# IDENTIFYING SURGICAL TRAUMA AND PREDICTING HEARING OUTCOMES USING ELECTROCOCHLEOGRAPHY DURING COCHLEAR IMPLANTATION

Christopher K. Giardina

A dissertation submitted to the faculty of the University of North Carolina at Chapel Hill and North Carolina State University in partial fulfillment of the requirements for the degree of Doctor of Philosophy in the Department of Biomedical Engineering in the School of Medicine.

Chapel Hill
2018

Approved by:

Lianne A. Cartee

Douglas C. Fitzpatrick

John H. Grose

Paul B. Manis

H. Troy Nagle

# ABSTRACT

Christopher K. Giardina: Identifying Surgical Trauma and Predicting Hearing Outcomes using Electrocochleography during Cochlear Implantation
(Under the direction of Douglas C. Fitzpatrick)

A patient receiving a cochlear implant (CI) has little predictive knowledge of how well he or she will ultimately perform in speech perception or hearing ability. Both pre- and intra-operative factors likely contribute to the wide variance in outcomes, but a key gap is identifying the specific causes. We have previously shown that assessing cochlear function with electrocochleography (ECochG) just prior to implantation can account for roughly half the variance in speech perception outcomes. However, surgical factors such as cochlear trauma during insertion and final implant positioning are also known to affect outcomes as well. This dissertation focuses on the use of extracochlear and intracochlear ECochG to identify trauma throughout CI insertion. An algorithm to determine the integrity of hair cell and neuronal generators from an ECochG recording was fundamental in this analysis. We also introduce two novel approaches to assess final CI positioning, using impedance and an intraoperative X-ray.

**Chapter 1** serves as a background to CI outcomes and intraoperative ECochG. **Chapter 2** describes initial experimentation, recording at a fixed, *extracochlear* location and examining reversible and permanent response drops (publication). To improve the analysis of ECochG, **Chapter 3** describes how an animal model with neurotoxins and ototoxins was used to develop a computational algorithm capable of estimating the contribution of hair cell and neuronal generators (publication co-written with Tatyana Khan). With this new tool, we were able to improve our speech prediction models, particularly in children with auditory neuropathy spectrum disorder. **Chapter 4** integrates the model into an analysis of *intracochlear* ECochG throughout CI insertion, particularly in deciding which response drops were likely to predict permanent hearing loss. Chapter 4 also serves as the primary

discussion of the thesis, comparing intra- and extracochlear ECochG and concluding with an evaluation of ECochG in accounting for outcomes and minimizing trauma. **Chapter 5** focuses on post-insertion positioning as a source of variance in outcomes, describing an impedance model to estimate array positioning (publication). **Chapter 6** highlights ongoing work, including extracochlear ECochG and hearing preservation, simultaneous intra- and extra-cochlear ECochG, and a tool to estimate CI positioning from an X-ray.

To my grandfathers, both for their curiosity and intellect:

CMSgt. Norris A. Cameron

USAF Strategic Air Command - Europe

Dr. David D. Giardina, M.D.

Yale Dept. of Radiology

# ACKNOWLEDGEMENTS

I would first like to sincerely thank the UNC MD/PhD program for their vote of confidence in accepting me into the University of North Carolina's MSTP program, and for their unwavering support as I complete this training. In particular, I'd like to acknowledge the professional and personal mentorship of Drs. Eugene Orringer, Mohanish Deshmukh, Toni Darville, Kimryn Rathmell, and David Siderovski. Just as important are Alison Regan and Carol Herion, who have helped me immensely to ensure that training progresses as smoothly as possible. Any person involved in the program can attest that Alison and Carol are consistently supportive, always willing to help, and astonishingly efficient.

I also thank Dr. Douglas Fitzpatrick, my primary research mentor, who on a daily basis provided critical, helpful feedback on all projects. He also allowed me flexibility in my research, encouraging independent projects which helped me grow as a scientist and researcher. He also ensured that I attended many international conferences, which fostered collaborations essential to this dissertation and my training at large. I also thank the members of my PhD committee, who have each provided unique and profound mentorship - Dr. Paul Manis provided scientific assistance regarding cochlear physiology, Dr. H. Troy Nagle provided advice on signal acquisition and instrumentation, Dr. Lianne Cartee was fundamental to my interpretation of bioelectricity, and Dr. John Grose provided expertise in understanding audiometric outcomes. I also thank my lab members Dr. Ken Hutson and Steve Pulver for their incredible, practical support in electrophysiology, and Dr. Tatyana Khan for our cooperative writing. I also acknowledge Dr. Devin Hubbard for academic support in recruiting undergraduate collaborators.

I am also grateful for the resolute and ongoing support of the surgical neurotologists who afforded me the opportunity to collect clinically-relevant data during their surgical procedures. Their patience throughout this process was extraordinary, particularly with such an active surgical center. I thank Drs. Harold Pillsbury, Craig Buchman, Oliver

Adunka, and Kevin Brown for both their professional mentorship and clinical expertise. I am also privileged to receive financial support from the National Institute on Deafness and Other Communication Disorders (NIDCD), who have supported me throughout my years of training.

Finally, I would like to acknowledge the essential support from family and friends throughout this process.

# TABLE OF CONTENTS

# LIST OF TABLES

# LIST OF FIGURES

# LIST OF ABBREVIATIONS

| | |
|---|---|
| $\mu$ | Period of the Unit Potential |
| $\mu$A | Microampere |
| $\mu$F | Microfarad |
| $\mu$M | Micromolar |
| $\mu$s | Microsecond |
| $\mu$V | Microvolt |
| $\Omega$ | Ohm |
| $\sigma$ | Width of the Cycle Histogram Distribution |
| $\varphi_{ANN}$ | Phase of the Auditory Nerve Neurophonic |
| $\varphi_{CM}$ | Phase of Cochlear Microphonic |
| $A_{ANN}$ | Amplitude of the Auditory Nerve Neurophonic |
| AB | Advanced Bionics |
| ABR | Auditory Brainstem Response |
| AC | Alternating Current |
| ACE | Advanced Combination Encoder |
| $A_{CM}$ | Amplitude of the Cochlear Microphonic |
| ADC | Analog-to-Digital Converter |
| AEP | Auditory-Evoked Potential |
| ANN | Auditory Nerve Neurophonic |
| ANOVA | Analysis of Variance |
| ANSD | Auditory Neuropathy Spectrum Disorder |
| AP | Anteroposterior |
| AzBio | Arizona Speech Score |
| BEDCS | Bionic Ear Data Collection System |
| BM | Basilar Membrane |
| CAP | Compound Action Potential |
| CF | Characteristic Frequency |
| CH | Cycle Histogram |

| | |
|---|---|
| CI | Cochlear Implant |
| CC | Cochlear Corporation |
| CIS | Continuous Interleaved Strategy |
| *CLDN14* | Claudin 14 gene |
| CM | Cochlear Microphonic |
| CMV | Cytomegalovirus |
| CNC | Consonant-Nucleus-Consonant |
| $C_p$ | Polarization Capacitance |
| CT | Computed Tomography |
| CVLT | California Verbal Learning Test |
| dB | Decibel |
| DC | Direct Current |
| DEG | Degree (angular), $^\circ$ |
| E1 | Electrode Array Contact 1 (apical contact of Advanced Bionics array) |
| EC | Extracochlear |
| ECE22 | Electrode Array Contact 22 (apical contact of Cochlear Corporation array) |
| ECAP | Electrically-evoked Compound Action Potential |
| ECochG | Electrocochleography |
| ECochG-TR | Electrocochleography Total Response |
| EFI | Electrical Field Imaging |
| EL | Electrode Array Contact |
| EPSP | Excitatory Postsynaptic Potential |
| EVA | Enlarged Vestibular Aqueduct |
| exp, $exp$ | Exponential Function |
| FDA | Food and Drug Administration |
| FFT | Fast Fourier Transform |
| *GJB2* | Connexin 26 gene |
| GND | Ground |
| HL | Hearing Level, Hearing Lost |

| | |
|---|---|
| HP | Hearing Preservation, Hearing Preserved |
| Hz | Hertz |
| $i$ | Current |
| i.p. | Intraperitoneal |
| IACUC | Institutional Animal Care and Use Committee |
| IC | Intracochlear |
| IHC | Inner Hair Cell |
| IQR | Interquartile Range |
| IRB | Institutional Review Board |
| KA | Kainic Acid |
| LF-PTA | Low Frequency Pure Tone Average |
| ln, $\ln$ | Natural Logarithm Function |
| lsqcurvefit | Least-square Curve Fitting Algorithm |
| LW | Lateral Wall |
| mA | Milliampere |
| mM | Millimolar |
| ms | Millisecond |
| mV | Millivolt |
| nHL | Normal Hearing Level |
| NIDCD | National Institute on Deafness and Other Communication Disorders |
| NIH | National Institutes of Health |
| OA | Ouabain |
| OHC | Outer Hair Cell |
| PM | Perimodiolar |
| Prom | Promontory |
| PTA | Pure-tone Average |
| $R_a$ | Access Resistance |
| RMS | Root-Mean Square |
| $R_p$ | Polarization Resistance |

| | |
|---|---|
| RW | Round Window |
| SD | Standard Deviation |
| SNHL | Sensorineural Hearing Loss |
| SOE | Spread of Excitation |
| SP | Summating Potential |
| SPEAK | Spectral PEAK |
| SPL | Sound Pressure Level |
| ST | Scala Tympani |
| SV | Scala Testibuli |
| $t$ | Time |
| *TECTA* | $\alpha$-tectorin gene |
| TR | Total Response (ECochG-TR) |
| TTX | Tetrodotoxin |
| UNC | University of North Carolina |
| UP | Unit Potential |
| $V_a$ | Access Voltage |
| $V_p$ | Polarization Voltage |
| $V_t$, $V_{tot}$ | Total Voltage |
| WHO | World Health Organization |
| $Z_p$ | Polarizaion Impedance |
| $Z_t$, $Z_{tot}$ | Total Impedance |

# CHAPTER 1: INTRODUCTION

## Overview

The cochlear implant (CI) is the most successful neural prosthesis to restore human sensory input, with electric stimulation of the auditory nerve clearly outperforming similarly designed devices which interface for visual or motor neuron rehabilitation (Zeng and Fay 2013). With an estimated 5% of the global population suffering from disabling hearing loss (World Health Organization, 2015), it is unsurprising then that as of 2012 over 312,000 devices have been implanted worldwide (Food and Drug Administration), and market analysts expect annual sales to jump from 45,000 implants a year in 2016 to 96,000 units a year by 2020 (Global Cochlear Implants Market, Technavio, 2018). Despite the successes of CI with auditory rehabilitation, there remain many unanswered questions regarding their efficacy – particularly why some individuals attain near-normal speech ability after implantation, whereas others struggle with open-set speech even after years of therapy.

For my dissertation, I have focused on using electrocochleography (ECochG), an electrophysiologic measurement made at the time of surgery, to identify intraoperative trauma associated with poorer hearing outcomes. Specifically, changes in ECochG responses throughout CI insertion were obtained at multiple recording sites and used to predict whether post-operative hearing thresholds were likely to remain intact.

This introductory chapter serves to provide a background to the topics discussed in this dissertation. The first section focuses on the biographical, anatomic, and device-specific factors that are known to affect outcomes. Next, the use of ECochG is discussed to explain how a single measure can help characterize cochlear health. The final section in this introduction describes how changes in ECochG can potentially be a marker of surgical trauma.

# Variability in Speech and Hearing Outcomes among Cochlear Implant Recipients

Although speech perception and hearing outcomes with CIs have improved on average over time, these outcomes are still highly variable (Holden, Finley et al. 2013). Accurate predictions would be useful in candidate selection, counseling patients before surgery, augmenting surgical techniques, improving electrode fitting and mapping, optimizing implant rehabilitative strategies, and eventually designing improved implant systems. It is therefore important to understand the underlying bases for the variance, with the goal of identifying and optimizing the limiting factors when possible.

## Biographical, Cognitive, Neural, and Device Programming Factors on Speech Outcomes

A myriad of patient-specific factors influence CI outcomes, including duration of deafness, duration of CI use, pre-operative speech ability, whether subjects were prelingual before implantation, cognitive ability, choice of CI stimulation paradigms, and method of fitting (Finley, Holden et al. 2008, Holden, Finley et al. 2013). However, as we will discuss below, none of these factors account for much of the variability seen because the causes of the variance are in general poorly known.

In adults, the main biographical factor typically seen to have a relationship with speech perception is duration of severe or profound hearing loss (e.g., Blamey, Arndt et al. 1996, Rubinstein, Parkinson et al. 1999, Blamey, Artieres et al. 2013, Holden, Finley et al. 2013). Blamey, Arndt et al. (1996) reported on 808 CI recipients and found a strong, negative relationship between duration of deafness and speech scores ($r^2$=13%), commented on the age of implantation as a factor, and were the first group to propose cognitive factors as being a potential contributor. Rubinstein, Parkinson et al. (1999) also found duration of deafness to be a factor but failed to show a strong connection between pre-implant speech ability and post-operative speech ability as Blamey et al had. However, because of the increasing use of hearing aids, the exact duration of sensorineural deafness is shortening

in the CI population – making it less of a predictive factor (Lazard, Vincent et al. 2012, Holden, Firszt et al. 2016).

The question of whether age at implantation is independently significant, or if it is merely a surrogate for cognitive ability or neural receptiveness to an implant, is controversial and ongoing. Leung, Wang et al. (2005) studied CI users over the age of 65 (n=258) and under the age of 65 (n=491) and found duration of deafness to be a strong predictor of speech discrimination ability within each group, but no difference in speech abilities between these two age groups. In 2011, Budenz, Cosetti et al. (2011) also found a strong relationship between duration of deafness and speech abilities and no relationship between age and outcomes (n=108). Conversely, in 2010 Friedland, Runge-Samuelson et al. (2010) found that in 56 subjects, age of implantation was a significant metric only after matching subjects by both pre-operative speech abilities and duration of deafness. In a larger study, Holden, Finley et al. (2013) found both age and duration of deafness to be significant contributors.

Cognitive factors including brain reorganization subsequent to reduced or absent input are also involved (Lee, Giraud et al. 2007, Moore and Shannon 2009, Strelnikov, Rouger et al. 2010, Anderson, Lazard et al. 2016), so education, verbal learning, and linguistic abilities are also studied alongside age of implantation and duration of deafness. Collison, Munson et al. (2004) found no relationship between cognitive ability or linguistic ability with outcomes (n=15), but in a slightly larger sample size (n=33) Heydebrand, Hale et al. (2007) found a strong between linguistic ability and speech outcomes – that 42% of the speech outcomes could be predicted by the California Verbal Learning Test (CVLT) (Delis, Kramer et al. 2000). When combining the factors from the CVLT with initial speech with an implant, and lip-reading abilities, the speech prediction improved to 82%. In children, age at implantation is a critical factor, with the earlier the implantation the better in cases of congenital hearing loss (Niparko, Tobey et al. 2010). General developmental progress, as well as educational, habilitative, and parental environments contribute additional variables, particularly in the youngest children who meet criteria for implantation prior to the acquisition of language (Blamey, Sarant et al. 2001, Baumgartner, Pok et al. 2002, Boons, Brokx et al. 2012, Dunn, Walker et al. 2014).

A factor that seems like it should affect outcomes is the prevalence of neural elements in the cochlea available for electrical stimulation. However, post-mortem analysis of surviving spiral ganglion cells and dendrites generally have not shown significant correlations with speech perception outcomes (Blamey 1997, Khan, Whiten et al. 2005, Nadol and Eddington 2006), although two recent studies (Seyyedi, Viana et al. 2014, Kamakura and Nadol 2016) have shown significant relationships between ganglion cell density and speech perception outcomes in small samples (n=6 and 16, respectively). A promising approach to directly measure the neural substrate is the electrically evoked compound action potential (ECAP). However, to date, this measurement has not shown a significant relationship to speech perception outcomes (reviewed by van Eijl, Buitenhuis et al. 2017). This may be due to the small dynamic range (Cohen 2009), similar to the dynamic range limitation seen with electrical stimulation in auditory nerve fibers (Kiang and Moxon 1972), which limits the ability to discriminate among subjects. Recently, ECAP techniques that exploit growth functions and refractoriness of the auditory nerve are showing correlation with neural survival in animal studies, and may lead to an advance in this area for CI subjects (Kang, Colesa et al. 2010, Kim, Abbas et al. 2010, Ramekers, Versnel et al. 2014, Zhou, Kraft et al. 2015, Strahl, Ramekers et al. 2016, Zhou and Pfingst 2016).

The range of residual neural substrate likely contributes to the wide variance in speech perception outcomes among the particular CI device stimulation strategies. A primary design decision is the choice of how electrodes are coupled and configured. Pfingst, Franck et al. (2001) compared monopolar to bipolar stimulation patterns, also altering distances between pairs of stimulating electrodes, and found that both factors could independently alter speech perception. Mens and Berenstein (2005) compared monopolar to quadripolar stimulation and found quantitative differences in spread of excitation, but no difference in speech perception with the new electrode configuration. Next, the choice of stimulation or processing algorithm must be considered. In 1988 Wilson, Finley et al. (1988) found interleaved strategies to offer superior performance. Some 20 years later, Skinner, Holden et al. (2002) compared three Cochlear processing algorithms, the SPEAK (Spectral PEAK), ACE (Advanced Combination Encoder), and CIS (Continuous Interleaved Strategy) strategies, and found users preferred all algorithms equally at onset– thus their recommendation

was that all users receive the ACE strategy, have parameters fitted, then begin to compare strategies rather than comparing different strategies from the onset of stimulation. With any stimulation strategy, it is known that proper device programming, or "fitting", to an individual subject is paramount to ensure the best speech outcomes possible (Skinner 2003), but variance among outcomes even after fitting remains high.

Considering audiologic, biographical, and device factors in either univariate or multivariate analysis, most studies account for only a limited amount of variance in speech perception outcomes using the implant alone in quiet. For instance, a recent multicenter study with 2251 subjects included fifteen pre- and post-surgical factors in a multivariate regression. Using nine variables, the authors were only able to account for 22% of the variance in monosyllabic word scores (Lazard, Vincent et al. 2012).

## Surgical Factors and Device Placement

In addition to the biographical, cognitive, and device stimulation paradigms, surgical factors including number of active electrodes, their scalar placement, depth of insertion, and distance from the modiolus are also markers for speech outcomes (Finley, Holden et al. 2008, Lazard, Vincent et al. 2012, Blamey, Artieres et al. 2013, Holden, Finley et al. 2013). Ideal placement of the CI is completely within the scala tympani (ST), coiled with contacts facing the spiral ganglion cells (Shepherd, Hatsushika et al. 1993). However, intra-insertion trauma can occur during surgical placement if an array penetrates the basilar membrane, which has been generally associated with poorer speech and hearing outcomes (reviewed by O'Connell, Hunter et al. 2016). In a cohort of 15 subjects, Skinner et al. found a strong, negative correlation between the number of electrodes in the scala vestibuli (SV) and Consonant-Nucleus-Consonant (CNC) speech score (Skinner, Holden et al. 2007). In 2013 Holden, Finley et al. (2013) updated their 2007 population to reflect a total of 114 subjects and continued to find an inverse relationship between number of electrodes in the SV and CNC scores. Aschendort et al also found higher speech scores in subjects with completely-within-ST positioning (Aschendorff, Kromeier et al. 2007). Finley et al. furthered this analysis to include both within-ST scalar positioning, as well as a metric for curvature ('wrapping factor') to both be significantly associated with better

speech perception outcomes (Finley, Holden et al. 2008). This latter, wrapping factor metric attempts to quantify the overall electrode placement relative to the modiolus, and is of significant interest because some implant designs are pre-coiled and "modiolar" whereas "lateral wall" arrays are designed to not interact with the modiolus as an attempt to avoid insertion trauma.

In 2010, researchers at Vanderbilt University developed and validated an algorithm which merged a pre-operative and post-operative computed tomography (CT) scan to determine precise electrode positioning within each scala (Schuman, Noble et al. 2010). With this tool, they found speech scores in 116 subjects were significantly better when implants resided completely within the ST (Wanna, Noble et al. 2014). This analysis was also used in a larger study of 220 subjects, where both CNC and Arizona Speech (AzBio) scores were better for ST than SV insertions (O'Connell, Cakir et al. 2016). Array designs were also found to differ significantly in terms of likelihood to penetrate the basilar membrane (BM). Specifically, modiolar arrays were significantly more likely to exit the ST, compared to lateral wall arrays (Wanna, Noble et al. 2014, Boyer, Karkas et al. 2015, O'Connell, Cakir et al. 2016). Subsequent analysis of modiolar and lateral wall arrays found lateral wall arrays afforded higher rates of completely-within-ST positioning, better speech scores overall, and also better speech scores after controlling for completely-within-ST positioning (O'connell, Hunter et al. 2016). These analyses also discovered that ST insertion, younger age, and greater angular insertion depth were associated with better speech performance. These same imaging techniques were also used to demonstrate that, among lateral wall arrays with completely-within-ST insertions, longer array lengths were associated with better post-operative speech ability (better CNC score) but poorer hearing ability (worse audiometric thresholds) (O'Connell, Hunter et al. 2017). That array length for completely-within-ST insertions affects postoperative hearing ability demonstrates there are more factors affecting insertion trauma than merely positioning within the ST; larger (longer) implants are associated with more robust fibrosis (Anderson, Rodriguez et al. 2008), a key step in the foreign body reaction which eventually leads to hearing loss (Jia, Wang et al. 2013).

An approach to account for, and possibly improve, outcomes would be to properly characterize the pre-operative cochlea, avoid surgical trauma, and assess post-operative positioning. Our approach to addressing these questions has primarily used a measurement called ECochG, which is the electric response generated by the cochlea to sound.

## Electrocochleography to Characterize Pre-Operative Cochlear Health

One way to probe the cochlea's functional status is with ECochG. In this section the history of ECochG, the cochlear and neural generators of the response, and the signal features will be discussed in relation to subjects receiving CIs.

### History of ECochG in Assessing the Cochlea

ECochG recordings were first made on the promontory in two humans undergoing surgery in 1935 (Fromm, Nylen et al. 1935), though no waveforms were published with the report. Better signal to noise ratio was paramount in recordings throughout the 1940s, wherein phase-locked responses to tones (later coined microphonics) were regularly obtained in subjects with normal hearing thresholds (Perlman and Case 1941, Lempert, Wever et al. 1947). Lempert, Wever et al. (1947) recorded from the round window (RW) of 11 cochleae with pathologies including tinnitus, otosclerosis, and Meniere's disease. ECochG during the next 20 years were advanced by Reuben, where microphonics were characterized from tuning forks (Ruben, Sekula et al. 1960) and clear compound action potentials (CAPs) were obtained at the RW (Ruben, Bordley et al. 1961). Reuben and Walker also quantified bone conduction latencies in mammals, and designated a shortening in latency before and after stapes surgery as evidence of improved acoustic conduction to the cochlea (Bordley, Ruben et al. 1964). Though still a largely exploratory technique, Ruben (1967) stated ECochG had three major implications: the correlation of physiological and psychoacoustic properties, the investigation of certain otologic diseases, and the diagnosis of deafness. By the mid-1980s, ECochG had a clinically important role in the diagnosis of Meniere's disease, but recent evidence implies the utility of ECochG may not be entirely

sufficient (Nguyen, Harris et al. 2010). It also temporarily played a role in the diagnosis of vestibular schwannoma until auditory brainstem responses (ABR) replaced the ECochG (Eggermont, Don et al. 1980). More recently, interest in ECochG has been revitalized in the characterization of cochlear health, particularly in subjects who are receiving cochlear implants and in diagnosing auditory neuropathy (Eggermont 2017, Fontenot, Giardina et al. 2017, Hornibrook 2017, Riggs, Roche et al. 2017, Santarelli, Starr et al. 2008) .

## Signal Components of the ECochG

The ECochG is the sound-evoked electrical response to stimuli (usually a tone, click or electrical pulse) containing contributions from inner hair cells, outer hair cells, and auditory nerve generators. The ECochG response to tones is rich and complex, with several distinct signal characteristics arising from different combinations of hair cell and neural generators. An example ECochG response is shown in Fig 1.1 , with the condensation/rarefaction (top row), difference (center row), and sum (bottom row) responses to a 500 Hz, 90 dB HL tone (waveform on left, fast Fourier Transform, FFT, on right) from the RW of a subject about to receive a CI. The components of the ECochG are the compound action potential (CAP), the cochlear microphonic (CM), the auditory nerve neurophonic (ANN) and the summating potential (SP). The CAP is seen as a transient deflection that represents synchronized neural activity to the onset of the stimulus. The ongoing part of the response to low frequency tones (Fig 1.1, 'CM/ANN' region) is a mixture of both hair cell and neural activity, assuming neural activity is present in a given case. The hair cell contribution is the CM, produced by mechanosensitive ion channels in the stereocilia of hair cells that open and close in response to displacement of the basilar membrane (Dallos 1973). The neural component is the ANN, which is produced by phase-locked responses of auditory nerve fibers (Snyder and Schreiner 1984, Henry 1995, He, Porsov et al. 2012, Forgues, Koehn et al. 2014, Lichtenhan, Hartsock et al. 2014, Verschooten and Joris 2014, Verschooten, Robles et al. 2015). Although there is variation by species, in general the phase-locking weakens above about 1000 Hz, and becomes negligible above 2-3 kHz (Weiss and Rose 1988). Most evidence supports a similar range for humans (Joris and Verschooten 2013). Thus, to frequencies above the phase-locking range the ongoing response is purely

CM, while to low frequencies it is CM plus the ANN. The majority of the spectral energy is found at the stimulus frequency in the condensation/rarefaction and difference curves (Fig 1.1, right column), and at twice the stimulus frequency in the summed response. There are some distortions (deviations from the purely sinusoidal stimulus in the recorded response) present at 1 kHz and 2 kHz on the response, representing some of the neural ANN. An additional component is a slow, cumulative shift from base-line during the tone stimulus, called the summating potential (SP). The SP is most evident to high frequencies and is derived from a mixture of hair cell and neural sources (Davis, Deatherage et al. 1958, Dallos, Schoeny et al. 1972, van Emst, Klis et al. 1995, Zheng, Ding et al. 1997, Durrant, Wang et al. 1998, Sellick, Patuzzi et al. 2003, Forgues, Koehn et al. 2014). In the summed response (Fig 1.1, bottom), the SP is depicted as a sustained, negative shift throughout the duration of the tone burst.

### ECochG in Subjects Receiving Cochlear Implants

Despite profound sensorineural deafness, it is possible to obtain ECochG at the RW in nearly 95% of subjects where CI is clinically indicated (Choudhury, Fitzpatrick et al. 2012). Recently, we found that measurements of residual cochlear physiology with ECochG just before implantation could account for 40-50% of the variance in speech perception outcomes in adults (McClellan, Formeister et al. 2014) and 33% of the variance in speech perception in children (Formeister, McClellan et al. 2015). The primary metric used is the ECochG Total Response (TR, ECochG-TR), and includes the sum of spectral magnitudes in the ongoing responses to tones of different frequency. Specifically, the 90 dB nHL (normal hearing level) tones are 250 Hz, 500 Hz, 750 Hz, 1 kHz, 2 kHz, and 4 kHz, chosen to roughly cover the range of speech. The TR in subjects varies with etiology, with lower responses in subjects with meningitis and larger responses with auditory neuropathy spectrum disorder (ANSD), but there was a difference in the TR between different age groups. The TR spans over 60 dB, and median TR for adults vs. children are within 5 dB of one another.

Because the TR focuses solely on the ongoing portion of the response, the CAP and SP are not considered in this metric and may provide prognostic value. To this end, we have previously attempted to quantify these responses in CI subjects. Unlike the ongoing

response, the CAP is seen in only about 50% of CI subjects, and when present can have a highly varied morphology making measurement difficult in some cases (Scott, Giardina et al. 2016). Examples of various CAP and SP morphologies are shown in Fig 1.2. In this subset of subjects, the CAP predicted 20% of the variance in speech outcomes, but the TR still was a much better predictor, predicting 43% of the variance. Additionally, the incorporation of the CAP to the TR added no predictive knowledge – that is to say the variance in the TR already completely accounted for any information the CAP could provide. The SP in CI subjects is highly variable, and deviations from recordings in normal cochleae have historically been attributed to endolymphatic hydrops (recently reviewed by Eggermont 2017, Hornibrook 2017). As such, most analyses in this thesis will involve metrics of the ongoing response.

## Changes in Electrocochleography to Identify Intra-Operative Trauma

Because the ECochG provides rich information about cochlear health, an approach to identify intraoperative surgical trauma is to implement ECochG throughout CI insertion.

### Assessing Trauma with an Animal Model

Several labs first began developing extracochlear ECochG measurement systems to monitor responses to auditory stimuli during implantation (Mandala, Colletti et al. 2012, Radeloff, Shehata-Dieler et al. 2012). However, these studies use threshold measurements, which by definition are of low signal to noise and only from a restricted part of the cochlea. In gerbil experiments, we showed that ECochG with a single low-frequency tone presented at high amplitude produces a cochlear response that is both easily analyzed and highly sensitive to small changes (Adunka, Mlot et al. 2010, Campbell, Suberman et al. 2010, Campbell, Suberman et al. 2010, Choudhury, Adunka et al. 2011, Demason, Choudhury et al. 2012). Specifically, the magnitude of the ongoing response is a better metric for trauma than the CAP (Demason, Choudhury et al. 2012). Consequently, overall trauma to any location may be detected as a loss in response magnitude. In the same studies, the

amount of trauma observed histologically were consistent with permanent or temporary loss of response. An intense, low frequency tone was chosen in order to maximize spread of excitation over the largest cochlear length possible. Fortuitously, in the noise damaged animal model (Suberman, Campbell et al. 2011, Choudhury, Adunka et al. 2014) and human implant subjects (Choudhury, Fitzpatrick et al. 2012, Fitzpatrick, Campbell et al. 2014) responses to low frequencies predominate. Importantly, this frequency is within the range of neural phase-locking, so that there is the possibility of analyzing neural and hair cell changes separately.

## Assessing Trauma in Cochlear Implant Recipients

By 2015, all the major implant manufacturers had begun facilitating the use of ECochG monitors: Dalbert et al. using custom Advanced Bionics software (Dalbert, Pfiffner et al. 2015), Campbell et al. working with Cochlear Corporation (Campbell, Kacier et al. 2015, Campbell, Kaicer et al. 2015), and also investigations from MED-EL (Youssef Adel 2015). Importantly, all of these groups are using our metric of a change in magnitude of the ongoing portion (often mis-identified as the 'CM' rather than 'CM&ANN') to indicate trauma. Over the subsequent 3 years, intracochlear ECochG recordings have continued to be performed by all manufacturers (Acharya, Tavora-Vieira et al. 2016, Campbell, Kaicer et al. 2016, Harris, Riggs et al. 2016, Campbell, Bester et al. 2017, Harris, Riggs et al. 2017, O'Connell, Holder et al. 2017, Dalbert, Pfiffner et al. 2018). Because the apical electrode is changing position during insertion, different geometry and proximity to sources will cause response changes which may make trauma harder to decipher than with extracochlear signals than with intracochlear signals. For this reason, extracochlear approaches continue to be investigated (Mandala, Colletti et al. 2012, Radeloff, Shehata-Dieler et al. 2012, Dalbert, Sim et al. 2014, Adunka, Giardina et al. 2015, Dalbert, Pfiffner et al. 2015, Dalbert, Sim et al. 2015, Dalbert, Huber et al. 2016, Dalbert, Pfiffner et al. 2018). However, there is no thorough comparison of the two approaches in the literature.

## Goals of the Thesis

The primary goal of this thesis was to evaluate the use of ECochG as a means of assessing and possibly avoiding insertion trauma during the surgery. To this purpose we assessed both extracochlear and intracochlear recording approaches. As part of comprehending the utility of the ECochG methods we also had to understand in detail the hair cell and neural sources of the recorded signal and their interactions. Thus, Chapter 2 describes extracochlear recording, Chapter 3 describes the development of a model of the ongoing response, Chapter 4 describes intracochlear recordings and serves as the primary discussion of the thesis, Chapter 5 presents a novel approach of imaging with impedance, and finally in Chapter 6 I present ongoing work.

# FIGURES

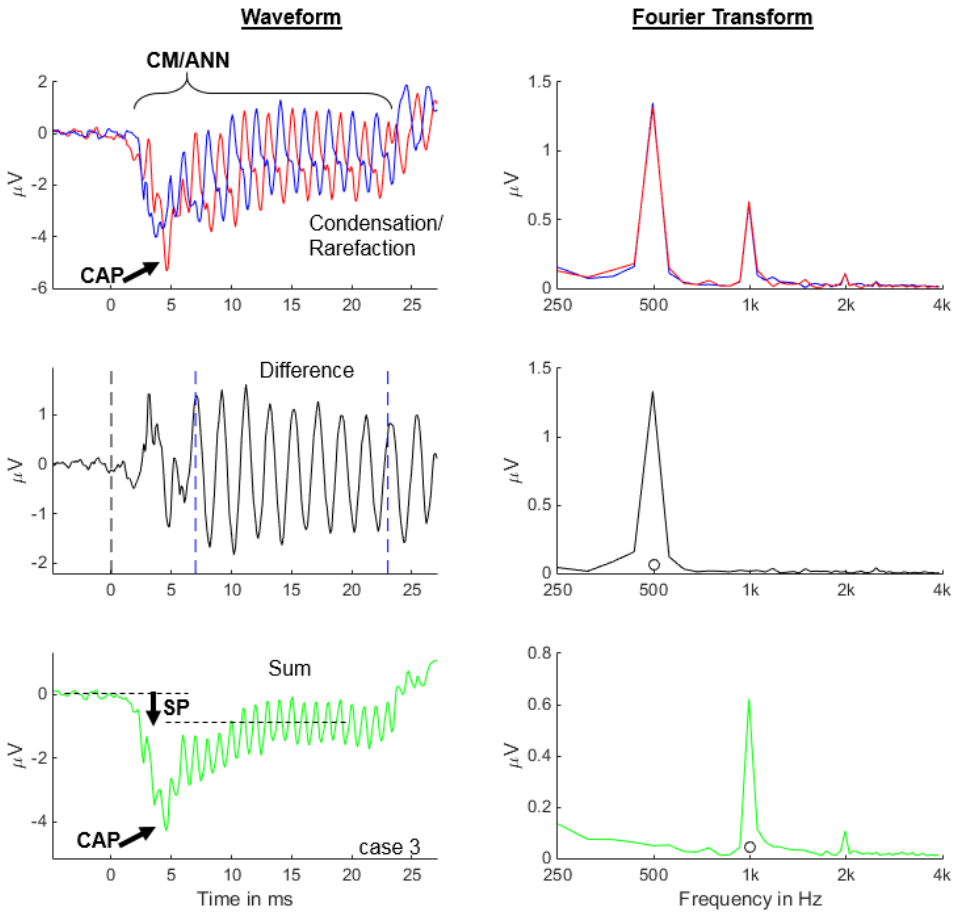


**Figure 1.1 - ECochG Response.**
Example response waveforms of Electrocochleography from the Round Window in a human subject. In response to the 500 Hz, 90 dB nHL tone burst presented with alternating polarity, the condensation/rarefaction responses (top row), difference (middle row), and sum (bottom row) are shown with waveforms on the left and response magnitudes on the right. The compound action potential (CAP) is an early-onset deflection of synchronized neural onset. The ongoing, phase-locked portion contains both the cochlear microphonic (CM) and the auditory nerve neurophonic (ANN). The summating potential (SP) is most readily seen in the sum waveform.

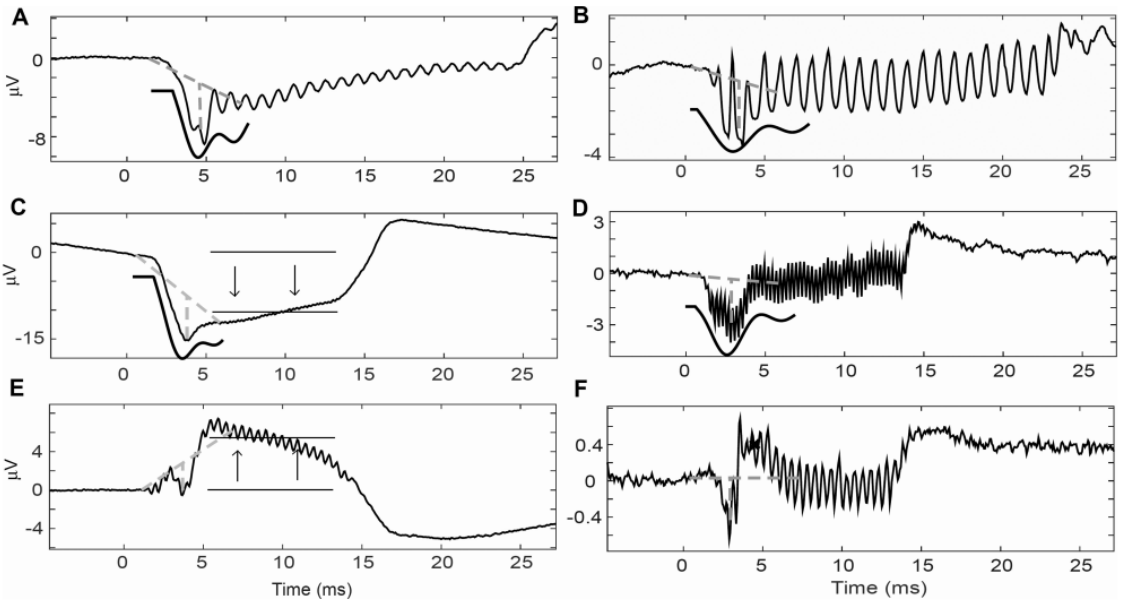


**Figure 1.2 - Compound Action Potential and Summating Potential in CI Subjects.** Six example waveforms of the sum response in six subjects demonstrate the variability in both morphology and strength of the compound action potential (CAP) and summating potential (SP). A. This response had a well-defined CAP to a low frequency (500 Hz) but no significant SP. B. This CAP to 500 Hz was obscured by the fine structure of the response. C. This apparent CAP to a 4 kHz tone was associated with a large SP (arrows). D. This CAP to a 4 kHz tone was shallow and spread in time. E. This CAP to a 1 kHz tone was also obscured by a SP, which was positive in this case. F. This CAP to a 2 kHz tone had a prominent P1, or positive, component (x). The fitting program was also unable to measure this CAP. (From Scott, Giardina et al. 2016).

## REFERENCES


Acharya, A. N., D. Tavora-Vieira and G. P. Rajan (2016). "Using the Implant Electrode Array to Conduct Real-time Intraoperative Hearing Monitoring During Pediatric Cochlear Implantation: Preliminary Experiences." Otology & Neurotology 37(2): e148-e153.

Adunka, O. F., C. K. Giardina, E. J. Formeister, B. Choudhury, C. A. Buchman and D. C. Fitzpatrick (2015). "Round window electrocochleography before and after cochlear implant electrode insertion." Laryngoscope.

Adunka, O. F., S. Mlot, T. A. Suberman, A. P. Campbell, J. Surowitz, C. A. Buchman and D. C. Fitzpatrick (2010). "Intracochlear recordings of electrophysiological parameters indicating cochlear damage." Otol Neurotol 31(8): 1233-1241.

Anderson, C. A., D. S. Lazard and D. E. Hartley (2016). "Plasticity in bilateral superior temporal cortex: Effects of deafness and cochlear implantation on auditory and visual speech processing." Hear Res.

Anderson, J. M., A. Rodriguez and D. T. Chang (2008). Foreign body reaction to biomaterials. Seminars in immunology, Elsevier.

Aschendorff, A., J. Kromeier, T. Klenzner and R. Laszig (2007). "Quality control after insertion of the nucleus contour and contour advance electrode in adults." Ear Hear 28(2 Suppl): 75S-79S.

Baumgartner, W. D., S. M. Pok, B. Egelierler, P. Franz, W. Gstoettner and J. Hamzavi (2002). "The role of age in pediatric cochlear implantation." Int J Pediatr Otorhinolaryngol 62(3): 223-228.

Blamey, P. (1997). "Are spiral ganglion cell numbers important for speech perception with a cochlear implant?" Am. J. Otolaryngol. 18(6 Suppl): S11-12.

Blamey, P., P. Arndt, F. Bergeron, G. Bredberg, J. Brimacombe, G. Facer, J. Larky, B. Lindstrom, J. Nedzelski, A. Peterson, D. Shipp, S. Staller and L. Whitford (1996). "Factors affecting auditory performance of postlinguistically deaf adults using cochlear implants." Audiol. Neurootol. 1(5): 293-306.

Blamey, P., F. Artieres, D. Baskent, F. Bergeron, A. Beynon, E. Burke, N. Dillier, R. Dowell, B. Fraysse, S. Gallego, P. J. Govaerts, K. Green, A. M. Huber, A. Kleine-Punte, B. Maat, M. Marx, D. Mawman, I. Mosnier, A. F. O'Connor, S. O'Leary, A. Rousset, K. Schauwers, H. Skarzynski, P. H. Skarzynski, O. Sterkers, A. Terranti, E. Truy, P. Van de Heyning, F. Venail, C. Vincent and D. S. Lazard (2013). "Factors affecting auditory performance of postlinguistically deaf adults using cochlear implants: an update with 2251 patients." Audiol Neurootol 18(1): 36-47.

Blamey, P., J. Z. Sarant, L. E. Paatsch, J. G. Barry, C. P. Bow, R. J. Wales, M. Wright, C. Psarros, K. Rattigan and R. Tooher (2001). "Relationships among speech perception, production, language, hearing loss, and age in children with impaired hearing." J Speech Lang Hear Res 44(2): 264-285.

Boons, T., J. P. Brokx, J. H. Frijns, L. Peeraer, B. Philips, A. Vermeulen, J. Wouters and A. van Wieringen (2012). "Effect of pediatric bilateral cochlear implantation on language development." Arch Pediatr Adolesc Med 166(1): 28-34.

Bordley, J. E., R. J. Ruben and A. T. Lieberman (1964). "Human cochlear potentials." The Laryngoscope 74(4): 463-479.

Boyer, E., A. Karkas, A. Attye, V. Lefournier, B. Escude and S. Schmerber (2015). "Scalar localization by cone-beam computed tomography of cochlear implant carriers: a comparative study between straight and periomodiolar precurved electrode arrays." Otology & Neurotology 36(3): 422-429.

Budenz, C. L., M. K. Cosetti, D. H. Coelho, B. Birenbaum, J. Babb, S. B. Waltzman and P. C. Roehm (2011). "The effects of cochlear implantation on speech perception in older adults." J Am Geriatr Soc 59(3): 446-453.

Campbell, A. P., T. A. Suberman, C. A. Buchman, D. C. Fitzpatrick and O. F. Adunka (2010). "Correlation of early auditory potentials and intracochlear electrode insertion properties: an animal model featuring near real-time monitoring." Otol Neurotol 31(9): 1391-1398.

Campbell, A. P., T. A. Suberman, C. A. Buchman, D. C. Fitzpatrick and O. F. Adunka (2010). "Flexible cochlear microendoscopy in the gerbil." Laryngoscope 120(8): 1619-1624.

Campbell, L., C. Bester, C. Iseli, D. Sly, A. Dragovic, A. W. Gummer and S. O'leary (2017). "Electrophysiological evidence of the basilar-membrane travelling wave and frequency place coding of sound in cochlear implant recipients." Audiology and Neurotology 22(3): 180-189.

Campbell, L., A. Kacier, R. Briggs and S. OLeary (2015). "Cochlear Response Telemetry: Real-Time Monitoring of Intraoperatice Electrocochleography." Poster Presentation at the 2015 Conference on Implantable Auditory Prostheses (CIAP).

Campbell, L., A. Kaicer, R. Briggs and S. O'Leary (2015). "Cochlear response telemetry: intracochlear electrocochleography via cochlear implant neural response telemetry pilot study results." Otol Neurotol 36(3): 399-405.

Campbell, L., A. Kaicer, D. Sly, C. Iseli, B. Wei, R. Briggs and S. O'Leary (2016). "Intraoperative Real-time Cochlear Response Telemetry Predicts Hearing Preservation in Cochlear Implantation." Otology & Neurotology 37(4): 332-338.

Choudhury, B., O. F. Adunka, O. Awan, J. M. Pike, C. A. Buchman and D. C. Fitzpatrick (2014). "Electrophysiologic consequences of flexible electrode insertions in gerbils with noise-induced hearing loss." Otol Neurotol 35(3): 519-525.

Choudhury, B., O. F. Adunka, C. E. Demason, F. I. Ahmad, C. A. Buchman and D. C. Fitzpatrick (2011). "Detection of intracochlear damage with cochlear implantation in a gerbil model of hearing loss." Otol Neurotol 32(8): 1370-1378.

Choudhury, B., D. C. Fitzpatrick, C. A. Buchman, B. P. Wei, M. T. Dillon, S. He and O. F. Adunka (2012). "Intraoperative round window recordings to acoustic stimuli from cochlear implant patients." Otol Neurotol 33(9): 1507-1515.

Cohen, L. T. (2009). "Practical model description of peripheral neural excitation in cochlear implant recipients: 1. Growth of loudness and ECAP amplitude with current." Hear Res 247(2): 87-99.

Collison, E. A., B. Munson and A. E. Carney (2004). "Relations among linguistic and cognitive skills and spoken word recognition in adults with cochlear implants." Journal of Speech, Language, and Hearing Research 47(3): 496-508.

Dalbert, A., A. Huber, D. Veraguth, C. Roosli and F. Pfiffner (2016). "Assessment of Cochlear Trauma During Cochlear Implantation Using Electrocochleography and Cone Beam Computed Tomography." Otology & Neurotology 37(5): 446-453.

Dalbert, A., F. Pfiffner, M. Hoesli, K. Koka, D. Veraguth, C. Roosli and A. Huber (2018). "Assessment of Cochlear Function during Cochlear Implantation by Extra-and Intracochlear Electrocochleography." Frontiers in neuroscience 12: 18.

Dalbert, A., F. Pfiffner, C. Roeoesli, K. Thoele, J. H. Sim, R. Gerig and A. M. Huber (2015). "Extra-and Intracochlear Electrocochleography in Cochlear Implant Recipients." Audiology and Neurotology 20(5): 339-348.

Dalbert, A., J. H. Sim, R. Gerig, F. Pfiffner, C. Roosli and A. Huber (2015). "Correlation of Electrophysiological Properties and Hearing Preservation in Cochlear Implant Patients." Otol Neurotol 36(7): 1172-1180.

Dalbert, A., J. H. Sim and A. M. Huber (2014). "Electrophysiologic Monitoring of Residual Hearing During and After Cochlear Implantation." Association for Research in Otolaryngology Abstracts 37: 317-318.

Dallos, P. (1973). The Auditory Periphery Biophysics and Physiology. New York, Academic Press, Inc.

Dallos, P., Z. G. Schoeny and M. A. Cheatham (1972). "Cochlear summating potentials. Descriptive aspects." Acta Otolaryngol Suppl 302: 1-46.

Davis, H., B. H. Deatherage, D. H. Eldredge and C. A. Smith (1958). "Summating potentials of the cochlea." Am J Physiol 195(2): 251-261.

Delis, D. C., J. Kramer, E. Kaplan and B. A. Ober (2000). CVLT-II: California verbal learning test: adult version, Psychological Corporation.

Demason, C., B. Choudhury, F. Ahmad, D. C. Fitzpatrick, J. Wang, C. A. Buchman and O. F. Adunka (2012). "Electrophysiological properties of cochlear implantation in the gerbil using a flexible array." Ear Hear 33(4): 534-542.

Dunn, C. C., E. A. Walker, J. Oleson, M. Kenworthy, T. Van Voorst, J. B. Tomblin, H. Ji, K. I. Kirk, B. McMurray, M. Hanson and B. J. Gantz (2014). "Longitudinal speech perception and language performance in pediatric cochlear implant users: the effect of age at implantation." Ear Hear 35(2): 148-160.

Durrant, J. D., J. Wang, D. L. Ding and R. J. Salvi (1998). "Are inner or outer hair cells the source of summating potentials recorded from the round window?" J Acoust Soc Am 104(1): 370-377.

Eggermont, J. J. (2017). "Ups and Downs in 75 Years of Electrocochleography." Front Syst Neurosci 11: 2.

Eggermont, J. J., M. Don and D. E. Brackmann (1980). "Electrocochleography and auditory brainstem electric responses in patients with pontine angle tumors." Annals of Otology, Rhinology & Laryngology 89: 1-19.

Finley, C. C., T. A. Holden, L. K. Holden, B. R. Whiting, R. A. Chole, G. J. Neely, T. E. Hullar and M. W. Skinner (2008). "Role of electrode placement as a contributor to variability in cochlear implant outcomes." Otol Neurotol 29(7): 920-928.

Fitzpatrick, D. C., A. T. Campbell, B. Choudhury, M. P. Dillon, M. Forgues, C. A. Buchman and O. F. Adunka (2014). "Round window electrocochleography just before cochlear implantation: relationship to word recognition outcomes in adults." Otol Neurotol 35(1): 64-71.

Fontenot, T. E., C. K. Giardina, H. F. Teagle, L. R. Park, O. F. Adunka, C. A. Buchman, K. D. Brown and D. C. Fitzpatrick (2017). "Clinical role of electrocochleography in children with auditory neuropathy spectrum disorder." International journal of pediatric otorhinolaryngology 99: 120-127.

Forgues, M., H. A. Koehn, A. K. Dunnon, S. H. Pulver, C. A. Buchman, O. F. Adunka and D. C. Fitzpatrick (2014). "Distinguishing hair cell from neural potentials recorded at the round window." J Neurophysiol 111(3): 580-593.

Formeister, E. J., J. H. McClellan, W. H. Merwin, 3rd, C. E. Iseli, N. H. Calloway, H. F. Teagle, C. A. Buchman, O. F. Adunka and D. C. Fitzpatrick (2015). "Intraoperative round window electrocochleography and speech perception outcomes in pediatric cochlear implant recipients." Ear Hear 36(2): 249-260.

Friedland, D. R., C. Runge-Samuelson, H. Baig and J. Jensen (2010). "Case-control analysis of cochlear implant performance in elderly patients." Arch Otolaryngol Head Neck Surg 136(5): 432-438.

Fromm, B., C. Nylen and Y. Zotterman (1935). "Studies in the mechanism of the Wever and Bray effect." Acta oto-laryngologica 22(3): 477-486.

Harris, M., W. Riggs, K. Koka, L. Litvak, P. Malhotra, A. Moberly, B. O'Connell, J. Holder, F. Di Lella, C. Boccio, G. Wanna, R. Labadie and O. Adunka (2016). "Real-time intracochlear electrocochleography obtained directly through a cochlear implant." Otol Neurotol.

Harris, M. S., W. J. Riggs, C. K. Giardina, B. P. O'connell, J. T. Holder, R. T. Dwyer, K. Koka, R. F. Labadie, D. C. Fitzpatrick and O. F. Adunka (2017). "Patterns Seen During Electrode Insertion Using Intracochlear Electrocochleography Obtained Directly Through a Cochlear Implant." Otology & Neurotology 38(10): 1415-1420.

He, W., E. Porsov, D. Kemp, A. L. Nuttall and T. Ren (2012). "The group delay and suppression pattern of the cochlear microphonic potential recorded at the round window." PLoS One 7(3): e34356.

Henry, K. R. (1995). "Auditory nerve neurophonic recorded from the round window of the Mongolian gerbil." Hear Res 90(1-2): 176-184.

Heydebrand, G., S. Hale, L. Potts, B. Gotter and M. Skinner (2007). "Cognitive predictors of improvements in adults' spoken word recognition six months after cochlear implant activation." Audiology and Neurotology 12(4): 254-264.

Holden, L. K., C. C. Finley, J. B. Firszt, T. A. Holden, C. Brenner, L. G. Potts, B. D. Gotter, S. S. Vanderhoof, K. Mispagel, G. Heydebrand and M. W. Skinner (2013). "Factors Affecting Open-Set Word Recognition in Adults With Cochlear Implants." Ear Hear.

Holden, L. K., J. B. Firszt, R. M. Reeder, R. M. Uchanski, N. Y. Dwyer and T. A. Holden (2016). "Factors Affecting Outcomes in Cochlear Implant Recipients Implanted With a Perimodiolar Electrode Array Located in Scala Tympani." Otol Neurotol 37(10): 1662-1668.

Hornibrook, J. (2017). "Tone Burst Electrocochleography for the Diagnosis of Clinically Certain Meniere's Disease." Front Neurosci 11: 301.

Jia, H., J. Wang, F. François, A. Uziel, J.-L. Puel and F. Venail (2013). "Molecular and cellular mechanisms of loss of residual hearing after cochlear implantation." Annals of Otology, Rhinology & Laryngology 122(1): 33-39.

Joris, P. X. and E. Verschooten (2013). "On the limit of neural phase locking to fine structure in humans." Adv Exp Med Biol 787: 101-108.

Kamakura, T. and J. B. Nadol, Jr. (2016). "Correlation between word recognition score and intracochlear new bone and fibrous tissue after cochlear implantation in the human." Hear Res 339: 132-141.

Kang, S. Y., D. J. Colesa, D. L. Swiderski, G. L. Su, Y. Raphael and B. E. Pfingst (2010). "Effects of hearing preservation on psychophysical responses to cochlear implant stimulation." J Assoc Res Otolaryngol 11(2): 245-265.

Khan, A. M., D. M. Whiten, J. B. Nadol, Jr. and D. K. Eddington (2005). "Histopathology of human cochlear implants: correlation of psychophysical and anatomical measures." Hear Res 205(1-2): 83-93.

Kiang, N. Y. and E. C. Moxon (1972). "Physiological considerations in artificial stimulation of the inner ear." Ann Otol Rhinol Laryngol 81(5): 714-730.

Kim, J. R., P. J. Abbas, C. J. Brown, C. P. Etler, S. O'Brien and L. S. Kim (2010). "The Relationship Between Electrically Evoked Compound Action Potential and Speech Perception: A Study in Cochlear Implant Users With Short Electrode Array." Otology & Neurotology 31(7): 1041-1048.

Lazard, D. S., C. Vincent, F. Venail, P. Van de Heyning, E. Truy, O. Sterkers, P. H. Skarzynski, H. Skarzynski, K. Schauwers, S. O'Leary, D. Mawman, B. Maat, A. Kleine-Punte, A. M. Huber, K. Green, P. J. Govaerts, B.

Fraysse, R. Dowell, N. Dillier, E. Burke, A. Beynon, F. Bergeron, D. Baskent, F. Artieres and P. J. Blamey (2012). "Pre-, per- and postoperative factors affecting performance of postlinguistically deaf adults using cochlear implants: a new conceptual model over time." PLoS One 7(11): e48739.

Lee, H. J., A. L. Giraud, E. Kang, S. H. Oh, H. Kang, C. S. Kim and D. S. Lee (2007). "Cortical activity at rest predicts cochlear implantation outcome." Cereb Cortex 17(4): 909-917.

Lempert, J., E. G. Wever and M. Lawrence (1947). "The cochleogram and its clinical application: a preliminary report." Archives of otolaryngology 45(1): 61-67.

Leung, J., N. Y. Wang, J. D. Yeagle, J. Chinnici, S. Bowditch, H. W. Francis and J. K. Niparko (2005). "Predictive models for cochlear implantation in elderly candidates." Arch Otolaryngol Head Neck Surg 131(12): 1049-1054.

Lichtenhan, J. T., J. J. Hartsock, R. M. Gill, J. J. Guinan, Jr. and A. N. Salt (2014). "The Auditory Nerve Overlapped Waveform (ANOW) Originates in the Cochlear Apex." J Assoc Res Otolaryngol.

Mandala, M., L. Colletti, G. Tonoli and V. Colletti (2012). "Electrocochleography during cochlear implantation for hearing preservation." Otolaryngol Head Neck Surg 146(5): 774-781.

McClellan, J. H., E. J. Formeister, W. H. Merwin, 3rd, M. T. Dillon, N. Calloway, C. Iseli, C. A. Buchman, D. C. Fitzpatrick and O. F. Adunka (2014). "Round window electrocochleography and speech perception outcomes in adult cochlear implant subjects: comparison with audiometric and biographical information." Otol Neurotol 35(9): e245-252.

Mens, L. H. and C. K. Berenstein (2005). "Speech perception with mono-and quadrupolar electrode configurations: a crossover study." Otology & Neurotology 26(5): 957-964.

Moore, D. R. and R. V. Shannon (2009). "Beyond cochlear implants: awakening the deafened brain." Nat Neurosci 12(6): 686-691.

Nadol, J. B., Jr. and D. K. Eddington (2006). "Histopathology of the inner ear relevant to cochlear implantation." Adv Otorhinolaryngol 64: 31-49.

Nguyen, L. T., J. P. Harris and Q. T. Nguyen (2010). "Clinical utility of electrocochleography in the diagnosis and management of Meniere's disease: AOS and ANS membership survey data." Otology & neurotology: official publication of the American Otological Society, American Neurotology Society [and] European Academy of Otology and Neurotology 31(3): 455.

Niparko, J. K., E. A. Tobey, D. J. Thal, L. S. Eisenberg, N. Y. Wang, A. L. Quittner, N. E. Fink and C. D. I. Team (2010). "Spoken language development in children following cochlear implantation." JAMA 303(15): 1498-1506.

O'Connell, B. P., J. T. Holder, R. T. Dwyer, R. H. Gifford, J. H. Noble, M. L. Bennett, A. Rivas, G. B. Wanna, D. S. Haynes and R. F. Labadie (2017). "Intra-and postoperative electrocochleography may be predictive of final electrode position and postoperative hearing preservation." Frontiers in neuroscience 11: 291.

O'Connell, B. P., J. B. Hunter, R. Gifford, A. Rivas, D. S. Haynes, J. H. Noble and G. B. Wanna (2016). "Electrode location and audiologic performance after cochlear implantation: a comparative study between Nucleus CI422 and CI512 electrode arrays." Otology & neurotology: official publication of the American Otological Society, American Neurotology Society [and] European Academy of Otology and Neurotology 37(8): 1032.

O'Connell, B. P., J. B. Hunter, D. S. Haynes, J. T. Holder, M. M. Dedmon, J. H. Noble, B. M. Dawant and G. B. Wanna (2017). "Insertion depth impacts speech perception and hearing preservation for lateral wall electrodes." The Laryngoscope 127(10): 2352-2357.

O'Connell, B. P., J. B. Hunter and G. B. Wanna (2016). "The importance of electrode location in cochlear implantation." Laryngoscope Investigative Otolaryngology 1(6): 169-174.

O'Connell, B. P., A. Cakir, J. B. Hunter, D. O. Francis, J. H. Noble, R. F. Labadie, G. Zuniga, B. M. Dawant, A. Rivas and G. B. Wanna (2016). "Electrode location and angular insertion depth are predictors of audiologic outcomes in cochlear implantation." Otology & neurotology: official publication of the American Otological Society, American Neurotology Society [and] European Academy of Otology and Neurotology 37(8): 1016.

Perlman, H. and T. Case (1941). "Electrical phenomena of the cochlea in man." Archives of Otolaryngology 34(4): 710-718.

Pfingst, B. E., K. H. Franck, L. Xu, E. M. Bauer and T. A. Zwolan (2001). "Effects of electrode configuration and place of stimulation on speech perception with cochlear prostheses." Journal of the Association for Research in Otolaryngology 2(2): 87-103.

Radeloff, A., W. Shehata-Dieler, A. Scherzed, K. Rak, W. Harnisch, R. Hagen and R. Mlynski (2012). "Intraoperative monitoring using cochlear microphonics in cochlear implant patients with residual hearing." Otol Neurotol 33(3): 348-354.

Ramekers, D., H. Versnel, S. B. Strahl, E. M. Smeets, S. F. Klis and W. Grolman (2014). "Auditory-nerve responses to varied inter-phase gap and phase duration of the electric pulse stimulus as predictors for neuronal degeneration." J Assoc Res Otolaryngol 15(2): 187-202.

Riggs, W. J., J. P. Roche, C. K. Giardina, M. S. Harris, Z. J. Bastian, T. E. Fontenot, C. A. Buchman, K. D. Brown, O. F. Adunka and D. C. Fitzpatrick (2017). "Intraoperative electrocochleographic characteristics of auditory neuropathy spectrum disorder in cochlear implant subjects." Frontiers in neuroscience 11: 416.

Ruben, R. (1967). "Cochlear potentials as a diagnostic test in deafness." Sensorineural hearing processes and disorders: 313-337.

Ruben, R., J. Bordley and A. Lieberman (1961). "Cochlear potentials in man." The Laryngoscope 71(10): 1141-1164.

Ruben, R., J. Sekula, J. Bordley, G. Knickerbocker, G. Nager and U. Fisch (1960). "Human Cochlea Responses to Sound Stimuli." Annals of Otology, Rhinology & Laryngology 69(2): 459-479.

Rubinstein, J. T., W. S. Parkinson, R. S. Tyler and B. J. Gantz (1999). "Residual speech recognition and cochlear implant performance: effects of implantation criteria." Am J Otolaryngol 20(4): 445-452.

Santarelli, R., A. Starr, H. J. Michalewski and E. Arslan (2008). "Neural and receptor cochlear potentials obtained by transtympanic electrocochleography in auditory neuropathy." Clin Neurophysiol 119(5): 1028-1041.

Schuman, T. A., J. H. Noble, C. G. Wright, G. B. Wanna, B. Dawant and R. F. Labadie (2010). "Anatomic verification of a novel method for precise intrascalar localization of cochlear implant electrodes in adult temporal bones using clinically available computed tomography." Laryngoscope 120(11): 2277-2283.

Scott, W. C., C. K. Giardina, A. K. Pappa, T. E. Fontenot, M. L. Anderson, M. T. Dillon, K. D. Brown, H. C. Pillsbury, O. F. Adunka, C. A. Buchman and D. C. Fitzpatrick (2016). "The Compound Action Potential in Subjects Receiving a Cochlear Implant." Otol Neurotol 37(10): 1654-1661.

Sellick, P., R. Patuzzi and D. Robertson (2003). "Primary afferent and cochlear nucleus contributions to extracellular potentials during tone-bursts." Hear Res 176(1-2): 42-58.

Seyyedi, M., L. M. Viana and J. B. Nadol, Jr. (2014). "Within-subject comparison of word recognition and spiral ganglion cell count in bilateral cochlear implant recipients." Otol Neurotol 35(8): 1446-1450.

Shepherd, R. K., S. Hatsushika and G. M. Clark (1993). "Electrical stimulation of the auditory nerve: the effect of electrode position on neural excitation." Hear Res 66(1): 108-120.

Skinner, M. W. (2003). "Optimizing cochlear implant speech performance." Annals of Otology, Rhinology & Laryngology 112: 4-13.

Skinner, M. W., L. K. Holden, L. A. Whitford, K. L. Plant, C. Psarros and T. A. Holden (2002). "Speech recognition with the nucleus 24 SPEAK, ACE, and CIS speech coding strategies in newly implanted adults." Ear and hearing 23(3): 207-223.

Skinner, M. W., T. A. Holden, B. R. Whiting, A. H. Voie, B. Brunsden, J. G. Neely, E. A. Saxon, T. E. Hullar and C. C. Finley (2007). "In vivo estimates of the position of advanced bionics electrode arrays in the human cochlea." Ann Otol Rhinol Laryngol Suppl 197: 2-24.

Snyder, R. L. and C. E. Schreiner (1984). "The auditory neurophonic: basic properties." Hear Res 15(3): 261-280.

Strahl, S. B., D. Ramekers, M. M. Nagelkerke, K. E. Schwarz, P. Spitzer, S. F. Klis, W. Grolman and H. Versnel (2016). "Assessing the Firing Properties of the Electrically Stimulated Auditory Nerve Using a Convolution Model." Adv Exp Med Biol 894: 143-153.

Strelnikov, K., J. Rouger, J. F. Demonet, S. Lagleyre, B. Fraysse, O. Deguine and P. Barone (2010). "Does brain activity at rest reflect adaptive strategies? Evidence from speech processing after cochlear implantation." Cereb Cortex 20(5): 1217-1222.

Suberman, T. A., A. P. Campbell, O. F. Adunka, C. A. Buchman, J. P. Roche and D. C. Fitzpatrick (2011). "A gerbil model of sloping sensorineural hearing loss." Otol Neurotol 32(4): 544-552.

van Eijl, R. H., P. J. Buitenhuis, I. Stegeman, S. F. Klis and W. Grolman (2017). "Systematic review of compound action potentials as predictors for cochlear implant performance." Laryngoscope 127(2): 476-487.

van Emst, M. G., S. F. Klis and G. F. Smoorenburg (1995). "Tetraethylammonium effects on cochlear potentials in the guinea pig." Hear Res 88(1-2): 27-35.

Verschooten, E. and P. X. Joris (2014). "Estimation of neural phase locking from stimulus-evoked potentials." J Assoc Res Otolaryngol 15(5): 767-787.

Verschooten, E., L. Robles and P. X. Joris (2015). "Assessment of the limits of neural phase-locking using mass potentials." J Neurosci 35(5): 2255-2268.

Wanna, G. B., J. H. Noble, M. L. Carlson, R. H. Gifford, M. S. Dietrich, D. S. Haynes, B. M. Dawant and R. F. Labadie (2014). "Impact of electrode design and surgical approach on scalar location and cochlear implant outcomes." Laryngoscope Epub ahead of print.

Weiss, T. F. and C. Rose (1988). "A comparison of synchronization filters in different auditory receptor organs." Hear Res 33(2): 175-179.

Wilson, B., C. Finley, B. Weber, M. White, J. Farmer, R. Wolford, M. Merzenich, D. Lawson, P. Kenan and R. Schindler (1988). "Comparative studies of speech processing strategies for cochlear implants." The Laryngoscope 98(10): 1069-1077.

Youssef Adel, T. R., Andreas Bahmer, and Uwe Baumann. (2015). "Recording Low-Frequency Acoustically Evoked Potentials using Cochlear Implants." Poster Presentation at the 2015 Conference on Implantable Auditory Prostheses (CIAP).

Zeng, F.-G. and R. R. Fay (2013). Cochlear implants: Auditory prostheses and electric hearing, Springer Science & Business Media.

Zheng, X. Y., D. L. Ding, S. L. McFadden and D. Henderson (1997). "Evidence that inner hair cells are the major source of cochlear summating potentials." Hear Res 113(1-2): 76-88.

Zhou, N., C. T. Kraft, D. J. Colesa and B. E. Pfingst (2015). "Integration of Pulse Trains in Humans and Guinea Pigs with Cochlear Implants." J Assoc Res Otolaryngol 16(4): 523-534.

Zhou, N. and B. E. Pfingst (2016). "Evaluating multipulse integration as a neural-health correlate in human cochlear-implant users: Relationship to forward-masking recovery." J Acoust Soc Am 139(3): EL70-75.

# CHAPTER 2: EXTRACOCHLEAR ECOCHG[1]

## Overview

Electrocochleography (ECochG) is increasingly being utilized as an intraoperative monitor of cochlear function during cochlear implantation (CI). Intracochlear recordings from the advancing electrode can be obtained through the device by on-board capabilities. However, such recordings may not be ideal as a monitor because the recording electrode moves in relation to the neural and hair cell generators producing the responses. The purposes of this study were to compare two extracochlear recording locations in terms of signal strength and feasibility as intraoperative monitoring sites, and to characterize changes in cochlear physiology during CI insertion. In 83 human subjects, responses to 90 dB nHL tone bursts were recorded both at the round window (RW) and then at an extracochlear position – either adjacent to the stapes or on the promontory just superior to the RW. Recording from the fixed, extracochlear position continued during insertion of the CI in 63 cases. Prior to CI insertion, responses to low-frequency tones at the RW were roughly 6 dB larger than when recording at either extracochlear site, but the two extracochlear sites did not differ from one another. During CI insertion, response losses from the promontory or adjacent to the stapes stayed within 5 dB in 61% (38/63) of cases, presumably indicating atraumatic insertions. Among responses which dropped more than 5 dB at any time during CI insertion, 12 subjects showed no response recovery while in 13 the drop was followed by partial or complete response recovery by the end of CI insertion. In cases with recovery the drop in response occurred relatively early (<15 mm insertion) compared to those where there was no recovery. Changes in response phase during the insertion occurred in some cases; these

[1]modified from: *Giardina, C. K., T. E. Khan, S. H. Pulver, O. F. Adunka, C. A. Buchman, K. D. Brown, H. C. Pillsbury and D. C. Fitzpatrick (2018). "Response Changes during Insertion of a Cochlear Implant Using Extracochlear Electrocochleography." Ear and Hearing. (ePub ahead-of-print)*

may indicate a change in the distributions of generators contributing to the response. Monitoring the ECochG during CI insertion from an extracochlear site reveals insertions that are potentially atraumatic, show interaction with cochlear structures followed by response recovery, or show interactions such that response losses persist to the end of recording.

## Introduction

Intra-insertion trauma during cochlear implantation (CI) is an important factor leading to poor speech and hearing outcomes (Finley, Holden et al. 2008, Adunka, Pillsbury et al. 2009, O'Connell, Hunter et al. 2016). A new approach using electrocochleography (ECochG) to monitor responses to auditory stimuli during insertion is under development in laboratories and is currently being implemented by implant manufacturers (Adunka, Giardina et al. 2015, Dalbert, Sim et al. 2015, Campbell, Kaicer et al. 2016, Dalbert, Huber et al. 2016, Harris, Riggs et al. 2016, Bester, Campbell et al. 2017) . The monitoring can be performed by recording from the electrode tip as it advances (Calloway, Fitzpatrick et al. 2014, Campbell, Kaicer et al. 2015, Acharya, Tavora-Vieira et al. 2016, Harris, Riggs et al. 2017, Harris, Riggs et al. 2017) or from a stable extracochlear location during the insertion (Mandala, Colletti et al. 2012, Radeloff, Shehata-Dieler et al. 2012, Dalbert, Sim et al. 2014). Both the intracochlear and extracochlear recording locations have strengths and weaknesses, and, ultimately, could be used in combination. Here, we evaluate different recording locations for the *extracochlear* placement, and describe the types of recordings, or 'insertion tracks' obtained during CI insertion.

Translocation of the CI from scala tympani into scala vestibuli during insertion is a major cause of basilar membrane trauma that has been correlated with poor speech perception outcomes (Skinner, Holden et al. 2007, Finley, Holden et al. 2008, Holden, Finley et al. 2013, O'Connell, Hunter et al. 2016) and loss of hearing thresholds in hearing preservation cases (Schuman, Noble et al. 2010, Noble, Labadie et al. 2011, Wanna, Noble et al. 2014, Wanna, Noble et al. 2015). In addition, despite implementing the techniques of 'soft' surgeries including selection of flexible, lateral wall electrodes, insertion through the round window (RW) to avoid drilling into the cochlea, protection from bone dust, and em-

ploying intraoperative and postoperative corticosteroids to minimize acute endocochlear inflammation (Skarzynski, Lorens et al. 2007, Adunka, Pillsbury et al. 2009, Von Ilberg, Baumann et al. 2011), only half the patients in hearing preservation surgeries have complete or nearly complete preservation (<10 dB loss) of thresholds across speech frequencies (Adunka, Pillsbury et al. 2009, Von Ilberg, Baumann et al. 2011, Skarzynski, Van de Heyning et al. 2013). These patients and others achieve maximal benefit if array insertion preserves both cochlear anatomy and auditory function, potentially in the electric-only hearing condition as well (Dalbert, Huber et al. 2016). Thus, there is a need for methods to monitor ongoing trauma to determine if it can be detected and avoided during surgery.

The use of ECochG to monitor physiological responses to sound during array insertion began in animal studies (Adunka, Mlot et al. 2010, Choudhury, Adunka et al. 2011, Demason, Choudhury et al. 2012) and is now being pursued in several clinics and by the implant manufacturers (Campbell, Kaicer et al. 2015, Acharya, Tavora-Vieira et al. 2016, Harris, Riggs et al. 2017). Stimulation with tones produce reliable, often large responses in >95% of CI subjects, including both adults and children (Choudhury, Fitzpatrick et al. 2012, Fitzpatrick, Campbell et al. 2014, McClellan, Formeister et al. 2014, Dalbert, Sim et al. 2015, Formeister, McClellan et al. 2015). Most subjects show sensitivity to frequencies of 1000 Hz and lower, with responses to 250 and 500 being largest on average. Response to higher frequencies of 2000 and 4000 Hz are seen in a minority of cases, except in children identified as ANSD where responses to high frequencies are typical (Fitzpatrick, Campbell et al. 2014, Riggs, Roche et al. 2017). A property of cochlear responses to low frequencies is that, because of the base-to-apex direction of the travelling wave, regions basal to the characteristic frequency (CF) region of the tone also contribute to the net response if the intensity is sufficient. For these reasons an intense, low frequency tone has become the stimulus of choice for characterizing cochlear response due to CI insertion (Calloway, Fitzpatrick et al. 2014, Adunka, Giardina et al. 2015, Campbell, Kacier et al. 2015, Dalbert, Pfiffner et al. 2015, Dalbert, Sim et al. 2015, Harris, Riggs et al. 2016, Harris, Riggs et al. 2017).

The recording capability currently being implemented by the implant companies is to record through the device, using the most apical contact as the recording electrode and

using the on-board amplifiers to collect data during acoustic stimulation and transmit this data through the coil and magnet for analysis. A major benefit of responses from an intracochlear electrode is that the responses are larger on average than extracochlear responses (Calloway, Fitzpatrick et al. 2014). However, recordings from the array can fluctuate independently of any change of output from the hair cell and neural response generators, due to the changing position of the recording electrode relative to the generators (Demason, Choudhury et al. 2012). Thus, the advantage of monitoring from a fixed, extracochlear location is that response fluctuations can only be due to changes in the cochlear generators, at the cost of a somewhat smaller signal.

Before 2016, only two reports had evaluated extracochlear ECochG during CI insertion, and both utilize measurements of response threshold – which requires recordings of low signal to noise ratio and only evoke responses from restricted parts of the cochlea – limiting the ability to obtain timely and useful measurements (Mandala, Colletti et al. 2012, Radeloff, Shehata-Dieler et al. 2012). To improve the technique of recording from a fixed, extracochlear location as the foundation for an intraoperative monitor of cochlear trauma, our first goal was to determine if different locations vary substantially in signal to noise characteristics. A second goal was to describe response 'tracks', or changes to suprathreshold tone bursts during insertion, for subjects receiving CIs.

## Materials and Methods

### Subjects

Eighty-three subjects undergoing CI surgery were enrolled in this study. Inclusion criteria allowed patients of any age, gender, hearing loss etiology, or residual hearing status (as determined by pure tone average, PTA, thresholds) to be included. Patients were excluded if they were undergoing revision surgery or were not fluent in English, requiring an interpreter. Future reports will consider audiometric outcomes but the broad inclusion criteria here were chosen to maximize the number of subjects for extracochlear signal analysis. Cochlear malformations were seen in only 4/83 subjects (2 Mondini and 2 enlarged vestibular aqueducts, EVA) but these subjects were still included to gain better perspec-

tive on the feasibility of intraoperative monitoring in all subjects. All research activity was performed with the approval of the institution's Institutional Review Board (UNC IRB Protocol No. 05-2616). Informed consent was obtained for subjects older than 18 years of age, parental permission was obtained for subjects under the age of 18, and assent was also acquired from subjects between 7 and 18 years of age.

### ECochG at the RW

Four surgeons performed all cochlear implantations. After anesthesia was induced, a foam earphone insert was placed in the ipsilateral ear canal for sound delivery and surface electrodes were placed on the contralateral mastoid and forehead for recording. A standard transmastoid facial recess approach was then utilized to expose the middle ear antrum and facial recess (Figure 2.1A) and identify the RW, stapes, and promontory (Figure 2.1B). Just before CI implantation, a monopolar electrode (Neurosign Surgical Inc. Part 3602-00, Carmarthenshire, UK) was placed in the RW niche. This served as the noninverting input while the surface electrodes at the contralateral mastoid and glabella served as the inverting input and the common, respectively. A Bio-logic Navigator Pro (Natus Medical Inc., San Carlos, CA) was used to record evoked responses to alternating polarity tone bursts (250 Hz, 500 Hz, 750 Hz, 1 kHz, 2 kHz, 4 kHz) at 90 dB HL (87 – 107 dB SPL) delivered by Etymotic ER-3b speakers to the foam insert in the ipsilateral auditory canal. The AEP system we utilized does not have in-ear microphone recording capability, but stimulation levels were calibrated from nHL to peakSPL using a 0.25 inch microphone and measuring amplifier (Bruel & Kjaer, Naerum, Denmark). Depending on signal strength and noise level, 50 to 500 repetitions per phase were collected at each stimulus frequency but the exact number of averages was at the discretion of the operator to minimize data collection time within the context of the surgery. Formal signal to noise analysis was performed post-operatively and is described in the ECochG Signal Analysis section of the paper.

### ECochG at Extracochlear Locations Before CI Insertion

Once the RW recordings were complete, a separate extracochlear electrode was placed at one of two sites between the RW and stapes footplate (S or P in Fig. 2.1B). Site S was ad-

jacent to and just inferior to the stapes footplate (Fig. 2.1B, “S”). Site P was anterosuperior to the RW on the promontory (Fig. 2.1B, “P”), which coincides with the location marked “2” on a promontory diagram identifying cochleostomy sites (Fig. 1B in (Iseli, Adunka et al. 2014) ). The decision regarding which recording site to use for a given subject was based primarily on surgeon preference, but all surgeons had experience with both recording locations.

The recording electrode for the stapes location was an insulated copper wire with a silver tip which is herein referred to as the “stapes electrode”. This electrode was threaded through the attic, its tip placed on the promontory just inferior to the stapes footplate, and its shaft held in place at the anterosuperior angle of the mastoidectomy cavity with bone wax (Fig. 2.1C). The electrode had a slight bend to avoid the ossicles and allow the tip to sit perpendicular to the bony surface of the cochlea. The wire was flexible enough that surgeons could easily bend it to better accommodate patient-specific anatomy, yet was also rigid enough to hold its form. Using braided wire improved the ability to put in flexible bends with a spring-like property. This strength was paramount for stability because the fixation of bone wax added a downward force to the wire which translated to holding it onto the bone.

The recording electrode used for the promontory location (”promontory electrode”) was a copper electrode with a 0.5 mm silver ball on the end held by a custom clamp which mounted to retractors already in the surgical field (Fig. 2.1D). Multiple degrees of freedom allowed the mount to first be manipulated and locked in position. Next the recording probe was placed through an aperture on the distal end of the mount before entering the superior portion of the facial recess and seated onto the promontory. To reduce surface impedance (1 kHz current between promontory electrode and surface skin electrode), a small piece of saline-soaked gelfoam was placed between the electrode tip and the promontory.

The responses at either the stapes or promontory positions were compared to responses at the RW within each subject in order to assess any change in response magnitude or quality when moving to either extracochlear site.

## Extracochlear ECochG during CI Insertion

With either extracochlear electrode in place, ECochG was performed to a single low frequency tone burst before, during and after insertion of the CI. The choice of stimulus frequency was either 250 Hz or 500 Hz at 90 dB HL, depending on which RW response was greater. Sequential responses to the tone bursts were assessed throughout CI insertion, each response coupled to an associated CI insertion depth, determined by the number of contacts inserted as reported by the surgeons during data acquisition. For example: "2 contacts inserted" with a MED-EL Standard array would be a 5.4 mm insertion depth (2.2 mm per contact + 1 mm inactive array housing apical to the tip contact), "12 contacts inserted" with this array would be 27.4 mm (26.4 mm active array + 1 mm apical housing) and a "fully inserted" array would be 31.5 mm. Because insertion speed is not perfectly smooth, it is also important to note that the amount of time between subsequent recordings is not equally spaced – that recording tracks are shown as a function of insertion depth and not of insertion time.

## ECochG Signal Analysis

Responses were analyzed using custom MATLAB routines (MathWorks, Natick, MA) and focused on the magnitude of the ongoing portion of the response waveform (windowed from 7 ms to 23 ms for 250 Hz or 7 ms to 21 ms for 500 Hz stimuli) to avoid the onset and offset characteristics of the CAP. The metric for response magnitude to a given stimulus was the sum of spectral peaks at the stimulus frequency and its higher harmonics. A spectral peak in the FFT was considered significant when its magnitude was more than three standard deviations (SD) greater than noise, where the noise level and SD were computed from 3 frequency bins on either side of the frequency of interest (62 Hz bins). The reason for summing the spectral peaks instead of measuring the root-mean square (RMS) value is to give particular significance to harmonic distortions in the magnitude calculation. This additional weighting is justified because the CM and ANN can combine at different phases, such that interference can reduce the fundamental magnitude but increase harmonic distortions (Forgues, Koehn et al. 2014).

At the RW, individual responses to several stimulus frequencies (250 Hz, 500 Hz, 750 Hz, 1 kHz, 2 kHz, 4 kHz) at 90 dB nHL were summed into the ECochG Total Response "TR" as described elsewhere (Fitzpatrick, Campbell et al. 2014, Formeister, McClellan et al. 2015). In short, the response to each stimulus frequency (in $\mu V$) was summed to a total response (in $\mu V$) before finally being converted to log-scale relative to a 1 $\mu V$ response. Thus the TR is represented in dB and represents a metric for residual cochlear health before CI insertion. Extracochlear responses during CI insertion were also converted to logarithmic scale (dB relative to 1 $\mu V$) and subsequent measures throughout CI insertion were assessed at this scale. Comparison of the initial response (before CI insertion) to the final response (after full CI insertion) was calculated as the overall response shift, a metric of possible trauma used by our group and others (Dalbert, Sim et al. 2014, Adunka, Giardina et al. 2015, Dalbert, Sim et al. 2015, Dalbert, Huber et al. 2016).

## Results

In 83 subjects, responses to acoustic tones were collected at the RW and then at an extracochlear site either adjacent to the stapes (n=29) or on the promontory (n=54). The design was to obtain responses at the RW in order to measure the residual physiology in each subject, move to a fixed extracochlear recording location to compare responses to those at the RW, and then continue extracochlear recording throughout CI insertion. Round window recordings were obtained in all 83 subjects. In nine cases, responses at the extracochlear site did not rise above the noise floor (3/29 at stapes, 6/54 at promontory), despite successful recordings at the RW. Among these 74 remaining cases, most attempts to monitor extracochlear responses throughout CI insertion were successful (n=63/74, 85%) while in a minority of cases (n=11/74, 15%) the recording electrode did not maintain constant contact during the insertion (4/26 at stapes, 7/48 at promontory). Of these final 63 successful cases with response tracks, 22 were recorded from the stapes location and 41 from the promontory. Demographic information and devices used in these subjects are described in Table 2.1.

## Responses at the Round Window

The TR was used as a basic metric for overall residual physiology (Fig. 2.2). Compared to our overall population database of 290 subjects (blue), the TRs of the 83 subjects in this study (red) had a larger initial RW responses (12.3 $\pm$ 10.4 dB vs. 5.29 $\pm$ 15.2 dB re 1 $\mu V$), and the difference was significant, t-test, t=4.7, df=161, p<0.001). Thus, our sample is representative of the general population of CI subjects with a slight bias towards larger initial responses. The white bars indicate the nine cases where no responses were obtained at the extracochlear location, despite a measurable RW response. These cases were not limited to low TRs, so it was not simply that the slightly smaller responses typical of the extracochlear location compared to the RW (see below) were below threshold.

## Comparison of Extracochlear Recording to Locations to RW

Two extracochlear recording sites were used to test whether location was a primary feature for success of the recordings, or if multiple locations could provide similar recording quality. Often, the morphology of the response waveforms (left panels in A-D) and peaks of the FFTs (right panels) were similar between the RW and the extracochlear site (e.g., Fig. 2.3A). The response from the fixed electrode was usually smaller than the RW (e.g., Fig. 2.3B), but in some cases the extracochlear response could be significantly larger than from the RW (e.g., Fig. 2.3C). The phase could either be similar (Fig. 2.3A and B) or different from the round window (Fig. 2.3C). In D, we show the case with the smallest signal recorded - this case had an amplitude in the FFT of 100 nV, which was still well above the minimum level for significance, typically about 20 nV for 500 repetitions.

There were a broad range of response magnitude changes when moving from the RW to either extracochlear site across subjects (Fig. 2.3E). Most changes were within 10 dB (dotted lines, n=49, or 66%) but changes could also include decreases greater than 10 dB (n=23, or 31%) as well as increases greater than 10 dB (n=2, or 3%). Within-subject changes in response magnitude showed significant drops when moving from the RW to the stapes (paired Wilcoxon Signed Rank test, z=2.80, p=0.005) and the RW to the promontory location (paired Wilcoxon Signed Rank test, z=4.23 p<0.001), but these drops were not different

from one another (Wilcoxon rank-sum test, z=-0.51, p=0.61). Overall, the median response near the stapes and promontory were 6.8 dB and 6.3 dB smaller than the RW, respectively (Fig. 2.3F). The median surface impedance at the RW was also slightly lower than at the stapes or the promontory (RW 7.0 kΩ IQR 1-10 kΩ, Stapes 8.0 kΩ IQR 4.25-14.5 kΩ, Promontory 12 kΩ, IQR 5-18 kΩ), however changes from RW to stapes or RW to promontory were not different (Wilcoxon rank-sum test, z=0.80, p=0.41). Additionally, there was no correlation between change in impedance and change in response magnitude (compared to the RW) for either extracochlear site (r=0.04, p>0.7). A correlation would have been expected if surface impedance were the sole or main contributor to response magnitude.

A possible explanation for the large response increases sometimes seen could be the presence of perilymph if the RW was inadvertently breached, causing conduction between the extracochlear electrode and the intracochlear environment where responses are known to be of greater magnitude (Calloway, Fitzpatrick et al. 2014, Dalbert, Pfiffner et al. 2015). To explore this, in a subset of subjects extracochlear responses were captured before and after surgically opening the RW (n=34). In these subjects the median change in response magnitude was just 0.7 dB higher than the response at the RW obtained prior to opening (Fig. 2.3F, red). This result indicates that perilymph is unlikely to be present at the extracochlear location very often, but can't be ruled out in individual cases. It is more likely that the change in recording site is biasing the recorded response towards a different set of generators than those at the RW. The change in phase for the case in Fig. 2.3C suggests that in this case of a large increase the sources of generators have indeed shifted with the change in location.

## Changes in Response during Insertion

During CI insertion, three overall patterns of response changes were identified. In some subjects, the responses were stable throughout the insertion (e.g., Fig. 2.4A). In others, the response was lower at the end of the insertion (e.g., Fig. 2.4B). Finally, in some subjects there was a magnitude drop mid-insertion which recovered by the end of insertion (Fig. 2.4C).

To estimate the size of response loss that might be considered significant, and to assess the 'test/retest' reliability of extracochlear recording during the insertion, we plotted a cumulative distribution function of the changes from one recording to the next for all recording pairs among the subjects (Fig. 2.5). Fifty-six percent of all response changes were 2 dB or less, 83% of changes were within 5 dB (Fig. 2.5, dashed line), and response shifts greater than 10 dB were seen in fewer than 3% of recording pairs. From these data, we deduced that response changes greater than 5 dB likely reflect physiological change rather than measurement variability.

Using this cutoff, each subject's response change throughout CI insertion was classified into one of three groups (Fig. 2.6). The left column in this figure shows the raw response tracks for individual subjects, and the right column shows the changes in response relative to their starting levels (by subtracting the initial response in dB). In the "No Change" group (Fig. 2.6A), magnitude losses were within 5 dB throughout all stages of the insertion (n=38, or 60.1%). In the second "Permanent Change" group, a response drop beyond 5 dB occurred monotonically with no recovery by the end of CI insertion (Fig. 2.6B, n=12, or 19.1%). For subjects in the last, "Reversible Change" group, responses at some point dropped by more than 5 dB and then at least partially recovered by the end of insertion (Fig. 2.6C, n=13, or 20.6%). Note that in this final group the overall response change from beginning to end could be more than 5 dB (n=8) or less than 5 dB (n=5) depending on the extent of response recovery. In one case, the response dropped nearly 25 dB and fully recovered by the end of CI insertion (Fig. 2.6C, arrow). Both recording locations were equally represented in each group, with 14 stapes and 24 promontory location subjects in the "No Change" group, 4 stapes and 9 promontory locations in the "Reversible Change" group, and 4 stapes and 8 promontory locations in the "Permanent Change" group. As such, group assignment was not significantly biased by recording location.

In the permanent change group there were no response drops beyond 5 dB until the CI had reached an insertion depth of at least 15 mm (Fig. 2.6B). Conversely, in the reversible change group (Fig. 2.6C), responses which dropped within the first 15 mm were all at least partially reversible by the end of insertion. This difference is shown in a histogram of the insertion depth where the response first dropped by 5 dB (Fig. 2.7). There was a significant

difference between the permanent and reversible change groups (Wilcoxon rank-sum test, U=147, p<1e-3), demonstrating that response drops early on in the insertion were more likely to be reversible whereas response losses at deeper depths were more likely to be permanent.

Summary distributions and statistical comparisons among the three groups are shown in Table 2.2. The pre-insertion RW response and the initial extracochlear responses were not significantly different among the three groups, which demonstrates that group classification was not influenced by pre-insertion responses. The final response was used to calculate the overall shift, which was significantly different between groups, an expected finding because this was the main criteria for separating tracks into groups. The largest shift at any insertion depth was not different between the permanent change and reversible change groups. Additionally, age ranges of subjects in the three groups were similar (1-87 years for "no change" group, 2-78 years for "permanent change" group and 1-76 years for "reversible change" group), and did not differ significantly from one another (1-way ANOVA of age by group, df=2, F= 2.15, p = 0.12).

In addition to response magnitude shifts with deeper insertions, changes in the phase of the ongoing response could also occur. To illustrate one of these cases, the responses are shown from the start of insertion (Fig. 2.8A, top row) to final CI position (Fig. 2.8A, bottom row). At each step, the condensation waveform (left column) and average cycle of the ongoing response (right column) are depicted. Between an insertion depth of 8 electrodes and 12 electrodes, the phase of the ongoing signal completely inverted (Fig. 2.8A, arrow). In this case the morphology of the CAP also changed from a single negative deflection to a larger, biphasic peak, but this was rare (4 subjects). Across all 63 subjects, shifts in the phase of the average cycle formed a continuum from small to large, with most cases showing a small phase shift and a minority of cases with large phase shifts (Fig. 2.8B). The median phase shift was 0 degrees with interquartile phase changes (box) between -31 and +43 degrees, and 99% limits shown (whiskers) with the 6 outliers beyond this range.

## Discussion

Preservation of cochlear integrity is important for maximizing speech outcomes with a CI (Finley, Holden et al. 2008, Wanna, Noble et al. 2014, O'Connell, Hunter et al. 2016). The current study compared approaches to extracochlear ECochG and characterized response changes during insertion, as a foundation for an intraoperative monitor of trauma. Responses at two extracochlear recording sites were slightly smaller than those at the RW, but were functionally comparable with each other in terms of signal strength and quality. Thus, the choice for the actual site of extracochlear electrode placement is not critical and can be obtained from multiple sites that are surgically accessible. Throughout CI insertion, most implantations (60%) showed no significant response change at any stage, with a minority (32%) showing an overall response loss greater than 5 dB, that may (or may not, see below) be due to trauma. Some responses (21%), declined in magnitude during the insertion but then recovered, particularly when these drops occurred within the first 15 mm of insertion. These temporary fluctuations indicate that using tone-evoked responses to distinguish between an atraumatic adjustment in micromechanics and gross anatomic trauma will likely necessitate more robust analysis than a magnitude change.

### Comparison of Responses at Extracochlear Recording Locations

In designing an ECochG system for assessing intraoperative changes in cochlear physiology, a preliminary factor to be addressed was the effect of different extracochlear recording sites on the measured response quality. Moving from the RW to adjacent the stapes or from the RW to the promontory resulted in a median decrease in response magnitude of -6.8 and -6.3 dB, respectively (Fig. 2.3E). Our initial hypothesis was that responses at any extracochlear location would be lower in magnitude than at the RW, due to higher surface impedance on the cochlear bone versus the membranous RW niche, and more bone resistance between the intracochlear generators and the recording site. Active electrode surface impedances (as measured by the BioLogic), particularly once a saline-soaked piece of gelfoam was placed between the recording probe and the cochlear surface, were only about 7 kΩ higher on average than those at the RW, and we did not see any evidence that

larger impedance differences produced large response differences (data not shown). Thus any significant drops in response magnitude, would more likely be from the bone rather than the surface impedance. However, there were also response increases present in some cases at either extracochlear site (Fig. 2.3). We have previously suggested that ECochG increases seen before and after implantation, when the recording electrode was removed from the RW and then replaced as close as possible to the original site, may have been due to contact with perilymph in the post-implant recordings (Adunka, Giardina et al. 2015), i.e., the electrode was essentially recording in an intracochlear environment where responses are known to be larger (Calloway, Fitzpatrick et al. 2014). However, this explanation cannot apply to the current results where care was taken to ensure the preliminary extracochlear recordings were made prior to opening the RW. An alternative hypothesis for why responses at the RW can differ so greatly from those at extracochlear sites is that the contributions of hair cell and neural populations differ when recording at the various extracochlear locations. Hair cell and neural potentials to the same frequency can interact constructively or destructively, with the presence of a CAP and prominent ANN distortions in the ongoing response as indicators of robust neural activity (Fontenot, Giardina et al. 2017, Riggs, Roche et al. 2017). This may also explain the shift in both phase and distortions when moving from the RW to the extracochlear site in Figure 2.3C which was independent of RW patency. These results imply the change in response when moving from the RW to an extracochlear site most likely involve a change in the specific population of recorded generators. And despite the overall lower median response magnitude at the various extracochlear sites from the round window, the main point for this study is that recordings from different extracochlear sites were well above the noise floor and functionally equivalent to one another. This finding should allow use of this technique at whichever extracochlear recording site is most surgically convenient, and to be applicable to most CI subjects.

### The Extracochlear Electrode Type

Although the two sites were functionally suitable for fixed ECochG, placing the associated recording electrodes through the attic or facial recess warranted very different

recording probes and surgical techniques. Specifically, these approaches differed in ease of placement, stability throughout CI insertion, and level of surgical obstruction in view or movement. When placing the flexible stapes electrode, the recording tip was threaded through the attic, maneuvering between the ossicles, and seated on a site inferior to the stapes footplate (Fig. 2.1C). A major advantage of this approach was that entering the antrum left the facial recess unobstructed during CI insertion. This recording site has also been utilized by Dalbert et al. (Dalbert, Sim et al. 2014, Dalbert, Huber et al. 2016), but they use a needle electrode. Because of this, we opted for a flexible braided wire that was anchored to the mastoidectomy cavity with bone wax. While usually successful (n=22/25), this approach could be unreliable if the electrode tip lost contact from the surface or if the wax holding the shaft in place dislodged from the bone. These led to an open recording circuit which could not be corrected while the array was being inserted. Conversely, the fixed promontory electrode clamps to retractors, is manipulated independently along multiple degrees of freedom, and small fasteners keep the electrode locked stationary throughout all subsequent steps (Fig. 2.1D). Placement of this electrode took longer than the stapes electrode but the mount ensured the electrode didn't spontaneously dislodge from the surface. A major limitation of entering the facial recess so close to the RW, however, was that it intruded upon the surgical view and was so close to the RW that in some cases (n=8/49) it could be bumped by insertion forceps. Even small displacements in recording location during insertion (viewed visibly through the surgical microscope) caused immediately visible shifts in the size and quality of the evoked responses which were clearly not due to changes in intracochlear mechanics or trauma.

## Changes in Response during Insertion

Most responses were stable throughout CI insertion (60%), but the transient response drops in 13 subjects (21%) has important implications for the use of the technology. Most important is that intermittent response losses may be the result of changes in cochlear physiology that do not lead to 'trauma,' or permanent damage to cochlear structures. ECochG magnitude shift is of particular interest because some groups have noted response drops

greater than 2.5 dB to be significant with regard to hearing preservation, and ECochG changes of 25 dB were predictive of complete hearing loss (Dalbert, Sim et al. 2015).

The largest temporary response loss in our study was 24 dB, which nearly returned to baseline (Fig. 2.6C, arrow). As such, a drop in response does not necessarily indicate permanent trauma. A similar result was seen in previous studies using gerbils, which demonstrated abrupt drops and recovery of responses could occur differentially across frequency as flexible electrodes were inserted into the cochlea (Demason, Choudhury et al. 2012). In that study, the response drops followed by recovery were interpreted as fixation of the basilar membrane due to electrode contact early in the insertion followed by the shaft losing contact with the membrane as the tip advanced around the end of the basal turn. That every response drop in the current study which occurred within the first 15 mm had at least some recovery (Fig. 2.7) suggests a similar mechanism as seen in gerbils, i.e., that early contact with the basilar membrane can resolve with further insertion. Exceeding this 15 mm threshold can result in more permanent losses, which may be most important in cases where hearing preservation is desired. Histological trauma to the cochlea is significantly greater when the array extends beyond the first turn (Adunka, Unkelbach et al. 2004, Adunka and Kiefer 2006) and for lateral wall arrays the first turn can be completed at roughly 20 mm of insertion (Franke-Trieger, Jolly et al. 2014). In subjects receiving lateral wall arrays, 20 mm arrays had higher hearing preservation rates and more stable hearing preservation over time than subjects receiving longer, 28 mm arrays (Suhling, Majdani et al. 2016). The upper limit of insertion depth in the current study suggests that most changes during the traverse of the first turn are indicative of cochlear mechanical effects but not of lasting anatomic trauma, and that an electrode emerging from the first turn of the cochlea may be at the highest risk of injuring the cochlea.

Atraumatic interactions between the array and the basilar membrane could also change the relative proportions of CM and ANN as the array is inserted, destructively or constructively interfering with each other, which could potentially cause magnitude fluctuations in the absence of trauma (Fontenot, Giardina et al. 2017). The transient response drops may also occur without any direct interaction between the array and the basilar membrane. One such scenario could be explained by models of basilar membrane stiffening or ST:SV

pressure ratio changes during CI insertion – which can negatively (or positively) affect response magnitude in the absence of cochlear trauma (Kiefer, Bohnke et al. 2006). These latter two explanations may shed light on why 7 subjects in this study (11%) had ECochG gains greater than 2.5 dB as a result of CI insertion, three of which grew more than 5 dB, paralleling results by Dalbert et al. who found that in 6 of 19 subjects (30%) increases in response occurred in at least one stimulation frequency as a result of CI insertion (Dalbert, Sim et al. 2015).

## Comparison with Intracochlear Recordings

Attempts to characterize trauma with intraoperative ECochG vary by approach – the largest distinction being whether the acoustic responses are measured from a location outside the cochlea or from within the cochlea, through the implant itself. Implant manufacturers are primarily testing intracochlear recording from the most apical contact as it advances (Adunka, Giardina et al. 2015, Dalbert, Sim et al. 2015, Acharya, Tavora-Vieira et al. 2016, Campbell, Kaicer et al. 2016, Dalbert, Huber et al. 2016, Harris, Riggs et al. 2016, Bester, Campbell et al. 2017). This technique has the advantage of increased signal to noise ratio, but the disadvantage that the movement of the electrode will change its relationship to the generators, so a stable response that can be used to detect trauma is not available. Extracochlear responses are smaller on average but do provide the stable recording site. A paradigm previously suggested (Dalbert, Sim et al. 2015) would be to use a mixed approach, in which trauma at the time of surgery is characterized with an extracochlear recording, while electrode placement relative to generators could be optimized with intracochlear recordings, which could also be used to monitor further trauma/fibrosis over time.

# TABLES

Table 2.1: Patient Demographics

| Characteristic | Count | % Total (Approx.) |
|---|---|---|
| Sex | | |
| Female | 32 | 51% |
| Male | 31 | 49% |
| Age at Implantation | | |
| 0 ≤ 5 yr old | 9 | 14% |
| 5 ≤ 18 yr old | 9 | 14% |
| 18 ≤ 80 yr old | 40 | 64% |
| 80 ≤ 90 yr old | 5 | 8% |
| SNHL Etiology | | |
| ANSD | 2 | 3% |
| Arachnoid Cyst | 1 | 2% |
| Barotrauma | 1 | 2% |
| CLDN14 mutation | 1 | 2% |
| Syndromic | 5 | 8% |
| Connexin 26 mutation | 1 | 2% |
| EVA | 2 | 3% |
| Meniere's | 5 | 8% |
| Meningitis | 1 | 2% |
| Mondini Malformation | 2 | 3% |
| Noise-Induced HL | 5 | 8% |
| Ototoxicity (Aminoglycoside) | 1 | 2% |
| Sudden SNHL | 7 | 11% |
| Unknown | 29 | 46% |
| Implanted Side | | |
| Left | 36 | 57% |
| Right | 27 | 43% |
| Device | | |
| Advanced Bionics MidScala | 1 | 2% |
| Cochlear 512 | 5 | 8% |
| Cochlear 522 | 3 | 5% |
| MED-EL Flex 24 | 9 | 14% |
| MED-EL Flex 28 | 17 | 27% |
| MED-EL Standard | 28 | 44% |
| Extracochlear Recording Site | | |
| Stapes Location | 22 | 35% |
| Promontory Location | 41 | 65% |

**Table 2.1 - Extracochlear Subject Demographics**

Demographics of subjects in the study with extracochlear recordings throughout CI insertion. Subjects included those of various ages, SNHL etiologies, devices, and residual hearing status. ANSD, auditory neuropathy spectrum disorder; CI, cochlear implantation; CLDN14, Claudin 14; EVA, enlarged vestibular aqueducts; SNHL, sensorineural hearing loss.

Table 2.2: Electrocochleography during CI Insertion

| | | Extracochlear Probe | | | |
|---|---|---|---|---|---|
| | Round Window ECochG-TR (dB re 1 µV) | Initial Response (dB re 1 µV) | Final Response (dB re 1 µV) | Overall Shift (dB re 1 µV) | Largest Shift (dB re 1 µV) |
| No Change Group (n = 38) | 11.7 ± 11.4 | -5.2 ± 8.2 | -5.7 ± 8.1 | **-0.5 ± 2.9** | -2.6 ± 1.5 |
| Permanent Change Group (n = 12) | 13.5 ± 9.6 | -2.4 ± 8.2 | -14.8 ± 7.3 | **-12.4 ± 5.8** | -12.4 ± 5.8 |
| Reversible Change Group (n = 13) | 10.7 ± 8.5 | -2.7 ± 8.5 | -10.7 ± 9.1 | **-8.0 ± 4.9** | -13.4 ± 5.7 |
| ANOVA F | 0.21 | 0.79 | 6.22 | 46.23 | 56.74 |
| Probability > F | 0.808 | 0.458 | 0.003 | **< 1 E-12** | **< 1 E-13** |

**Table 2.2 - Extracochlear ECochG and Response Patterns**
Electrocochleography characteristics throughout CI insertion for the three groups. Round window responses did not differ between groups nor did the initial extracochlear magnitudes. The final response, overall shift, and largest response shift differed between groups. ANOVA, analysis of variance; CI, cochlear implantation; ECochG, electrocochleography; TR, total response.

## FIGURES

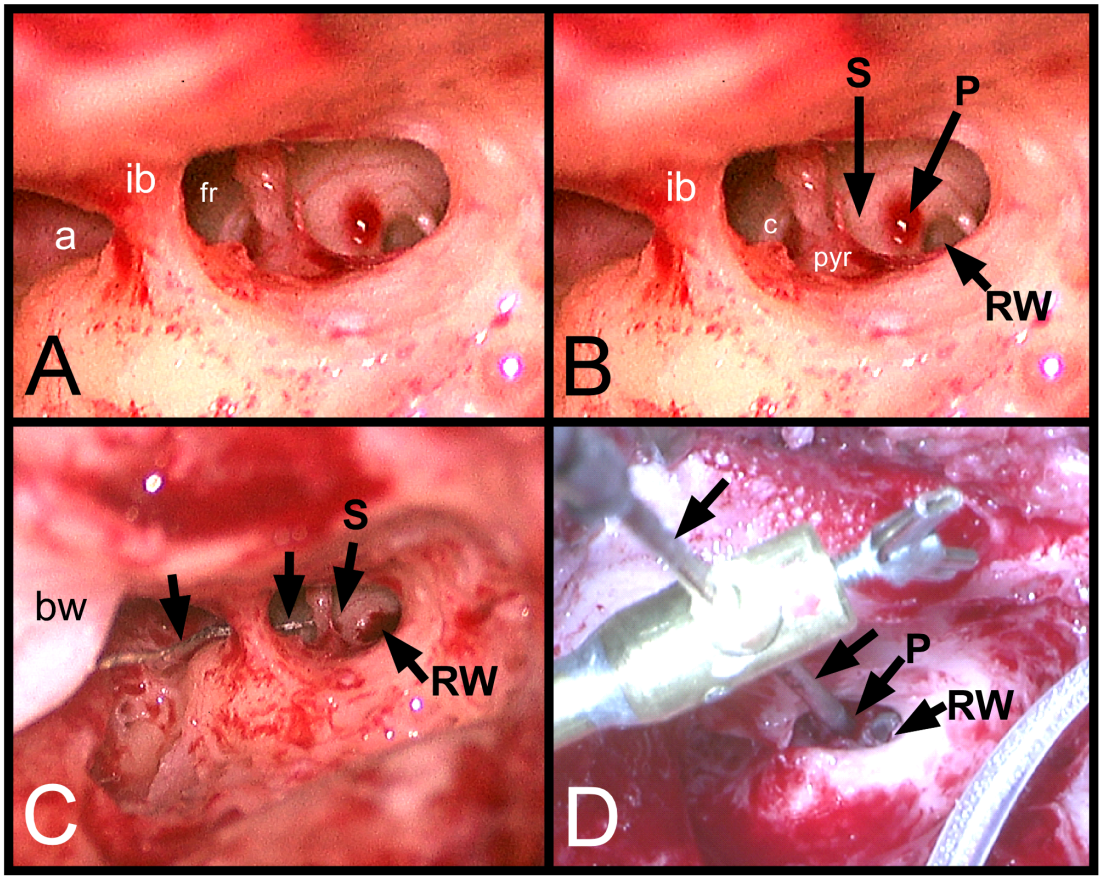


**Figure 2.1 - Surgical anatomy and extracochlear recordings sites**
(A) Mastoidectomy cavity reveals the attic (a), incus buttress (ib), and facial recess (fr). (B) Recording sites for extracochlear recordings are adjacent the stapes (S) and on the promontory (P) just superior and anterior to the round window (RW). (C) Stapes electrode threads through the attic and under the incus buttress and is held in place with a piece of bone wax (bw). (D) Promontory electrode extends from a custom rigid electrode mount (arrows) which is fixed to the retractors.

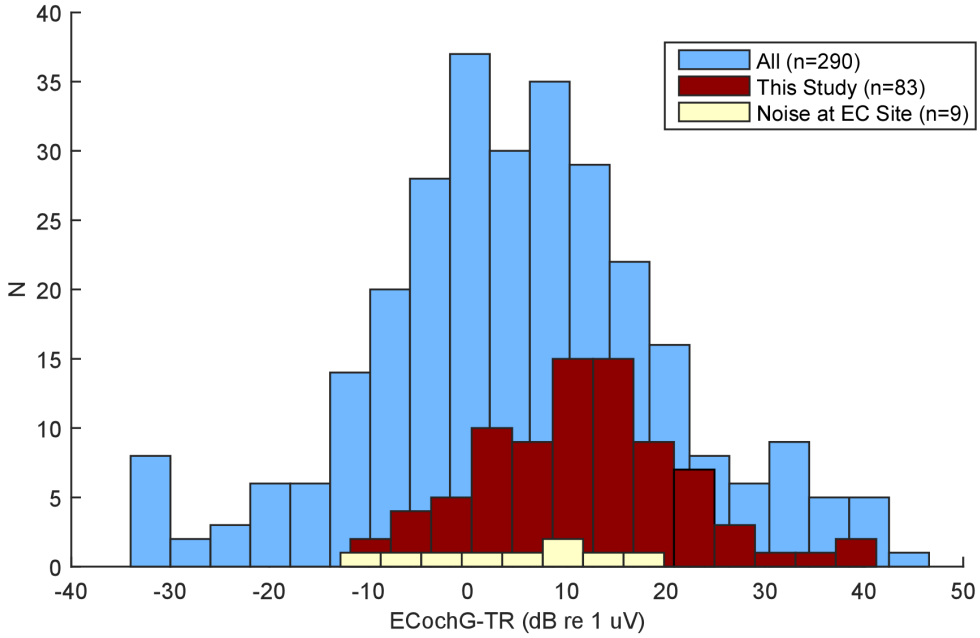


**Figure 2.2 - Distribution of Total Response from the Round Window**
Distribution of Total Response (ECochG-TR, see methods) from round Window electrocochleography just prior to insertion. The distribution of TRs across subjects in this study (red) was significantly higher than the magnitude of all subjects in our database (blue). Noise at the extracochlear recording site precluding inclusion was more likely in subjects with smaller RW responses (beige) but there was no consistent cutoff.

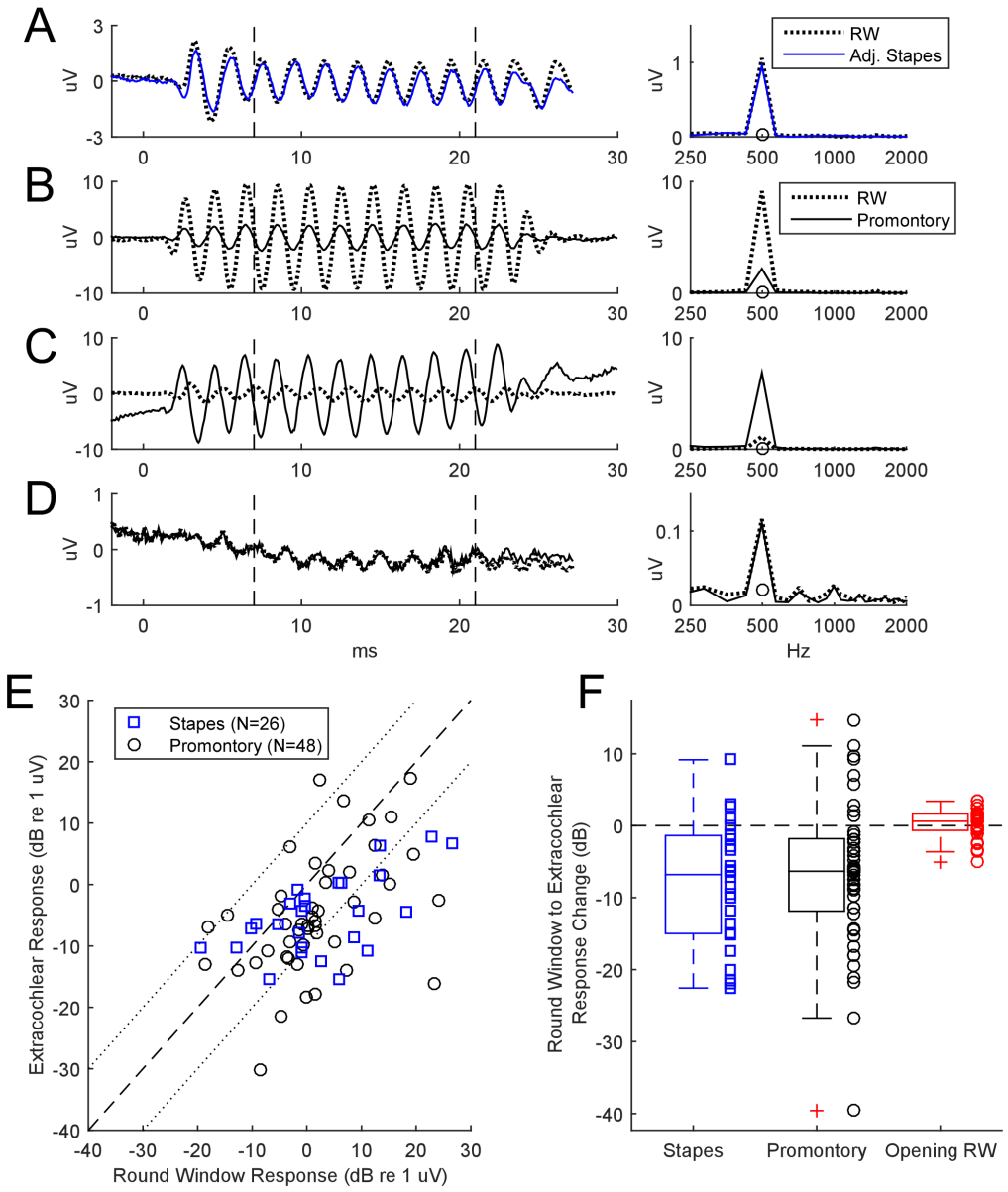


**Figure 2.3 - Magnitude of Extracochlear Responses compared to Round Window responses**

Recordings at the RW could be of similar morphology to those at the extracochlear site (A), smaller than extracochlear responses (B), or larger than the extracochlear site (C). The smallest response measured was just above the noise floor (D). Across all subjects, extracochlear magnitudes were typically smaller than those at the RW but changes included increases as well as decreases (E). Moving to an extracochlear site was roughly 7 dB smaller than those at the RW but did not differ between stapes and promontory locations. Additionally, these changes in response were not explained by opening the RW (red). *note:* uV $= \mu V$

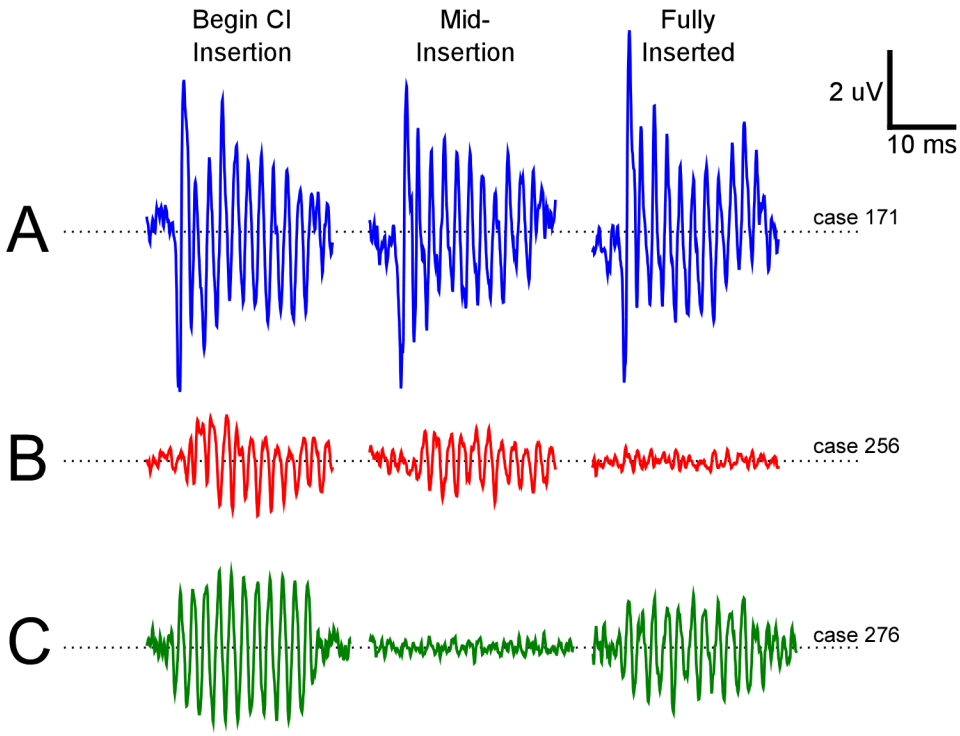


**Figure 2.4 - Extracochlear Response Waveforms during CI Insertion**
Three patterns emerged were seen (A) steady responses throughout the insertion, (B) a drop in response which persisted to the end of insertion, and (C) responses which dropped mid-insertion but recovered at deeper insertion depths. *note:* uV $= \mu V$

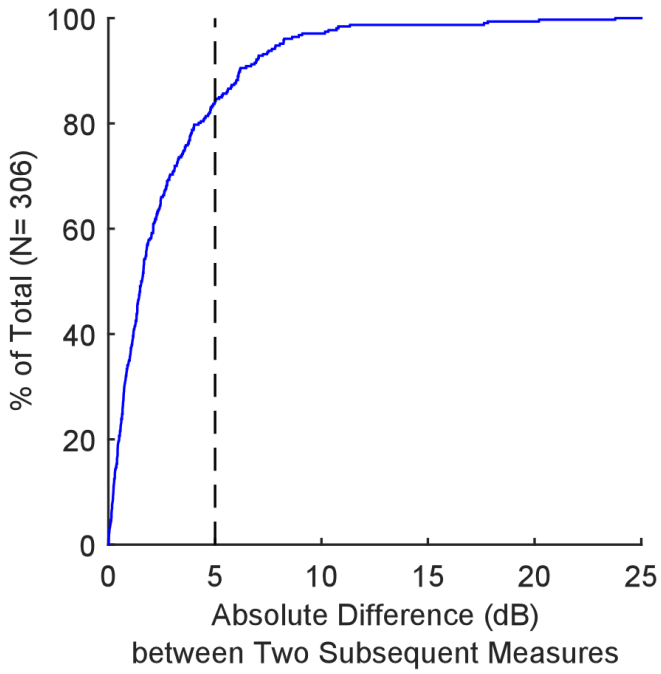


**Figure 2.5 - Extracochlear Response Drops across all subjects**
Incremental response drops from one recording to the next, cumulative across all subjects and depths. This plot was used to judge test/retest reliability and estimate when a response was rare enough that it was likely not due to simple variability in measurement. The dotted line at 5 dB is on the knee of the distribution and encompasses 83% of all increments, so a criterion of 5 dB was used to indicate a significant change response.

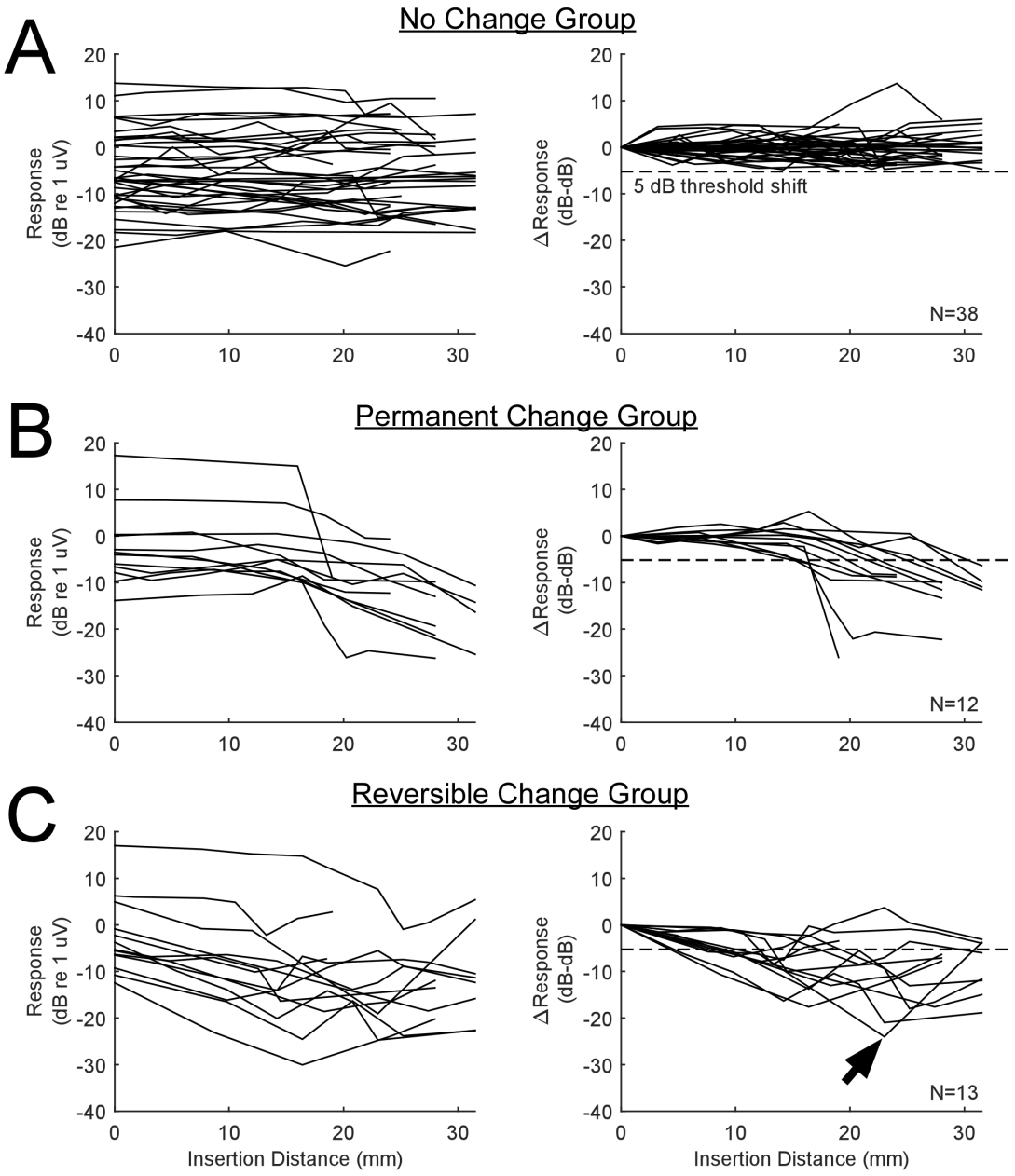


**Figure 2.6 - Extracochlear Response Tracks**

Phenotypes of response changes across all subjects. (A) In the majority of subjects, response magnitude changed by < 5 dB throughout insertion depth, and were in the "No Change" group. (B) In 12 subjects, the response magnitude dropped below 5 dB and did not recover, and were assigned to the "Permanent Change" group. (C) In the "Reversible Change" group, 13 subjects showed a response change below 5 dB which at least partially recovered by the end of insertion. The case at the arrow dropped by more than 5 dB at 12 mm insertion and by a total of 25 dB overall, but was nearly fully recovered by the end of insertion. *note:* uV $= \mu V$

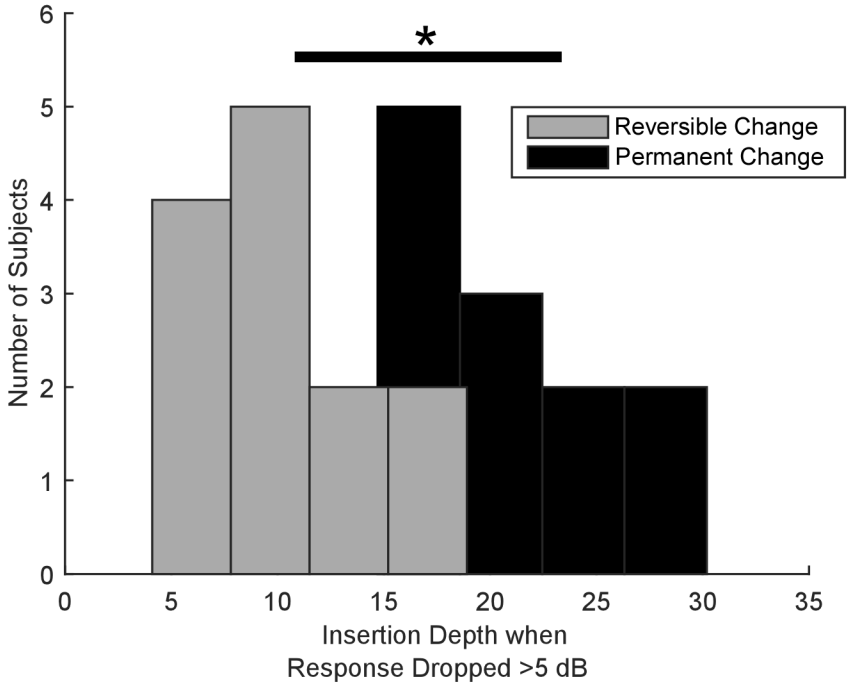


**Figure 2.7 - Insertion Depth when Response Dropped**
Insertion depth when response dropped by 5 dB. In the Reversible Change group, initial response drops usually occurred within the first 15 mm. In the Permanent Change group, primary response drops occurred at deeper insertion depths. *The difference in the distributions was significant (t-test, $t=4.7$, $df=161$, $p<0.001$).

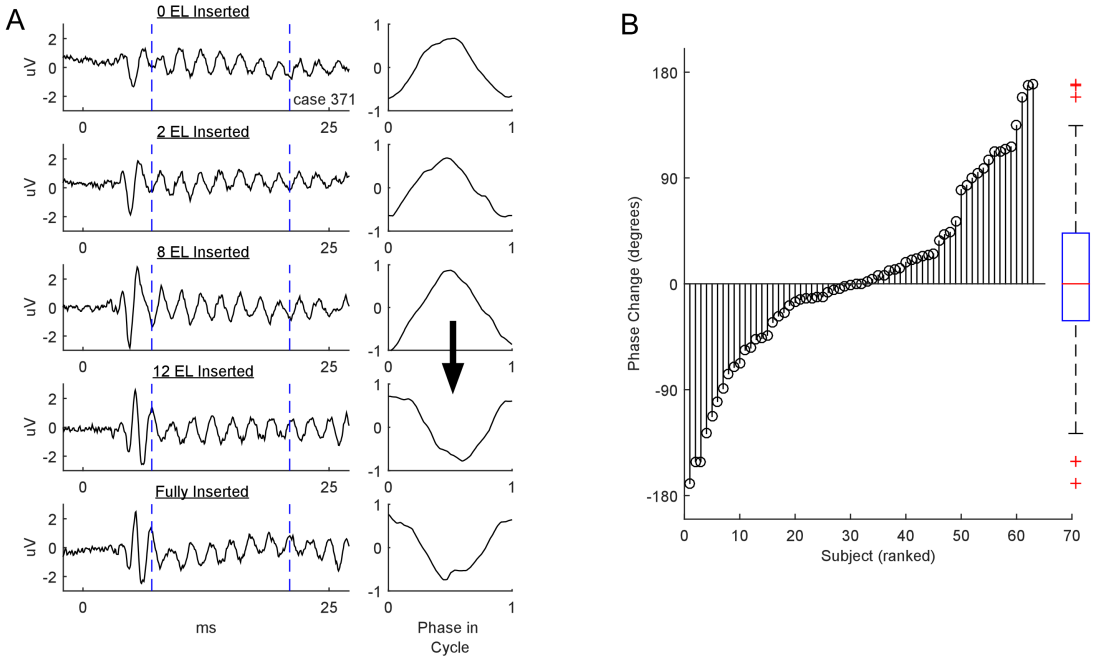


**Figure 2.8 - Extracochlear Phase Inversion**

Inversion of response phase throughout CI insertion. (A) Left column represents waveform response while the right column represents the average cycle of the ongoing segment throughout 5 stages of CI insertion. An inversion of phase (arrow) during the latter stage occurred despite no change in response magnitude. (B) Phase change across all subjects. The majority of phase changes were small, with a median change of 0 degrees, but there was complete distribution across the full range. *note:* uV $= \mu V$

# REFERENCES


Acharya, A. N., D. Tavora-Vieira and G. P. Rajan (2016). "Using the Implant Electrode Array to Conduct Real-time Intraoperative Hearing Monitoring During Pediatric Cochlear Implantation: Preliminary Experiences." Otology & Neurotology 37(2): e148-e153.

Adunka, O. and J. Kiefer (2006). "Impact of electrode insertion depth on intracochlear trauma." Otolaryngology-Head and Neck Surgery 135(3): 374-382.

Adunka, O., M. H. Unkelbach, M. MacK, M. Hambek, W. Gstoettner and J. Kiefer (2004). "Cochlear implantation via the round window membrane minimizes trauma to cochlear structures: a histologically controlled insertion study." Acta oto-laryngologica 124(7): 807-812.

Adunka, O. F., C. K. Giardina, E. J. Formeister, B. Choudhury, C. A. Buchman and D. C. Fitzpatrick (2015). "Round window electrocochleography before and after cochlear implant electrode insertion." Laryngoscope.

Adunka, O. F., S. Mlot, T. A. Suberman, A. P. Campbell, J. Surowitz, C. A. Buchman and D. C. Fitzpatrick (2010). "Intracochlear recordings of electrophysiological parameters indicating cochlear damage." Otol Neurotol 31(8): 1233-1241.

Adunka, O. F., H. Pillsbury and C. Buchman (2009). "Minimizing intracochlear trauma during cochlear implantation."

Bester, C. W., L. Campbell, A. Dragovic, A. Collins and S. J. O'Leary (2017). "Characterizing Electrocochleography in Cochlear Implant Recipients with Residual Low-Frequency Hearing." Frontiers in Neuroscience 11.

Calloway, N. H., D. C. Fitzpatrick, A. P. Campbell, C. Iseli, S. Pulver, C. A. Buchman and O. F. Adunka (2014). "Intracochlear electrocochleography during cochlear implantation." Otol Neurotol 35(8): 1451-1457.

Campbell, L., A. Kacier, R. Briggs and S. OLeary (2015). "Cochlear Response Telemetry: Real-Time Monitoring of Intraoperatice Electrocochleography." Poster Presentation at the 2015 Conference on Implantable Auditory Prostheses (CIAP).

Campbell, L., A. Kaicer, R. Briggs and S. O'Leary (2015). "Cochlear response telemetry: intracochlear electrocochleography via cochlear implant neural response telemetry pilot study results." Otol Neurotol 36(3): 399-405.

Campbell, L., A. Kaicer, D. Sly, C. Iseli, B. Wei, R. Briggs and S. O'Leary (2016). "Intraoperative Real-time Cochlear Response Telemetry Predicts Hearing Preservation in Cochlear Implantation." Otology & Neurotology 37(4): 332-338.

Choudhury, B., O. F. Adunka, C. E. Demason, F. I. Ahmad, C. A. Buchman and D. C. Fitzpatrick (2011). "Detection of intracochlear damage with cochlear implantation in a gerbil model of hearing loss." Otol Neurotol 32(8): 1370-1378.

Choudhury, B., D. C. Fitzpatrick, C. A. Buchman, B. P. Wei, M. T. Dillon, S. He and O. F. Adunka (2012). "Intraoperative round window recordings to acoustic stimuli from cochlear implant patients." Otol Neurotol 33(9): 1507-1515.

Dalbert, A., A. Huber, N. Baumann, D. Veraguth, C. Roosli and F. Pfiffner (2016). "Hearing Preservation After Cochlear Implantation May Improve Long-term Word Perception in the Electric-only Condition." Otology & Neurotology 37(9): 1314-1319.

Dalbert, A., A. Huber, D. Veraguth, C. Roosli and F. Pfiffner (2016). "Assessment of Cochlear Trauma During Cochlear Implantation Using Electrocochleography and Cone Beam Computed Tomography." Otology & Neurotology 37(5): 446-453.

Dalbert, A., F. Pfiffner, C. Roeoesli, K. Thoele, J. H. Sim, R. Gerig and A. M. Huber (2015). "Extra-and Intracochlear Electrocochleography in Cochlear Implant Recipients." Audiology and Neurotology 20(5): 339-348.

Dalbert, A., J. H. Sim, R. Gerig, F. Pfiffner, C. Roosli and A. Huber (2015). "Correlation of Electrophysiological Properties and Hearing Preservation in Cochlear Implant Patients." Otol Neurotol 36(7): 1172-1180.

Dalbert, A., J. H. Sim and A. M. Huber (2014). "Electrophysiologic Monitoring of Residual Hearing During and After Cochlear Implantation." Association for Research in Otolaryngology Abstracts 37: 317-318.

Demason, C., B. Choudhury, F. Ahmad, D. C. Fitzpatrick, J. Wang, C. A. Buchman and O. F. Adunka (2012). "Electrophysiological properties of cochlear implantation in the gerbil using a flexible array." Ear Hear 33(4): 534-542.

Finley, C. C., T. A. Holden, L. K. Holden, B. R. Whiting, R. A. Chole, G. J. Neely, T. E. Hullar and M. W. Skinner (2008). "Role of electrode placement as a contributor to variability in cochlear implant outcomes." Otol Neurotol 29(7): 920-928.

Fitzpatrick, D. C., A. T. Campbell, B. Choudhury, M. P. Dillon, M. Forgues, C. A. Buchman and O. F. Adunka (2014). "Round window electrocochleography just before cochlear implantation: relationship to word recognition outcomes in adults." Otol Neurotol 35(1): 64-71.

Fontenot, T. E., C. K. Giardina and D. C. Fitzpatric (2017). "A Model-Based Approach for Separating The Cochlear Microphonic From The Auditory Nerve Neurophonic in The Ongoing Response Using Electrocochleography." Frontiers in Neuroscience(Ahead of Print).

Fontenot, T. E., C. K. Giardina and D. C. Fitzpatrick (2017). "A Model-Based Method for Separating The Cochlear Microphonic From The Auditory Nerve Neurophonic in The Ongoing Response to Tones In Electrocochleography." Frontiers in Neuroscience In Press.

Forgues, M., H. A. Koehn, A. K. Dunnon, S. H. Pulver, C. A. Buchman, O. F. Adunka and D. C. Fitzpatrick (2014). "Distinguishing hair cell from neural potentials recorded at the round window." J Neurophysiol 111(3): 580-593.

Formeister, E. J., J. H. McClellan, W. H. Merwin, 3rd, C. E. Iseli, N. H. Calloway, H. F. Teagle, C. A. Buchman, O. F. Adunka and D. C. Fitzpatrick (2015). "Intraoperative round window electrocochleography and speech perception outcomes in pediatric cochlear implant recipients." Ear Hear 36(2): 249-260.

Franke-Trieger, A., C. Jolly, A. Darbinjan, T. Zahnert and D. Mürbe (2014). "Insertion depth angles of cochlear implant arrays with varying length: a temporal bone study." Otology & Neurotology 35(1): 58-63.

Harris, M. S., W. J. Riggs, C. K. Giardina, B. P. O'Connell, J. T. Holder, R. T. Dwyer, K. Koka, R. F. Labadie, D. C. Fitzpatrick and O. F. Adunka (2017). "Patterns Seen During Electrode Insertion Using Intracochlear Electrocochleography Obtained Directly Through a Cochlear Implant." Otol Neurotol.

Harris, M. S., W. J. Riggs, K. Koka, L. M. Litvak, P. Malhotra, A. C. Moberly, B. P. O'connell, J. Holder, F. A. Di Lella and C. M. Boccio (2017). "Real-time intracochlear electrocochleography obtained directly through a cochlear implant." Otology & Neurotology 38(6): e107-e113.

Holden, L. K., C. C. Finley, J. B. Firszt, T. A. Holden, C. Brenner, L. G. Potts, B. D. Gotter, S. S. Vanderhoof, K. Mispagel, G. Heydebrand and M. W. Skinner (2013). "Factors Affecting Open-Set Word Recognition in Adults With Cochlear Implants." Ear Hear.

Iseli, C., O. F. Adunka and C. A. Buchman (2014). "Scala tympani cochleostomy survey: A follow-up study." The Laryngoscope 124(8): 1928-1931.

Kiefer, J., F. Bohnke, O. Adunka and W. Arnold (2006). "Representation of acoustic signals in the human cochlea in presence of a cochlear implant electrode." Hear Res 221(1-2): 36-43.

Mandala, M., L. Colletti, G. Tonoli and V. Colletti (2012). "Electrocochleography during cochlear implantation for hearing preservation." Otolaryngol Head Neck Surg 146(5): 774-781.

McClellan, J. H., E. J. Formeister, W. H. Merwin, 3rd, M. T. Dillon, N. Calloway, C. Iseli, C. A. Buchman, D. C. Fitzpatrick and O. F. Adunka (2014). "Round window electrocochleography and speech perception outcomes in adult cochlear implant subjects: comparison with audiometric and biographical information." Otol Neurotol 35(9): e245-252.

Noble, J. H., R. F. Labadie, O. Majdani and B. M. Dawant (2011). "Automatic segmentation of intracochlear anatomy in conventional CT." Biomedical Engineering, IEEE Transactions on 58(9): 2625-2632.

O'Connell, B. P., J. B. Hunter and G. B. Wanna (2016). "The importance of electrode location in cochlear implantation." Laryngoscope Investigative Otolaryngology 1(6): 169-174.

Radeloff, A., W. Shehata-Dieler, A. Scherzed, K. Rak, W. Harnisch, R. Hagen and R. Mlynski (2012). "Intraoperative monitoring using cochlear microphonics in cochlear implant patients with residual hearing." Otol Neurotol 33(3): 348-354.

Riggs, W. J., J. P. Roche, C. K. Giardina, M. S. Harris, Z. J. Bastian, T. E. Fontenot, C. A. Buchman, K. D. Brown, O. F. Adunka and D. C. Fitzpatrick (2017). "Intraoperative Electrocochleographic Characteristics of Auditory Neuropathy Spectrum Disorder in Cochlear Implant Subjects." Front Neurosci 11: 416.

Schuman, T. A., J. H. Noble, C. G. Wright, G. B. Wanna, B. Dawant and R. F. Labadie (2010). "Anatomic verification of a novel method for precise intrascalar localization of

cochlear implant electrodes in adult temporal bones using clinically available computed tomography." Laryngoscope 120(11): 2277-2283.

Skarzynski, H., A. Lorens, A. Piotrowska and I. Anderson (2007). "Preservation of low frequency hearing in partial deafness cochlear implantation (PDCI) using the round window surgical approach." Acta oto-laryngologica 127(1): 41-48.

Skarzynski, H., P. Van de Heyning, S. Agrawal, S. Arauz, M. Atlas, W. Baumgartner, M. Caversaccio, M. de Bodt, J. Gavilan and B. Godey (2013). "Towards a consensus on a hearing preservation classification system." Acta Oto-Laryngologica 133(sup564): 3-13.

Skinner, M. W., T. A. Holden, B. R. Whiting, A. H. Voie, B. Brunsden, J. G. Neely, E. A. Saxon, T. E. Hullar and C. C. Finley (2007). "In vivo estimates of the position of advanced bionics electrode arrays in the human cochlea." Ann Otol Rhinol Laryngol Suppl 197: 2-24.

Suhling, M.-C., O. Majdani, R. Salcher, M. Leifholz, A. Büchner, A. Lesinski-Schiedat and T. Lenarz (2016). "The impact of electrode array length on hearing preservation in cochlear implantation." Otology & Neurotology 37(8): 1006-1015.

Von Ilberg, C. A., U. Baumann, J. Kiefer, J. Tillein and O. F. Adunka (2011). "Electric-acoustic stimulation of the auditory system: a review of the first decade." Audiology and Neurotology 16(Suppl. 2): 1-30.

Wanna, G. B., J. H. Noble, M. L. Carlson, R. H. Gifford, M. S. Dietrich, D. S. Haynes, B. M. Dawant and R. F. Labadie (2014). "Impact of electrode design and surgical approach on scalar location and cochlear implant outcomes." Laryngoscope Epub ahead of print.

Wanna, G. B., J. H. Noble, R. H. Gifford, M. S. Dietrich, A. D. Sweeney, D. Zhang, B. M. Dawant, A. Rivas and R. F. Labadie (2015). "Impact of Intrascalar Electrode Location, Electrode Type, and Angular Insertion Depth on Residual Hearing in Cochlear Implant Patients: Preliminary Results." Otology & Neurotology 36(8): 1343-1348.

# CHAPTER 3: MODEL OF THE ONGOING RESPONSE[1]

## Overview

Electrocochleography (ECochG) is a potential clinically valuable technique for predicting speech perception outcomes in cochlear implant (CI) recipients, among other uses. Current analysis is limited by an inability to quantify hair cell and neural contributions which are mixed in the ongoing part of the response to low frequency tones. Here, we used a model based on source properties to account for recorded waveform shapes and to separate the combined signal into its components. The model for the cochlear microphonic (CM) was a sinusoid with parameters for independent saturation of the peaks and the troughs of the responses. The model for the auditory nerve neurophonic (ANN) was the convolution of a unit potential and population cycle histogram with a parameter for spread of excitation. Phases of the ANN and CM were additional parameters. The average cycle from the ongoing response was the input, and adaptive fitting identified CM and ANN parameters that best reproduced the waveform shape. Test datasets were responses recorded from the round windows of CI recipients, from the round window of gerbils before and after application of neurotoxins, and with simulated signals where each parameter could be manipulated in isolation. Waveforms recorded from 284 CI recipients had a variety of morphologies that the model fit with an average $r^2$ of $0.97 \pm 0.058$ (standard deviation). With simulated signals, small systematic differences between outputs and inputs were seen with some variable combinations, but in general there were limited interactions among the parameters. In gerbils, the CM reported was relatively unaffected by the neurotoxins. In contrast, the ANN was strongly reduced and the reduction was limited to frequencies of

[1]modified from: *Fontenot, T. E., C. K. Giardina and D. C. Fitzpatrick (2017). "A Model-Based Approach for Separating the Cochlear Microphonic from the Auditory Nerve Neurophonic in the Ongoing Response Using Electrocochleography." Frontiers in Neuroscience (11):592*

1000 Hz and lower, consistent with the range of strong neural phase-locking. Across human CI subjects, the ANN contribution was variable, ranging from nearly none to larger than the CM. Development of this model could provide a means to isolate hair cell and neural activity that are mixed in the ongoing response to low-frequency tones. This tool can help characterize the residual physiology across CI subjects, and can be useful in other clinical settings where a description of the cochlear physiology is desirable.

## Introduction

Electrocochleography is the recording of electrical potentials produced by the cochlea in response to stimulation. It has been extensively used to evaluate peripheral auditory system physiology, and is used clinically to identify hydrops in Meniere's patients and other retrocochlear pathologies (Schmidt, Eggermont et al. 1974, Gibson and Beagley 1976). It has also drawn interest for the study of auditory neuropathy spectrum disorder (ANSD, Santarelli 2010, Rance and Starr 2015). Recently, ECochG has been used to account for speech perception outcomes in cochlear implant (CI) recipients (Fitzpatrick, Campbell et al. 2014, McClellan, Formeister et al. 2014, Formeister, McClellan et al. 2015) and is showing promise for detecting intraoperative trauma in CI patients (Adunka, Mlot et al. 2010, Mandala, Colletti et al. 2012, Radeloff, Shehata-Dieler et al. 2012, Calloway, Fitzpatrick et al. 2014, Campbell, Kaicer et al. 2015, Dalbert, Sim et al. 2015, Dalbert, Huber et al. 2016, Bester, Campbell et al. 2017). Liberman and colleagues, among others, have investigated various aspects of ECocG for detecting evidence of cochlear synaptopathy, or hidden hearing loss (Liberman, Epstein et al. 2016). Analysis of the hair cell and neural contributions to ECochG responses recorded in CI recipients is the main objective of this study.

The responses from the cochlea to sounds consist of several distinct signals which overlap in time. The compound action potential (CAP) occurs near the onset of the response to stimuli with fast rise times, and has a purely neural source produced by the synchronous action potential produced to onsets of sound. The alternating-current (AC) component of the ECochG response is a mixture of the cochlear microphonic (CM) and auditory nerve

neurophonic (ANN). The CM is produced by transducer current through stereocilia of hair cells in response to basilar membrane movement, and is thus phase-locked to all tone frequencies. The ANN is the evoked potential correlate of phase-locked responses in neural fibers, which is strong only to frequencies below roughly 2000 Hz. The direct current (DC) response to tones is the summating potential (SP) which is derived from a complex mixture of hair cell (Davis, Deatherage et al. 1958, Dallos 1973, Zheng, Ding et al. 1997, Durrant, Wang et al. 1998) and neural (van Emst, Klis et al. 1995, Sellick, Patuzzi et al. 2003, Forgues, Koehn et al. 2014) sources.

There are several cases where it would be useful to separate the CM from the ANN in the ongoing portion of the response to tones. These include a non-invasive way to estimate the upper limit of phase locking (Verschooten and Joris 2014, Verschooten, Robles et al. 2015); as a screen for low frequency hearing loss (Lichtenhan, Cooper et al. 2013, Lichtenhan, Hartsock et al. 2014); and to determine the proportions of hair cell and neural activity in the responses of CI recipients, which are most reliably elicited by low frequency stimuli (Choudhury, Fitzpatrick et al. 2012). Historically, the ANN was considered the principal source of the 2nd harmonic (Henry 1995, Lichtenhan, Cooper et al. 2013, Chertoff, Kamerer et al. 2015). However, asymmetries of the transduction process also produce even harmonics in the CM (Teich, Keilson et al. 1989, Santos-Sacchi 1993, Forgues, Koehn et al. 2014). The periodicity of both the CM and the ANN reflect the stimulus frequency, thus, both potentials contribute to the magnitude of the first harmonic peak (Snyder and Schreiner 1984, Forgues, Koehn et al. 2014, Verschooten, Robles et al. 2015). Masking has been used to recover the proportion of the neural response removed by adaptation, based on the idea that only neural signals show such adaptation (Snyder and Schreiner 1984, Sparacino, Milani et al. 2000, Verschooten, Robles et al. 2015). However, this approach only quantifies the neural proportion that adapts to the masker, and cannot quantify the total amount of neural response within the signal.

The approach presented here uses discrete analytic models of the expected ANN and CM waveforms in order to separate them in the combined signal, as would be acquired in a clinical setting. By varying the proportions of expected CM and ANN, and the phases between them, we can determine the best fit for the parameters to match the recorded

waveforms. To validate the approach we first show that the model is able to fit the complex waveforms recorded from human CI subjects. We then examine the parametric performance of the model using artificially mixed signals, and show results from animals before and after application of the neurotoxins kainic acid (KA), tetrodotoxin (TTX) and ouabain (OA) to the round window. Finally, the model is used to examine the CM and ANN in responses from CI recipients.

## Materials and Methods

Three data sets were used in the experimental design: human CI recipients, gerbils and simulated signals created by varying the parameters of interest.

### Human Subjects

All adult and pediatric patients who were scheduled for CI at University of North Carolina Hospitals in 2011-2017 were eligible to be enrolled in the study. Thus, the sample population (N=285) includes the heterogeneity of conditions leading to a recommendation for a CI. Non-native English speakers, children of non-native speakers, and those undergoing revision surgery or with severe inner ear malformations (cochlear atresia, etc.) were excluded. The recordings in human CI recipients were carried out in accordance with the recommendations of Declaration of Helsinki guidelines as reviewed and approved by the Institutional Review Board at University of North Carolina. All subjects gave written informed consent in accordance with the Declaration of Helsinki. Parental consents were obtained for all pediatric subjects and assent was obtained for pediatric subjects at least 7 years old.

The recording procedures for pediatric and adult CI recipients have been previously described (Choudhury, Fitzpatrick et al. 2012, McClellan, Formeister et al. 2014, Formeister, McClellan et al. 2015). A Biologic Navigator PRO (Natus Medical Inc., San Carlos, CA) was used for acoustic stimulation and ECochG recordings. The stimuli were delivered through an in-ear foam insert attached to a speaker (Etymotic ER3b) by a sound tube. Stimuli were alternating phase tone bursts from 250 to 4000 Hz presented at 90 dB nHL (from

108-114 dB peak SPL for 250-2 kHz, 95 dB for 4 kHz). Rise/fall times were 1 ms or 1 cycle, whichever was longer. Calibration of sound levels was by a 1/4" microphone and measuring amplifier ((Bruel & Kjaer, Nærum, Denmark)). Distortion at these sound levels for the second harmonic was from -37 to -67 dB compared to the fundaments for frequencies of 1-2 kHz, but was -26 dB for 4 kHz. The third harmonic was <-40 dB compared to the fundamental for all frequencies.

A standard transmastoid facial recess approach was used to surgically access the round window. The recording used surface electrodes on the forehead contralateral mastoid as ground and reference electrode, respectively. The active electrode a stainless-steel monopolar probe (Neurosign; Magstim Co., Wales, UK) placed in the round window niche. The ECochG recordings were obtained immediately before CI insertion. Recording epochs were 512 points each, from 32 ms for 250-1000 Hz (16000 Hz sampling rate) to 10.66 ms for 2000 and 4000 Hz (48000 Hz sampling rate). Filter settings were 10 Hz high-pass and low passes were 5,000 Hz for 250-1000 Hz, and 15,000 Hz for 2 and 4 kHz.

### Recordings in Gerbils

The experiments with gerbils (*Meriones unguiculatus*) were carried out in accordance with the standards of the National Institutes of Health and Committee on Care and Use of Laboratory Animals. All procedures were reviewed and approved by the Institutional Animal Care and Use Committee (IACUC) at the University of North Carolina.

Gerbils with clean middle ears had ECochG recordings using the same equipment as in the human recordings. Anesthesia, surgery and ECochG recording procedures have been previously described (Forgues, Koehn et al. 2014). Animals were sedated using sodium pentobarbital (10 mg/kg, i.p.) and anesthetized with urethane (1.5 g/kg, i.p.), Atropine was used to control respiratory secretions. The animal was maintained at 38°C using a heating pad. Needle electrodes were placed at the base of the tail and contralateral neck muscles for the ground and reference inputs, respectively. A sealed sound tube was then placed within the external auditory canal. After surgical exposure of the round window, the Neurosign electrode was placed inside the niche. Tone bursts of 250 to 8000 Hz over levels from 30-80 dB SPL were presented with the same stimulus/recording conditions as for the humans.

Additional frequencies in some cases included 375 and 8000 Hz; both had second and third harmonic distortion levels of less than -50 dB compared to the fundamental.

The neurotoxins KA, TTX and OA were used to obtain signals with diminished neural contribution. Different substances were used because the material was available from other experiments, and because the use of multiple compounds can help avoid the possibility of one or the other having unexpected actions on hair cells in addition to nerve fibers. KA is a glutamate analogue and destroys the nerve terminals by excitotoxicity; TTX blocks sodium channels and thus removes the spiking component of the neural response, and OA inhibits the sodium-potassium ATPase also blocking the nerve from firing as well as further depolarizing, but without physically removing the nerve terminal. Six animals were used for each substance. The neurotoxins were applied for 1 hour to the round window following baseline ECochG recordings. The toxins were dissolved in lactated Ringer's solutions for KA, and artificial perilymph for TTX and OA. Specifically, the artificial perilymph contained 127.5 mM NaCl, 3.5 mM KCl, 25 mM $NaHCO_3$, 1.3 mM $CaCl_2$, 1.2 mM $MgCl_2$, 0.75 mM $NaH_2PO_4$, and 11 mM Glucose (Mikulec, Plontke, et al. 2009). The solutions were warmed to 38°C before use. The KA (Sigma USA #K0250) was 60 or 100 mM; the TTX was 15 $\mu$M (Tocris Bioscience, #1069) and the OA (Calbiochem, #4995) was 1 or 10 mM. These high concentrations were used because the solution needed to overcome the pharmacokinetics associated with dissolving through the RW and permeating through the scala. After application the solutions was wicked from the round window and replaced with vehicle alone. The ECochG recording series was then performed again.

## Signal Analysis

Figure 1A depicts a typical ECochG response to a 500 Hz condensation-phase tone bursts with the ongoing portion highlighted (green area). Within this region, the CM and ANN are mixed together, with both following the amplitude changes in the tone. Each cycle of the ongoing portion of the response was combined to produce an "average cycle" (Figure 1B). The mixture of the CM and ANN affect the distortions in the response, compared to the sinusoidal stimulus (dashed green line). This average cycle became the input that the model attempted to fit.

The time waveforms were analyzed with using fast Fourier Transforms (FFTs) and the magnitude peaks to the stimulus frequency and its harmonics were considered significant if they exceeded the noise by more than three standard deviations, as measured from three bins on either side of the peaks. Typically, the minimum detectable signal was approximately 20 nV after 500 repetitions (-34 dB re 1 $\mu V$).

For the human CI subjects, evidence of neural activity from CI recipients was graded based on a visual assessment of the response, including evaluation for the presence of a CAP and ANN across the frequency range (Riggs, Roche et al. 2017). Briefly, a CAP was typically detected as a negative deflection within the first few ms of the response (although some were delayed as long as 10 ms, see Scott, Giardina et al. 2016, Abbas, Tejani et al. 2017). The ANN was determined to be present when the average cycle deviated from a possible shape attributable to the CM alone, as further described below. The CAP and ANN were each scored over the range of 0-2, so the range of 'nerve scores' was from 0-4. A zero for the CAP or ANN indicated no conclusive evidence of presence; one indicated present but small (in the case of the CAP), or with clear but relatively minor distortions in the average cycle (in the case of the ANN); while two indicated large (in the case of CAP) or with strong distortions (for the ANN). The shapes of the average cycle that indicated the presence of the ANN was strongly influenced by the animal work reported in part here. For examples of human CI cases with each nerve score, see Riggs et al. (2017). It was the need for an objective means of determining the presence of the ANN that prompted the development of the model reported here. The nerve score is useful as an independent means of assessing neural activity (see Figure 3.11).

## Conceptual Basis for the Model

The conceptual basis for the individual contributions of CM and ANN used in the model are depicted in Figure 3.2. The source of the CM is the transducer current through mechanosensitive channels in the stereocilia of hair cells. The input-output function of the current flow is typically modeled as an asymmetrically saturating second-order Boltzmann function (Santos-Sacchi 1993, Sirjani, Salt et al. 2004, Ramamoorthy, Deo et al. 2007). To a low intensity stimulus (Figure 3.2A), the hair cell movement is within the

linear range of the function producing a sinusoidal CM. To a moderate intensity stimulus (Figure 3.2B), the hair cell movement can saturate in one direction producing a partially rectified signal, depending on the degree of distance of the operating point, or proportion of open channels at rest, from the midpoint of the function. For a high intensity stimulus, the movement saturates in both directions of the CM waveform (Figure 3.2C). Thus, the CM can be represented as a sinusoid at the stimulus frequency, with two additional parameters of saturation of the peak and trough of response, to capture both asymmetric and symmetric saturation.

As with the CAP, the ANN can be described as the convolution of a unit potential (UP), which is the shape of a single action potential as it appears at the round window (Kiang, Moxon et al. 1976, Prijs 1986, Versnel, Prijs et al. 1992), and the cumulative post-stimulus time histogram, or summed histogram of all responding auditory nerve fibers (Goldstein and Kiang 1958, Snyder and Schreiner 1984, Chertoff 2004). For low frequency tones, the post-stimulus time histograms of auditory nerve fibers shows cyclic firing to the positive-going half-phase of the stimulus (Rose, Brugge et al. 1967). By folding across stimulus cycles, the resulting cycle histogram (CH) resembles the half-wave rectified form of the phase-locking. The curve shown (Figure 3.2E) has been stretched to be more than a half-cycle to simulate the spread in phase associated with inclusion of fibers at more basal positions on the basilar membrane as the intensity is varied (Kim and Molnar 1979).

## Implementation of the Model

The CM was described by Equation 1. A sinusoid (Equation 1a) was defined in time ($t$, in seconds) with frequency ($f$, in Hz) equal to the stimulus frequency and amplitude ($A_{CM}$, in $\mu V$) and starting phase ($\varphi_{CM}$, in cycles) as parameters. Additional parameters were upper and lower cutoffs that represented saturation of the peak and trough independently (Equation 1b). The $A_{CM}$ was allowed to vary between 0 and 5x the maximum of the input

signal. The phase boundaries were from -2 to 2 cycles. Boundaries of clipping the peak and trough were 50% of the maximum or minimum input, respectively.

$$CM_{sine}(t) = A_{CM} \times sin\Big(2 \times \pi(ft - \varphi_{CM})\Big) \tag{1a}$$

$$CM(t) = \left\{ \begin{array}{ccc} UpperCutoff & \text{if} & CM_{sine}(t) > UpperCutoff \\ CM_{sine}(t) & \text{if} & Lowercutoff \leq CM_{sine}(t) \leq UpperCutoff \\ LowerCutoff & \text{if} & CM_{sine}(t) < LowerCutoff \end{array} \right\} \tag{1b}$$

To fit the neural contributions to the ongoing response, the UP was described as a single cycle of a sinusoid at 1100 Hz. This frequency was selected based on pilot studies where values over the range of 800-1200 Hz were tested, where 1100 Hz provided the best fits on average. The UP has also been previously modeled using a dampened sinusoid (Chertoff 2004) but we found that a peak in a second cycle of the UP introduced distortions not reflective of those seen in the physiological data, producing poor fits. The cycle histogram (CH), was described as a lognormal probability distribution function (Equation 2) which describes when neural spikes are most likely to fire. Probability in the CH is highest during the phase of basilar membrane motion that depolarizes hair cells, and is zero for the hyperpolarizing direction because the spike rate cannot go below zero (although spontaneous activity can be modulated) (Rose, Brugge et al. 1967). The width of the CH distribution curve ($\sigma$) was determined by the 'SOE' parameter, which was allowed to range from 0.35 to 0.65 of the stimulus cycle. The lower limit was chosen because it is sharper than the vector strength of a typical nerve fiber over most frequencies and intensities, so a sharper cycle histogram for the population is not expected. The upper limit was chosen because there is a natural limit for SOEs greater than one cycle, because only the cyclic part of the ANN contributes to the ac component of the ongoing response as because a constant level of firing occurs as the cycle histogram from different regions overlap.

$$CH(t) = \frac{1}{(\sigma\sqrt{2\pi})t} \exp\left(\frac{-(\ln t - \mu)^2}{2\sigma^2}\right) \tag{2}$$

$t$ = timeline of the CH, $\mu$ = period of the UP, $\sigma$ = SOE

Convolution of the UP and the CH, multiplied by an ANN amplitude term, $A_{ANN}$, was performed to yield a single cycle of ANN (Equation 3). The $A_{ANN}$ was allowed to vary between 0 and 5 times the maximum of the input signal.

$$ANN(t) = A_{ANN} \times \Big( CH(t) * UP(t) \Big) \tag{3}$$

Phase shift ($\varphi_{ANN}$) was a parameter applied to the convolved signal using MATLAB function 'circshift' which discretely shifts the array circularly. It could vary over the range of -2 to 2 cycles.

$$ECochG_{model}(t) = ANN(t) + CM(t) \tag{4}$$

A schematic representation of the analytical process performed by the computational model is shown in Figure 3.3. To fit an observed ECochG using the model, the averaged ongoing response was evaluated using a nonlinear least squares curve fitting function (MATLAB function 'lsqcurvefit') which calculated optimized values of the CM and ANN parameters ($A_{CM}$, $A_{ANN}$, $\varphi_{CM}$, $\varphi_{ANN}$, SOE, peak saturation and trough saturation) based on Equation 4. The specific least-squares algorithm implemented used the "trust-region-reflective" approach because the model was defined with specified equations (Equations 1-4) and the parameters were bounded. Optimized parameters were returned when the output waveform approximated the input signal, using the default optimality tolerance of $1x10^{-6}$.

Goodness of fit was evaluated using regression analysis to calculate the degree of correlation (r) and determination coefficient ($r^2$) between the average cycle of the recorded ECochG and one cycle of the modeled ECochG. Frequency spectra of the modeled ECochG and the individually modeled CM and ANN components were also computed using FFTs.

The model reports the amount of "CM" and "ANN" required to best fit the input waveforms. However for various reasons described throughout the manuscript these modeled results are not identical to the actual amounts of CM and ANN that produced the wave-

forms, only an approximation of them. To avoid calling them "mCM" and "mANN" throughout, for example, it should be understood that the reported CM and ANN represent these approximations.

### Generation of Simulated Signals for Model Testing

In addition to the human and animal data sets from ECochG, a third data set was a series of simulated signals where the values of each parameter were systematically varied. These simulated signals served to determine the model's ability to detect the changes and observe the effects of the change in each parameter on the others. The simulated signals used the same fitting functions for the CM and ANN as described above.

## Results

### Modeled Fits to the Average Cycles from Human CI Recipients

The fits between recorded waveforms used as inputs and the outputs produced by mixing parameters of the CM and ANN are shown in Figure 3.4. The examples in Figure 3.4A-E were chosen to illustrate the variety of waveform morphologies seen to low frequency tones. The waveforms show the inputs and modeled outputs to two concatenated average cycles (left panels), and the spectra show the magnitudes of the individual CM and ANN components (right panels). Some of the responses showed strong distortions compared to the sinusoidal stimuli (e.g., A and E), while in others the distortions were smaller (B, C and D). Metrics used to compare the average cycle and model fit were the correlation coefficient (r) between the two (from the xcorr function in MATLAB) and the coefficient of determination ($r^2$). The additional examples in Figure 3.4F-J show responses and the modeled fits across a wider range of stimulus frequencies (250-2000Hz) and in subjects with a variety of hearing loss etiologies. The case shown in F, reported as ANSD, showed extreme distortions and a strong ANN to a 250 Hz tone. Another case with a specific type of ANSD, cochlear nerve deficiency (G) had very small distortions or ANN, as did a case with an unknown cause of sensorineural hearing loss. Distortions could be present to 1000 Hz (I), while to 2000 Hz it was absent; in this case there was only saturation (J).

Figure 3.4K demonstrates the distribution of the fits produced by the model based on the analysis of all of the ECochG signals from 284 CI recipients. The mean $r^2$ produced by the model, based on analysis of 1241 signals recorded, was $0.97 \pm 0.051$ (standard deviation).

The data in Figure 3.4 indicates the model can accurately reproduce the recorded waveforms from CI subjects, and that the ANN/CM ratio reported follows the degree of distortions (other than saturation that can be attributed to the CM) in the waveforms. This data suggests that the model is a plausible means to analyze the responses to assess the underlying sources. We will test this idea with three data sets, first with simulated signal that can be varied parametrically, second with data from gerbils before and after application of neurotoxins to the round window, and finally in the sample population of CI subjects.

### Assessment of the Model Using Simulated Signals

To help understand interactions between ANN and CM that help fit particular shapes, and to evaluate possible interactions between parameters returned by the model, we simulated waveforms with parametric variations using the same equations for the CM and ANN that the model used to fit ECochG signals. In figure 5, we show effects of variation of the phase between the CM and ANN when the amplitudes of each remained the same. This manipulation resulted in waveforms which closely resembled the physiologic signals we have collected from experiments with human CI recipients (see Figures, 3.4E, 3.4I, and 3.4E for analogs of 3.A, 3.B and 3.C, respectively). The phase relationship also changed the overall peak to peak magnitude of the ongoing response, which was at its largest when the two signals were in phase (Figure 3.5A) and smallest when out of phase (Figure 3.5C), due to constructive and destructive interference.

The effects of parametric variations of the inputs on the outputs of the model are shown in Figure 3.6. The parameter that was varied is indicated for each column (A-F) and the outputs of the model are shown in the rows. Each panel shows the output to a series of 100 input signals. The input values are indicated by black lines. Only small deviations were seen in the amplitudes of the CM and ANN (top row) and the phases between them (second row), with the largest deviation occurring to the CM amplitude as symmetric saturation

increased (D, top row, blue trace). For the trough saturation (third row, green trace) a relatively large deviation occurred as the ANN became large (A), but this had only a small effect on the CM amplitude. The peak saturation parameter (third row, black trace) and the SOE, showed small deviations that were associated with minor effects on the CM and ANN amplitudes, and did not affect the phase measurement. These results indicate the model can detect independent parameter changes in the underlying formulae, and that interactions of the parameters do occur, but do not appear to be major.

### Modeled Fits of the ECochG Signals from Gerbils before and after Application of Neurotoxins

The previous data showed that the model provided good fits to the raw curves and tracks the changes in simulated signals. To further assess how well it could capture the ANN and CM in ECochG responses, experiments using neurotoxins were performed in gerbils. Expected effects of the neurotoxins included 1) a reduced proportion of ANN, 2) little or no effect on the CM, 3) low-pass filtering of the ANN compared to the CM due to the range of phase-locking in auditory nerve fibers, and 4) greater compression of the rate-level function in the ANN compared to the CM; i.e., there should be a greater proportion of ANN to low and moderate intensities than to high intensities in low frequency sounds. These features, if captured by the model, could then be experimentally related to the ANN.

Examples of the effects of the different neurotoxins are shown in Figure 3.7. The frequency/intensity combination in each response was 500 Hz at 50 dB SPL. This stimulus was chosen for illustration because: 1) the phase-locking is expected to be strong to this low frequency, so a large ANN is expected; 2) the ANN should be proportionally larger compared to the CM than would be the case at higher intensities; and 3) the 500 Hz region is relatively apical in the gerbil cochlea, so it represents a site where the spread of the neurotoxin can be assessed. In addition, 500 Hz is the 'sweet-spot' for human CI subjects, where the responses tend to be the largest, so the choice is relevant for our main purpose. The left column shows responses from three gerbils (A1-3) prior to any drug application. Each case shows the signal waveform and the model fit (top) and the FFT of the ANN as reported by the model (bottom). Both the waveforms and FFT are normalized by the maximum firing

rate. The numbers in the FFTs are the ANN/CM ratio reported by the model. For each neurotoxin (B-D), the three examples (1-3) were chosen to cover the range of distortions remaining; cases in row 1 had the least remaining distortion, those in row 2 an intermediate level, and those in row 3 were at the upper end of distortions seen for that drug. The 'Post-KA' responses (C) are from the same gerbils as the 'Pre-KA' responses (A). The main results were that application of the drugs removed most of the distortions compared to the Pre-KA responses, and that the ratio of ANN/CM reported decreased. Application of TTX (B) resulted in more complete removal of the distortions and reported reduction in the ANN compared to KA (C), or OA (D), although with each substance cases with nearly complete reported removal of the ANN occurred (e.g., row 1).

The population data for the gerbil experiments across frequencies and intensities is shown in Figure 3.8. The four columns, representing the responses recorded in gerbils before application of any neurotoxin (A) and the effects of the drugs (B-D) are the same as the previous figure. The rows represent the CM (top) and ANN (middle) reported by the model which were used to calculate the 'ANN/CM index' (bottom). The index is an alternate method for reporting the proportion of ANN using the formula (ANN-CM)/(ANN+CM), so that negative values indicate CM larger than ANN (-1 is all CM), 0 indicates equal amounts of CM and ANN, and positive values indicate greater ANN than CM (+1 is all ANN). A larger range of frequencies and intensities was tested in the KA experiments compared to when TTX or OA was used. Across the top row, the use of the neurotoxins had little effect on the CM, although to low intensities in the post KA cases the values reported for 750 and 1000 Hz were reduced (arrows). For the ANN, in the pre-drug condition (A) there was a considerable effect of frequency with both the ANN (middle) and the ANN/CM index (bottom). This bias of the ANN toward low frequencies is expected from neural phase-locking. However, to achieve this effect in the case of the ANN magnitude the values reported as 5% or less of the total were scored as a zero, because the model rarely produced an ANN much smaller than 5%. Without this cut-off the ANN reported for high frequencies and high intensities was only slightly lower than for low frequencies; i.e., because the responses themselves were so large even a small percentage produced a relatively large ANN. The cut-off did not affect any of the measurements to low frequencies (<= 1000 Hz) in the pre-

drug condition, and the cut-off was not used for the ANN/CM index, so the low pass filtering of the ANN compared to the CM is clear from the model.

In the post-drug conditions (Figure 3.8, B-D), the ANN was reduced compared to the predrug condition, but large values were still reported to high intensities. These large values were probably due to a mixture of two effects. First, the effects of the drug were variable, so some ANN left over after drug application on average is expected. Second, in the post-drug condition the need for the 5% cut-off comes into play for low frequencies as well as high frequencies. The ANN/CM index appeared to capture the effect of the neurotoxins more accurately than the raw numbers. Note that as in the examples presented earlier (Figure 3.7) the OA had the least effect.

Another way to assess the effect of the neurotoxin is to compute the difference between the pre and post drug conditions reported by the model. In Figure 3.9 we show this data for control cases where only vehicle (lactated Ringer's or artificial perilymph) was applied to the round window as well as for when neurotoxins were applied. In the control cases with lactated Ringer's as the vehicle (Figure 3.9A), a non-specific effect of time is evident by the small decrease in response of the CM and ANN. This is the main reason the frequency and intensity combination were decreased in later experiments. With this smaller stimulus set and change and using artifical perilymph as the vehicle (Figure 3.9C), the changes in the CM and ANN were much less. After KA (Figure 3.9B), the subtraction showed the CM to 750 and 1000 Hz at the lowest intensity (30 dB SPL) to be reduced by a relatively large amount (arrow), as shown in the previous figure with the raw data. The CM after KA, TTX, and OA (Figures 3.9B, D, and E) showed no changes in the CM compared to controls. For the KA (B) and TTX (D), the ANN was reduced to frequencies of 1000 Hz and below for intensities below 70 dB SPL. To low frequencies at high intensities and for high frequencies the effects of these neurotoxins were small. the the ANN showed the greater effect of KA than the CM, with the CM similar to the control. The OA showed the same trends but with smaller effect.

With the KA and the TTX, the reduction of the ANN was less substantial for high than for low intensities, corresponding to the larger remaining ANN to high intensities. However, the expected effect is that the largest reduction in the ANN would be to high

intensities, since the neurotoxin would have the greatest effect on the cochlear base, thus blocking spread of excitation. Remaining ANN from the apex would be relatively less affected by the neurotoxin. Thus, less ANN than was actually removed was detected when it is was a small or neligible fraction of the total response at the beginning, and more of the response was estimated to remain than was likely to actually be present. To help understand possible reasons for these results, Figure 3.10 depicts examples of waveforms and spectra to 1 and 4 kHz before and after the application of TTX, presented at 80 dB SPL. To the 1 kHz tone, some ANN is expected prior to TTX, but at such a high intensity it should be small relative to the CM. After TTX the ANN should be small or negligible. To the 4 kHz tone there should be no ANN either before of after TTX. However, all four of these responses were reported by the model to have considerable ANN - from 7-17% of the CM. In addition, all were accompanied by a similar waveform. To be called purely CM, the model expects a sine wave that can be saturated in the peaks and/or troughs. However, responses shown had a declining, rather than purely saturated, response at the peak (arrows). Although many of the pre and post-TTX responses to high frequencies (and post-TTX to low frequencies) had ANN/CM ratios below 0.05, for those that exceeded this cut-off the waveform shape shown here was often encountered.

### The CM and ANN in Human CI Recipients as Determined by the Model

The data presented to this point support the ability of the model to reproduce waveform shapes in CI subjects (Figure 3.4), and the parameters identified provide reasonable estimates of the CM and ANN for most frequency/intensity combinations before and after neurotoxins (Figures 3.7-3.10). Here, we apply the model to the population of CI recipients (Figure 3.11). For 500 Hz stimuli at 90 dB nHL, the magnitude of the reported ANN was typically lower than for the CM. On average, this difference was 14.7 $\pm$ 13.9 dB (standard deviation). However, there was a general trend for a larger ANN as the CM increased. This trend is expected to the degree that a larger response indicates both larger CM and ANN. However, the data indicated by the 'X' symbols are the cases where the ANN/CM ratio was less than 0.05, and in some of these cases, such as for cochlear nerve deficiency (see Figure 3.4G), it is highly likely that the ANN would be small or absent. Thus, as with

the animal data, the model as currently implemented does not allow for small or absent ANN when the overall response is very large. The average reduction compared to the CM in these cases where the ANN ratio was <0.05 was 26.2 dB, so this appears to be essentially a lower limit for the ANN using the model. Figure 11B shows there was a wide variety in the proportion of the ANN across cases. In the large majority of cases (93%) the ANN/CM index was negative, indicating a predominance of CM over ANN (mean index of -0.56 $\pm$ 0.31, or an average of about 3.5 time larger CM than ANN). However, a number of cases had an ANN approaching 50% of the CM (index of 0), and in some the ANN contribution was reported as larger than the CM.

To assess the effects of frequency, the ECochG signals belonging to each individual were categorized based on a visual assessment of the neural activity, including evaluation for the presence of a CAP and ANN across the frequency range (see Methods). The data for the CM was not well-ordered by the amount of neural activity (Figure 3.11C), and showed only a small frequency effect (these cases show only responses that were significant for each frequency, so the numbers are smaller for 2 and 4 kHz compared to 250-1000 Hz). In contrast, the reported ANN supported the results of the subjective assessment (Figures 3.11D and E). As with the gerbil data, a non-linearity at ANN/CM ratio of 0.05 was applied forcing lower ratios to have zero ANN (Figure 3.11D). The CM/ANN index showed a similar trend as the ANN magnitude without no non-linearity used (Figure 3.11E). For cases with the highest nerve score the cut-off frequency for the ANN was similar to that seen in the NH gerbils, while the responses in cases with the lowest nerve scores were similar to that seen with gerbils after neurotoxins.

## Discussion

Although the responses to tones have long been known to contain both CM and ANN, methods to quantitatively separate them have been largely lacking. Here, we created an analytic model of the CM and ANN intended to separate and estimate the magnitudes of these two components of the ongoing response. We used the model to analyze ECochG responses recorded in CI recipients, NH gerbils before and after application of a neurotoxin, and sim-

ulated ECochG signals. The model succeeded in capturing the overall shapes of waveforms in CI subjects (Figure 3.4), was affected in generally predicable ways by parametric manipulation of simulated signals (Figures 3.5-3.6), captured aspects of the responses expected after application of neurotoxins in gerbils (Figures 3.7-3.10) and provided estimates of the ANN and CM in human CI subjects that generally matches that of a subjective estimate of neural activity (Figure 3.11). However, the model also showed limitations, of which the most important were to overestimate the amount of ANN in cases where little or none is expected, such as after neurotoxins or in some CI subjects, and to underestimate the amount of ANN when the CM is extremely large, such as to high intensities in normal hearing animals.

### Need for the Model

Masking techniques can reveal the presence of the ANN in many cases, but can quantitatively recover only the amount that is masked, which for suprathreshold stimuli in single unit studies is not the entire neural component (Smith 1977, Harris and Dallos 1979). In addition, in CI subjects the stimulus levels are already very high (typically >100 dB peakSPL), so maskers have to be presented at levels that can be prohibitive. In addition, recovery from masking is relatively slow (Snyder and Schreiner 1985, Verschooten, Robles et al. 2015), a major issue with intraoperative techniques. We have tried numerous other methods to quantify the ANN to low frequency stimuli in animals and CI subjects prior to adopting the modeling method used here. As described in Figure 3.2D, the ANN has inherent asymmetry due to the half-wave rectification of phase-locking in auditory nerve fibers. Thus, the ANN typically contributes a robust 2nd harmonic in the response. This has also been called the 'auditory nerve overlapped waveform' (Lichtenhan, Cooper et al. 2013, Lichtenhan, Hartsock et al. 2014). However, the 2nd harmonic is not a quantitative measure of neural contribution because most of the energy of this waveform is periodic at the stimulus frequency, i.e., in the first harmonic, where it is mixed with the CM. The ANN and CM are produced by independent processes that can have different spatial distributions in the cochlea, which results in highly variable phase relationship between the two signals. Therefore, the proportion of ANN present in the first harmonic cannot be

predicted by the sizes of the higher harmonics alone. Finally, the second harmonic is not entirely ANN, as high stimulus intensities can cause asymmetric and symmetric saturation of the CM which results in even and odd order harmonics as well (Teich, Keilson et al. 1989).

In addition to investigating measurements of each harmonic and the total harmonic distortion, we have used cross-correlation and error measures between the average cycle and a sinusoidal representation of the stimulus, as well as shape distortions in the response such as the form factor, crest factor, and skew. The spectral and time-based approaches both identified features indicative of the ANN in many cases, such as the presence of 2nd harmonic, low correlation with a sinusoid, low form factor, high crest factor, or high skew. While these approaches are not quantitative, in most cases their results agreed with our visual assessment of the waveforms. However, with each measure there were clear false positive and false negatives in terms of identifying the degree of ANN, based on visual examination of the average cycle for distortions indicative of neural activity that has been our 'gold standard' for identifying the presence of ANN. This visual approach is strongly informed by the animal experiments with neurotoxins, where absence of the ANN was indicated by the loss of the distortions except for saturation that can be attributed to the CM.

It was because of these issues that we considered the approach of using an adaptive model which treats the ECochG waveform as the sum of the discrete CM and ANN signals. This approach depends on accuracy of the equations used to estimate the physiological processes, which, we have only partially achieved in this early implementation. Based on our experience up to this point, physiological signals in which the ANN is either very small or exceptionally large relative to the CM are challenging for the model to analyse.

### Basis of the Model: The CM

The CM was modeled as a sinusoid with parameters of peak and trough saturation. A benefit of this method is that it does it requires no a priori knowledge or assumptions about the shape of the function or operating point – the proportion of open channels in hair cell stereocilia in the absence of sound stimulation. In a population response the

shape of input/output function will be affected by the spatial extent of responding hair cells which will be stimulated at different effective levels according to their distance from the characteristic frequency locus of the stimulation frequency. In addition, the CM will be a mixture of contributions from outer and inner hair cells, which can have different operating points. By using such a simple and hard-edged description we probably underestimate the complexity of the responses produced by hair cells. In particular, responses in gerbils without ANN, either after neurotoxins or to high frequencies before neurotoxins, show what resemble cycle-by-cycle-adaptation to high intensity sounds (Figure 3.10). It is not clear what drives this small decline in response during each cycle in some cases. If such adaptation were present in the model it might reduce some of the response interpreted as ANN that is really CM.

### Basis of the Model: The ANN

The ANN was modeled as the convolution of the UP and CH, and included a parameter to represent the effect of SOE. This convolution procedure is similar to the convolution of the UP and PST histogram that has been used successfully to model the CAP (Goldstein and Kiang 1958, Chertoff 2004) with the cyclic firing to low frequencies in the PST collapsed to produce the CH (Snyder and Schreiner 1984). After piloting a range of frequencies, the UP was ultimately modeled as a single cycle of an 1100 Hz sinusoid. The use of a single cycle is similar to the UP determined from experimental data (Versnel, Schoonhoven et al. 1992), although we have not yet implemented the exact shape they described. A better approximation of the UP is also an improvement to the model that should be implemented. The shape of the CH was modeled as a stretched lognormal probability density equation, with the variable width of the curve ($\sigma$) representing the SOE. These equations represent a version of the underlying processes, and a more accurate description of the actual physiology is likely to be achieved if a biophysically-based model were used (Carney and Yin 1988, Meddis 1988, Meddis, Lecluyse et al. 2013, Zilany, Bruce et al. 2014).

### Results with the Model: Simulated Signals

With simulated waveforms as inputs the model was able to reproduce the values of the parameters across the range encountered physiologically. This simulation was presented in detail to 500 Hz, since that is a frequency where both the CM and ANN can have a wide range of relative values. The features reproduced with the most accuracy were CM amplitude, ANN amplitude, and the phase difference between them. The model reported a small degree of primarily saturation, primarily in the trough, when the ANN amplitude exceeded the CM amplitude. This deviation was accompanied by small deviations in the reported CM and ANN amplitudes. The model was less precise with its estimation of SOE, however, inaccuracies in that parameter did not seem to affect other parameters of the ANN component.

One purpose in using the simulated signals was to assess the effects of phase differences between the ANN and CM on the ECochG waveforms and compare them to the distortions commonly seen in the human and gerbil data. We found that manipulating the phase resulted in a variety of waveforms which closely resembled the physiologic signals we have collected from experiments with the animal model and human CI recipients. The phase relationship also changed the magnitude of the ongoing response, which was at its largest when the two signals were in phase and smallest when out of phase; i.e., there was constructive and destructive interference. This effect has implications for studies of ECochG as a monitoring tool for cochlear trauma during CI surgery. Many of these studies use 500 Hz tones as a stimulus, and some monitor the magnitude of the response, either as an RMS signal (Campbell, Kaicer et al. 2015, Campbell, Kaicer et al. 2016) or as the peak of the spectrum at the stimulus frequency (Koka, Saoji et al. 2016). Because of the expected effect of phase interactions, which was demonstrated here in the model, in the past we (Fitzpatrick, Campbell et al. 2014, McClellan, Formeister et al. 2014, Formeister, McClellan et al. 2015) and others (Dalbert, Sim et al. 2014, Dalbert, Huber et al. 2016) have summed the peaks of the spectrum of the response to each stimulus frequency as the measure of response magnitude. By summing the spectral peaks, rather than calculating their RMS value as would be done to reproduce the time waveform, the contributions of

the distortions to the overall signal are given more weight. While summing rather than squaring the response peaks partially mitigates the effect of phase when assessing the magnitude of the ECochG response, the model offers the possibility of measuring the potentials separately and thus accurately measuring the overall response independent of phase effects.

### Results with the Model: Studies Using Gerbils

The results from the gerbil indicate that the model captures some important features of phase-locking in the auditory nerve across frequency and intensity. It reports a larger CM than ANN, with the major effects of neurotoxins limited to the ANN. In the case of KA we did see some effect of KA on the CM at a few frequency/intensity combinations, but this was not seen with the other neurotoxins. However, the vehicle was also different between the experiments (lactated Ringer's for KA and artificial perilymph for the others) so it hard to know what to attribute this difference to. The proportion of the ANN relative to CM is strongly reduced to high frequencies compared to low, with the cut-off between 1000 and 2000 Hz, consistent with the range where phase-locking in gerbil auditory nerve fibers has the greatest synchrony (Ohlemiller and Siegel 1998, Versteegh, Meenderink et al. 2011). The relationship with intensity is similar to that expected from compression of the ANN relative to the CM, which is that the proportion of ANN is much greater to low intensities compared to high. Thus, the model does identify the major features of phase-locking expected from single unit studies and extrapolated to a population response.

The major limitation in the model was the report of substantial ANN in cases where little or no neural responses were expected (e.g. high frequency stimulus, or after treatment with a neurotoxin). Large values of ANN were reported when the CM was large, even if the overall percentage reported was relatively low. To help mitigate this error, we set values of ANN to be zero when the ANN/CM ratio was less than 0.05. There is evidence (Figure 3.10) that the flaw lies in an incomplete modeling of processes which can affect the CM waveform morphology. A promising direction is to allow some adaptation in the response on a cycle-by-cycle basis. The model also struggled with some responses to low frequencies presented at low to moderate intensities - these signals tended to have the largest ANN and produce

highly complex waveforms. While the model accurately identified large ANN amplitude in these cases, the correlations between the input and the model signals tended to be lower than the average, suggesting possible areas of improvement in the implementation of UP, CH and SOE.

Application of KA also resulted in a small decline of the CM signal magnitude to low frequencies (750 and 1000 Hz) and intensities (30 dB SPL), suggesting the neurotoxin affected hair cells, or that the model was incorrectly assigning some of the ANN to the CM prior to KA application. A similar change in the CM did not happen with either TTX or OA. A small effect of KA on the CM has previously been reported in other animal models (Zheng, Wang et al. 1996, Sun, Hashino et al. 2001). In addition, although we have not examined the question in detail, some effect on the CM, either an increase or decrease, can be expected in individual cases due to changes in the efferent system that can affect the operating point of outer hair cells. Such changes are expected once the afferent input is removed, but the direction may vary across cases.

The frequency range of ANN reported by the model is a close match to the range where the ANN was detected in a spectral analysis using some of the same KA data (Forgues, Koehn et al. 2014). It is also similar to the range of the 'auditory nerve overlapped potential,' reported in similar experiments in other species (Lichtenhan, Cooper et al. 2013, Lichtenhan, Hartsock et al. 2014). In contrast to the evoked potential results, single units in gerbils can show phase-locking to frequencies up to 3-4 kHz (Versteegh, Meenderink et al. 2011), as is also reported in other species (Johnson 1980, Weiss and Rose 1988). There are at least two reasons why the ANN in ECochG recordings may have a more limited phase-locking range than the single units. The first is that the ANN may only be detectable over the range of phase-locking where the synchrony is the highest. In gerbils and most species there is a steep decline in the vector strengths of single units beyond about 1000 Hz. The second is that will also be low-pass filtering of the ANN due to the overall UP duration of approximately 1 ms (period of 1000 Hz sinusoid), as previously suggested by Lichtenhan et al. (2013). Due to the UP's relatively long duration, overlapping responses to higher frequency stimuli may reduce the cyclic component in the evoked response.

A main assumption of the model is that the ongoing response consists of only the ANN and CM. This misses at least one known source of cochlear electrical responses – the dendritic current that is produced from the sum of synaptic currents in auditory nerve fiber terminals (Dolan, Xi et al. 1989). Since the dendritic potential is not based on spikes, the correlate of the UP would be the excitatory postsynaptic potentials (EPSP) from transmitter-gated channels. TTX blocks only the action potentials and should not affect these EPSPs, unlike KA which removes the nerve terminal, and OA which prevents further depolarization. This dendritic current is not currently considered in the model. By initial application of TTX followed by KA, the dendritic contribution can be isolated as the difference of the response seen after each compound. Preliminary results from this experiment show the dendritic response to be present but smaller than the spiking component. Future iterations of the model will need to consider both sources of neural contributions to the ongoing response to better account for recorded waveform shapes.

Finally, the model does not include separate functions for inner and outer hair cells. This is reasonable given that the recordings from the round window are the sum of all contributions to the CM, which include both types of hair cells. However, it would be important to know whether the asymmetries are different in the two cell types, which could also be approached pharmacologically in gerbils, as it has in guinea pigs (van Emst, Klis et al. 1995, van Emst, Klis et al. 1996).

## Results with the Model: Human CI Subjects

The results of model analysis of the signals recorded in human CI subjects are encouraging, however, issues similar to those in the animal experiments were present. The reported CM was on average larger than the ANN, by 26 dB on average. This corresponds with our expectation that the ECochG responses in CI subjects are dominated by the CM, which is the reason why the measure of 'total response' (sum of all significant responses to harmonics 1-3 across a range of tone burst frequencies) account for more of the variance in outcomes in adults (>40%, Fitzpatrick, Campbell et al. 2014, McClellan, Formeister et al. 2014) and in older children (>30%, Formeister, McClellan et al. 2015) than does audiometric or biographic data (Lazard, Vincent et al. 2012). That is, the proposed explanation

for correlation of outcomes with a signal dominated by the CM in these studies is that the degree of hair cell survival is a better correlate to 'cochlear health' than is the degree of intact connections with nerve fibers. Here, the CM did not show a low-pass cut-off frequency, consistent with the animal data and basilar membrane movement. Furthermore, it was not correlated with the degree of neural activity determined subjectively, and which was a good fit with the results for ANN, further supporting the view that the CM and ANN in CI subjects do not provide identical information regarding outcomes.

In the population-wide results, as in the gerbil data, the model did not always report a small ANN for cases where the CM/ANN ratio was small; instead, enough ANN was reported for it to scale with the size of the CM. As was discussed with the gerbil results, it may be that the shape of the CM is more complex than a sinusoid with parameters of asymmetric and symmetric saturation, such that any waveform abnormalities beyond those would likely be attributed to the ANN. The importance of this issue is that to the degree the reported ANN is covariant with the CM rather than independent, its value as a predictive measure for speech perception outcomes with the CI recipients is limited.

Unlike gerbils, the phase-locking range in the human auditory nerve is unknown. There are some indications that human phase-locking could go to higher frequencies than found in animal single unit studies (Moore, Glasberg et al. 2006), but the more general view is that the weight of evidence supports a range of up to about 1.5 kHz for strong phase-locking, i.e., similar to other species (Joris and Verschooten 2013). Here we are able to report that the frequency range of the ANN estimated by the model (and seen visually in the average cycle) is similar to that in the gerbil.

A model based on an analytic description of hair cell and neural contributions to the ongoing responses to low frequency tones was used to separate the ECochG signals into their individual components. This analytical tool can help characterize the residual physiology CI recipients, and can be useful in other clinical settings where a description of the cochlear physiology is desirable.

# FIGURES

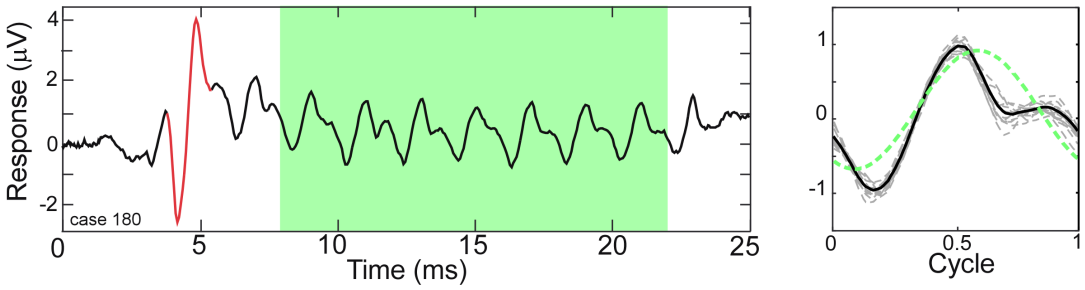


**Figure 3.1 - ECochG response to a tone burst from a human CI subject.**
A. A Human ECochG response to a 500 Hz tone burst presented in condensation phase. The ongoing portion is highlighted (green area). The CAP is shown in red. B. Each cycle in the ongoing response (dashed lines) and the 'average cycle' (solid line). The presence of the ANN causes distortions in the response compared to a reference sinusoid (dotted line).

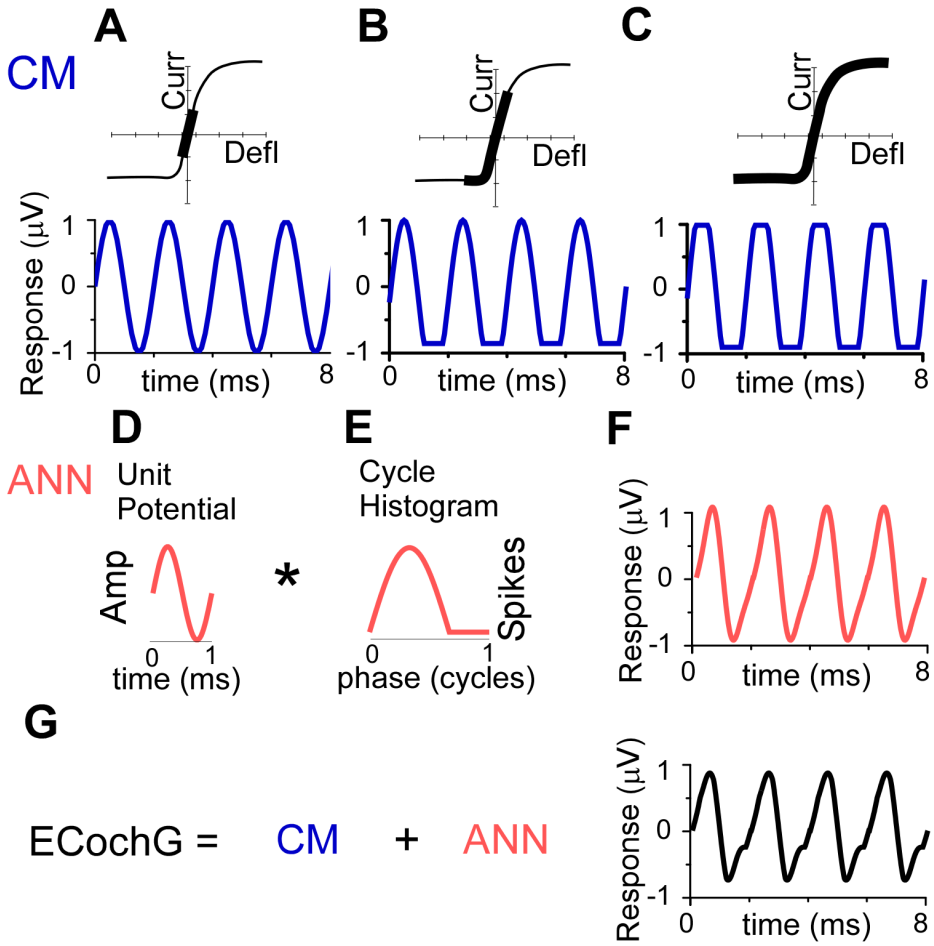


**Figure 3.2 - Conceptual basis of the model**

Conceptual basis of the model for the ongoing part of the ECochG response to low frequency tones. (A-C) The CM. To a low stimulus intensity (A), the hair cell stereociliary motion and channel openings operate symmetrically within the input-output function (top, black bar), producing a sinusoidal CM response (bottom). (B) With increasing stimulus intensity, asymmetric saturation can occur if the operating point (average state of the channels at rest) is displaced from the center of the function (top), producing a CM saturated only to one side of motion, in this case the trough of the CM (bottom). (C) With a high stimulus intensity, symmetric saturation occurs with maximal deflection at both ends of the oscillation (top), creating a CM with saturation to both the peak and trough. (D-F) The ANN is created by the convolution of the unit potential (D) and the population cycle histogram (E). The unit potential is the shape of a single action potential at the round window, and the cycle histogram is the sum of action potential firing in the population of the across all responding nerve fibers. Because the cycle histogram is derived by folding the periods in the post-stimulus time histogram, this process is identical to that previously modeled to produce the CAP (see text for references). The non-linearities inherent in this process will always create a distorted version of the cyclic response (F). (G) The ongoing ECochG represents the sum of the CM and ANN.

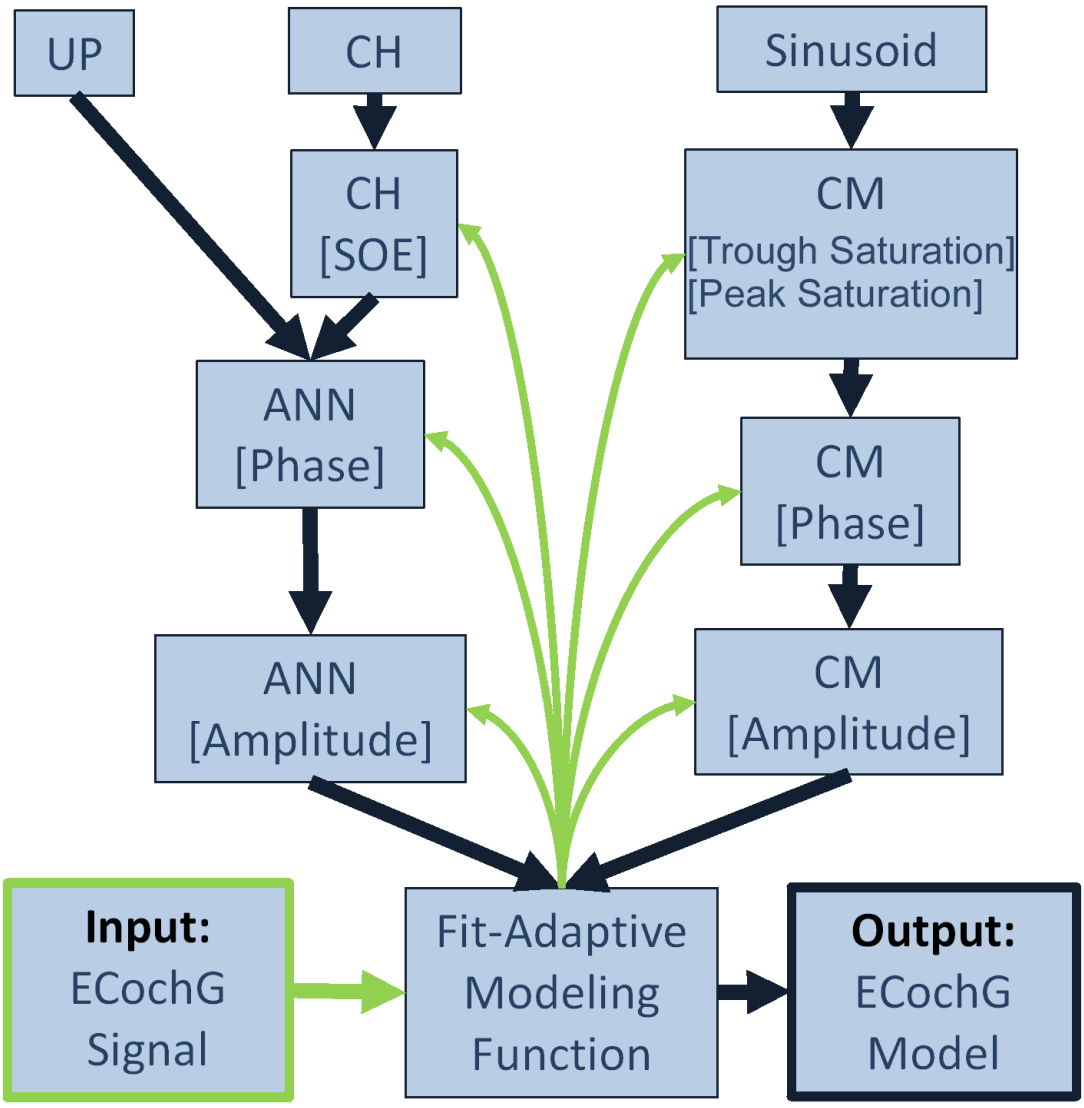


**Figure 3.3 - Block Diagram of Model Parameters**

The ongoing portion of a recorded/input ECochG signal (lower left corner) is the basis for a fit-adaptive modelling function (center, bottom). To estimate the hair cell contribution (right column), the fitting function generates a sinusoidal CM at the stimulus frequency and optimizes the coefficients for amplitude and phase, and saturation of the peaks and troughs of the response. To estimate the neural contribution (left column), a unit potential is convolved with a cycle histogram of variable spread of excitation (SOE) and the resulting ANN amplitude and phase are also optimized. The output of the model is the estimated ongoing ECochG and its associated CM and ANN parameters (lower right corner).

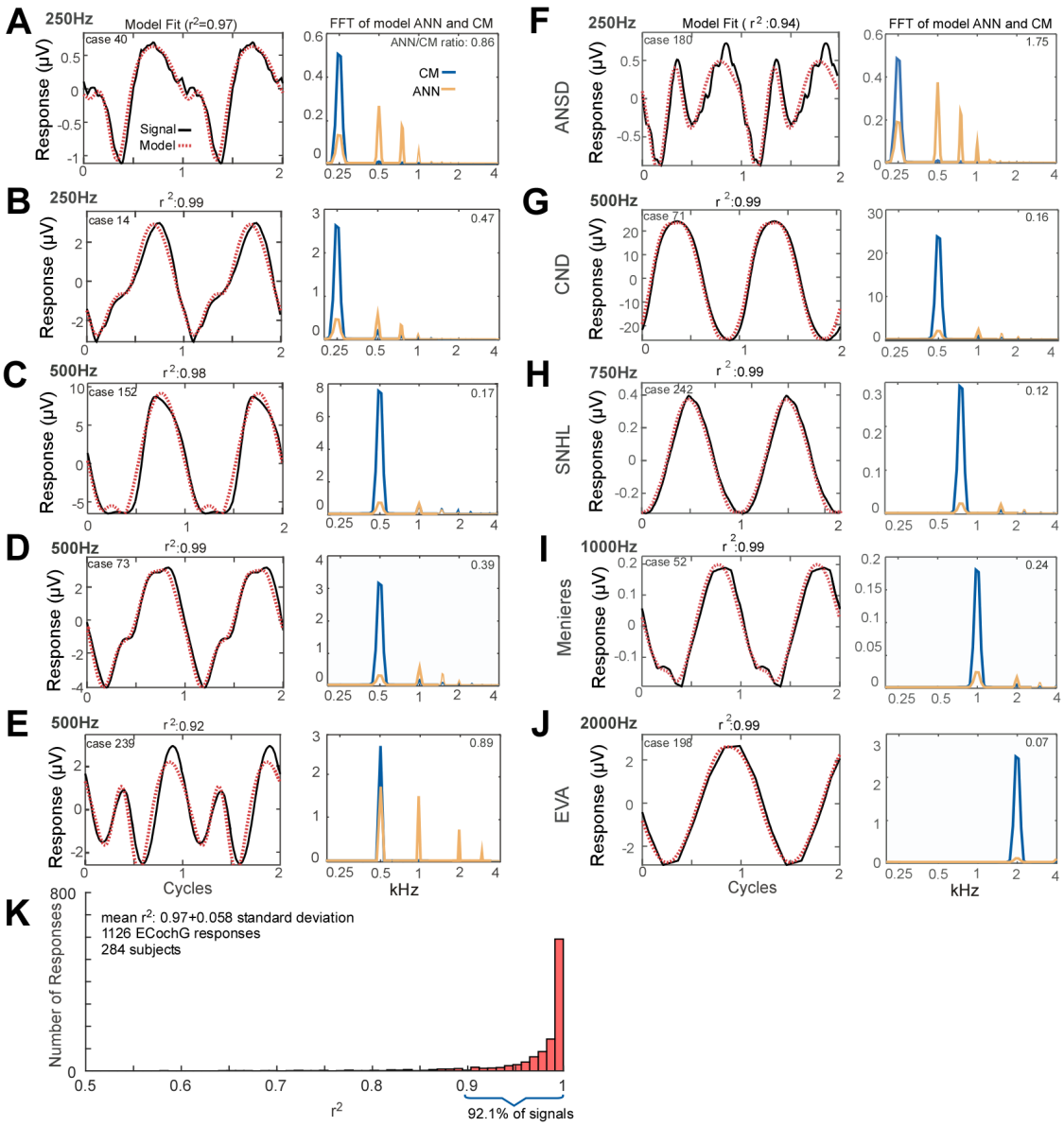


**Figure 3.4 - Model fits to ECochG responses in human subjects.**
(A-E) Responses from different subjects to 250 Hz (A and B) or 500 Hz (C-E) show that the output of the model (left panels, red, dotted line) is able to reproduce the wide variety of waveforms seen in human CI subjects (solid black lines). From the model, the spectra of the CM and ANN used to produce the fit can be produced (right panels). For each case the linear fit between the two curves was described by the $r^2$ value, and the ANN/CM ratio is given for the spectra. (F-J). Similar to the previous examples, except these cases are from subjects with different hearing loss etiologies, to indicate the heterogeneity of causes leading to cochlear implantation (ANSD-auditory nerve spectrum disorder; CND-cochlear nerve deficiency, SNHL- unknown cause of sensineural hearing loss, Meniere's - Meniere's disease, EVA- enlarge vestibular aqueduct). The responses are shown in order of increasing stimulus frequency. The spectrum of the ANN is slightly displaced for clarity. (K) Across all recordings (n=1126) from 284 subjects, the model was able to fit observed ECochG signals with an mean $r^2$ of 0.97 $\pm$ 0.058 (standard deviation).

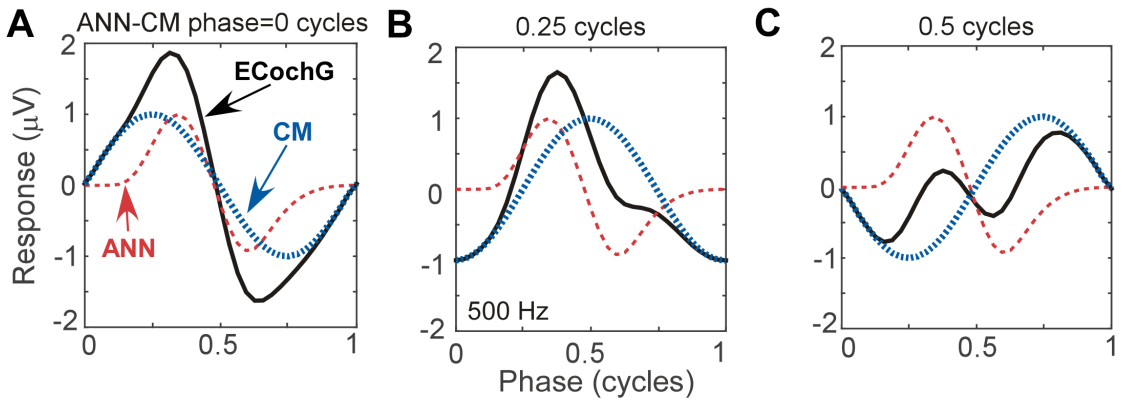


**Figure 3.5 - Waveforms generated using simulated signals varied in phase.** (A) When the CM and ANN are in phase, the waveform is only slightly distorted, and the amplitude is maximal. (B) When the CM and ANN are 1/4 cycle out of phase, the distortion increases. (C) When the CM and ANN are 1/2 cycle out of phase the distortion is even greater and the overall response magnitude is at a minimum.

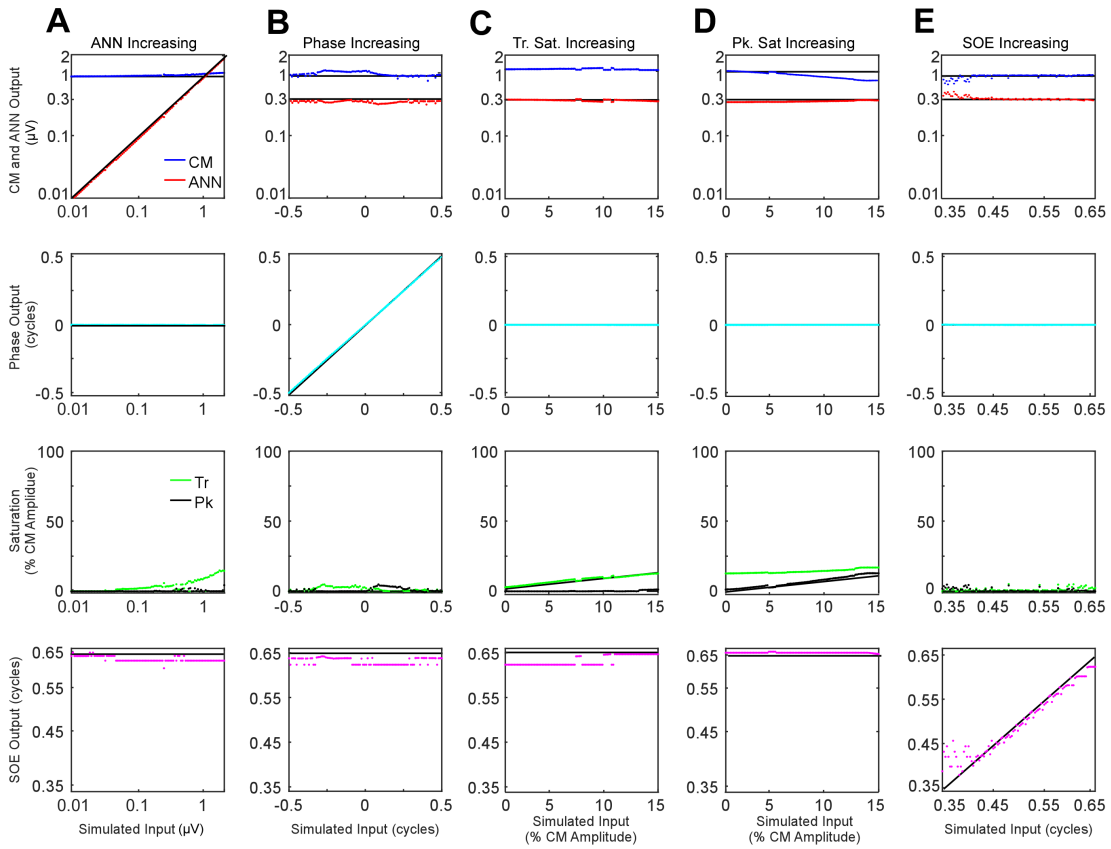


**Figure 3.6 - Parametric examination of model outputs to simulated signals.** The parameter varied is changed along the columns (A-E), and the responses obtained for each parameter is varied by row. (A) The ANN amplitude was gradually increased from 0.01 to 2 $\mu V$ with CM amplitude of 1 $\mu V$, no phase difference between the two signal components or trough or peak saturation, and SOE of 0.65 cycles. (B) The phase difference between the two CM and ANN was gradually increased from -0.5 to 0.5 cycle while CM amplitude was 1 $\mu V$, no trough or peak saturation, and ANN amplitude was 0.3 $\mu V$ with SOE of 0.65 cycle. (C) The trough saturation of the CM component was varied from 0 to 15% of the CM amplitude with no peak saturation, the ANN amplitude was 0.3 $\mu V$ in dB and SOE 0.65 cycles while the phase difference between the two signal components was zero. (D). The degree of peak saturation of CM was varied from zero to approximately 10% of the CM amplitude of 1 $\mu V$ while trough saturation was stable at 15% of the CM amplitude; ANN amplitude was 0.43 $\mu V$ in dB, SOE 0.65 cycles and phase difference between the two components zero. (E) The SOE increased from 0.35 to 0.65 cycles while the CM amplitude was 1 $\mu V$, ANN amplitude was 0.3 $\mu V$ and no trough or peak saturation and the phase difference between these two signal components was zero.

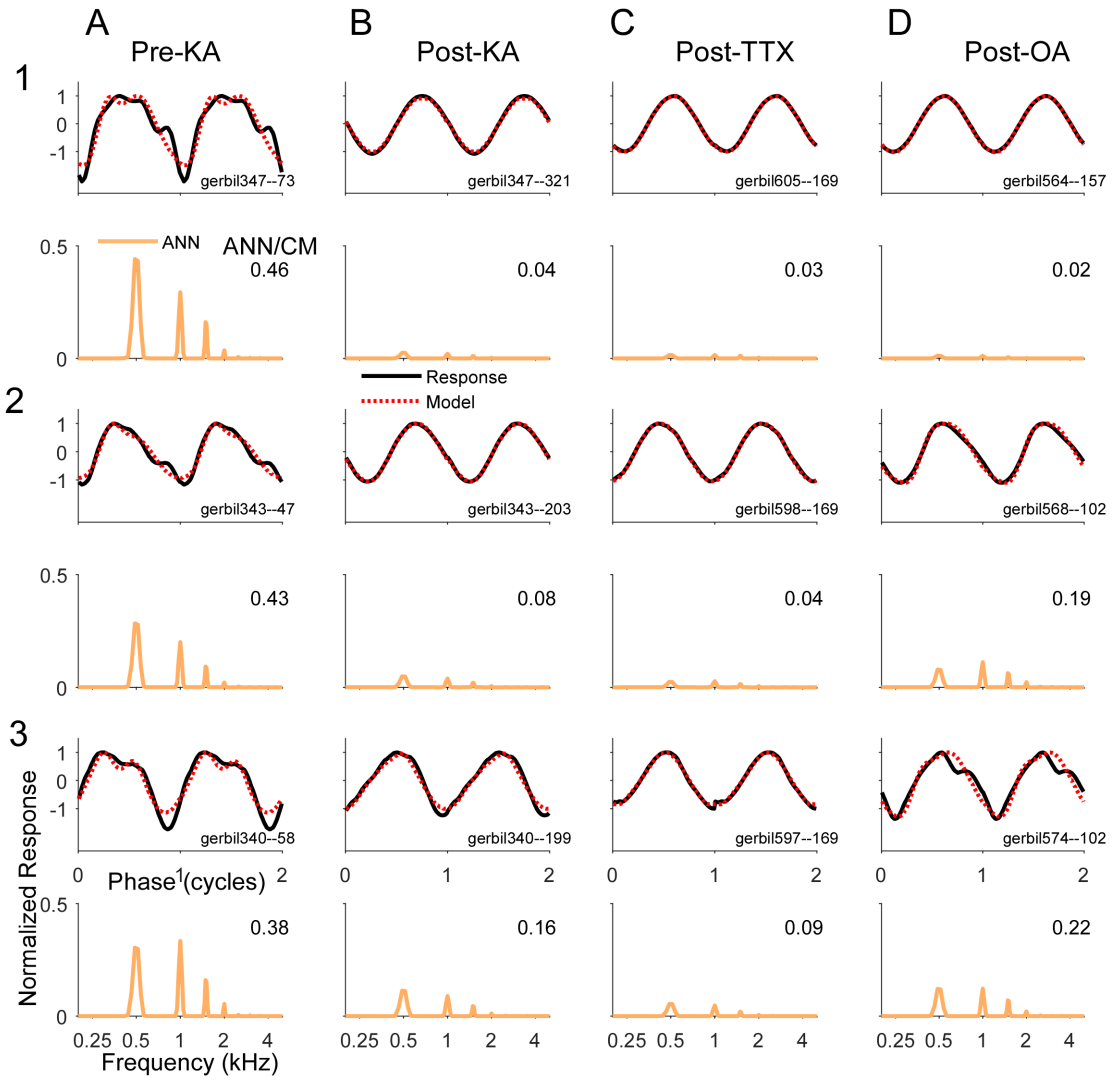


**Figure 3.7 - Examples of waveforms and frequency spectra at 50 dB SPL**
Examples of waveforms and frequency spectra of ECochG signals in response to 500 Hz tone burst at 50 dB SPL (A). Three examples (1-3) recorded prior to KA. The waveforms shown strong distortions and in the ECochG and model waveforms (top panels) and the ANN has multiple harmonics in its spectra (bottom panels). Both sets of data were normalized by the maximum response. The numbers in the spectra represent the ANN/CM ratio. The CM is not shown. (B-D) Three examples each (1-3) recorded after KA, TTX and OA, respectively. The waveforms show less distortion and smaller ANN/CM ratios, although the ANN is not completely removed in most cases. The cases (1-3) are in order of least to most remaining ANN for that drug. The Pre-Drug condition for TTX and OA are not shown, but were similar to that for Pre-KA.

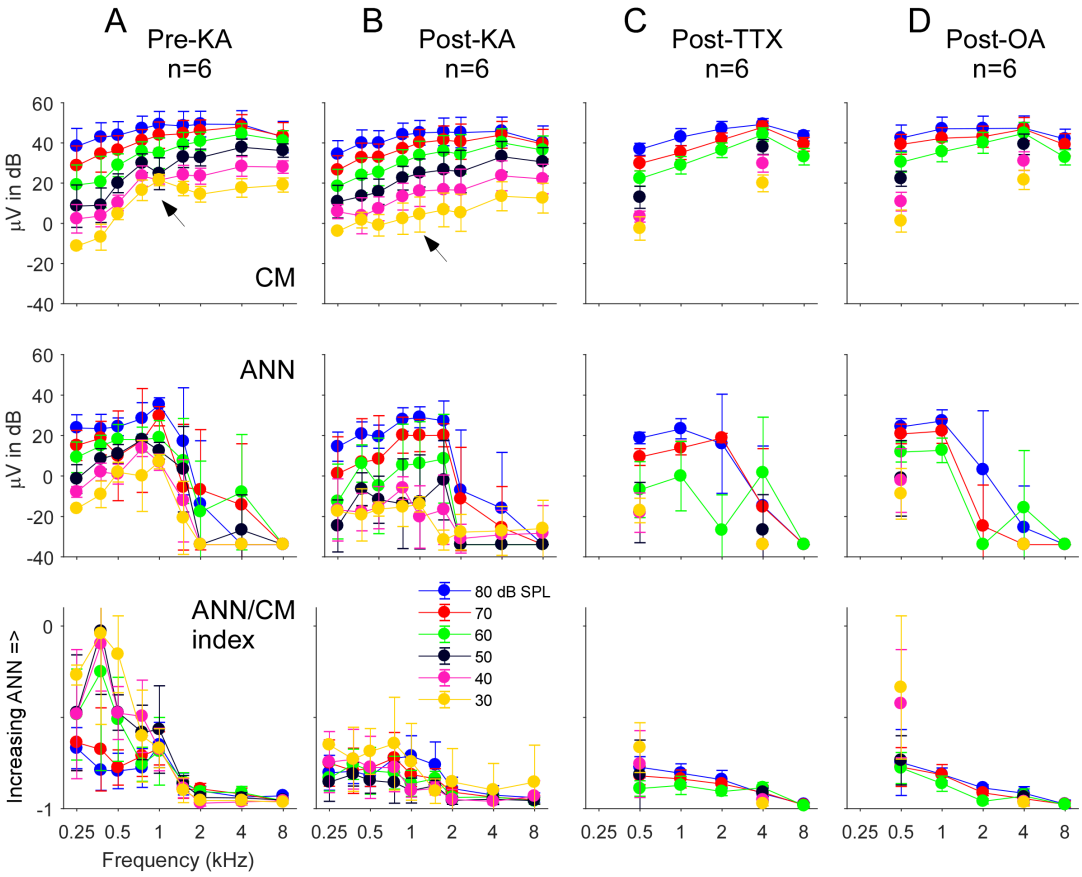


**Figure 3.8 - The CM, ANN and ANN/CM index reported by the model as functions of frequency and intensity**

(A). The Pre-KA condition. The CM shows an orderly pattern of CM across frequency and intensity, with no cut-off to higher frequencies. The arrow represents a small discontinuity to low frequencies (750 and 1000 Hz) and intensities (30-50 dB SPL). The ANN shows a low-pass cut-off to frequencies >1000 Hz. However, a non-linearity was introduced - all responses where the ANN/CM ratio was <5% were considered no response (see Text for further explanation). The ANN/CM index, where no non-linearity was introduced, also showed the low pass cut-off to frequencies >1000 Hz. (B-D). Responses after KA, TTX and OA, respectively. The Pre-Drug condition for TTX and OA are not shown, but were similar to that for Pre-KA. A smaller range of frequencies and intensities was tested with TTX and OA that with KA. In general, the CM was little affected by the neurotoxin. However, the discontinuity seen in the CM was not present after KA (arrow). The ANN/CM index was also reduced to low intensities, but was already small at high intensities so a change was difficult to detect. The reduction in the ANN and ANN/CM index was greater for KA and TTX than OA. Errors bars are standard deviation.

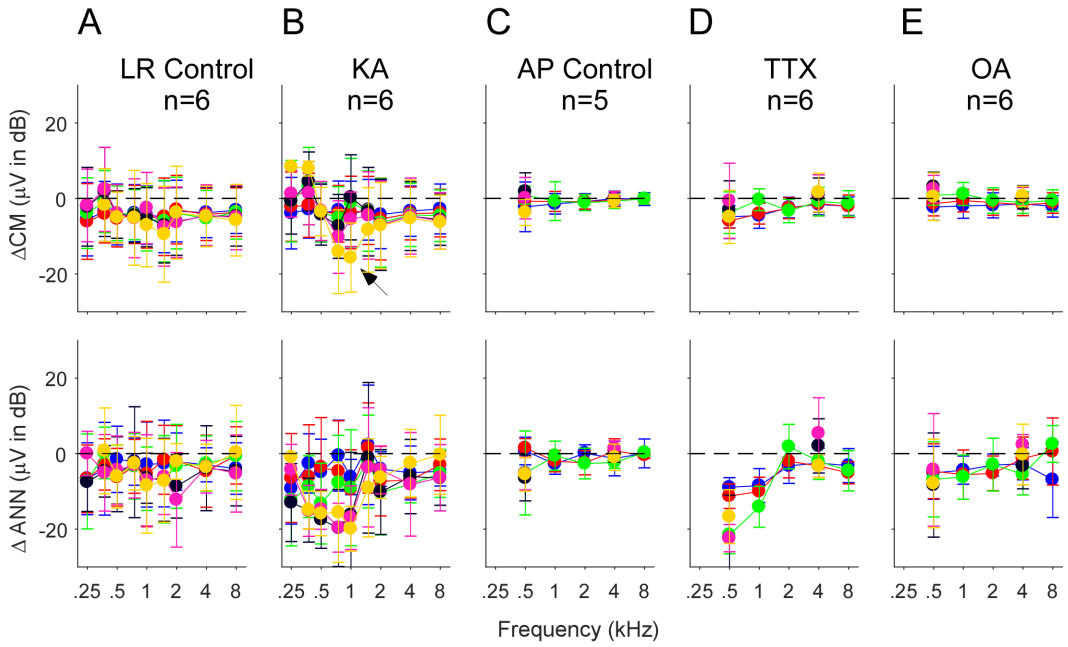


**Figure 3.9 - CM and ANN before and after vehicle or vehicle+neurotoxin**
Difference in the CM (top row) and ANN (bottom row) before and after application of vehicle only or vehicle + neurotoxins. Each subtraction is paired between the Pre and Post data for each animal. (A and C). Control cases where vehicle only was applied to the round window. For the lactated Ringer's (LR) there was a small reduction in both the CM and ANN that could be related to the passage of time (A). For the artificial perilymph (AP), the smaller frequency and intensity range decreased the time between recordings, and the reduction in the CM and ANN was smaller (C). (B, D and E). Responses after KA, TTX and OA, respectively. After KA (B), the reduction in the CM to 750 and 1000 Hz, also shown in the previous figure, was greatest to the lowest intensity (arrow). After TTX (D), the reduction in the ANN was large at 500 and 1000 Hz, and similar to controls the higher frequencies. After OA (E), the reduction to the lower frequencies was smaller than with KA or TTX. Errors bars are standard deviation.

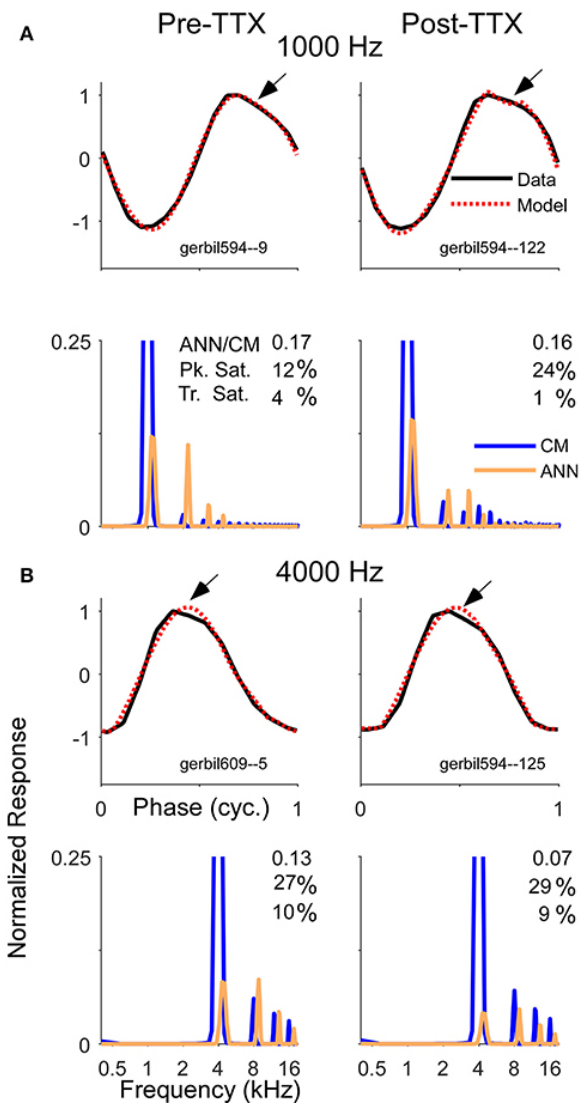


**Figure 3.10 - Average Cycles and Spectra at 80 dB SPL**

Examples of average cycle waveforms and frequency spectra in response to tone bursts at 80 dB SPL. These examples depict a particular type of ECochG response that does not conform to the shapes expected for CM. To the 1000 Hz (A) and 4000 Hz stimuli (B) there was a sloping response to the clipped peak of the average cycle (arrows). To a 1000 Hz stimulus at this sound level the ANN should be a relatively small proportion of the response, and smaller still after TTX. For the 4000 Hz stimulus there should be little or no ANN either before or after TTX. Thus, these waveforms are likely to be nearly-pure CM. The model did capture considerable clipping of the CM, indicated by the large saturation values reported for the peak (Pk. Sat.) and smaller values for the trough (Tr. Sat.). However, the spectrum of each modeled waveform showed considerable ANN even after TTX, suggesting the model interpreted the sloping shape of the CM as ANN. The waveforms and the spectra are normalized to the amplitude of CM contribution measured by the model. The CM of the first harmonic is off-scale to emphasize the higher harmonics, which were present due to the clipping. The spectrum of the ANN is slightly displaced for clarity.

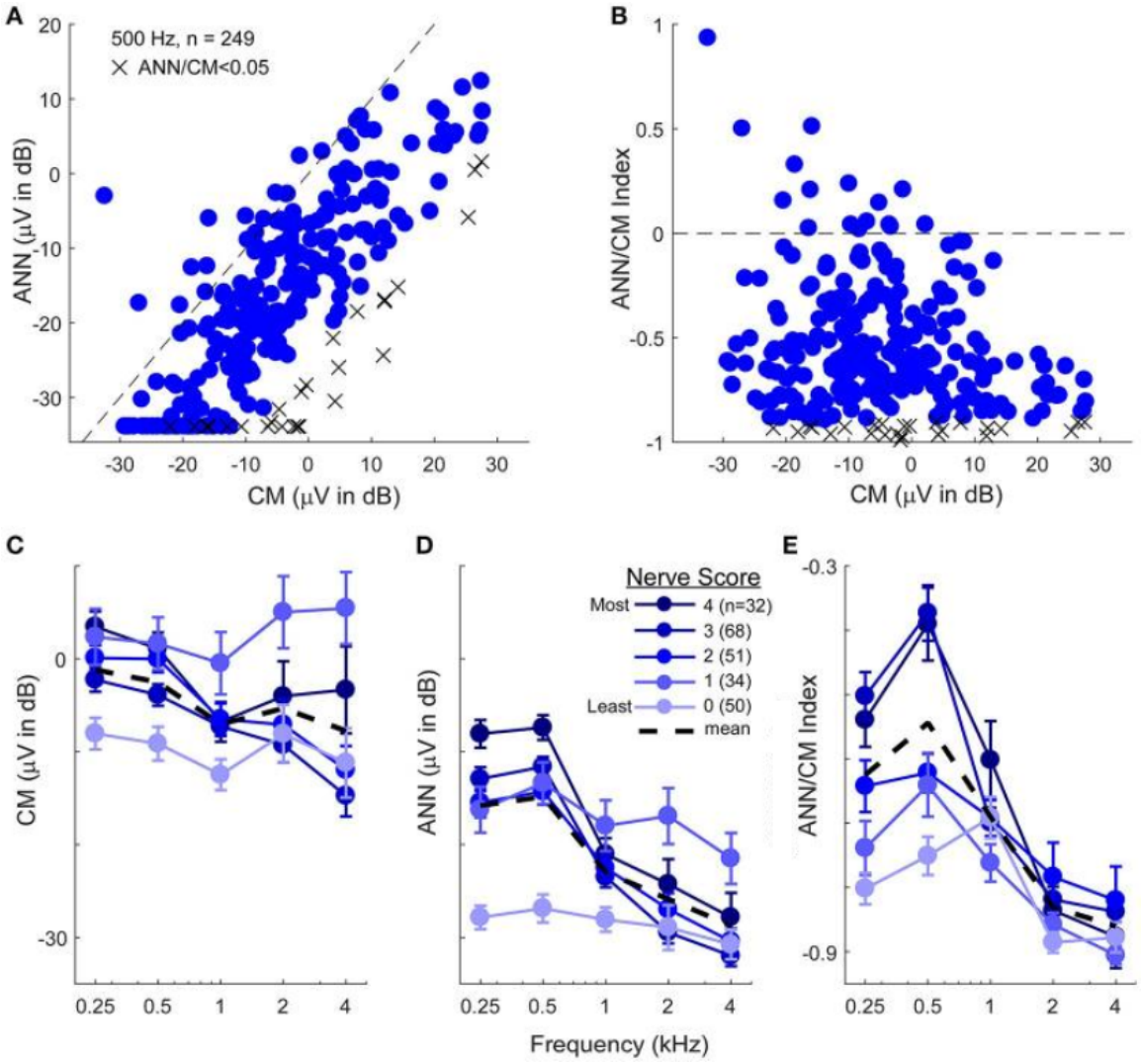


**Figure 3.11 - The CM and ANN in human CI subjects**

(A) In 249 subjects with significant responses (see Methods) to 500 Hz tone bursts at 90 dB HL the ANN amplitude was generally smaller than the CM (below the line of equality, dashed) but the two were positively correlated ($r=0.75$, $p<0.001$). Symbols with an X had an ANN/CM ratio less than 0.05. (B) The ANN/CM index of the same subjects. On this scale an index of -1 is all CM, 0 is equal amount of CM and ANN, and 1 is all ANN. Usually the CM was greater than the ANN, although in a number of cases they were nearly equal, and in a few the ANN was larger than the CM (C-E). The CM (C), ANN (D) and ANN/CM index (D) as a function of frequency and with the parameter of 'nerve score,' which is a subjective scaling of the neural activity in each cases based on visual observation of the CM and ANN. There was no trend for the subjective nerve activity to reflect the size of the CM, in contrast, the size of the ANN and the ANN/CM index reflected the nerve activity. Both also showed low-pass filtering of similar to that in gerbil. The responses included for each frequency had to be significant (see Methods) so the numbers of cases differ by a small amount for 250-1000 Hz (>80% of cases have significant responses to these frequencies) but are fewer to 2 and 4 kHz (43 and 26%, respectively). Errors bars in C-E are standard error.

# REFERENCES


Abbas, P. J., V. D. Tejani, R. A. Scheperle and C. J. Brown (2017). "Using Neural Response Telemetry to Monitor Physiological Responses to Acoustic Stimulation in Hybrid Cochlear Implant Users." Ear Hear 38(4): 409-425.

Adunka, O. F., S. Mlot, T. A. Suberman, A. P. Campbell, J. Surowitz, C. A. Buchman and D. C. Fitzpatrick (2010). "Intracochlear recordings of electrophysiological parameters indicating cochlear damage." Otol Neurotol 31(8): 1233-1241.

Bester, C. W., L. Campbell, A. Dragovic, A. Collins and S. J. O'Leary (2017). "Characterizing Electrocochleography in Cochlear Implant Recipients with Residual Low-Frequency Hearing." Front Neurosci 11: 141.

Calloway, N. H., D. C. Fitzpatrick, A. P. Campbell, C. Iseli, S. Pulver, C. A. Buchman and O. F. Adunka (2014). "Intracochlear electrocochleography during cochlear implantation." Otol Neurotol 35(8): 1451-1457.

Campbell, L., A. Kaicer, R. Briggs and S. O'Leary (2015). "Cochlear response telemetry: intracochlear electrocochleography via cochlear implant neural response telemetry pilot study results." Otol Neurotol 36(3): 399-405.

Campbell, L., A. Kaicer, D. Sly, C. Iseli, B. Wei, R. Briggs and S. O'Leary (2016). "Intraoperative Real-time Cochlear Response Telemetry Predicts Hearing Preservation in Cochlear Implantation." Otol Neurotol 37(4): 332-338.

Carney, L. H. and T. C. Yin (1988). "Temporal coding of resonances by low-frequency auditory nerve fibers: single-fiber responses and a population model." J Neurophysiol 60(5): 1653-1677.

Chertoff, M. E. (2004). "Analytic treatment of the compound action potential: estimating the summed post-stimulus time histogram and unit response." J Acoust Soc Am 116(5): 3022-3030.

Chertoff, M. E., A. M. Kamerer, M. Peppi and J. T. Lichtenhan (2015). "An analysis of cochlear response harmonics: Contribution of neural excitation." J Acoust Soc Am 138(5): 2957-2963.

Choudhury, B., D. C. Fitzpatrick, C. A. Buchman, B. P. Wei, M. T. Dillon, S. He and O. F. Adunka (2012). "Intraoperative round window recordings to acoustic stimuli from cochlear implant patients." Otol Neurotol 33(9): 1507-1515.

Dalbert, A., A. Huber, D. Veraguth, C. Roosli and F. Pfiffner (2016). "Assessment of Cochlear Trauma During Cochlear Implantation Using Electrocochleography and Cone Beam Computed Tomography." Otol Neurotol 37(5): 446-453.

Dalbert, A., J. H. Sim, R. Gerig, F. Pfiffner, C. Roosli and A. Huber (2015). "Correlation of Electrophysiological Properties and Hearing Preservation in Cochlear Implant Patients." Otol Neurotol 36(7): 1172-1180.

Dalbert, A., J. H. Sim and A. M. Huber (2014). "Electrophysiologic Monitoring of Residual Hearing During and After Cochlear Implantation." Association for Research in Otolaryngology Abstracts 37: 317-318.

Dallos, P. (1973). The Auditory Periphery Biophysics and Physiology. New York, Academic Press, Inc.

Davis, H., B. H. Deatherage, D. H. Eldredge and C. A. Smith (1958). "Summating potentials of the cochlea." Am J Physiol 195(2): 251-261.

Dolan, D. F., L. Xi and A. L. Nuttall (1989). "Characterization of an EPSP-like potential recorded remotely from the round window." J Acoust Soc Am 86(6): 2167-2171.

Durrant, J. D., J. Wang, D. L. Ding and R. J. Salvi (1998). "Are inner or outer hair cells the source of summating potentials recorded from the round window?" J Acoust Soc Am 104(1): 370-377.

Fitzpatrick, D. C., A. T. Campbell, B. Choudhury, M. P. Dillon, M. Forgues, C. A. Buchman and O. F. Adunka (2014). "Round window electrocochleography just before cochlear implantation: relationship to word recognition outcomes in adults." Otol Neurotol 35(1): 64-71.

Forgues, M., H. A. Koehn, A. K. Dunnon, S. H. Pulver, C. A. Buchman, O. F. Adunka and D. C. Fitzpatrick (2014). "Distinguishing hair cell from neural potentials recorded at the round window." J Neurophysiol 111(3): 580-593.

Formeister, E. J., J. H. McClellan, W. H. Merwin, 3rd, C. E. Iseli, N. H. Calloway, H. F. Teagle, C. A. Buchman, O. F. Adunka and D. C. Fitzpatrick (2015). "Intraoperative round window electrocochleography and speech perception outcomes in pediatric cochlear implant recipients." Ear Hear 36(2): 249-260.

Gibson, W. P. and H. A. Beagley (1976). "Electrocochleography in the diagnosis of acoustic neuroma." J Laryngol Otol 90(2): 127-139.

Goldstein, M. H. and N. Y. S. Kiang (1958). "Synchrony of neural activity in electric responses evoked by transient acoustic stimuli." J. Acoust. Soc. Am. 30: 107–114.

Harris, D. M. and P. Dallos (1979). "Forward masking of auditory nerve fiber responses." J Neurophysiol 42(4): 1083-1107.

Henry, K. R. (1995). "Auditory nerve neurophonic recorded from the round window of the Mongolian gerbil." Hear Res 90(1-2): 176-184.

Johnson, D. H. (1980). "The relationship between spike rate and synchrony in responses of auditory-nerve fibers to single tones." J Acoust Soc Am 68(4): 1115-1122.

Joris, P. X. and E. Verschooten (2013). "On the limit of neural phase locking to fine structure in humans." Adv Exp Med Biol 787: 101-108.

Kiang, N. Y. S., E. C. Moxon and A. R. Kahn (1976). The relationship of gross potentials recorded from cochlea to single unit activity in the auditory nerve. Electrocochleography. R. J. Ruben, C. Elberling and G. Salomon. Baltimore, University Park Press: 95-115.

Kim, D. O. and C. E. Molnar (1979). "A population study of cochlear nerve fibers: comparison of spatial distributions of average-rate and phase-locking measures of responses to single tones." J Neurophysiol 42(1 Pt 1): 16-30.

Koka, K., A. A. Saoji and L. M. Litvak (2016). "Electrocochleography in Cochlear Implant Recipients With Residual Hearing: Comparison With Audiometric Thresholds." Ear Hear.

Lazard, D. S., C. Vincent, F. Venail, P. Van de Heyning, E. Truy, O. Sterkers, P. H. Skarzynski, H. Skarzynski, K. Schauwers, S. O'Leary, D. Mawman, B. Maat, A. Kleine-Punte, A. M. Huber, K. Green, P. J. Govaerts, B. Fraysse, R. Dowell, N. Dillier, E. Burke, A. Beynon, F. Bergeron, D. Baskent, F. Artieres and P. J. Blamey (2012). "Pre-, per- and postoperative factors affecting performance of postlinguistically deaf adults using cochlear implants: a new conceptual model over time." PLoS One 7(11): e48739.

Liberman, M. C., M. J. Epstein, S. S. Cleveland, H. Wang and S. F. Maison (2016). "Toward a Differential Diagnosis of Hidden Hearing Loss in Humans." PLoS One 11(9): e0162726.

Lichtenhan, J. T., N. P. Cooper and J. J. Guinan, Jr. (2013). "A new auditory threshold estimation technique for low frequencies: proof of concept." Ear Hear 34(1): 42-51.

Lichtenhan, J. T., J. J. Hartsock, R. M. Gill, J. J. Guinan, Jr. and A. N. Salt (2014). "The Auditory Nerve Overlapped Waveform (ANOW) Originates in the Cochlear Apex." J Assoc Res Otolaryngol.

Mandala, M., L. Colletti, G. Tonoli and V. Colletti (2012). "Electrocochleography during cochlear implantation for hearing preservation." Otolaryngol Head Neck Surg 146(5): 774-781.

McClellan, J. H., E. J. Formeister, W. H. Merwin, 3rd, M. T. Dillon, N. Calloway, C. Iseli, C. A. Buchman, D. C. Fitzpatrick and O. F. Adunka (2014). "Round window electrocochleography and speech perception outcomes in adult cochlear implant subjects: comparison with audiometric and biographical information." Otol Neurotol 35(9): e245-252.

Meddis, R. (1988). "Simulation of auditory-neural transduction: further studies." J Acoust Soc Am 83(3): 1056-1063.

Meddis, R., W. Lecluyse, N. R. Clark, T. Jurgens, C. M. Tan, M. R. Panda and G. J. Brown (2013). "A computer model of the auditory periphery and its application to the study of hearing." Adv Exp Med Biol 787: 11-19; discussion 19-20.

Mikulec, A. A., S. K. Plontke, J. J. Hartsock, and A. N. Salt (2009). "Entry of substances into perilymph through the bone of the otic capsule following intratympanic applicatons in guinea pigs: Implications for local drug delivery in humans." Otology & Neurotology 30(2): 131-138.

Moore, B. C., B. R. Glasberg, H. J. Flanagan and J. Adams (2006). "Frequency discrimination of complex tones; assessing the role of component resolvability and temporal fine structure." J Acoust Soc Am 119(1): 480-490.

Ohlemiller, K. K. and J. H. Siegel (1998). "Temporal aspects of the effects of cooling on responses of single auditory nerve fibers." Hear Res 123(1-2): 78-86.

Prijs, V. F. (1986). "Single-unit response at the round window of the guinea pig." Hear Res 21(2): 127-133.

Radeloff, A., W. Shehata-Dieler, A. Scherzed, K. Rak, W. Harnisch, R. Hagen and R. Mlynski (2012). "Intraoperative monitoring using cochlear microphonics in cochlear implant patients with residual hearing." Otol Neurotol 33(3): 348-354.

Ramamoorthy, S., N. V. Deo and K. Grosh (2007). "A mechano-electro-acoustical model for the cochlea: response to acoustic stimuli." J Acoust Soc Am 121(5 Pt1): 2758-2773.

Rance, G. and A. Starr (2015). "Pathophysiological mechanisms and functional hearing consequences of auditory neuropathy." Brain 138(Pt 11): 3141-3158.

Riggs, W. J., J. R. Roche , C. K. Giardina, M. S. Harris, Z. J. Bastian, T. E. Fontenot, C. A. Buchman, K. D. Brown, O. F. Adunka and D. C. Fitzpatrick (2017). Intraoperative Electrocochleographic Characteristics of Auditory Neuropathy Spectrum Disorder In Cochlear Implant Subjects. Frontiers in Neuroscience, in press.

Rose, J. E., J. F. Brugge, D. J. Anderson and J. E. Hind (1967). "Phase-locked response to low-frequency tones in single auditory nerve fibers of the squirrel monkey." J Neurophysiol 30(4): 769-793.

Santarelli, R. (2010). "Information from cochlear potentials and genetic mutations helps localize the lesion site in auditory neuropathy." Genome Med 2(12): 91.

Santos-Sacchi, J. (1993). "Harmonics of outer hair cell motility." Biophys J 65(5): 2217-2227.

Schmidt, P. H., J. J. Eggermont and D. W. Odenthal (1974). "Study of meniere's disease by electrocochleography." Acta Otolaryngol Suppl 316: 75-84.

Scott, W. C., C. K. Giardina, A. K. Pappa, T. E. Fontenot, M. L. Anderson, M. T. Dillon, K. D. Brown, H. C. Pillsbury, O. F. Adunka, C. A. Buchman and D. C. Fitzpatrick (2016). "The Compound Action Potential in Subjects Receiving a Cochlear Implant." Otol Neurotol 37(10): 1654-1661.

Sellick, P., R. Patuzzi and D. Robertson (2003). "Primary afferent and cochlear nucleus contributions to extracellular potentials during tone-bursts." Hear Res 176(1-2): 42-58.

Sirjani, D. B., A. N. Salt, R. M. Gill and S. A. Hale (2004). "The influence of transducer operating point on distortion generation in the cochlea." J Acoust Soc Am 115(3): 1219-1229.

Smith, R. L. (1977). "Short-term adaptation in single auditory nerve fibers: some post-stimulatory effects." J Neurophysiol 40(5): 1098-1111.

Snyder, R. L. and C. E. Schreiner (1984). "The auditory neurophonic: basic properties." Hear Res 15(3): 261-280.

Snyder, R. L. and C. E. Schreiner (1985). "Forward masking of the auditory nerve neurophonic (ANN) and the frequency following response (FFR)." Hear Res 20(1): 45-62.

Sparacino, G., S. Milani, V. Magnavita and E. Arslan (2000). "Electrocochleography potentials evoked by condensation and rarefaction clicks independently derived by a new numerical filtering approach." Audiol Neurootol 5(5): 276-291.

Sun, H., E. Hashino, D. L. Ding and R. J. Salvi (2001). "Reversible and irreversible damage to cochlear afferent neurons by kainic acid excitotoxicity." J Comp Neurol 430(2): 172-181.

Teich, M. C., S. E. Keilson and S. M. Khanna (1989). "Rectification Models in Cochlear Transduction." Acta Oto-Laryngologica: 235-240.

van Emst, M. G., S. F. Klis and G. F. Smoorenburg (1995). "Tetraethylammonium effects on cochlear potentials in the guinea pig." Hear Res 88(1-2): 27-35.

van Emst, M. G., S. F. Klis and G. F. Smoorenburg (1996). "4-Aminopyridine effects on summating potentials in the guinea pig." Hear Res 102(1-2): 70-80.

Verschooten, E. and P. X. Joris (2014). "Estimation of neural phase locking from stimulus-evoked potentials." J Assoc Res Otolaryngol 15(5): 767-787.

Verschooten, E., L. Robles and P. X. Joris (2015). "Assessment of the limits of neural phase-locking using mass potentials." J Neurosci 35(5): 2255-2268.

Versnel, H., V. F. Prijs and R. Schoonhoven (1992). "Round-window recorded potential of single-fibre discharge (unit response) in normal and noise-damaged cochleas." Hear Res 59(2): 157-170.

Versnel, H., R. Schoonhoven and V. F. Prijs (1992). "Single-fibre and whole-nerve responses to clicks as a function of sound intensity in the guinea pig." Hear Res 59(2): 138-156.

Versteegh, C. P., S. W. Meenderink and M. van der Heijden (2011). "Response Characteristics in the Apex of the Gerbil Cochlea Studied Through Auditory Nerve Recordings." J Assoc Res Otolaryngol.

Weiss, T. F. and C. Rose (1988). "A comparison of synchronization filters in different auditory receptor organs." Hear Res 33(2): 175-179.

Zheng, X. Y., D. L. Ding, S. L. McFadden and D. Henderson (1997). "Evidence that inner hair cells are the major source of cochlear summating potentials." Hear Res 113(1-2): 76-88.

Zheng, X. Y., J. Wang, R. J. Salvi and D. Henderson (1996). "Effects of kainic acid on the cochlear potentials and distortion product otoacoustic emissions in chinchilla." Hear Res 95(1-2): 161-167.

Zilany, M. S., I. C. Bruce and L. H. Carney (2014). "Updated parameters and expanded simulation options for a model of the auditory periphery." J Acoust Soc Am 135(1): 283-286.

# CHAPTER 4: INTRACOCHLEAR ECOCHG[1]

## Overview

Electrocochleography (ECochG) obtained through a cochlear implant (CI) is increasingly being tested as an intraoperative monitor during implantation with the goal of reducing trauma during insertion, preserving residual hearing, and improving speech perception. The purpose of this study was to characterize intracochlear ECochG responses to sound throughout insertion in a range of array types and, when applicable, relate these intraoperative measures to postoperative hearing preservation. The ECochG signal in CI subjects is complex, consisting of hair cell and neural generators with differing distributions depending on the etiology and history of hearing loss. Consequently, a focus was to observe and characterize response changes as an electrode advances. In 36 human subjects, responses to 90 dB nHL tone bursts were recorded both at the round window (RW) and then through the apical contact of the CI as the array advanced into the cochlea. The specific intracochlear recording setup used a sterile clip in the surgical field, attached to the ground of the implant with a software-controlled short to the apical contact. The end of the clip was then connected to standard audiometric recording equipment. The stimulus used during insertion was 500 Hz tone bursts at 90 dB nHL. Audiometry for cases with intended hearing preservation (12 subjects) were correlated with intraoperative recordings. Successful intracochlear recordings were obtained in 28 subjects. For the eight unsuccessful cases, the clip introduced excessive line noise which saturated the amplifier. Among the successful subjects, the initial intracochlear response was a median 5.8 dB larger than the response at the RW. Throughout insertion, modiolar arrays showed median response drops

[1]modified from: *Giardina, C. K, K. A. Brown, O. F. Adunka, C. A. Buchman, K. A. Hutson, H. C. Pillsbury, and D. C. Fitzpatrick (2018). "Intracochlear Electrocochleography: Response Patterns during Cochlear Implantation and Hearing Preservation." Ear and Hearing (accepted)*

after stylet removal while in lateral wall arrays the maximal median response magnitude was typically at the deepest insertion depth. Across all array types, four main patterns of response magnitude were seen: increases >5 dB (12/28) or steady responses within 5 dB (4/28), or drops >5 dB (from the initial response) occurring early (< 15 mm deep, 7/28), or later in the insertion (5/28). Hearing preservation, defined as <80 dB threshold at 250 Hz, was obtained in 9/12 subjects. In these subjects, an intracochlear loss of response magnitude afforded a prediction model with poor sensitivity and specificity, which improved when phase, latency and proportion of neural components was considered. The change in hearing thresholds across cases was significantly correlated with various measures of the absolute magnitudes of response, including RW response, starting response, maximal response, and final responses (p's<0.05, min of 0.0001 for the maximal response, all r's > 0.57, max of 0.80 for the maximal response). Monitoring the cochlea with intracochlear ECochG during CI is feasible and patterns of response vary by device type. Changes in magnitude alone during a track did not account for hearing preservation rates, but considerations of phase, latency and neural contribution can help to interpret the changes seen and improve sensitivity and specificity. The correlation between the absolute magnitude of the ECochG and the hearing threshold changes suggest that 'cochlear health,' which varies by subject, plays an important role.

## Introduction

Minimizing cochlear trauma during insertion of a cochlear implant array could improve speech perception outcomes and help preserve residual hearing when it is present. Surgical techniques have been implemented to minimize intra-insertion trauma including the use of shorter, lateral wall arrays and round window (RW) insertions rather than drilling cochleostomies (Adunka, Pillsbury et al. 2009). Despite these attempts, greater than 50% of subjects lose at least 10 dB in hearing across frequencies, presumably due to intraoperative trauma to the basilar membrane and/or postoperative fibrosis (Jurawitz, Büchner et al. 2014, Santa Maria, Gluth et al. 2014, Kamakura and Nadol 2016, O'Connell, Holder et al. 2017). Objective measures to detect and ideally avoid insertion trauma are an area of

current exploration, but one technique showing promise is electrocochleography (ECochG). As a surrogate for basilar membrane (BM) integrity, a working hypothesis by our group and others is that a reduction in physiological responses from the cochlea in response to sound during CI insertion could signify acute trauma leading to loss of residual hearing and/or poor speech perception outcomes (Dalbert, Sim et al. 2014, Adunka, Giardina et al. 2015, Dalbert, Sim et al. 2015, Dalbert, Huber et al. 2016). ECochG responses can be acquired throughout CI insertion at either an extracochlear site (Mandala, Colletti et al. 2012, Radeloff, Shehata-Dieler et al. 2012, Dalbert, Pfiffner et al. 2018, Giardina, Khan et al. 2018) or from an intracochlear site through the apical array contact as it is inserted (Calloway, Fitzpatrick et al. 2014, Campbell, Kaicer et al. 2015, Acharya, Tavora-Vieira et al. 2016, Campbell, Kaicer et al. 2016, Campbell, Bester et al. 2017, Harris, Riggs et al. 2017, Harris, Riggs et al. 2017, O'Connell, Holder et al. 2017). We recently compared and evaluated extracochlear recording sites for this purpose (Giardina, Khan et al. 2018) and here are considering the strengths and weakness of intracochlear recordings. In particular, we describe the response patterns for three different array types, and comment on a variety of intraoperative metrics that could be useful to account for hearing preservation or loss.

Studies in animals support the possibility that ECochG can be used to detect acute trauma during insertion. Using a rigid intracochlear electrode designed to penetrate the basilar membrane, and verified histologically, drops in the response magnitudes to tones occurred that did not recover when the electrode was withdrawn (Adunka, Mlot et al. 2010, Choudhury, Adunka et al. 2011, Ahmad, Choudhury et al. 2012). However, when a flexible electrode was used, drops in ECochG response magnitude could be reversible when the electrode was withdrawn, and in these cases histological examination verified that basilar membrane integrity was maintained (Demason, Choudhury et al. 2012). The most sensitive metric was a drop in the ongoing response magnitude to a tone, containing the cochlear microphonic (CM) and auditory nerve neurophonic (ANN), rather than changes in the compound action potential (CAP). In a study using animals with high-pass noise induced hearing loss, intended to mimic the condition of many CI subjects who have a high-frequency sloping hearing loss, trauma in the basal regions was found to affect the

magnitude of a response to low frequency tones whose responses elements are located far apically (Choudhury, Adunka et al. 2011). Thus, the results of these animal studies indicated that 1) the CM was a more sensitive detector of trauma than the CAP, 2) responses from all parts of the cochlea could be obtained even if the generators, i.e. those neural and hair cell elements responsive to sound, were restricted to the apical region, and 3) reductions in response magnitudes to intense sound were a sensitive measure of interactions between an inserted array and cochlear tissues. Recent studies with normal-hearing animals demonstrate responses to higher frequency stimuli can also help elucidate basilar membrane trauma (Lo, Bester et al. 2017). Additionally, in human CI subjects with large degrees of high frequency hearing loss, markers such as CAP amplitude are highly variable and of limited utility in predicting speech outcomes with the implant (Scott, Giardina et al. 2016). As such, the ongoing response magnitude to an intense, low-frequency (500 Hz) tone is the metric most studied with regard to basilar membrane trauma in CI subjects.

There are currently two approaches to intracochlear recording. Both approaches use array contacts as the recording electrodes, but they differ in the means of outside connection to the contact and subsequent amplification and digitization. In one approach, recordings are digitized by the CI itself, and data are reported directly through the device's telemetry (Acharya, Tavora-Vieira et al. 2016, Campbell, Kaicer et al. 2016, Harris, Riggs et al. 2017, O'Connell, Holder et al. 2017). While familiar to set up, since it uses the same connection to the magnet used for intraoperative impedance testing, data acquisition is limited in terms of available gain, sampling rates and time windows for recording, which affect both the sensitivity and the time required for recordings. The second approach is to use standard audiologic recording equipment that connects directly to the CI, using a clip in the surgical field attached to the device's ground, and software through the CI that creates a connection between the ground and the most-apical contact on the array (Harris, Riggs et al. 2017). For this study we used the clip approach to maximize sensitivity and speed of the recordings.

With either recording approach various response patterns are observed as the array advances deeper into the cochlea. When recording from a modified MED-EL lateral wall array with a direct connection (no processor) to an exposed wire connected to the apical

contact during a temporary insertion, response magnitudes tended to increase with depth, although this increase did not happen in all cases (Calloway, Fitzpatrick et al. 2014). With the Advanced Bionics MidScalar arrays (Harris, Riggs et al. 2017, O'Connell, Holder et al. 2017), responses remained steady, increased, or increased and then decreased with depth. With Cochlear Corporation's Slim Straight (CI422/522) arrays, responses grew immediately, and a late drop in CM amplitude was associated with subsequent hearing loss (Campbell, Kaicer et al. 2016, Campbell, Bester et al. 2017).

The ECochG is a complex signal, and major hurdles remain in determining which parts of the signals and what types of changes indicate that trauma is occurring, and whether these changes in response are array-specific. The purpose of this study was to characterize intracochlear ECochG responses throughout CI insertion in a variety of array types and, when applicable, relate these intraoperative metrics to postoperative hearing preservation.

# Materials and Methods

## Subjects and Inclusion Criteria

A primary goal was to assess intracochlear responses across a broad range of recipients and device types, so inclusion criteria allowed CI recipients of any age, deafness etiology, and audiometric hearing status to participate. To this end, 36 subjects receiving CIs were enrolled, which included 5 adults, 18 children aged 2-18 years old, and 13 children under 2 years of age (Table 4.1). Twelve subjects had some degree of pre-operative hearing, and were more likely to receive lateral wall arrays, as is described below in the section on audiology. Software to use the clip recording system was available for Cochlear Corporation or Advanced Bionics arrays. Patients were excluded if they required an English interpreter, had anatomic malformations or if the procedure was a revision/replacement. All research was approved by the institution IRB (UNC IRB Protocol No. 05-2616). Consent was obtained for subjects over the age of 18, parental permission was required for subjects under the age of 18, and children aged 7 to 18 were also asked for assent with age-appropriate forms.

## Surgical Approach and Recording Setup at the Round Window

Anesthesia was induced and a foam in-ear insert connected to an Etymotic ER-3b speaker was placed in the ipsilateral external canal for delivery of acoustic stimulation. For recording, reference and common electrodes were adhesive surface electrodes placed on the contralateral mastoid and forehead, respectively. A transmastoid facial-recess approach was then performed by surgeons to expose the round window niche. Acoustic stimuli were delivered and evoked responses recorded with the Bio-logic Navigator Pro (Natus Medical Inc., San Carlos, CA). For preliminary recordings before implantation, a Neurosign monopolar electrode (Neurosign Surgical Inc. Part 3602-00, Carmarthenshire, UK) was placed within the RW niche and served as the active recording input. Acoustic stimuli were alternating polarity tone bursts (250 Hz, 500 Hz, 750 Hz, 1 kHz, 2 kHz, 4 kHz) at 90 dB nHL. Tone bursts were shaped by a Blackman window and had a rise/fall length of one cycle or 1 ms, whichever was longer, and plateau lengths of 20 cycles or 20 ms, whichever was longer. Stimuli were presented at 17.3 Hz and digitized at a sample rate of 16 kHz except for the 4 kHz stimuli, which was presented at 23.3 Hz and digitized at a sample rate of 48 kHz. The amplifier gain was 50,000x and the bandpass filter was set from 10 Hz to 5 kHz for all stimuli except 4 kHz, which had a bandpass upper limit of 10 kHz.

## Recording through the CI with the clip during Insertion

The monopolar electrode was then removed from the field and the CI processor was seated under the temporalis muscle. With a sterile ultrasound drape, a telemetry magnet was placed over the skin above the processor and a laptop established a connection with the implanted device. Software provided allowed the array's apical contact to be shorted to the extracochlear cylindrical ground rod (Cochlear Corporation ECE1 contact) or ground ring (Advanced Bionics IE1 contact). In both approaches, the software ultimately created a direct electrical connection between the deepest (apical) array contact and the BioLogic recording device through the clip connection which was electrically isolated from the surgical field. For the CI512 device, the array was inserted through a cochleostomy whereas the CI522 and AB MidScala devices were advanced through the RW.

Using the set-up described above, responses to a 500 Hz tone at 90 dB nHL were collected throughout all stages of CI insertion, and the associated insertion depth for each recording was reported orally by the surgeons. In this way, response 'tracks', or magnitude changes throughout insertion, could be plotted as a function of insertion depth. The tones were delivered at 500 Hz and 90 dB nHL, with a rise/fall time of 1 ms, presented at a 17.3 Hz stimulus rate. While the stimuli was the same as that presented at the round window, line noise when recording through the clip necessitated lowering the gain to 20,000x and narrowing the cutoffs of the band-pass filter to frequencies between 300 Hz and 5 kHz.

### ECochG Signal Analysis

Recordings at the RW and through the intracochlear clip system were exported to MATLAB (MathWorks, Natick, MA) and analyzed postoperatively. Responses were windowed with a Blackman function to isolate the ongoing portion, typically from 7 to 23 ms, and the response magnitude of the averaged waveform was calculated as the sum of spectral peaks at the fundamental stimulus frequency and the next two harmonics with significant peaks. A response peak was considered significant when its amplitude was at least 3 standard deviations above the noise floor, which was computed from the average FFT magnitude of the 3 frequency bins adjacent to the stimulus frequency. As described previously, the ongoing portion to a low frequency (like 500 Hz) can contain both the cochlear microphonic (CM) and auditory-nerve neurophonic (ANN) (Forgues, Koehn et al. 2014, McClellan, Formeister et al. 2014, Fontenot, Giardina et al. 2017) so distortions producing multiple, large spectral peaks in the responses to single tones were common. In addition to the spectrum of the ongoing response, the 'average cycle,' or average across all condensation and rarefaction (shifted in time to match the condensation) phase cycles in the ongoing response, was examined for evidence of the ANN. Animal studies using neurotoxins have identified distortions due to the ANN in the average cycle that are not always detectable in the spectrum (Fontenot, Giardina et al. 2017, Riggs, Roche et al. 2017). At the RW prior to insertion, the 'Total Response' (TR) is the sum of individual response magnitudes to 250 Hz, 500 Hz, 750 Hz, 1 kHz, 2 kHz, and 4 kHz at 90 dB nHL (Fitzpatrick, Campbell et al. 2014, McClellan, Formeister et al. 2014). Throughout CI insertion, response tracks are sequential

responses to a 500 Hz, 90 dB nHL tone. Depending on signal to noise, 50 to 500 averages were collected per evoked response.

### Audiometry

As standard of care, all subjects had unaided audiometric thresholds evaluated prior to implantation to determine residual hearing status and aid in device selection. Most subjects (n=24/36) were conventional implant candidates where preserving residual hearing was not a goal and mainly received the modiolar CI512 array to maximize electric hearing (n=20/24), the AB MidScala array (n=3/24), and in one case the lateral wall CI522 (n=1/24). The 12 subjects where preoperative hearing was sufficient to preserve (typically HL at 250 Hz <= 80 dB HL) received CI422/522 arrays (n=10/12) or AB MidScala arrays (n=2/12). In these subjects, post-operative audiometry was performed at the time of activation (median 1 month after surgery); in 3 cases the first audiometric evaluation was at around 3-6 months, and in 3 cases hearing thresholds improved around the 3 month mark (compared to thresholds at activation) so these thresholds were used as their post-operative HL instead. Hearing was considered preserved if post-operative HL at 250 Hz was < 80 dB HL and the low frequency pure-tone average (LF-PTA, average of 125 Hz, 250 Hz, 500 Hz, and 1 kHz) was also < 80 dB HL.

## Results

Thirty-six subjects were enrolled in the current study (Table 4.1). The study included both children (n= 31) and adults (n=5) with a variety of etiologies. Most of the devices were from Cochlear Corporation (n=31) with the others from Advanced Bionics (n=5).

### Round Window responses and Intracochlear Recordings through the Clip

The first experimental measurements were responses recorded at the RW using the Neurosign electrode and responses were above the noise floor in almost all subjects (n=35/36). Recording through the CI using the clip method was then attempted in all subjects. These intracochlear recordings were successful in 28/36 cases (25 Cochlear Corporation and 3

Advanced Bionics). In 8 cases, AC power-associated noise (60 Hz in the USA) that saturated the recording amplifier precluding successful recordings (6 Cochlear Corporation and 2 Advanced Bionics). Three of these were early cases where the recording amplifier settings were the same as at the RW, which prompted us to lower the gain and narrow the filter settings to better deal with the noise through the clip. To investigate whether there was a RW signal cutoff which would predict whether intracochlear signals could be measured, the ECochG-TR for subjects with significant intracochlear responses were compared with those subjects without intracochlear responses, and also to the overall distribution of subjects in our database (Fig 4.1). The cases where intracochlear responses failed to reach significance were on the lower end of the ECochG-TR distribution, but there was no clear magnitude cutoff where a low RW response would preclude the possibility of obtaining successful intracochlear recordings. The TR of the cases successfully recorded (red) spanned the range of our University of North Carolina population database, and the means of the distributions were not significantly different (t-test, $5.1 \pm 15.5$ dB vs. $0.5 \pm 18.9$ dB, t=1.42, df=42, p=0.17).

Examples of intracochlear response waveforms collected in 3 subjects are displayed in Fig. 4.2. With Cochlear Corporation's software, a trigger artifact is seen prior to sound onset (0 ms) and recovery from the artifact extends into the early response to the sound (Fig 4.2A and 4.2B, top rows). Because this trigger pulse was always of the same polarity, it was largely eliminated in the ECochG difference waveform (Fig. 4.2A and 4.2B, middle row) but present in the summed response (Fig. 4.2A and 4.2B, bottom row). In addition to the onset pulse, the clip set-up was also sensitive to AC noise, and evoked responses could be seen riding on top of slower 60 Hz waves in some cases (Fig. 4.2B, top and bottom rows) which in the USA have a characteristic signal period of 16.7 ms. No trigger artifact occurs with the Advanced Bionics software (Fig 4.2C, top row).

The differences between the RW and intracochlear responses, taken at the initial entrance of the electrode into the cochlea, are shown in Fig. 4.3. This initial recording location was typically 2.7 mm inside the RW but could be as far as 7 mm. This distance was largely device dependent: in the case of the CI512 it was difficult to get multiple response points before it came off the stylet, as a smooth motion is critical for proper modiolar placement.

In most cases (n=18/28) the intracochlear response magnitude was at least 2 dB larger than the response at the RW (example case in Fig. 4.3A), but the two responses could also be of similar magnitude (n=3, example case in Fig. 4.3B) or even demonstrate a 2 dB smaller response inside the cochlea than the response previously recorded at the RW (n=7, example case in Fig. 4.3C). Across all the 28 subjects with successful recordings (Fig. 4.3D, circles), the initial intracochlear responses were a median 5.8 dB larger than those at the RW, similar to previous reports (Calloway, Fitzpatrick et al. 2014), and the values were positively correlated with those obtained from the RW response ($r^2$ = 0.51, Fig. 4.3D, dashed line).

## Changes in Response during CI Insertion

In cases where detectable responses were seen through the clip system, recording continued throughout all stages of CI insertion. In an example case with a CI522 array (Fig 4.4) response waveforms were taken at 5 points throughout a slow, continuous insertion (Fig. 4.4A, demonstrating the difference curves), and the associated response magnitudes at each insertion depth are plotted as a 'track' (Fig. 4.4B). The '0 mm insertion depth' marks the first response just inside the cochlea. In this case, the response began around 12 dB (re 1 $\mu V$) and grew to a maximum 29.6 dB around an insertion depth of 24 mm, and further advancement of the array to its final insertion depth of 25 mm was associated with a 0.5 dB drop in response magnitude.

Response tracks for all subjects are overlaid by array type in Fig. 4.5. In the top row, response change (in dB) from the interpolated response at 1 mm is plotted for each track. The bottom row shows the median change (in linear units) with semi interquartile ranges (line and grey bars, respectively) for all responses. For the 14 cases with the modiolar hugging CI512 array (Fig. 4.5A), a few showed large increases early in the insertion (top row) while some showed only small or no increases in response. On average, the median response (Fig. 4.5A, bottom) grew as the array was inserted through the cochleostomy, reached a maximum (white arrow) near 14.2 mm, and then dropped prior to the end. This depth corresponds to when the array was advanced off the stylet and began coiling towards the modiolus. In the 11 subjects who received CI422/522 lateral wall arrays (Fig 4.5B), the responses either grew or stayed relatively steady; there were no large drops (top row). This

array does not have a stylet and is not precoiled, and the median response (bottom row) was steady until a rise at the end, so that the maximal median response was at the full insertion depth of 25 mm (white arrow). The depth of maximal median response differed significantly between these two array types (Wilcoxon rank-sum test, U=17.3, p=0.001), but the magnitude achieved at these depths did not differ (Wilcoxon rank-sum test, U=64, p=0.49). In the 3 subjects that received Advanced Bionics MidScala devices with successful insertion tracks (Fig. 4.5C), one increased early in the insertion, then dropped but recovered, another stayed relatively steady during the insertion, and the third showed a response drop early that then remained steady (Fig. 4.5C, top row). The median track showed a decline, but with only 3 cases the effect of each case was large, and this decline on average was caused by just one case (Fig 4.5C, bottom row). Taken as a whole, the individual tracks and the trends in median response demonstrate that there is substantial variability in intracochlear response patterns by both device type (modioloar vs. lateral wall) and manufacturer.

It is reasonable to assume that a response drop indicates some mechanical interaction between the electrode and responding elements that might indicate burgeoning cochlear trauma. However, an example (Fig. 4.6) indicates that a response drop can also be caused by interactions between different sources that produce the ongoing responses. In this case, the response magnitude dropped by nearly 10 dB and then recovered to within 3 dB of the starting value (Fig. 4.6A). Because the CI's apical contact was moving deeper into the cochlea during this process, this shifting recording site was biased by immediately-adjacent generators. Hair cell and neural sources responding to the same stimulus frequency can constructively or destructively interfere depending on the relative strength and phase difference between them (Forgues, Koehn et al. 2014, McClellan, Formeister et al. 2014, Fontenot, Giardina et al. 2017). Evidence that this process is occurring can be seen through changes in phase, spectrum and latency. The phase changes are shown in the 'average cycles' Figs. 4.6B-D, left, see Methods). The response (solid lines) and the best-fit sinusoids simulating the stimulus (dashed lines) show phase shifts, which are greater than 1 cycle across these points. The spectrum of the ongoing response also changed, with more second harmonic in the bottom spectrum panel (Fig. 4.6D, arrow). This increase of the second

harmonic could be interpreted as an increase in neural activity in the form of the ANN, but an examination of the average cycle reveals distortions that are consistent with neural activity in all three curves (Riggs, Roche et al. 2017). In addition, since the ANN is periodic with the low frequency stimulus, some energy, usually most, will appear in the first harmonic (500 Hz). The first harmonic is largest in the top panel, but instead of indicating little nerve it is more likely that most of the ANN is appearing in the first harmonic in this waveform configuration. Thus, both hair cell and neural sources can overlap differently at different positions within the cochlea, producing changing patterns in both amplitude and phase as the array advances. Finally, the entire response shows a latency shift of 2.57 ms over this time frame (Fig. 4.6E), consistent with the phase change seen in the average cycle, and giving a direction to them. Thus, changes in the way different generators of the cochlea are interacting at different locations is the most likely source of the observed drop in magnitude, rather than trauma.

## Patterns of Response Tracks During Insertion and Rates of Hearing Preservation

Demographics and hearing outcomes for the 12 subjects where hearing preservation was an intended goal are listed in Table 4.2. With the definition of hearing preservation as threshold <80 dB at 250 Hz, hearing was preserved in 9/12 subjects, while in 3 subjects hearing loss was immediately apparent at the first post-operative visit.

A goal of this study was to analyze tracks and observe features that might be related to atraumatic vs. traumatic insertions. To this end, we first hypothesized that a response track with an increase or stable level throughout insertion likely meant no or minimal trauma, whereas a drop in response could mean trauma. We first used a 5 dB cutoff to categorize response tracks into one of four groups- an overall growth in response, a steady response, an early drop in response, or a late drop in response (Fig. 4.7). We separated the early and late drops because we recently found that a drop in extracochlear response which occurred early in the insertion process (< 15 mm) was likely to demonstrate some level of response recovery, whereas a drop which occurred deeper than this was likely to be permanent (Giardina, Khan et al. 2018). Specifically, the track categories were defined by

an overall (start to finish) response increase >5 dB during the insertion (n=12, Fig. 4.7A), steady responses within 5 dB throughout insertion (n=4, Fig. 4.7B), tracks with an early drop (>5 dB from the starting value before 15 mm) in response during insertion (n=7, Fig. 4.7C), and those with a late drop (after 15 mm) in response during insertion (n=5, Fig. 4.7D). Tracks are colored blue if hearing was preserved, red if hearing was lost, and black for subjects where hearing preservation was not intended and therefore not measured.

We expected that tracks in the "growth" and "steady" categories (n=16/28) would indicate atraumatic insertions, and that the latter "early drop" and 'late drop" categories (n=12/28) could indicate trauma. Six of the 9 cases with hearing preserved resided in the growth/stable categories (Fig. 4.7A,B), but 3 of the 9 were in the early drop category (Fig. 4.7C). In the 3 subjects who lost hearing, 2 showed overall gains in response (Fig. 4.7A), while one showed a late drop (Fig. 4.7D). In summary, the increase/steady ECochG categories included 66% of the hearing preserved cases but also 66% of the hearing lost cases, and the two ECochG response loss categories included 33% of the hearing preserved cases and 33% of the hearing loss cases. These results imply that an overall change in ECochG magnitude, on its own, does not detect all trauma that occurs, and that response drops >5 dB can occur without a profound loss in hearing.

A more thorough analysis of the waveforms can help explain why some magnitude drops were likely not associated with trauma – i.e. why blue tracks where hearing was preserved were found in response drop categories (Fig. 4.7C), and also why some cases did not show a drop along the track as large as 5 dB but still lost hearing (Fig. 4.7A, red). Earlier in Fig. 4.6, a large, but reversible response drop was attributed to a changing phase relationship between hair cells and neuronal sources (CM and ANN, respectively) interfering destructively as the array advanced. This case illustrated case was actually one of the three in the "early drop" category (Fig. 4.7C), which had preserved hearing. A second case in this category also demonstrated this phase-shifting phenomenon, and also had preserved hearing. Figure 4.8 shows the third case with preserved hearing from the early drop category (Fig. 4.8, left panels A-C), and its waveforms, alongside another case with preserved hearing that was in the steady growth category (Fig 4.8, right panels D-F). In the first subject of Fig. 4.8 (left, A-C) the waveforms reveal another apparent interaction

between CM and ANN, this time without a change in phase. In this track, the response dropped by about 10 dB between 6 and 11 mm of insertion depth (Fig. 4.8A). Before the change, the average cycle shows a large, nearly-sinusoidal response with a peak in the best-fit sine at 0.15 cycles (Fig. 4.8B). At the next insertion depth (Fig. 4.8C), the response became more distorted (Fig 4.8B,C arrows), which is a sign of a changing proportion of neural and hair cell generators (Riggs, Roche et al. 2017), but the phase of the best-fit sine only shifted to 0.12 cycles, a change of 0.03 cycles. Using an algorithm we previously developed to approximate the relative contribution of ANN and CM in each response (Fontenot, Giardina et al. 2017), it was found that the percentage of ANN/CM increased from 9 to 25%. In review, all three cases of hearing preservation which showed a large, early drop in response also demonstrated concurrent shifts in the phase or proportion of ANN/CM, implying again these drops were from shifting sources rather than overt trauma.

Conversely, a response drop that occurs without an associated change in phase or ANN may be a more likely indication of trauma. This result appeared to be the case for each of the three cases that lost hearing. Examination of the two cases that lost hearing in Fig. 4.7A (red tracks) show response drops of less than 5 dB along the track, while the case that lost hearing in Fig. 4.7D has a larger drop. Closer examination of the average cycles in these three cases did not reveal a change in phase, but the signal to noise ratios were low making the use of the average cycle either visually or in the model less reliable. That large drops without indications of shifting sources in the CM and ANN can occur is shown by a case in Fig. 4.8D-F. This case had a large increase in response from start to finish and was placed in the 'steady growth' category in Fig. 4.7A. However, there was a 4.3 dB drop at the end, which was not associated with any change in shape or phase of the average cycle, and the proportion of ANN to CM remained similar between E and F. This therefore represents a case where trauma might have been predicted, but the hearing loss was small, 0 dB at 250 Hz and only 10 dB at 500 Hz (case 471, Table 4.2).To quantify these observations, we constructed contingency tables designed around detecting trauma using ECochG as a predictor of loss of hearing (Fig. 4.9). In the first model (Fig. 4.9A), we used the 5 dB cutoffs from Fig. 4.7 to categorize whether ECochG appeared traumatic. Four cases dropped below 5 dB, but only one of them lost hearing. Conversely, most tracks (8/12)

appeared atraumatic and 6 had preserved hearing. In the contingency table, this 5 dB cutoff afforded a model with only 33% sensitivity and 67% specificity for trauma detection predicting hearing loss. We tested the range of cutoff dB values from 1-20, and the value with the largest average sensitivity/specificity was found when using a 2 dB cutoff (Fig. 4.9B). Using this new cutoff, the sensitivity jumped to 100% - all cases where hearing was not preserved had at least some drops. However, most cases with hearing preservation also had drops, so the specificity was low, only 44%. We then investigated the nature of the drops, under the assumption that drops associated with shifts in phase or composition of the response (ANN) do not necessarily indicate trauma and hearing loss, while drops without such shifts are indicative of trauma (Fig. 4.9C). None of the 3 cases that lost hearing showed such shifts when drops were seen, with the caveat noted above that the S/N ratio in these cases was low. Of the 5 cases with drops where hearing was preserved, four showed clear evidence of shifts in phase or ANN/CM ratio that indicated changing interactions among different sources. The one case that showed no phase or composition changes was illustrated in Fig. 4.8D-F. Thus, with these new criteria, ECochG as a marker to identify hearing loss had a specificity of 89% - while retaining a sensitivity of 100%. In sum, steady increases in ECochG likely indicate there is no trauma occurring, while response drops on their own are an unreliable marker, but analysis of the waveforms may be crucial in deciphering whether trauma is in fact occurring.

### Response Metrics and Changes in Absolute Hearing Thresholds

In addition to the bimodal metric of hearing preserved vs. lost, we further explored the relationship between ECochG magnitude and the amount of audiometric threshold increase at 500 Hz in all hearing preservation subjects (Fig. 4.10). When the tracks were plotted on an absolute scale (Fig 4.10A), the tracks with lower absolute magnitudes were more likely to be associated with hearing loss (red vs. blue). To explore this trend, the initial value, maximal value, and final value from each track (in absolute scale, i.e dB 1 $\mu V$) were then compared to threshold increase. Because multiple comparisons were made from the same observations, a Bonferroni correction was applied to the level of significance such that the necessary alpha needed to reject the null hypothesis became 0.01 instead of

0.05. We found significant or nearly significant correlations between the starting intracochlear magnitude (r= –0.72, p=0.014, Fig. 4.10B), the final intracochlear magnitude (r= –0.79, p=0.002, Fig. 4.10C), and the maximum intracochlear response measured during the insertion (r= –0.80, p=0.002, Fig. 4.10D) with the amount of hearing loss. These results indicate that the absolute degree of hearing loss tends to be greater with those who start with smaller cochlear responses overall. In contrast, the pattern of change in ECochG magnitude was not sufficient on its own to predict which subjects would most likely lose hearing (Fig. 4.10E, red vs. blue) and, as expected from the previously presented results (Fig. 4.9A,B) there was no correlation between the overall change in response magnitude (start to finish) throughout insertion (p=0.61, Fig. 4.10F) or the size of the largest response drop (p=0.32, Fig. 4.10G) and the amount of behavioral hearing loss at 500 Hz.

Given the response magnitude of the tracks was correlated with hearing loss, we then asked whether the response recorded at the RW prior to insertion was similarly correlated. The response magnitude at the RW to 500 Hz was correlated with the amount of hearing loss (r= –0.59, p=0.04, Fig 4.11A), as was the TR (r= –0.61, p=0.03, Fig. 4.11B). These findings demonstrate that the pre-operative health of the cochlea as assessed with RW recordings is an indicator of how much the hearing is likely to change due to surgery – with healthier cochleae incurring smaller losses.

## Discussion

The idea behind using ECochG during insertion of a cochlear implant array is that a change in the cochlear response to sound could be a metric to determine when trauma is impending or actively occurring. To this end, we used intracochlear ECochG to record patterns of response changes during insertion for several array types and used subsequent hearing loss as a metric for trauma in a subset of cases where hearing preservation was a goal. The first finding was that intracochlear response patterns can be partially explained by array type; particularly that stylet removal in modiolar-hugging arrays was associated with a drop in response which was not seen with lateral wall arrays. We then demonstrated that some ECochG response drops could be reversible and likely atraumatic, if the drops

were associated with concurrent changes in phase or distortions indicative of a destructive interference between hair cell and neural generators. In the hearing preservation cases, all cases with monotonically increasing responses demonstrated preserved hearing, while those recordings with any drops included both hearing preserved and hearing lost subjects. There was no magnitude cutoff for these drops that could reliably predict which subjects would lose hearing. However, many of the drops were associated with changes in phase or in the proportion of ANN, indicating changing source relationships rather than trauma could be the cause for the drops. When these factors were taken into account the sensitivity and specificity for detecting loss of hearing was better than measures based on magnitude alone. Additionally, it was found that the absolute size of ECochG response magnitudes, rather than changes in magnitude during the track, was the best predictor of the amount of postoperative threshold shift.

### Technical issues of intracochlear recording

Responses just within the cochlea were typically 5 dB larger than those at the RW, consistent with our previous study (Calloway, Fitzpatrick et al. 2014). However, failures to obtain significant intracochlear responses occurred, and these were usually due to the increased line noise when using the clip recording approach. We have not determined why this noise using the clip is present, compared either with extracochlear recordings or through telemetry from the device. It is likely to be due to a higher impedance pathway between the external amplifier and array contact as the connection is made using the clip and shorting through the device to connect to the external ground. Noise precluded recording in 8 of the 36 subjects, usually early cases in the study until we changed the hi-pass filter to 300 Hz and reduced the gain to avoid saturation of the amplifier. The only previous study with the clip was reported from 2 subjects and successful recordings were achieved both times (Harris, Riggs et al. 2017), however those recordings were made after some early experience with the clip and a passive hi-pass filter was introduced prior to amplification to reduce the noise.

Recording with the clip system has strengths and weaknesses compared to recording through the telemetry. The clip system is an extra step to setup and has the line noise prob-

lem as mentioned, but data acquisition is faster than with telemetry because there is no wireless data transfer step. Additionally, the individual recording windows with telemetry are only 3 ms with the Cochlear Corporation system (Campbell, Kaicer et al. 2015) and 1.7 ms with the MED-EL system (Adel, Rader et al. 2015), so longer responses can only be acquired by collecting separate, shorter recordings at different delays relative to the stimulus and then piecing them together. The AB system does not have this limitation (Harris, Riggs et al. 2017). Additionally, the on-board analog-to-digital converter (ADC) of the CI processor is of much lower resolution than that of standard audiometric hardware (such as the BioLogic) which are specifically designed to detect ECochGs. The telemetry approach was reverse-engineered to measure ECochGs rather than electrically-evoked neural responses. The telemetry approach is, however, simpler to setup and recordings can be made throughout the rest of the surgery and post-operatively (Dalbert, Pfiffner et al. 2015, Koka, Saoji et al. 2017), whereas the clip needs to be removed to complete the surgery.

### Patterns of Response throughout CI Insertion

Recording from the apical contact throughout CI insertion provides a wealth of information regarding the interaction between the array and cochlear structures. For the cases with successful intracochlear recordings throughout insertion, response changes could be partially explained by the array type. For instance, magnitude drops were seen after stylet removal in the CI512's perimodiolar array (Fig. 4.5A, white arrow), a step which allows the array to coil inwards towards the BM, causing mechanical dampening of the BM or even translocation through it – processes which are known to cause response reductions in animal models (Demason, Choudhury et al. 2012, Lo, Bester et al. 2017). Conversely, the CI522 lateral wall array demonstrated on average a relatively steady median response with insertion depth until an increase was seen near the end of insertion. Examples going into this median were a mixture, including some increasing, some flat, and some decreasing. The increase of the median magnitude at deeper insertion depths indicates more consistency across cases as the array approached apical regions. The variety of patterns seen with the CI522 (Fig. 4.5B, top row) differs from previous studies, where the responses in

general were consistently increasing (Campbell, Kaicer et al. 2015, Campbell, Kaicer et al. 2016).

Across all arrays, four major patterns of response were seen: increases in response with insertion depth, steady responses throughout insertion, drops in magnitude early in the insertion, and late drops in magnitude during insertion (Fig. 4.7). We separated the drops into early and late categories and used a 5 dB cutoff because we found drops in extracochlear ECochG beyond 5 dB that occurred in the first 15 mm of insertion were more likely to show some level of response recovery (Giardina, Khan et al. 2018). In the current study, 7 of the 13 recordings with losses greater than 5 dB showed some degree of recovery. These reversible changes are important, because an ongoing hypothesis is that any response drop could indicate trauma.

A reversible change could indicate a physical interaction with the membrane, which isn't necessarily traumatic. It is possible that a drop occurs because the array interacts with the basilar membrane in a temporary, atraumatic way, as the array slides past the first turn. Our categorizing drops as "early" versus a "late" uses a cutoff of 15 mm insertion depth, which is of anatomic significance because it marks the approximate lateral wall depth of the basal turn (Kawano, Seldon et al. 1996, Franke-Trieger and Mürbe 2015). Among the responses with early drops (n=8, Fig. 4.7C), 5 were at least partially reversible (63%) and among the late drops (n=5, Fig. 4.7D), only 2 were partially reversible (40%). This pattern where early drops are more likely to be reversible than late drops is a finding consistent with previous data collected using extracochlear ECochG (Giardina, Khan et al. 2018).

Response drops during insertion can also occur without any mechanical interaction with the BM, because of a changing recording location passing across a region of heterogeneous intracochlear generators. Responses to the 500 Hz tone from different parts of the cochlea can overlap, interfering either constructively or destructively as the array moves through the cochlea, causing changes in the magnitude and phase of the net response (Fig. 4.6). Thus, response decrements at any given position cannot definitively be attributed to trauma. To help overcome this problem, it is first necessary to consider how generators can be distributed at different cochlear regions, and what their effects on the net response

would be at different recording locations. These overlapping responses could come from hair cells (the CM), from the auditory nerve (ANN), or from the interaction between CM and ANN. The CM makes up the bulk of the ECochG response in CI subjects (Fontenot, Giardina et al. 2017) so changes in its sources should have the largest effects. In cases with responses to frequencies higher than 500 Hz, particularly 2 and 4 kHz (as was the case in the subject shown in Fig. 4.6), the CM recorded will include the summed response from two cochlear regions with different properties. One region of generators is the basal segment of the cochlea with CFs higher than the 500 Hz tone, where the traveling wave will pass through quickly and responses to a wide extent of the cochlea will be in phase. The other region is the part of the cochlea near the CF, where the traveling wave slows down and responses occur with a longer latency and rapidly changing phase to allow for maximal BM displacement and tonotopic resolution (Robles and Ruggero 2001). Thus, when the electrode first enters the cochlea, it will "see" the more basal region with in-phase responses, but as the array advances apically through this high frequency region the tip electrode will get increasingly more input from the CF region, which is at a different phase due to the slowing of the traveling wave (van der Heijden and Versteegh 2015, Campbell, Bester et al. 2017). As the proportion of the response from the CF region increases, the phase difference between the base and CF increases, causing sources between these regions to interact destructively ultimately resulting in a drop in the net response. With even further insertion the response increases again as it becomes dominated by the single source, now located deeper in the cochlea, with a longer latency. These different possibilities indicate that it will be necessary to use as much information as is available to accurately interpret reductions in responses as either a changing phase relationship or possible trauma.

### Response Patterns and Hearing Preservation

An initial hypothesis was that increasing or steady responses would indicate an atraumatic insertion, whereas drops in magnitude during insertion would likely indicate immediate insertion trauma. This is the basic metric used in most previous studies. Campbell et al. reported the response track as a binary metric – whether the ongoing response magnitude was preserved or not by the end of insertion, although the criterion for preserva-

tion was not given (Campbell, Kaicer et al. 2016). In 15 hearing-preservation subjects, they found patients with preserved ECochG (n=7) responses at the end of surgery had 15 dB better low-frequency hearing postoperatively than those who demonstrated ECochG losses (n=8) during surgery. This was an early indication that surgical trauma detectable by ECochG could affect hearing preservation. Dalbert, Pfiffner et al. (2018) recorded intracochlear tracks in 3 hearing-preservation subjects and found slowly growing responses associated with hearing preservation in 2 subjects, and a response that grew and then dropped in the third subject – who completely lost hearing. Harris et al. further stratified response tracks into 3 categories – Type A, B, and C (Harris, Riggs et al. 2017). Type A demonstrated an overall increase in amplitude from beginning to end of insertion, analogous to the "CM preserved" category used by Campbell, Kaicer et al. (2017) and our 'overall growth' category. Harris's Type B had a maximal value at the beginning of insertion and drops throughout insertion, similar to our early drop category, and their Type C had a similar response magnitude at the beginning and end, but a maximal response magnitude mid-insertion, similar to the "CM not preserved" category used by Campbell, and our late drop category. While it was hypothesized that subjects in Harris's B and C categories would have incurred trauma, only a few of the 17 subjects in their study had any meaningful preoperative hearing so no conclusions could be drawn regarding track pattern and hearing preservation. Acharya, Tavora-Vieira et al. (2016) recorded intracochlear responses during CI insertion in two pediatric subjects and found the first subject, with stable intracochlear responses, had complete hearing preservation whereas the second subject, with a mild drop in response, had a small degree of hearing loss. O'Connell, Holder et al. (2017) studied intra-insertion ECochG in 13 subjects and utilized post-operative imaging to determine the absolute scalar position, because scalar translocation is associated with hearing loss (Finley, Holden et al. 2008, O'Connell, Hunter et al. 2016). The patterns of response change in the cohort with completely-within-ST insertions were similar in both magnitude and pattern to those insertions which translocated into the SV, implying scalar displacement was not easily recognizable by shifts in magnitude alone. In short, interest in intracochlear ECochG as a predictor of hearing preservation is robust, but groups are coming to differing conclusions regarding which ECochG changes are normal, and which indicate trauma.

As described above, all these previous studies reported only magnitude changes during the insertion. In our hearing preservation sample (n=12), there was no obvious trend between response drop and rates of hearing preservation; drops in response occurred in some subjects with preserved hearing (Fig. 4.7C), and some subjects with increasing or steady responses essentially lost all hearing postoperatively (Fig. 4.7A). A specificity/sensitivity analysis showed little indication that a metric based on magnitude drop with an arbitrary cut-off value (5 dB in this case) would prove useful (Fig. 4.9A), and the best cut-off (2 dB) had 100% sensitivity but only 44% specificity (Fig. 4.9B). In contrast to a sole reliance on magnitudes, a more promising result was obtained when the relationship between magnitude and phase changes was considered - with the sensitivity remaining at 100% but the specificity increasing to 89% (Fig. 4.9C). The one outlier was the case from Fig. 4.7D-F, where a 4.3 dB drop in ECochG was seen, without a clear change in phase or ANN/CM ratio, but hearing was well preserved.

Although not seen in our limited data set, it is also possible that a completely atraumatic insertion is seen on ECochG during insertion, yet near-total loss of hearing occurs post-operatively (Campbell, Kaicer et al. 2016). The mechanism for this would be a foreign body reaction that occurs hours to weeks after implantation (Anderson, Rodriguez et al. 2008), eventually leading to fibrosis and loss of hearing (Jia, Wang et al. 2013). With a larger sample size, we would expect to see more cases with profound hearing loss despite an apparently atraumatic ECochG.

### Implications for using ECochG as a runtime monitor of insertion trauma

In designing a system to monitor cochlear responses and detect trauma, an initial design decision is whether to monitor these responses from within the cochlea (intracochlear recordings) or from a fixed location outside of the cochlea (extracochlear recordings). Each approach has its own benefits, and they provide complementary yet distinct information regarding the state of the cochlea. For a fixed extracochlear electrode, any measured change in response must inherently be due to a change in the cochlea's ability to transduce acoustic energy into electric responses. Models have shown a completely-within-tympani (atraumatic) insertion shouldn't significantly affect BM propagation energy (Greene, Mattingly

et al. 2015), so any extracochlear response change must be the result of a change in intracochlear fluid pressure gradients, basilar membrane displacement pattern, basilar membrane integrity, or a change in the generators themselves. The fixed recording location, often placed near the base, may be biased towards immediately-adjacent (high-CF) generators, but this stability in location minimizes other confounders such as movement artifact that may be important when analyzing intracochlear recordings.

A substantial benefit to intracochlear recordings, compared to extracochlear recordings, are the higher signal to noise ratios, which minimizes the number of responses needed to obtain a significant response and aids in the speed of feedback to surgeons. However, the shift of recording location as the array advances, coupled with different distributions of generator sources due to individual etiologies and histories of hearing loss leading to cochlear implantation, introduces confounders. This report demonstrates that a significant drop in intracochlear response pattern can be hypothesized to be traumatic or atraumatic due to changing relationships to generators as the contact advances. While we had some post-hoc success in accounting for the responses seen in relation to hearing outcomes, the ability to account for the various possible patterns in near-real time would seem to require a priori knowledge of what might be expected in each case. However, there are possible ways to normalize for the pattern seen during a track. One way is to monitor if consecutive contacts after the apical electrode are following the same track as they pass the same region in the cochlea, i.e., that they are observing comparable responses at the same location in the cochlea in all respects (amplitude, phase and ANN/CM composition). Another way would be to monitor responses at the most basal electrode, shifting the contact number as each enters the cochlea. This way would be pseudo-extracochlear in the sense of recording from a stable location, but would gain the benefit of signal to noise from the intracochlear location and requires no separate hardware or software.

## Cochlear Health and Hearing Preservation

A fundamental issue in using intra-operative ECochG tracks to predict hearing loss is that ECochG and hearing ability are related, but not synonymous. Audiometric thresholds are determined by the lowest acoustic intensity needed to stimulate the most sensitive

fibers and elicit an audible precept (Musiek and Baran 2007) and thus relies on complete connections between hair cells and the auditory nerve. In contrast, the ECochG response is dominated by hair cell rather than neural activity, and the two are not strongly related (Riggs, Roche et al. 2017). Our finding that the overall size of the ECochG response is related to hearing preservation suggests that 'cochlear health', measured at the RW or an intracochlear site, is an important factor. This trend was seen across various indicators of response magnitude, both from the round window prior to insertion and when taken during the track. It may be that cochleae with larger responses are more resistant to post-insertion intracochlear inflammatory damage, retaining more complete connections between inner hair cells and auditory nerve fibers. We are not aware that this possible indicator of hearing preservation has been previously considered. It may be necessary to use overall magnitudes, in addition to track changes, to characterize each cochlea.

# TABLES

Table 4.1: Patient Demographics

| Characteristic | Count | % Total (Approx.) |
|---|---|---|
| Sex | | |
| Female | 21 | 58% |
| Male | 15 | 42% |
| Age at Implantation | | |
| 0 ≤ 2 yr old | 13 | 36% |
| 3 ≤ 5 yr old | 9 | 25% |
| 6 ≤ 18 yr old | 9 | 25% |
| 18 ≤ 72 yr old | 5 | 14% |
| SNHL Etiology | | |
| ANSD | 8 | 22% |
| Autoimmune | 1 | 3% |
| *CLDN14* mutation | 2 | 6% |
| CMV | 2 | 6% |
| Connexin 26 (*GJB2*) mutation | 2 | 6% |
| EVA | 2 | 6% |
| *TECTA* mutation | 2 | 6% |
| Trauma | 1 | 3% |
| Unknown | 16 | 44% |
| Implanted Side | | |
| Left | 17 | 47% |
| Right | 19 | 53% |
| Device | | |
| Advanced Bionics MidScala | 5 | 14% |
| Cochlear 512 | 20 | 56% |
| Cochlear 422/522 | 11 | 31% |

**Table 4.1 - Intracochlear Subject Demographics**

Patient Demographics. Thirty-six subjects were enrolled in the study, with slightly more women than men. The age at implantation ranged from 9 months to 72 years of age. Sensorineural hearing loss etiologies include auditory neuropathy spectrum disorder (ANSD), genetic causes, and trauma, but most subjects had an unknown etiology. Implant sides were represented roughly equally and devices used include the AB MidScala, and Cochlear Corporation's CI512, and CI422/522 arrays.

Table 4.2: Hearing Preservation

| | | | | | HL at 250 Hz (dB HL) | | HL at 500 Hz (dB HL) | | LF PTA (dB HL) | | |
|---|---|---|---|---|---|---|---|---|---|---|---|
| Subject | ID | Age/Sex | Etiology | Device | Pre-operative | Post-operative | Pre-operative | Post-operative | Pre-operative | Post-operative | HP Category |
| 1 | 270 | 62 F | Unknown | CI 422 | 45.0 | 80.0 | 55.0 | 90.0 | 52.5 | 83.7 | Loss |
| 2 | 297 | 4 M | ANSD | CI 422 | 10.0 | 20.0 | 55.0 | 55.0 | 53.3 | 53.6 | Preserved |
| 3 | 335 | 1 F | ANSD | AB MidScala | N/A | N/A | 80.0 | 80.0 | 81.7 | 79.8 | Preserved |
| 4 | 368 | 5 F | *CLDN14* | CI 522 | 25.0 | 30.0 | 50.0 | 60.0 | 56.7 | 52.6 | Preserved |
| 5 | 379 | 13 M | Unknown | CI 522 | 15.0 | 25.0 | 25.0 | 45.0 | 36.7 | 48.3 | Preserved |
| 6 | 391 | 2 M | ANSD | CI 522 | 60.0 | 60.0 | 60.0 | 60.0 | 70.0 | 68.8 | Preserved |
| 7 | 414 | 14 M | EVA | CI 522 | 55.0 | 80.0 | 60.0 | 80.0 | 62.5 | 81.8 | Loss |
| 8 | 416 | 14 F | Unknown | CI 522 | 30.0 | 90.0 | 50.0 | 105.0 | 47.5 | 90.4 | Loss |
| 9 | 447 | 5 F | *CLDN14* | CI 522 | 15.0 | 20.0 | 45.0 | 70.0 | 42.5 | 61.8 | Preserved |
| 10 | 466 | 3 M | ANSD | CI 522 | 55.0 | 55.0 | 55.0 | 50.0 | 67.5 | 66.7 | Preserved |
| 11 | 471 | 14 F | Hypoxia | CI 522 | 15.0 | 15.0 | 50.0 | 60.0 | 31.3 | 43.4 | Preserved |
| 12 | 476 | 11 F | Unknown | CI 522 | 60.0 | 70.0 | 75.0 | 80.0 | 67.5 | 77.5 | Preserved |

**Table 4.2 - Intracochlear ECochG and Hearing Preservation Rates**
Candidates for hearing preservation arrays and surgical consideration were when behavioral thresholds at 250 Hz were <80 dB HL, and the low-frequency pure tone average (LF PTA), at 125 Hz, 250 Hz, 500 Hz, and 1 kHz, was also <80 dB HL. Post-operative hearing was taken within the first 3 months of implant activation and hearing was categorized as preserved if unaided thresholds remained <80 dB for both 250 Hz and the LFPTA.

# FIGURES

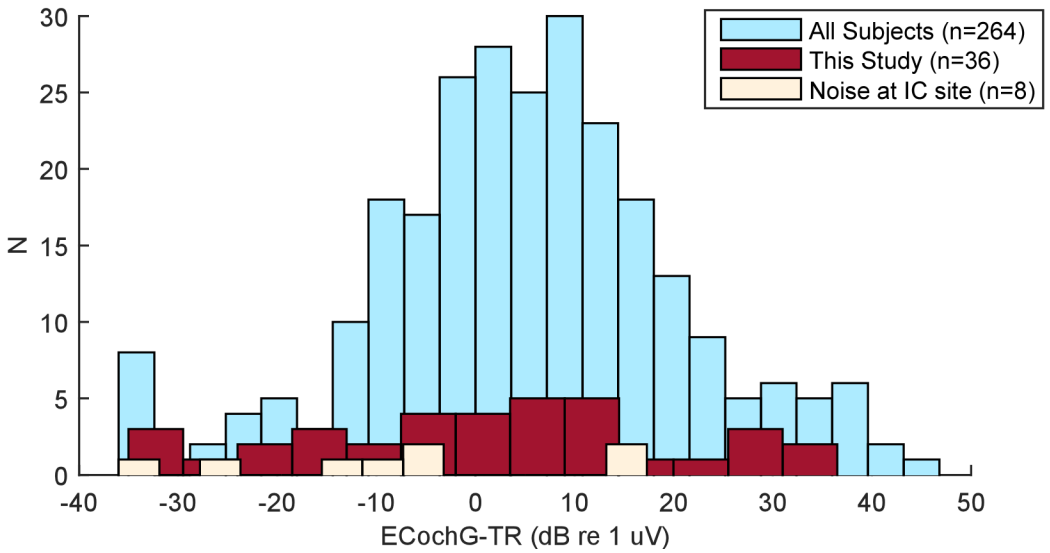


**Figure 4.1 - Distribution of ECochG-TR**

Distribution of Total Response (ECochG-TR, see methods) from round window electrocochleography just prior to insertion. The distribution of TRs across subjects in this study (red) was not significantly different from the distribution in our larger database (teal). Noise when recording at the intracochlear site precluded recordings in 8 subjects, and while these subjects had smaller RW responses (beige), there wasn't a clear RW magnitude cutoff which would predict whether intracochlear recordings would be feasible. *note:* uV $= \mu V$

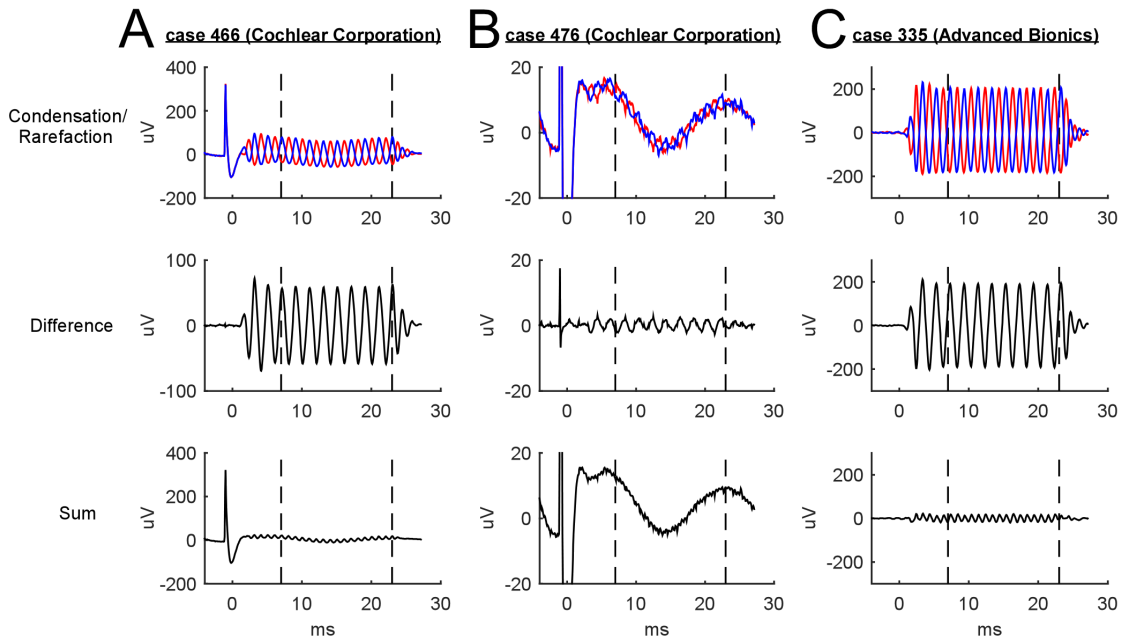


**Figure 4.2 - Intracochlear Waveforms**

Example waveforms when recording through the intracochlear clip system. (A) A trigger artifact can be seen when using Cochlear Corporation's software. (B) For smaller responses, the clip system is also sensitive to line noise (typically 60 Hz). (C) In Advanced Bionics arrays, there is no trigger artifact but 60 Hz noise can be seen (though not in this case). *note:* uV $= \mu V$

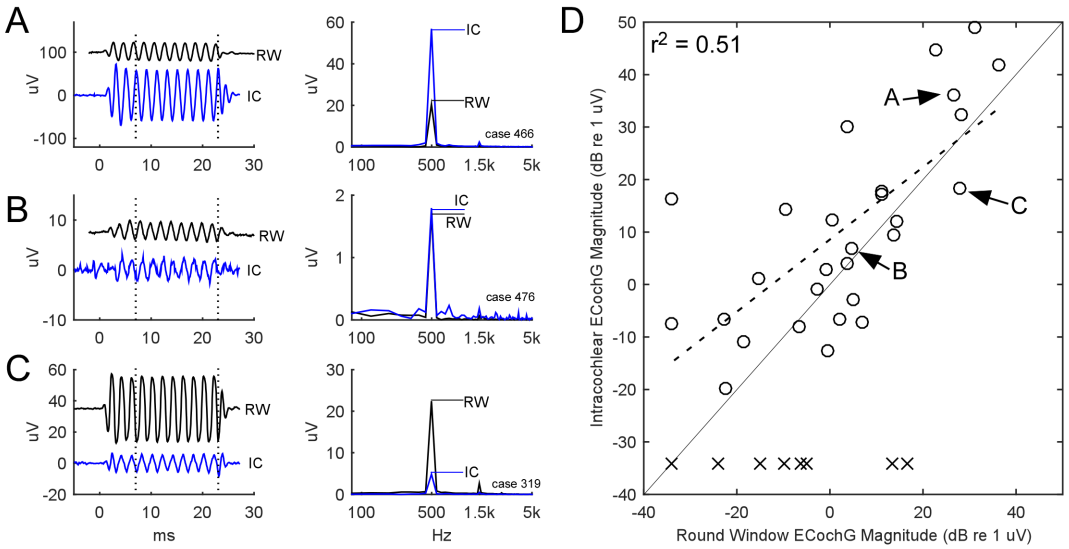


**Figure 4.3 - Intracochlear vs. RW Magnitude**

Comparison of intracochlear response magnitude to those at the RW. Intracochlear responses could be (A) larger than the RW, (B) of similar magnitude to the RW, or (C) smaller than the RW. (D) Across all 36 subjects, 28 intracochlear responses were above the noise floor among these, the median intracochlear response was 5.8 dB larger than the RW, and correlated positively ($r^2 = 0.51$). Labels within (D) refer to the subjects illustrated in (A) to (C), while the 'x' symbols refer to cases with intracochlear noise which precluded subsequent analysis. *note:* uV $= \mu V$

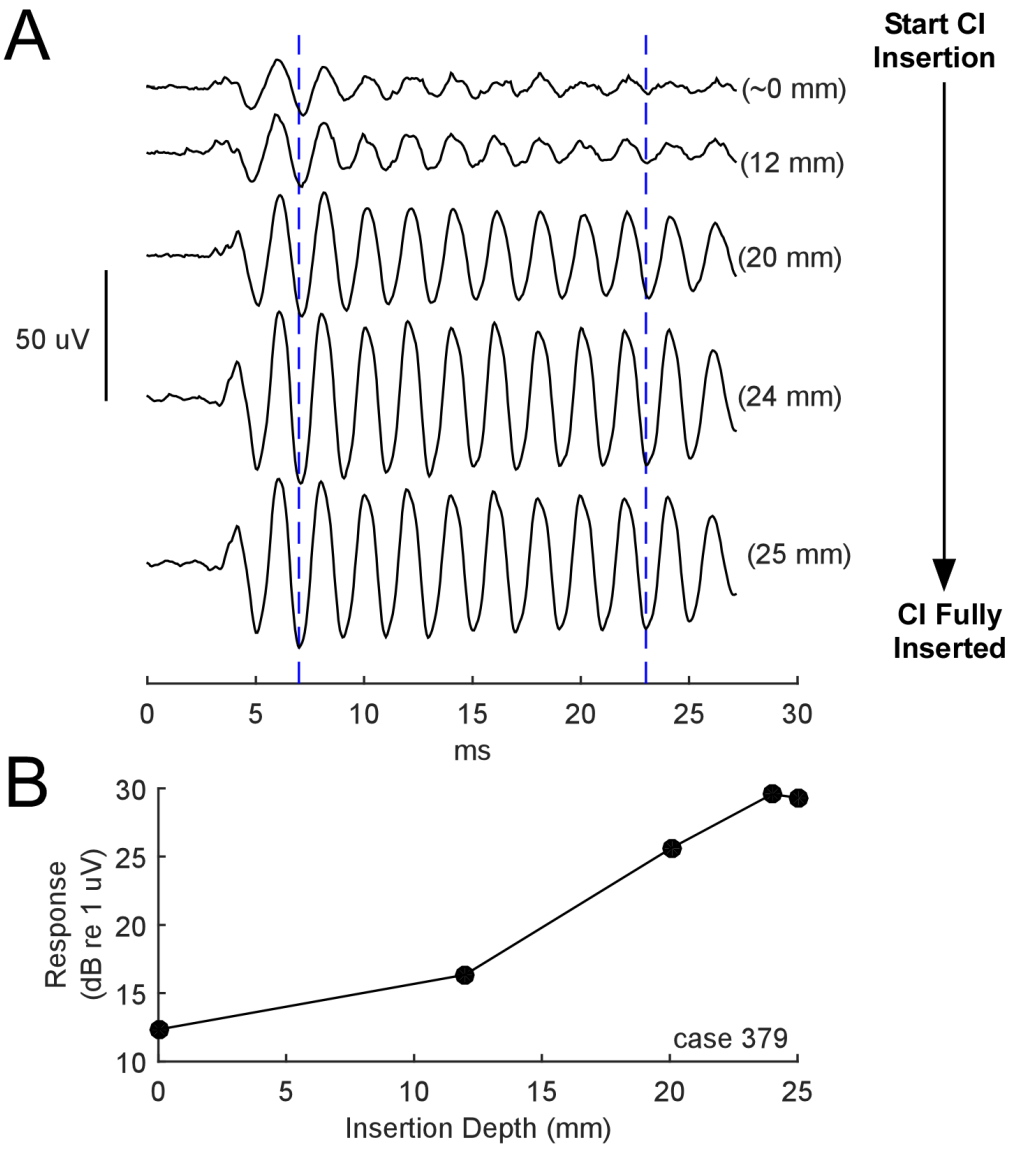


**Figure 4.4 - Intracochlear Response Tracks**

(A) Response waveforms to a 90 dB, 500 Hz tone in one subject were assessed at 5 stages during CI insertion. (B) Plotting the response magnitude of the ongoing response as a function of insertion depth reveals a "Response Track". *note:* uV $= \mu V$

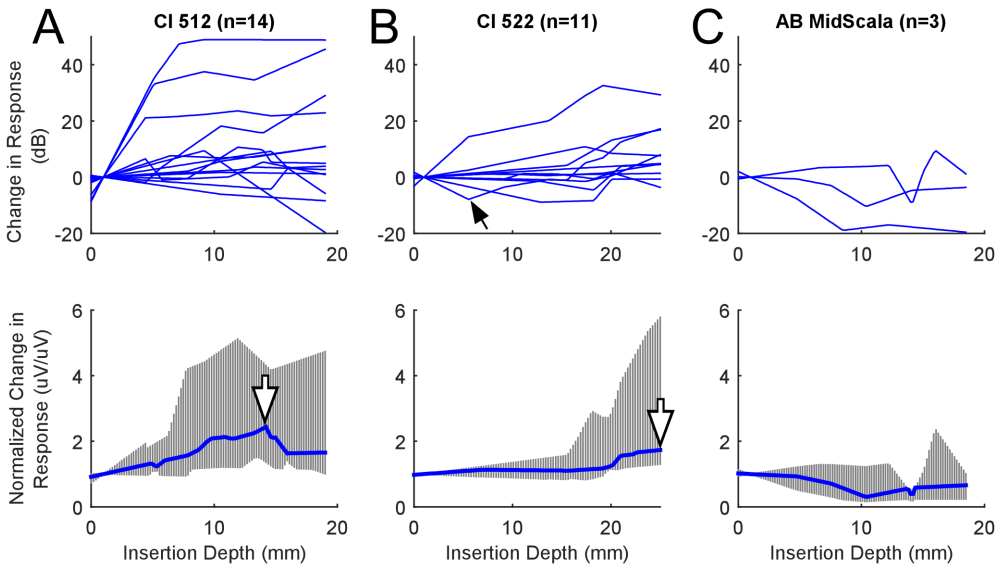


**Figure 4.5 - Response Tracks by Device Type**

Response Tracks vary by device type. (A) In the Cochlear Corporation CI512 array, responses in dB scale (top row) typically demonstrate early growth, and response magnitude when normalized in $\mu V$ (bottom row) demonstrates the median response was greatest at an insertion depth of 14.2 mm (white arrow). (B) In the Cochlear Corporation 422/522 arrays, responses in dB could dip (n=3, black arrow) but most growths were steady and in $\mu V/\mu V$ scale (bottom row) the maximal median response was achieved at the deepest insertion depth (white arrow). (C) in Advanced Bionics MidScala devices, sample size was limited but responses were steady and in one case dropped with depth. *note:* uV $= \mu V$

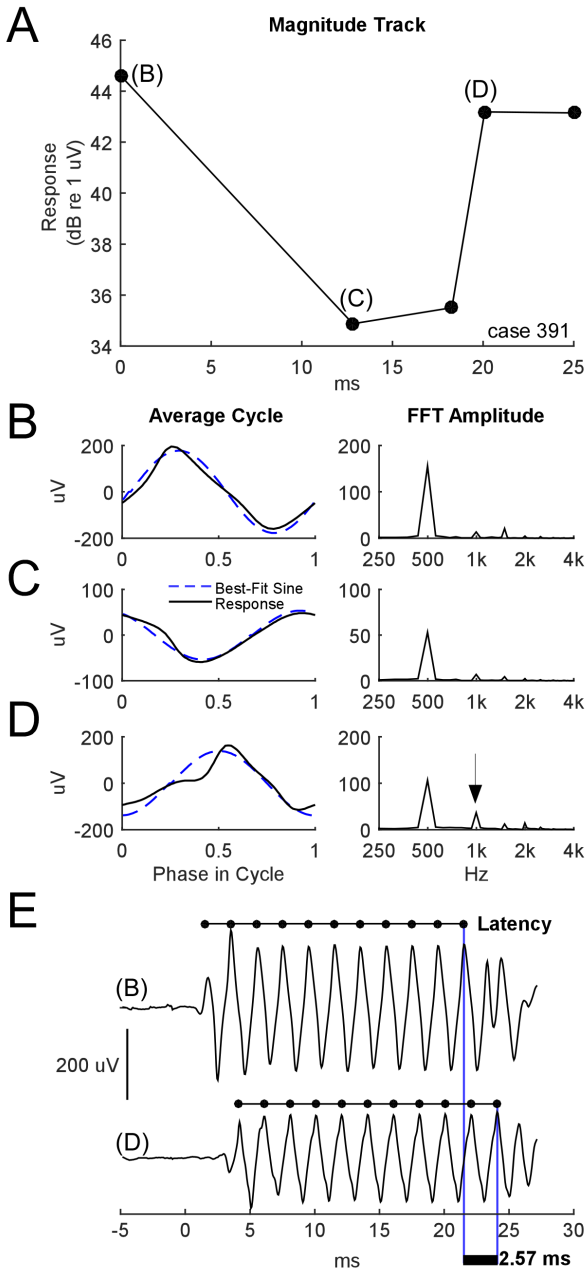


**Figure 4.6 - Response Drops with Phase Shifts**

Response magnitude could drop because of differences in phase relationship of generators rather than trauma. (A) A Response Track for one subject shows a large drop (10 dB) which recovered to within 3 dB by the end of insertion. (B) Average cycles from the ongoing response (left) at the starting point demonstrates a large response at the fundamental frequency evident in the FFT (right). (C) Mid-insertion, the phase inverts. (D) By the end of insertion, the phase again reverts and the response contains more distortions (arrow), indicating the array is likely recording from a different population of generators than those at the first intracochlear location. (E) This phase change is due to a latency shift beyond a cycle. *note:* uV $= \mu V$

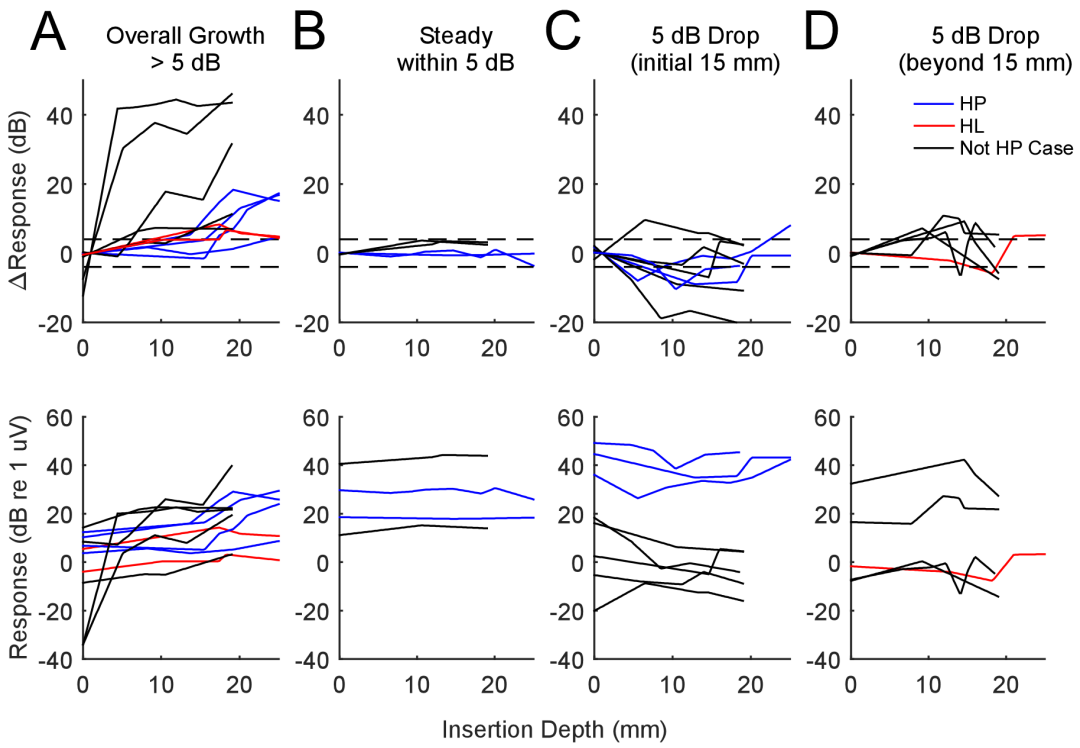


**Figure 4.7 - Response Tracks by Response Pattern**
Categories were (A) Overall growth of 5 dB by the end of insertion, (B), a response which remained $\pm$ 5 dB throughout insertion, (C) an early drop of >5 dB during insertion, and (D) a late drop in response during insertion. The top row demonstrates change in response (dB) whereas the bottom row shows dB re 1 $\mu V$. Cases in blue are cases where hearing was preserved, red demonstrate hearing was lost, and black are for subjects where preservation was not a goal. As is evident, there isn't a clear pattern category which contains the hearing preserved vs. lost subjects, implying trauma can occur with or without a characteristic response pattern. Note: in the top row of panel A there are two red tracks which mostly overlap, but are more distinct in absolute scale on the bottom row. *note:* uV $= \mu V$

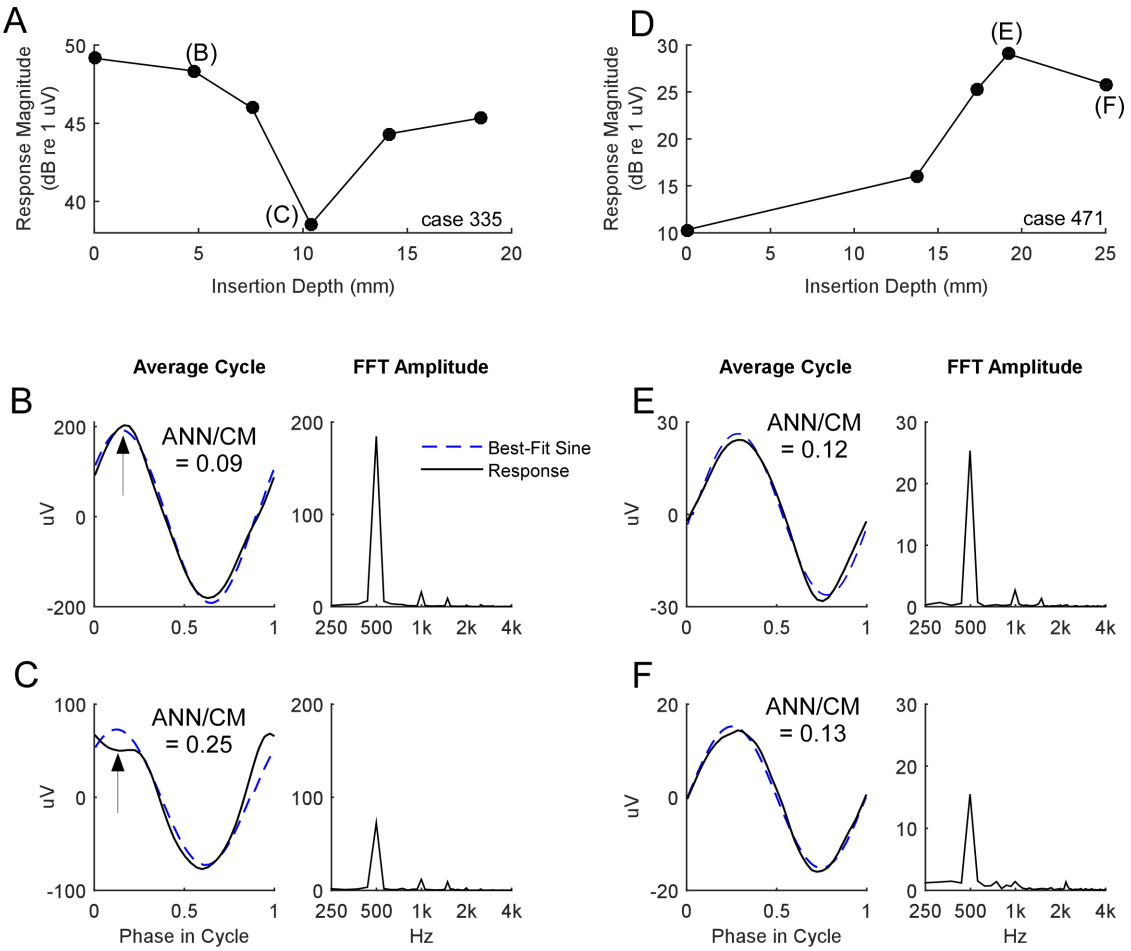


**Figure 4.8 - Response Drops without Phase Shifts**

Response drops in two subjects without a concurrent change in phase. The first subject demonstrates (A) a 10 dB drop between (B) and (C). While the phase of the best-fit sine doesn't change between (B) and (C), the proportion of neural activity is seen by both the distortions in the average cycle (arrows) and the changing proportion of ANN/CM (see methods for this calculation). In a second subject, a response drop of 4.3 dB (D) shows no change in phase or proportion of ANN/CM. *note:* uV $= \mu V$

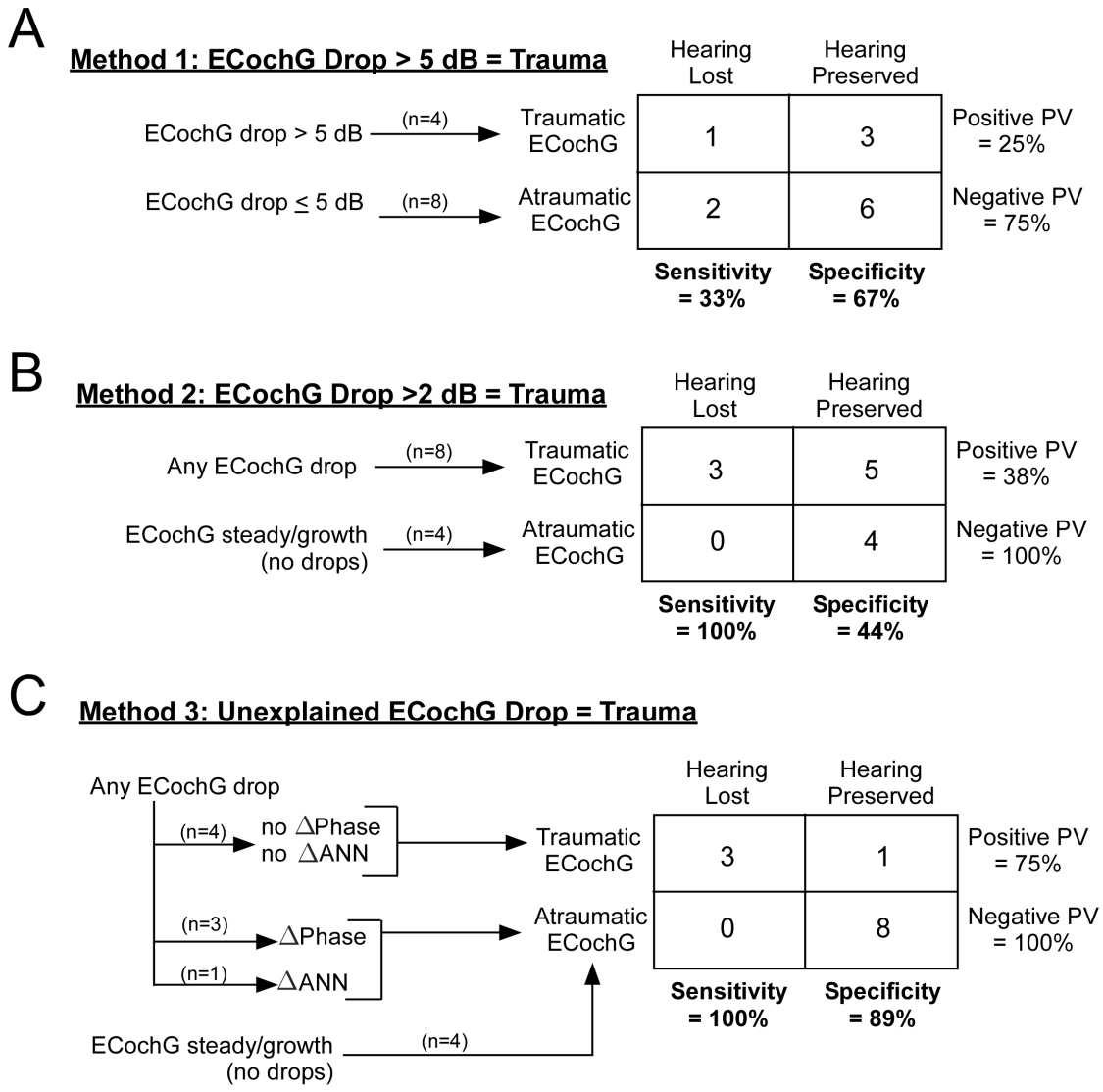


**Figure 4.9 - Contingency Tables to Identify Trauma**

Contingency tables for using three approaches of ECochG to identify trauma leading to hearing loss. In the first model (A), a 5 dB cutoff is used to connote trauma, which was associated with poor sensitivity and specificity. (B) The best magnitude cutoff we found, 2 dB, properly identified all cases of hearing loss but the specificity was poor. (C) Using magnitude drops and analysis of phase and ANN/CM, the sensitivity remained high and the specificity was improved. PV, predictive value.

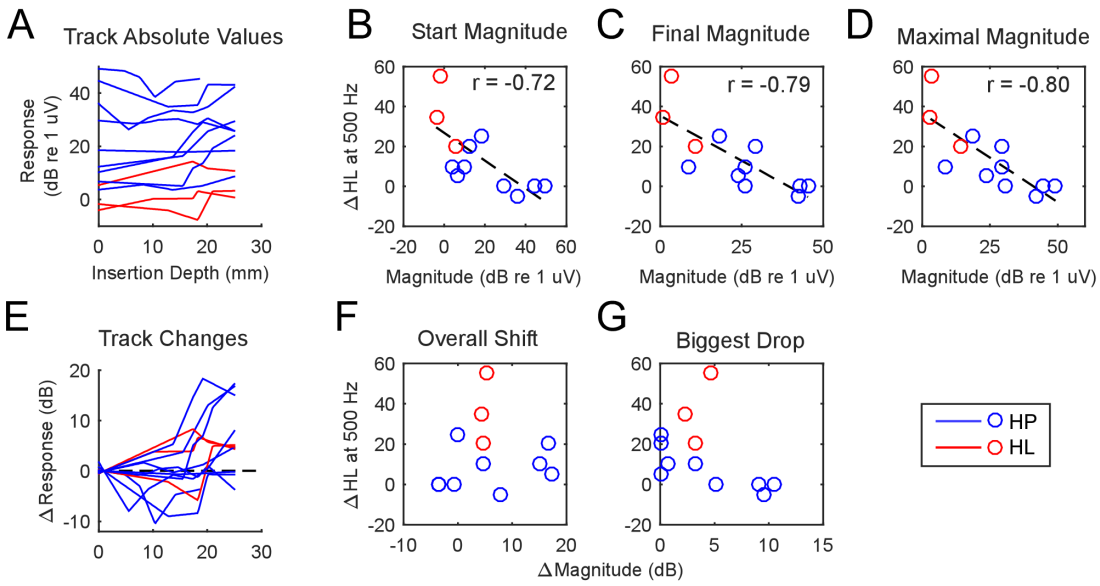


**Figure 4.10 - Response Tracks and Absolute Hearing**

Response Tracks for Hearing Preservation cases and Relationship between hearing loss at 500 Hz and intraoperative track magnitudes. (A) The absolute track values demonstrate those who lost hearing (red) had smaller responses. Specifically, the starting magnitude (B), final magnitude (C), and maximal magnitude (D) all correlated significantly with amount of threshold gain. (E) The change in response does not in and of itself help predict which cases will have preserved hearing versus hearing loss. Changes in response magnitude including the overall growth (B) and the largest drop (C) were not correlated with hearing loss. *note:* uV $= \mu V$

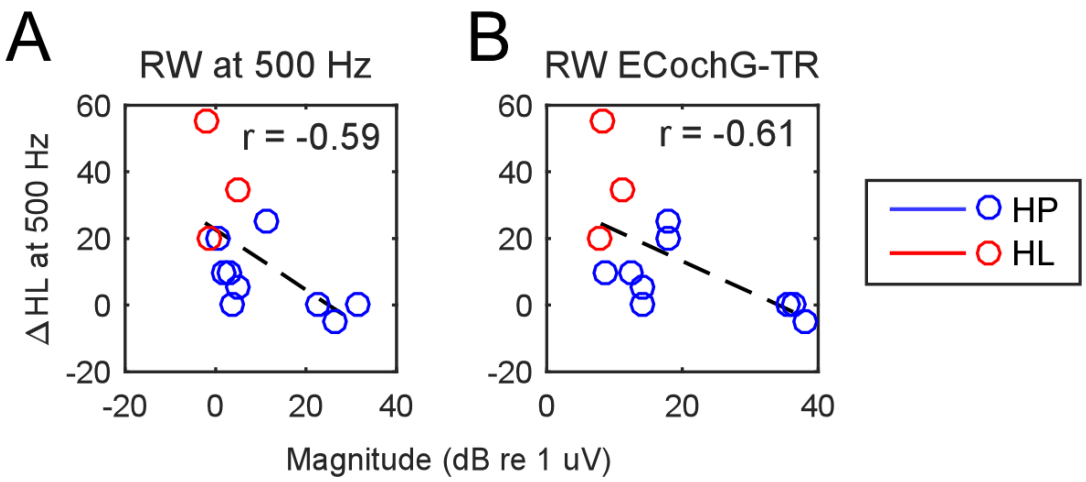


**Figure 4.11 - RW Magnitudes and Absolute Hearing**
Relationship between Round Window (RW) response magnitudes prior to CI insertion and subsequent hearing loss at 500 Hz. (A) The magnitude of the response to a 90 dB, 500 Hz tone correlated with the degree of hearing loss. (B) Across a broad range of stimulus frequencies (see ECochG-TR in methods), the total response (TR) also correlates with degree of hearing loss. *note:* uV $= \mu V$

# REFERENCES


Acharya, A. N., D. Tavora-Vieira and G. P. Rajan (2016). "Using the Implant Electrode Array to Conduct Real-time Intraoperative Hearing Monitoring During Pediatric Cochlear Implantation: Preliminary Experiences." Otology & Neurotology 37(2): e148-e153.

Adel, Y., Y. Rader, A. Bahmer and U. Baumann (2015). Recording Low-Frequency Acoustically Evoked Potentials using Cochlear Implants. 2015 Conference on Implantable Auditory Prostheses.

Adunka, O. F., C. K. Giardina, E. J. Formeister, B. Choudhury, C. A. Buchman and D. C. Fitzpatrick (2015). "Round window electrocochleography before and after cochlear implant electrode insertion." Laryngoscope.

Adunka, O. F., S. Mlot, T. A. Suberman, A. P. Campbell, J. Surowitz, C. A. Buchman and D. C. Fitzpatrick (2010). "Intracochlear recordings of electrophysiological parameters indicating cochlear damage." Otol Neurotol 31(8): 1233-1241.

Adunka, O. F., H. Pillsbury and C. Buchman (2009). "Minimizing intracochlear trauma during cochlear implantation."

Ahmad, F. I., B. Choudhury, C. E. De Mason, O. F. Adunka, C. C. Finley and D. C. Fitzpatrick (2012). "Detection of intracochlear damage during cochlear implant electrode insertion using extracochlear measurements in the gerbil." Laryngoscope 122(3): 636-644.

Anderson, J. M., A. Rodriguez and D. T. Chang (2008). Foreign body reaction to biomaterials. Seminars in immunology, Elsevier.

Calloway, N. H., D. C. Fitzpatrick, A. P. Campbell, C. Iseli, S. Pulver, C. A. Buchman and O. F. Adunka (2014). "Intracochlear electrocochleography during cochlear implantation." Otol Neurotol 35(8): 1451-1457.

Campbell, L., C. Bester, C. Iseli, D. Sly, A. Dragovic, A. W. Gummer and S. O'leary (2017). "Electrophysiological evidence of the basilar-membrane travelling wave and frequency place coding of sound in cochlear implant recipients." Audiology and Neurotology 22(3): 180-189.

Campbell, L., A. Kaicer, R. Briggs and S. O'Leary (2015). "Cochlear response telemetry: intracochlear electrocochleography via cochlear implant neural response telemetry pilot study results." Otol Neurotol 36(3): 399-405.

Campbell, L., A. Kaicer, D. Sly, C. Iseli, B. Wei, R. Briggs and S. O'Leary (2016). "Intraoperative Real-time Cochlear Response Telemetry Predicts Hearing Preservation in Cochlear Implantation." Otology & Neurotology 37(4): 332-338.

Choudhury, B., O. F. Adunka, C. E. Demason, F. I. Ahmad, C. A. Buchman and D. C. Fitzpatrick (2011). "Detection of intracochlear damage with cochlear implantation in a gerbil model of hearing loss." Otol Neurotol 32(8): 1370-1378.

Dalbert, A., A. Huber, D. Veraguth, C. Roosli and F. Pfiffner (2016). "Assessment of Cochlear Trauma During Cochlear Implantation Using Electrocochleography and Cone Beam Computed Tomography." Otology & Neurotology 37(5): 446-453.

Dalbert, A., F. Pfiffner, M. Hoesli, K. Koka, D. Veraguth, C. Roosli and A. Huber (2018). "Assessment of Cochlear Function during Cochlear Implantation by Extra-and Intracochlear Electrocochleography." Frontiers in neuroscience 12: 18.

Dalbert, A., F. Pfiffner, C. Roeoesli, K. Thoele, J. H. Sim, R. Gerig and A. M. Huber (2015). "Extra-and Intracochlear Electrocochleography in Cochlear Implant Recipients." Audiology and Neurotology 20(5): 339-348.

Dalbert, A., J. H. Sim, R. Gerig, F. Pfiffner, C. Roosli and A. Huber (2015). "Correlation of Electrophysiological Properties and Hearing Preservation in Cochlear Implant Patients." Otol Neurotol 36(7): 1172-1180.

Dalbert, A., J. H. Sim and A. M. Huber (2014). "Electrophysiologic Monitoring of Residual Hearing During and After Cochlear Implantation." Association for Research in Otolaryngology Abstracts 37: 317-318.

Demason, C., B. Choudhury, F. Ahmad, D. C. Fitzpatrick, J. Wang, C. A. Buchman and O. F. Adunka (2012). "Electrophysiological properties of cochlear implantation in the gerbil using a flexible array." Ear Hear 33(4): 534-542.

Finley, C. C., T. A. Holden, L. K. Holden, B. R. Whiting, R. A. Chole, G. J. Neely, T. E. Hullar and M. W. Skinner (2008). "Role of electrode placement as a contributor to variability in cochlear implant outcomes." Otol Neurotol 29(7): 920-928.

Fitzpatrick, D. C., A. T. Campbell, B. Choudhury, M. P. Dillon, M. Forgues, C. A. Buchman and O. F. Adunka (2014). "Round window electrocochleography just before cochlear implantation: relationship to word recognition outcomes in adults." Otol Neurotol 35(1): 64-71.

Fontenot, T. E., C. K. Giardina and D. C. Fitzpatrick (2017). "A Model-Based Approach for Separating the Cochlear Microphonic from the Auditory Nerve Neurophonic in the Ongoing Response Using Electrocochleography." Frontiers in neuroscience 11.

Forgues, M., H. A. Koehn, A. K. Dunnon, S. H. Pulver, C. A. Buchman, O. F. Adunka and D. C. Fitzpatrick (2014). "Distinguishing hair cell from neural potentials recorded at the round window." J Neurophysiol 111(3): 580-593.

Franke-Trieger, A. and D. Mürbe (2015). "Estimation of insertion depth angle based on cochlea diameter and linear insertion depth: a prediction tool for the CI422." European Archives of Oto-Rhino-Laryngology 272(11): 3193-3199.

Giardina, C. K., T. E. Khan, S. H. Pulver, O. F. Adunka, C. A. Buchman, K. D. Brown, H. C. Pillsbury and D. C. Fitzpatrick (2018). "Response Changes During Insertion of a Cochlear Implant Using Extracochlear Electrocochleography." Ear and Hearing.

Greene, N. T., J. K. Mattingly, H. A. Jenkins, D. J. Tollin, J. R. Easter and S. P. Cass (2015). "Cochlear implant electrode effect on sound energy transfer within the cochlea during acoustic stimulation." Otology & neurotology: official publication of the American

Otological Society, American Neurotology Society [and] European Academy of Otology and Neurotology 36(9): 1554.

Harris, M. S., W. J. Riggs, C. K. Giardina, B. P. O'Connell, J. T. Holder, R. T. Dwyer, K. Koka, R. F. Labadie, D. C. Fitzpatrick and O. F. Adunka (2017). "Patterns Seen During Electrode Insertion Using Intracochlear Electrocochleography Obtained Directly Through a Cochlear Implant." Otology & Neurotology.

Harris, M. S., W. J. Riggs, K. Koka, L. M. Litvak, P. Malhotra, A. C. Moberly, B. P. O'connell, J. Holder, F. A. Di Lella and C. M. Boccio (2017). "Real-time intracochlear electrocochleography obtained directly through a cochlear implant." Otology & Neurotology 38(6): e107-e113.

Jia, H., J. Wang, F. François, A. Uziel, J.-L. Puel and F. Venail (2013). "Molecular and cellular mechanisms of loss of residual hearing after cochlear implantation." Annals of Otology, Rhinology & Laryngology 122(1): 33-39.

Jurawitz, M.-C., A. Büchner, T. Harpel, M. Schüssler, O. Majdani, A. Lesinski-Schiedat and T. Lenarz (2014). "Hearing preservation outcomes with different cochlear implant electrodes: Nucleus® Hybrid™-L24 and Nucleus Freedom™ CI422." Audiology and Neurotology 19(5): 293-309.

Kamakura, T. and J. B. Nadol (2016). "Correlation between word recognition score and intracochlear new bone and fibrous tissue after cochlear implantation in the human." Hearing research 339: 132-141.

Kawano, A., H. L. Seldon and G. M. Clark (1996). "Computer-aided three-dimensional reconstruction in human cochlear maps: measurement of the lengths of organ of Corti, outer wall, inner wall, and Rosenthal's canal." Annals of Otology, Rhinology & Laryngology 105(9): 701-709.

Koka, K., A. A. Saoji and L. M. Litvak (2017). "Electrocochleography in cochlear implant recipients with residual hearing: comparison with audiometric thresholds." Ear and hearing 38(3): e161-e167.

Lo, J., C. Bester, A. Collins, C. Newbold, A. Hampson, S. Chambers, H. Eastwood and S. O'Leary (2017). "Intraoperative force and electrocochleography measurements in an animal model of cochlear implantation." Hearing research.

Mandala, M., L. Colletti, G. Tonoli and V. Colletti (2012). "Electrocochleography during cochlear implantation for hearing preservation." Otolaryngol Head Neck Surg 146(5): 774-781.

McClellan, J. H., E. J. Formeister, W. H. Merwin, 3rd, M. T. Dillon, N. Calloway, C. Iseli, C. A. Buchman, D. C. Fitzpatrick and O. F. Adunka (2014). "Round window electrocochleography and speech perception outcomes in adult cochlear implant subjects: comparison with audiometric and biographical information." Otol Neurotol 35(9): e245-252.

Musiek, F. E. and J. A. Baran (2007). The auditory system: anatomy, physiology and clinical correlates, Allyn & Bacon.

O'Connell, B. P., J. T. Holder, R. T. Dwyer, R. H. Gifford, J. H. Noble, M. L. Bennett, A. Rivas, G. B. Wanna, D. S. Haynes and R. F. Labadie (2017). "Intra-and postoperative electrocochleography may be predictive of final electrode position and postoperative hearing preservation." Frontiers in neuroscience 11: 291.

O'Connell, B. P., J. B. Hunter and G. B. Wanna (2016). "The importance of electrode location in cochlear implantation." Laryngoscope Investigative Otolaryngology 1(6): 169-174.

Radeloff, A., W. Shehata-Dieler, A. Scherzed, K. Rak, W. Harnisch, R. Hagen and R. Mlynski (2012). "Intraoperative monitoring using cochlear microphonics in cochlear implant patients with residual hearing." Otol Neurotol 33(3): 348-354.

Riggs, W. J., J. P. Roche, C. K. Giardina, M. S. Harris, Z. J. Bastian, T. E. Fontenot, C. A. Buchman, K. D. Brown, O. F. Adunka and D. C. Fitzpatrick (2017). "Intraoperative electrocochleographic characteristics of auditory neuropathy spectrum disorder in cochlear implant subjects." Frontiers in neuroscience 11: 416.

Robles, L. and M. A. Ruggero (2001). "Mechanics of the mammalian cochlea." Physiological reviews 81(3): 1305-1352.

Santa Maria, P. L., M. B. Gluth, Y. Yuan, M. D. Atlas and N. H. Blevins (2014). "Hearing preservation surgery for cochlear implantation: a meta-analysis." Otology & Neurotology 35(10): e256-e269.

Scott, W. C., C. K. Giardina, A. K. Pappa, T. E. Fontenot, M. L. Anderson, M. T. Dillon, K. D. Brown, H. C. Pillsbury, O. F. Adunka and C. A. Buchman (2016). "The Compound Action Potential in Subjects Receiving a Cochlear Implant." Otology & neurotology: official publication of the American Otological Society, American Neurotology Society [and] European Academy of Otology and Neurotology 37(10): 1654-1661.

van der Heijden, M. and C. P. Versteegh (2015). "Energy flux in the cochlea: Evidence against power amplification of the traveling wave." Journal of the Association for Research in Otolaryngology 16(5): 581-597.

# CHAPTER 5: IMPEDANCE AND POSITIONING[1]

## Overview

Improper electrode placement during cochlear implant (CI) insertion can adversely affect speech perception outcomes. However, the intraoperative methods to determine positioning are limited. Because measures of electrode impedance can be made quickly, the goal of this study was to assess the relationship between CI impedance and proximity to adjacent structures. An Advanced Bionics CI array was inserted into a clear, plastic cochlea one electrode contact at a time in a saline bath (9 trials). At each insertion depth, response to biphasic current pulses were used to calculate access resistance ($R_a$), polarization resistance ($R_p$), and polarization capacitance ($C_p$). These measures were correlated to actual proximity as assessed by microscopy using linear regression models. Impedance increased with insertion depth and proximity to the inner wall. Specifically, $R_a$ increased, $C_p$ decreased, and $R_p$ slightly increased. Incorporating all impedance measures afforded a prediction model (r = 0.88) while optimizing for sub-mm positioning afforded a model with 78.3% specificity. Impedance in vitro greatly changes with electrode insertion depth and proximity to adjacent structures in a predicable manner. Assessing proximity of the CI to adjacent structures is a significant first step in qualifying the electrode-neural interface. This information should aid in CI fitting, which should help maximize hearing and speech outcomes with a CI. Additionally, knowledge of the relationship between impedance and positioning could have utility in other tissue implants in the brain, retina, or spinal cord.

[1]modified from: *Giardina, C. K., E. S. Krause, K. Koka and D. C. Fitzpatrick (2018). "Impedance Measures During in vitro Cochlear Implantation Predict Array Positioning." IEEE Transactions on Biomedical Engineering 65(2): 327-335.*

## Introduction

Cochlear implantation (CI) is a major advance in auditory rehabilitation. Although speech perception outcomes with CIs have improved on average over time, these outcomes are still highly variable (Fitzpatrick, Campbell et al. 2014). Biographical factors, audiological factors, and surgical approach can only account for 25% of the variance in speech outcomes (Lazard, Vincent et al. 2012), and up to 40% when incorporating the magnitude of tone-evoked responses of the cochlea just before implantation (McClellan, Formeister et al. 2014). A substantial portion of the remaining variance is likely due to positioning of the CI relative to the auditory nerve as a result of implantation (Adunka, Giardina et al. 2015).

An ideally placed CI electrode is completely contained within the scala tympani (ST), coiled along the curvature of the cochlea and facing inwards towards the modiolus, a bony structure which contains the auditory nerve's spiral ganglion cell bodies. Recent improvements in post-insertion imaging have strengthened the intuitive relationship between major placement errors, i.e., electrodes that traverse from ST (correct placement) into scala vestibuli (adjacent structure), and poor speech perception outcomes (Finley, Holden et al. 2008, Holden, Finley et al. 2013, Tan, Holland et al. 2015, O'Connell, Hunter et al. 2016).

Yet even for completely-within-ST insertions, speech outcomes are still highly variable (O'Connell, Cakir et al. 2016) and may be influenced by differences in the proximity to and integrity of the electrode-neural interface (DeVries, Scheperle et al. 2016). For instance when individual CI electrode contacts are farther from the modiolus the stimulus current level needed to activate adjacent neurons is greater (Shepherd, Hatsushika et al. 1993), which can increase the spread of excitation and the risk of channel-channel interactions known to inhibit speech discrimination (Jones, Ho Won et al. 2013). As such, it would be useful to assess the proximity of each electrode contact to the modiolar wall in order to optimize stimulation parameters to obtain the best possible speech outcomes (Holden, Finley et al. 2013).

Correct placement by surgeons has always been the goal during implantation (Maneva 1970), but visual inspection of the implant is limited to the site of insertion and tactile per-

ception is limited in its ability to predict overall cochlear positioning (Kratchman, Schuster et al. 2016). Post-operative CT imaging is the best way to determine positioning, but is not routinely performed in adults and because of the radiation risk it will never be routinely performed in children. However, intra-operative device testing is almost universally employed (Busby, Plant et al. 2013). Three measures which can be rapidly assessed from the implant at the time of implantation include electrically-evoked neural responses, electric field imaging (EFI), and impedances (Mens 2007).

The clinical utility of evoked responses in assessing electrode positioning is highly variable. Mittmann, Ernst et al. (2015) found a correlation between evoked response thresholds and completely-within-scala positioning, while Miller, Brown et al. (2008) found no correlation of response thresholds to either intrascalar position or outcomes. In a study of 2,365 CI insertions in human adults, the relationship between electrode-to-modiolus distance and the minimum current level to reach response threshold was significant, but very weak within a given array type (r=0.12) (Davis, Zhang et al. 2016). As such, evoked responses are not a reliable contributor to determining electrode geometry relative to adjacent structures.

With regard to EFI, Vanpoucke, Zarowski et al. (2004) thoroughly modeled the equivalent circuit of a CI within the ST. The model was able to detect major placement errors, including tip-rollover of the implant and ossification of the cochlea, but was not utilized to predict the relative medio-to-lateral orientation within a scala (Vanpoucke, Boermans et al. 2012). A final metric, impedance, is typically used to assess CI integrity after implantation yet unique recent approaches to impedance measurement have gleaned additional information about the electrode's surroundings and proximity to adjacent tissue.

One experimental approach, utilized by Tan, Svirsky et al. (2013), analyzed impedance of electrode contacts at two stages during CI insertion: before and after stylet removal, a surgical step in some CI models which tightly wraps the array around the modiolus of the cochlea. They used fluoroscopy to confirm that stylet removal successfully caused the array to coil inwards and increases were seen in impedance at nearly every CI contact, consistent with models which describe the electrode-electrolyte interface and electrolyte-tissue interface as major contributors to resistance (Vanpoucke, Zarowski et al. 2004). This same

approach was also employed by Pile, Sweeney et al. (2016) who similarly found the change in impedance across electrodes increased after stylet removal, and could vary by surgical insertion technique. Tykocinski, Cohen et al. (2005) followed post-insertion impedance in CI subjects over time, further characterizing the electrode-electrolyte interface to track inflammation and fibrosis.

The common approach utilized by these three groups to compare changes in impedance is paramount, because impedance on its own is not correlated with CI positioning (Saunders, Cohen et al. 2002). This is because differences in baseline impedances between CI electrode contacts can routinely vary by kΩ (Hughes 2012), completely obscuring changes in the aforementioned studies which could be within hundreds of Ω. A technique for characterizing the electrode-saline interface of an implant before introducing biologic tissue has been utilized in other applications (Nag, Sikdar et al. 2015) but has not been utilized in CI arrays, and was the foundation for this research.

The goal of this study was to determine the relationship between CI impedance and proximity to adjacent structures in a saline environment. Our approach was to assess impedance across all contacts of a CI throughout sub-steps of insertion into a plastic cochlea submerged in saline. Our hypothesis was that impedance characterization of the electrode-saline interface before CI insertion would allow changes in impedance during insertion to sensitively infer electrode proximity to adjacent structures.

## Materials and Methods

### Cochlear Implant and Current Pulse Stimuli

An Advanced Bionics (AB) Hi-Focus 1j CI electrode array was used for all experiments (Valencia, CA, USA). The AB 1j electrode array has 16 individual platinum contacts (E1 to E16) which curl inwards, towards the modiolus. Contacts are spaced apart by 1.1 mm, leading to an overall active array length of 17 mm. At the base of the implant array there is a full-circumference ground electrode (Fig. 5.1, top), but the processor case can also be used as a ground in a clinical setting. Electrode contacts and the ground are individually shielded within a flexible silicon carrier and connected internally to the processer via

platinum-iridium wires. Each electrode is driven by a separate current source, and the processor has a built-in amplifier with an analog-to-digital converter which can sample at 56 kHz with 9 bit resolution (Fig. 5.1, center). Sampled data is sent via telemetry from the implant's magnet to the processor and interpreted with Advance Bionics Bionic Ear Data Collection System (BEDCS) software. Stimuli were biphasic pulses with an amplitude of 34 $\mu A$ lasting 179.6 $\mu s$ per phase, separated by 100 ms to minimize any interference with charging between subsequent pulses. At a 56 kHz sample rate, 33 samples per recording epoch were taken in monopolar recording mode, that is to say the recording electrode and stimulating electrode were the same, and potentials were recorded relative to the ring electrode ground.

## Calculation of Access Resistance and Polarization Impedance

The approach used here is described by Tykocinski, Cohen et al. (2005), who model the CI electrode-electrolyte interface as a resistor and capacitor in parallel, and the and bulk tissue resistance as a resistor in series. The implant generates a current pulse which passes from an electrode contact through the surrounding medium and returns on the ring ground (Fig. 5.1, bottom). The major sources of impedance are the bulk resistance through the cochlear tissue ($R_a$) and the impedance at the electrode-electrolyte interface ($Z_p$), which are in series. Polarization Impedance ($Z_p$) is composed of both resistive ($R_p$, Faradaic Resistance) and capacitive ($C_p$, double layer capacitance) elements in parallel.

The response waveform (Fig. 5.2, center) to a long stimulus pulse (Fig. 5.2, top) of an implant in saline demonstrates the two sources of voltage increase consistent with this model: an immediate voltage increase from the frequency-independent resistive elements between the contact and the ground (access voltage, $V_a$) and a slowly-rising limb demonstrating a charge accumulation at the electrode-electrolyte interface (polarization voltage, $V_p$) as in (1).

$$V_{tot}(t) = V_a + V_p(t) \tag{1}$$

Calculation of access resistance is simply the access voltage at the first sampled time point in $V_a$ divided by the current pulse amplitude (2).

$$R_a(t) = \frac{V_a}{i} \tag{2}$$

The total polarization impedance is the voltage growth after the first time point until the end of the first phase divided by the current used (3).

$$Z_p(t)\Big|_{180\mu s} = \frac{V_p(t)\big|_{180\mu s}}{i} \tag{3}$$

Unlike the $R_a$, $Z_p$ changes as a function of time. In our model, the relationship between $R_p$, $C_p$, and $Z_p$ are described as a standard RC circuit:

$$V_p(t) = i * Z_p(t) \tag{4}$$

$$Z_p(t) = R_p\left[1 - \exp\left(\frac{-t}{Rp * Cp}\right)\right] \tag{5}$$

Using MATLAB (MathWorks, Natick, MA) to fit the $Z_p$(t) segment of the measured response (4) to the model function (5), it is possible to approximate magnitudes of $R_p$ and $C_p$ (Fig. 5.2, bottom).

## Recording Impedance in the Plastic Cochlea During CI Insertion

The AB CI was placed in a saline bath alongside a clear, 3D printed plastic cochlea. The cochlea was printed to mimic the approximate size of the human ST (Cohen, Xu et al. 1996, Clark, Warren et al. 2011), but was slightly wider due to constraints in fabrication. Just inside the RW, the plastic ST is roughly twice the diameter of a human ST (as determined by studies of human cochlear histology) but by 4 mm of insertion depth our plastic cochlea ST size is within 0.35 mm of real cochleae (Wysocki 1999). At the deepest level the CI was inserted (17 mm), the plastic lateral wall is 1.8 mm from the modiolus, slightly larger than the human ST width at this depth, which ranges from 1.25 to 1.6 mm (-SD to +SD) Wysocki 1999). Post-operative CT imaging of CI subjects receiving this exact AB array had contacts

which ranged from 0.4 to 1.75 mm to the modiolus (Davis, Zhang et al. 2016). As such our plastic cochlea is much wider than a human cochlea at the base, but differences from 4 mm of insertion to full insertion depth were usually within 0.2 mm and were thus considered negligible.

With the CI still in saline and completely outside the plastic cochlea, baseline measurements of electrode impedances were sequentially made between each contact and the ground ring (E1 to ring, E2 to ring, ... E16 to ring). Next, the implant array was inserted one electrode contact into the plastic cochlea, such that E1 was just inside the cochlea while E2 to E16 were still outside. Impedances were again assessed for all 16 contacts. For the rest of the implantation, each time after the CI was inserted one electrode contact deeper, impedances were again assessed across all contacts (Fig. 5.3). Thus there were 17 recording locations (saline + 16 CI insertion depths) during which all 16 electrode contacts were individually assessed, totaling 272 impedance recordings per CI insertion. Recordings at each contact were normalized by subtracting the impedance component values in saline. Nine complete CI insertions were performed.

### Imaging to Determine CI Positioning

The 3D printed cochlea was completely transparent, and allowed for microscopy at all stages of CI insertion. A Zeiss (Oberkochen, DE) Axioskop microscope with was used with accompanying Canon (Tokyo, JP) EOS digital camera and software to acquire a high resolution photograph at each CI insertion depth (Fig. 5.4A). In this way, each time an impedance measurement was made for a given electrode contact, it would also be possible to determine the associated distance of that contact to the inner wall (Fig. 5.4B).

### Impedance Modeling to Predict CI Positioning

The goal of the study was to determine if CI positioning of each electrode contact could be predicted solely from impedance measures. Specifically, to determine if a model could be developed which input the overall CI insertion depth, specific electrode number, and recorded impedance response to predict the distance of that contact to the modiolus (6).

$$\begin{aligned} PredictedDistanceToModiolus &= f\big(V(t)\big)\Big|_{EL,Depth} \\ &= f\big(R_a, R_p, C_p\big)\Big|_{EL,Depth} \end{aligned} \tag{6}$$

To test this hypothesis, impedance measures and exact positioning of each contact throughout all CI insertions were used to make a database where each depth/electrode combination had associated impedance values ($R_a$, $R_p$, $C_p$) and a precise modiolar distance per microscopy. With this, SPSS Version 24 software (IBM Corporation, Armonk, NY) optimized a linear regression model which accepted insertion depth, $R_a$, $R_p$, and $C_p$ as independent variables to predict the dependent outcome metric – distance to the modiolus.

An ancillary goal of this study was to determine if impedance measures could predict when any electrode contact was within a millimeter of the modiolus, as a marker for near-modiolar positioning as is desirable for some pre-curved arrays. Using a subset of the full-insertion dataset, a second model was created – which was designed to optimize for when any electrode contact was within 1 mm of the modiolus (a Boolean) rather than accuracy across any distance (continuous). Both models were assessed by introducing ANOVA predictor variables sequentially and determining if any increase in the adjusted $r^2$ was significant by an F-test.

# Results

## Impedance and Insertion Depth

When solely observing the voltage response waveforms of the deepest/apical electrode (E1) during several stages of CI insertion (Fig. 5.5, top), it is clear that there is a direct relationship between insertion depth and recorded voltage amplitude (Fig. 5.5, bottom). Deeper locations within the plastic cochlea have a more resistive path to ground, necessitating an increase in the required CI's voltage to allow the fixed current pulse level. Consistent with this observation, in a fully-inserted CI (Fig. 5.6, top), waveform amplitudes

across multiple EL contacts demonstrate that deeper electrodes have higher waveform amplitudes (Fig. 5.6, bottom).

Trends in $R_a$, $Z_p$, $Z_t$ (total impedance), $R_p$, and $C_p$, across all contacts for 4 different insertion depths are depicted in Fig. 5.7. Each column represents a CI insertion depth while each row demonstrates microscopy of the CI when the data were collected (Fig. 5.7, top row), trends in $R_a$, $Z_p$, and $Z_t$ at each electrode contact (Fig. 5.7, center row), and characterization of polarization components $R_p$ and $C_p$ (Fig. 5.7, bottom row). Column one shows the array with only a single contact inserted into the ST. At this depth, there have been no appreciable changes in any impedance measures compared to those in saline. Column 2 demonstrates 9 contacts inserted. At this depth, the total impedance $Z_t$ is driven mostly by $R_a$, and those electrode contacts which were visually inspected to be closer to the modiolus (black arrow) had much higher rates of impedance growths than the mid-scalar electrodes closer to the RW. With 12 electrode contacts inserted (Column 3), electrodes 4-7 were closer to the modiolus and again $R_a$ growths (black arrow) were much higher than the linear growth pattern observed on electrodes both deeper and shallower. The final column represents a full insertion, during which all electrodes are more lateral and far from the modiolus, demonstrating a fairly linear growth in $R_a$ as a function of depth with a small increase in $Z_p$. No appreciable changes in either $R_p$ or $C_p$ occurred during any insertion.

## Insertion Depth and Proximity to the Modiolar Wall

The first 100 degrees of rotation of the cochlea has a wider radius of curvature than the remaining two turns running towards the apex (Clark, Warren et al. 2011). As such, the CI array changes its medio-lateral positioning throughout insertion. By analyzing the proximity of any contact by cochlear position (1=base, 16=apex), microscopy revealed that this particular CI array had a reproducible range of distances to the modiolus (Fig. 5.8). At the base of the cochlea, the distance from electrodes to the modiolus was large. As the electrode approached the basal turn of the cochlea, roughly around position 8, the array was consistently close to this inner edge. Throughout the rest of the insertion, the array remained roughly 1.5 mm away from the modiolar wall.

### Impedance and Proximity to the Modiolar Wall

When analyzing changes in impedance (relative to saline) as a function of cochlear position, $R_a$ shows a positive trend increasing with depth (Fig. 5.9, top left), $R_p$ does not drastically change with depth (Fig. 5.9, center left), and $C_p$ decreases with depth (Fig. 5.9, bottom left). Incorporating microscopy into the dataset, individual measurements in the left column of Fig. 5.9 were ranked and colored by proximity to the modiolus - where a red circle indicates a closer position to the modiolus, a blue circle indicates a far position from the modiolus, and a black circle was a midscalar position. At a given cochlear position, the range of impedances for $R_a$ could be partially explained by the electrode proximity (Fig. 5.9, top right). However, trends of proximity were not so obvious with $R_p$ (Fig. 5.9, center right) or $C_p$ (Fig. 5.9, bottom right).

### Impedance Model to Predict Modiolar Distance of Electrode Contacts

The trends between impedance measures and proximity which were introduced visually (Fig. 5.8) were fully realized in a linear regression model. The independent variables of this model are designed to be the metrics available to the surgeon at the time of surgery – a given CI insertion depth (d) and an array contact (EL), with the associated calculated impedance measures ($R_a$, $R_p$, and $C_p$). The dependent variable to be predicted is the distance from contact to the modiolus, in mm. The linear regression optimization algorithm introduced these variables in a stepwise fashion, creating 5 models and evaluating whether each variable significantly increased the adjusted $r^2$ (Table 5.1, models [a] through [e]).

The majority of the observed variance (59%) in electrode-to-modiolus distance can be explained solely with $R_a$, while incorporating insertion depth and electrode number added 9% each to the adjusted $r^2$. While still significant, $C_p$ and $R_p$ contributed just 2.5% collectively to the explained variance. Ultimately, a Pearson correlation of 0.885 could be achieved with the Table 5.1 model [e], herein called Model 1.

### Impedance Model to Predict Submillimeter Proximity to Modiolus

During the experiments performed, 267 individual electrode contacts were found to be microscopically within 1 mm of the modiolus. Using these sub-millimeter cases as inputs to the model in Model 1, the predicted distances were greater than 1 mm in nearly 77% of recordings. Such underestimation of proximity is not ideal. As such, a new model was created utilizing training data solely from electrode contacts which were closer to the modiolus (Table 5.2). In this model, the output metric was a boolean – whether the contact was within 1 mm of the modiolus – rather than an estimated distance as was the case in Model 1.

A linear regression model introduced these same variables in a stepwise fashion but here the best model resulted with a Pearson correlation of 0.717 with Table 5.2 model [e], herein called Model 2. The adjusted $r^2$ of this model is slightly lower than that of Model 1, but the rate of false negatives when detecting sub-mm proximity dropped from 77% to 22.1%. In addition to better detection of sub-mm positioning, Model 2 also reduced the rate of false-positives (array contacts being flagged <1 mm despite actually being farther from the modiolus) from 43% to 25%.

## Discussion

Qualifying the electrode-neural interface in cochlear implant recipients is crucial for understanding the variance in speech perception outcomes. A key component of this interface is the positioning, or geometry, of the electrode array relative to cochlear anatomy. This report introduces impedance collection throughout many stages of CI insertion, and expands upon existing impedance models for approximating CI positioning in situ.

First the plastic ST model was used to determine the relationship between derived CI impedance measures and proximity to adjacent structures at 16 discrete steps during CI insertion. We found that the total impedance increased with both insertion depth and proximity to adjacent structures –consistent with Tan, Svirsky et al. (2013) and Pile, Sweeney et al. (2016) who demonstrate an increase in overall ($R_a$) impedance after stylet removal.

In our Model 1, $R_a$ accounted for the majority (59%) of the adjusted $r^2$, while the addition of electrode number and insertion depth brought this correlation to 0.76. Polarization components $R_p$ and $C_p$ added a small but significant amount to this correlation.

Because of the profound interest by some implant manufacturers to place the implant either as close to the modiolus as possible to minimize current spread, or intentionally as far from the modiolus as possible to avoid modiolar insertion trauma, we also wanted to determine if impedance could detect when any given contact was grossly lying along the modiolar wall or along the lateral wall. One manufacturer, for example, produces precurved arrays which have a median modiolar distance of 0.4 mm in vivo whereas their lateral wall arrays have a median modiolar distance of 1.2 mm (Davis, Zhang et al. 2016). In fact, their perimodiolar arrays with electrode-modiolar distances greater than 1 mm in this study were considered outliers. With this cutoff in mind, Model 2 was created, wherein the metric to be optimized was a Boolean – whether any contact was within 1 mm of the modiolus – even at the expense of knowing the precise modiolar distance as in Model 1.

A comparison of Model 1 and Model 2 (Table 5.3) demonstrates that Model 1 is better for determining precise positioning anywhere within the ST, but Model 2 is much more sensitive and specific to detecting which electrodes are very close proximity to the modiolus. As such, each model provides discrete but complimentary information regarding the position of the electrode relative to the modiolus, which may be clinically valuable in assessing the electrode-neural interface. In addition, implementation of an approach like Model 2 throughout CI insertion may also be advantageous if a surgeon wanted to receive intraoperative feedback on whether the cochlear implant is approaching adjacent tissue structures (Mandala, Colletti et al. 2012, Radeloff, Shehata-Dieler et al. 2012). The speed of the measurements being less than 1 ms per electrode, and the ability to concurrently use the processor case as the ground electrode, make the runtime feedback a feasible goal. However, the role of impedance as a metric for trauma is not currently known, as penetration damage from the array tip, for example, could occur despite recording contacts being appropriately distanced from tissue.

Currently, the use of intraoperative impedance testing only occurs only after full CI insertion, and is used to confirm CI processor function and identify malfunctioning array

contacts (Busby, Plant et al. 2013). Electrodes which are shorting have abnormally low impedances, whereas electrodes with an open or disconnected contact have abnormally high impedances. Functioning devices are manufactured to satisfy a range of acceptable impedance tolerances, but slight differences between contacts are not uncommon. As such, a single post-insertion impedance scan is not sufficient to determine which electrodes are closest to the modiolus (Saunders, Cohen et al. 2002); differences can be due to factors both within the CI or at the CI interface rather than reflecting the environment around the device. To minimize this confounder, it is absolutely paramount that the impedance of each individual electrode contact is characterized in saline before CI insertion; the trends noted in this report were not robust when analyzing impedance without first doing so. This may become even more important when utilizing this approach in living tissue, when slight discrepancies in individual electrode contact impedances can lead to drastic differences in recordings to biphasic current stimulation (Limnuson, Lu et al. 2014). In the surgical setting, an approach to obtain pre-insertion impedance measures could include briefly flooding the surgical field and immersing the array with saline, while a more elegant approach may be to use the first non-artifact impedance measure from each contact throughout insertion as its own baseline.

The vast majority of CI current in vivo is confined to the ST, with a ST conductance roughly 100x greater than transversal current pathways towards the modiolus (Vanpoucke, Zarowski et al. 2004). When current is limited to the ST, the return path to ground becomes longer and the cochlear conductive space becomes narrower as the electrode advances deeper. This may explain why total impedance increases with both insertion depth and proximity to the modiolar walls (Tan, Svirsky et al. 2013, Pile, Sweeney et al. 2016), consistent with our results in this study where the plastic model afforded no “leaky” transverse channels whatsoever. In addition to current not returning through the modiolus, our plastic model also negates the possibility of current favoring a path out of the ST apex and through the facial canal rather than towards the RW (Vanpoucke, Zarowski et al. 2004). This characteristic also likely explains why the polarization resistance and capacitance of the surface monolayer was negative compared to saline; that is to say patterns of inductance were more easily obtained down the ST than in an open body of saline. Recordings

in vivo also necessarily introduce bone, which will increase the $R_a$ portion of the necessary return path depending on temporal bone thickness (Tang, You et al. 2008). The roles of polarization impedance, specifically $R_p$ and $C_p$, played a minimal role in assessing positioning in the plastic model but may be much more integral in cadaveric or living cochlear models because of the current pathways outside the ST, comprising a variety of tissue types and interfaces between them. In fact, polarization impedance comprised nearly 2/3 of the total impedance across CI contacts within the first week after CI implantation (Tykocinski, Cohen et al. 2005).

Knowledge of array positioning has been previously used to optimize speech coding strategies during rehabilitation for individual subjects, by reprogramming and deactivating contacts to limit spread of excitation (Noble, Gifford et al. 2014). As such, attempts to assess positioning are clinically worthwhile, particularly for those where imaging is unavailable. Future studies will thus be directed at characterizing the relationship between impedance measures and CI positioning in temporal bone and cadaveric models.

## Conclusions

Components of electrode impedance change during CI insertion due to proximity to local sources. Building a template of CI electrode insertions with intraoperative insertion depth and impedance measures can accurately predict the positioning of the CI array during insertion in a plastic ST model. Of the metrics obtained, access Resistance ($R_a$) is the best at inferring positioning of electrode contacts to the wall of the cochlear model, while polarization resistance and capacitance significantly contributed to a smaller degree. Impedances normalized to saline aided in the creation of two regression models to predict 1) overall electrode positioning in terms of proximity to the modiolus and 2) predict whether contacts were grossly located along the modiolar or lateral wall.

# TABLES

TABLE 5.1
MODELS FOR ESTIMATING PROXIMITY OF ALL ELECTRODE CONTACTS TO MODIOLUS AT ANY STAGE OF CI INSERTION

| | R | $R^2$ | Adj. $R^2$ | Std. Error of Estimate | $\Delta R^2$ | $\Delta F$ | Sig. $\Delta F$ |
|---|---|---|---|---|---|---|---|
| [a] | 0.767 | 0.588 | 0.588 | 1.392 | 0.588 | 3282 | < 1E-14 |
| [b] | 0.820 | 0.673 | 0.672 | 1.241 | 0.085 | 596.6 | < 1E-14 |
| [c] | 0.871 | 0.758 | 0.758 | 1.066 | 0.086 | 814.9 | < 1E-14 |
| [d] | 0.874 | 0.764 | 0.764 | 1.053 | 0.006 | 57.9 | < 1E-14 |
| **[e]** | **0.885** | **0.783** | **0.783** | **1.010** | **0.019** | **200.8** | **< 1E-14** |

[a] Predictors: Ra,
[b] Predictors: Ra, Insertion Depth
[c] Predictors: Ra, Insertion Depth, EL
[d] Predictors: Ra, Insertion Depth, EL, Cp
[e] Predictors: Ra, Insertion Depth, EL, Cp, Rp

**Table 5.1 - Model 1: Impedance Models for Overall Positioning**
The independent variables of this model are designed to be the metrics available to the surgeon at the time of surgery – a given CI insertion depth (d) and an array contact (EL), with the associated calculated impedance measures ($R_a$, $R_p$, and $C_p$). The dependent variable to be predicted is the distance from contact to the modiolus, in mm. The linear regression optimization algorithm introduced these variables in a stepwise fashion, creating 5 models and evaluating whether each variable significantly increased the adjusted $r^2$ (models [a] through [e]).

TABLE 5.2
MODELS FOR ESTIMATING PROXIMITY OF ARRAY TO MODIOLUS WITHIN 1 MM DURING CI INSERTION

| | R | $R^2$ | Adj. $R^2$ | Std. Error of Estimate | $\Delta R^2$ | $\Delta F$ | Sig. $\Delta F$ |
|---|---|---|---|---|---|---|---|
| [a] | 0.662 | 0.379 | 0.438 | 0.693 | 0.439 | 782.9 | < 1E-14 |
| [b] | 0.687 | 0.485 | 0.484 | 0.664 | 0.047 | 90.5 | < 1E-14 |
| [c] | 0.703 | 0.495 | 0.493 | 0.658 | 0.009 | 18.0 | < 1E-14 |
| [d] | 0.710 | 0.504 | 0.502 | 0.652 | 0.010 | 19.2 | < 1E-14 |
| **[e]** | **0.717** | **0.514** | **0.512** | **0.646** | **0.010** | **20.3** | **< 1E-14** |

[a] Predictors: Ra
[b] Predictors: Ra, EL
[c] Predictors: Ra, EL, Cp
[d] Predictors: Ra, EL, Cp, Rp
[e] Predictors: Ra, EL, Cp, Rp, Insertion Depth

**Table 5.2 - Model 2: Impedance Models for Detecting sub-Millimeter Positioning**
The independent variables of this model are designed to be the metrics available to the surgeon at the time of surgery – a given CI insertion depth (d) and an array contact (EL), with the associated calculated impedance measures ($R_a$, $R_p$, and $C_p$). Like Table 5.1, the dependent variable to be predicted is the distance from contact to the modiolus, in mm. Unlike Table 5.1, the model in this linear regression optimization algorithm was heavily weighted towards detecting sub-mm proximity. Again these independent variables were introduced in a stepwise fashion, creating 5 models and evaluating whether each variable significantly increased the adjusted $r^2$ (models [a] through [e]).

TABLE 5.3
COMPARISON OF MODELS FOR ARRAY POSITIONING

$$\text{PredictedDistanceToModiolus} = \beta_0+\beta_1\cdot\text{Depth}+\beta_2\cdot\text{EL}+\beta_3\cdot R_a+\beta_4\cdot R_p+\beta_5\cdot C_p$$

| | **Model 1** | **Model 2** |
|---|---|---|
| Utility | **Accurate positioning of any electrode** | **Detecting any electrode within 1 mm of modiolus** |
| $\beta_0$ | 5.054 | 2.310 |
| $\beta_1$ | -0.241 | -0.090 |
| $\beta_2$ | 0.170 | 0.134 |
| $\beta_3$ | -0.176 | -0.063 |
| $\beta_4$ | 0.236 | 0.074 |
| $\beta_5$ | -275.383 | -112.601 |
| Pearson R | **0.885** | 0.717 |
| Sensitivity to ≤ 1 mm | 22.1 % | **78.3 %** |
| Specificity to > 1mm | 56.8 % | **75.0 %** |

**Table 5.3 - Comparison of Impedance Models**

A comparison of the parameters and efficacy of Models 1 and 2 in demonstrate their utility. Model 1 (Table 5.1) accurately predicts the location of any electrode with a stronger correlation than Model 2. However, it is less sensitive and less specific to detecting sub-mm proximity. Model 2 affords much better sensitivity and specificity to this 1 mm cutoff, at the expense of overall precision in positioning (smaller r).

# FIGURES

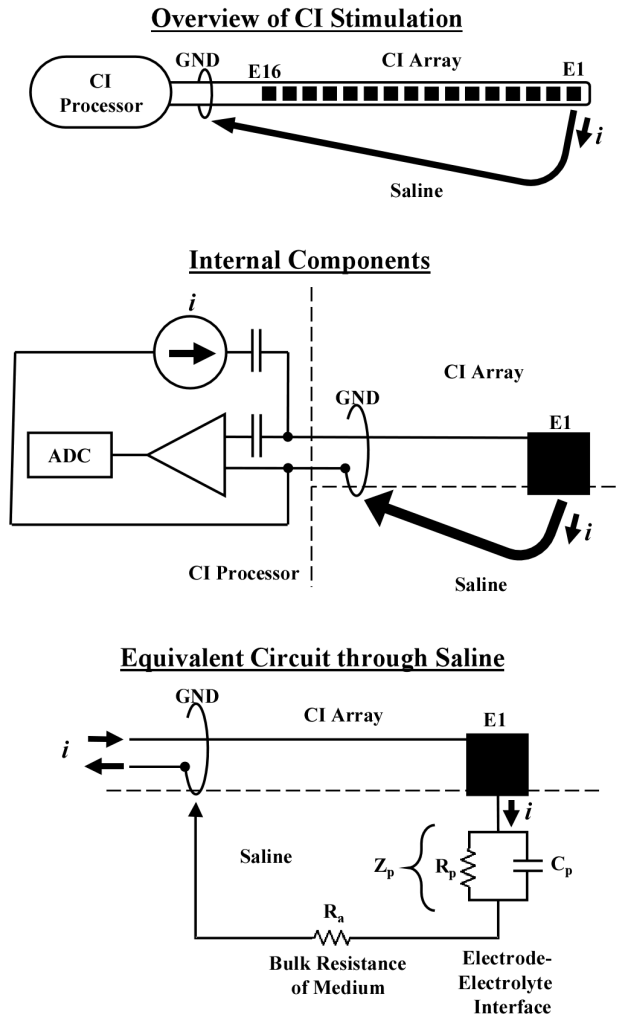


**Figure 5.1 - Equivalent Circuit in Saline**

(top) Current passes from each cochlear implant (CI) electrode contact, E1 for example, through the surrounding medium and returns at the ring ground. (center) The processor contains a current source and ADC while the array contains contacts which interface with saline. (bottom) Major contributors to impedance for a single cochlear implant contact include the bulk resistance of the medium (access resistance, $R_a$), and the polarization impedance of the electrode-electrolyte interface ($Z_p$), which can be modelled as a parallel circuit with polarization resistance ($R_p$) and capacitance ($C_p$).

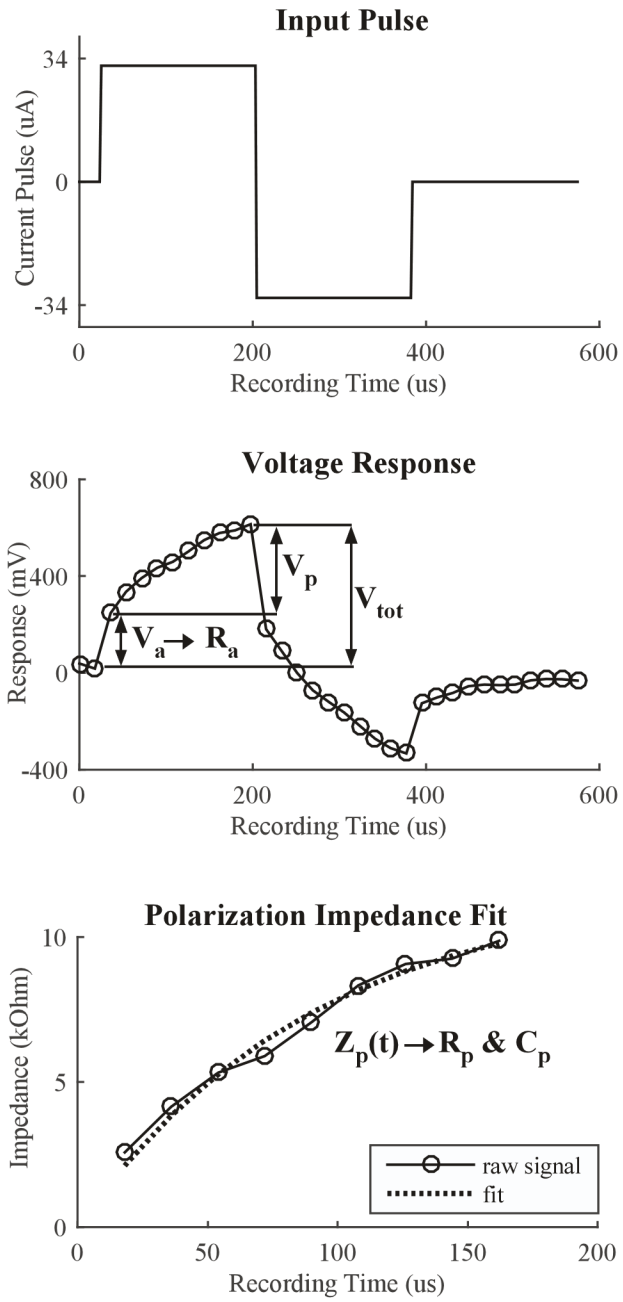


**Figure 5.2 - Impedance Waveforms and Fit**

Stimulus, Recording, and Analysis of Impedance. (top) The CI generates a biphasic square pulse. The measured response (middle) includes an immediate jump in voltage ($V_a$) and a polarizing growth ($V_p$). $V_a$ is used to calculate $R_a$ while $V_p$ is split into $R_p$ and $C_p$ (bottom) by modelling the circuit as a resistor and capacitor in parallel, after subtracting $R_a$. *note:* uA $= \mu A$, us $= \mu s$

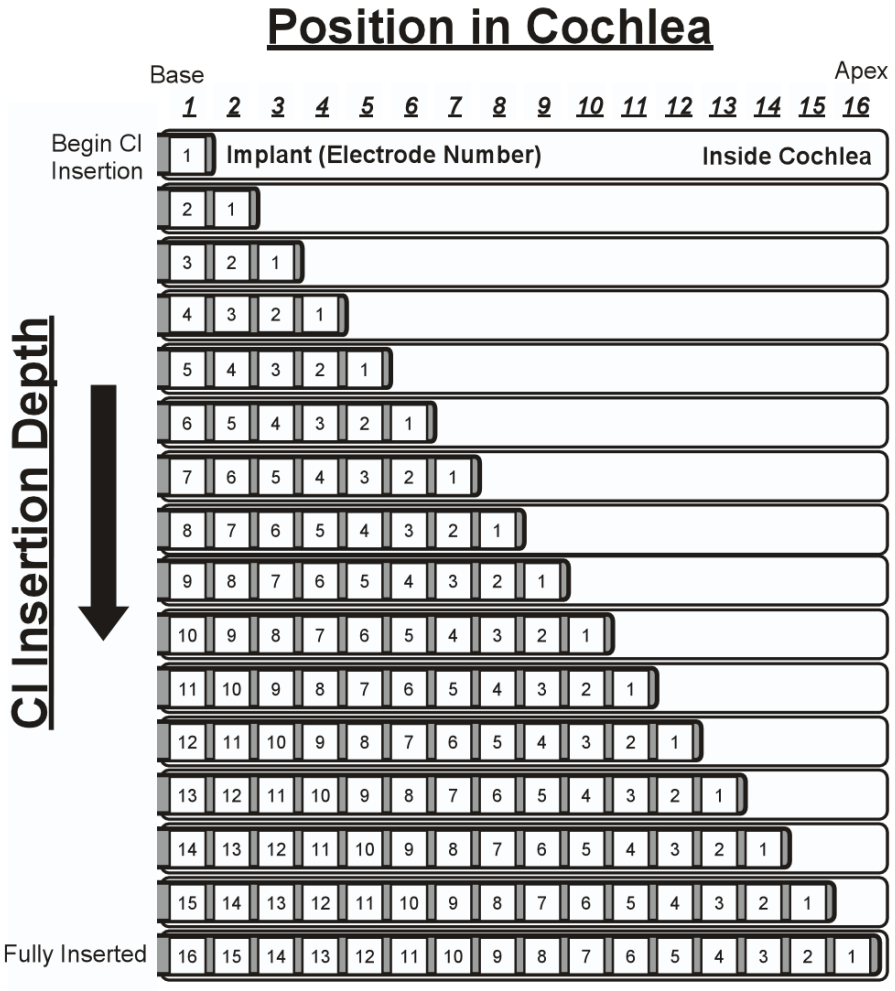


**Figure 5.3 - Position in Cochlea and Insertion Depth**
Relationship between Position in Cochlea and Insertion Depth. Each row represents a depth the CI is inserted into the model cochlea, and each boxed number is an electrode contact. Each column is the position of the cochlea. E1 is the deepest electrode throughout insertion.

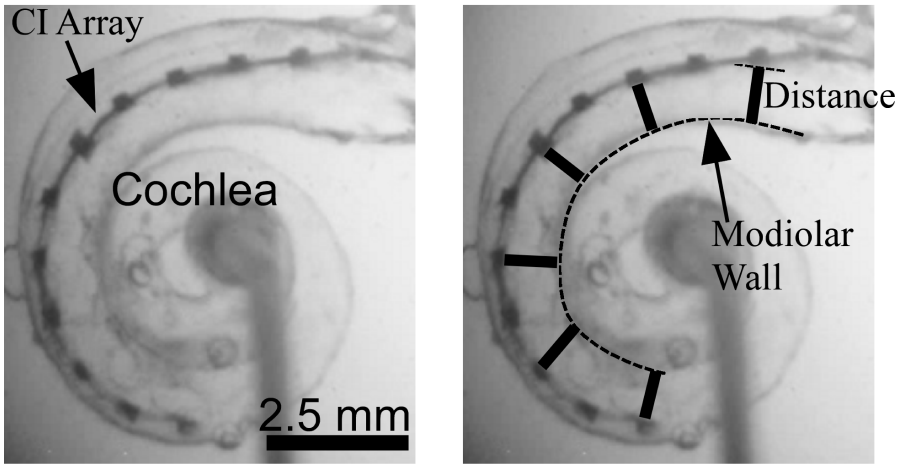


**Figure 5.4 - Microscopy and CI Position**
From a micrograph of the CI array in a plastic cochlea model (a), it is possible to assess the distance (b, solid bar) from each contact to the modiolar wall (b, dashed line).

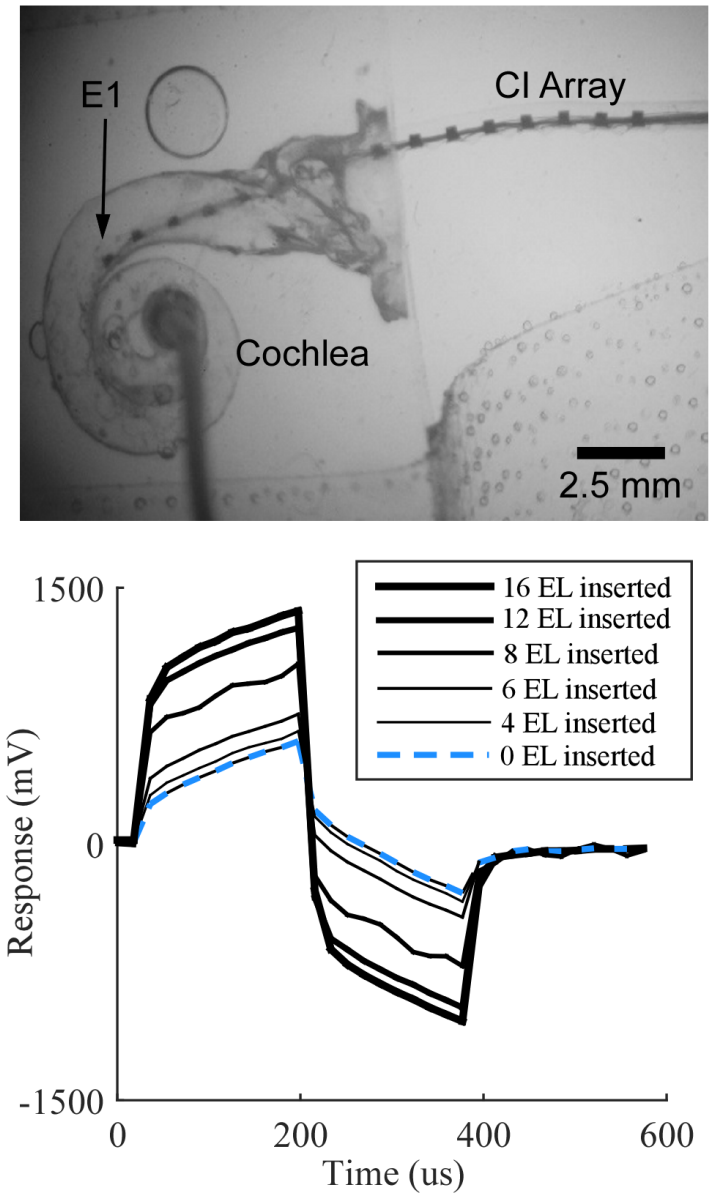


**Figure 5.5 - Impedance and Insertion Depth**
Relationship between E1 response magnitude and insertion depth during CI insertion. (top) Microscopy of mid-CI insertion, just before CI insertion (1 EL contact into the cochlea) and during insertion (8 EL contacts inserted). (bottom) The voltage required to allow the current pulse increases with E1 insertion depth. Grossly, total impedance of E1 grows with insertion depth. *note:* us $= \mu s$

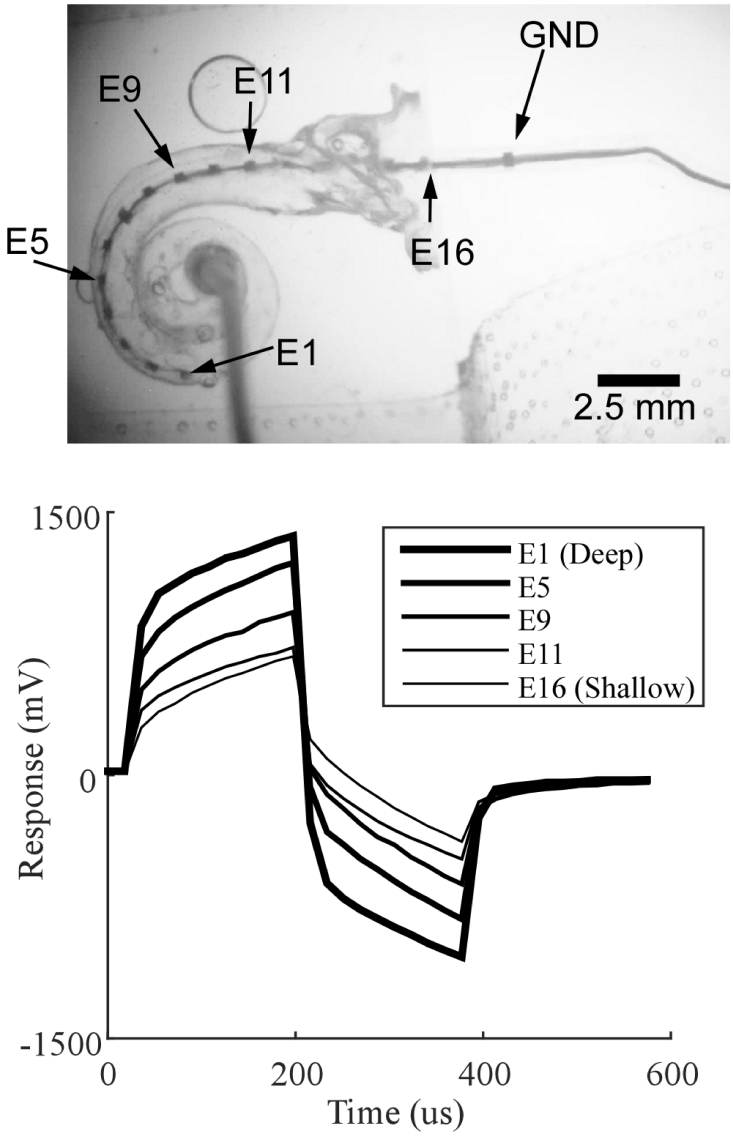


**Figure 5.6 - Impedance and Contact Number**
Relationship between response magnitude and electrode contact in a fully-inserted CI. (top) demonstrates a fully inserted CI and corresponding electrode contact numbers. (bottom) demonstrates response magnitude is greatest for the deepest electrode contacts.
*note:* us $= \mu s$

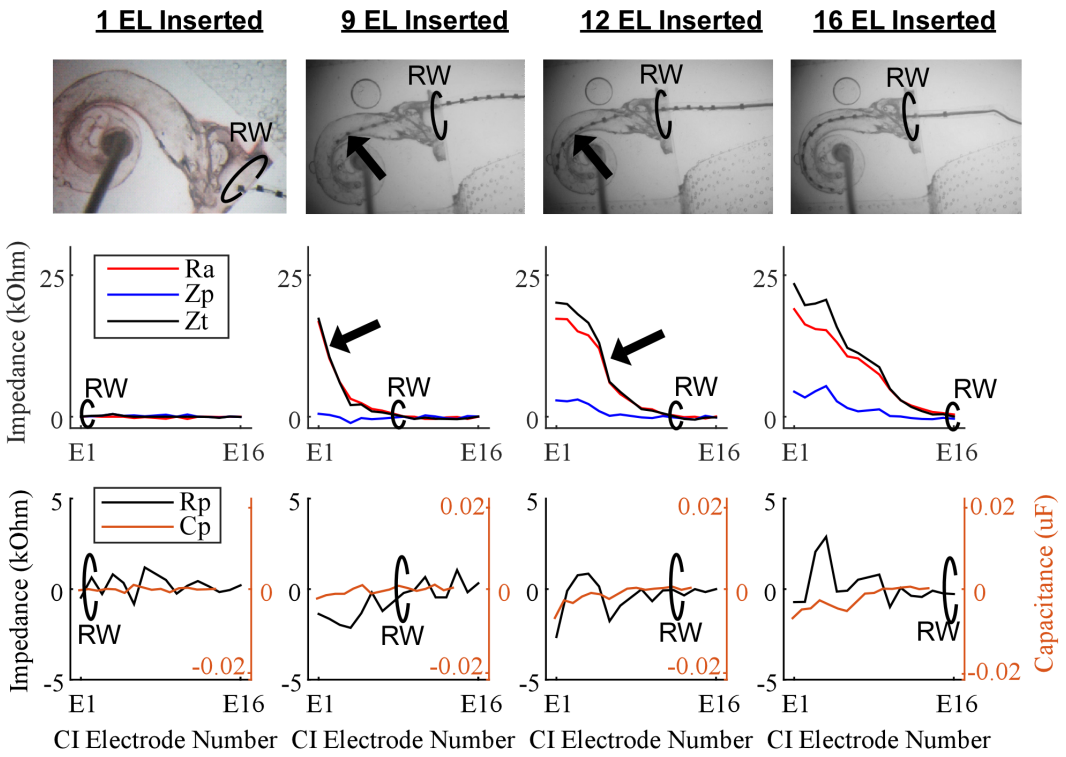


**Figure 5.7 - Impedance throughout CI Insertion**

Components of impedance across all CI electrode contacts at 4 stages of CI insertion normalized by saline. (Column 1) with 1 EL inserted (Row 1), $R_a$, $Z_p$, and $Z_t$ are the same as in saline (Row 2). Row 3 demonstrates splitting of $Z_t$ into $R_p$ and $C_p$. At 9 EL inserted (Column 2), exponential growth in $Z_t$ is dominated by $R_a$, and these apical electrodes are close to the modioloar wall (arrow). At 12 EL inserted (Column 3), electrode contacts 4-8 are close to the modioloar wall and demonstrate exponential growth in $R_a$. At full CI insertion, (Column 4), no electrodes are significantly close to the inner modiolar wall and $Z_t$ is roughly linear. *note:* uF $= \mu F$

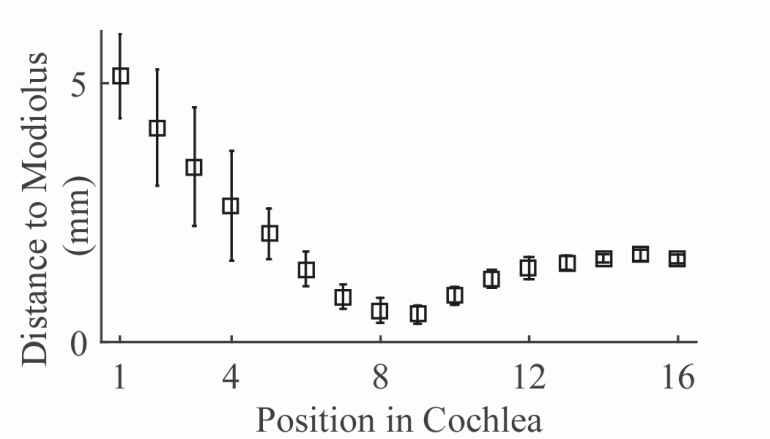


**Figure 5.8 - Patterns of Electrode Proximity**
Array contacts passing the base of the cochlea (position 1) are further in proximity than those passing the basal turn (position 8). Toward the apex (position 8), the array bows out to roughly 1.5 mm.

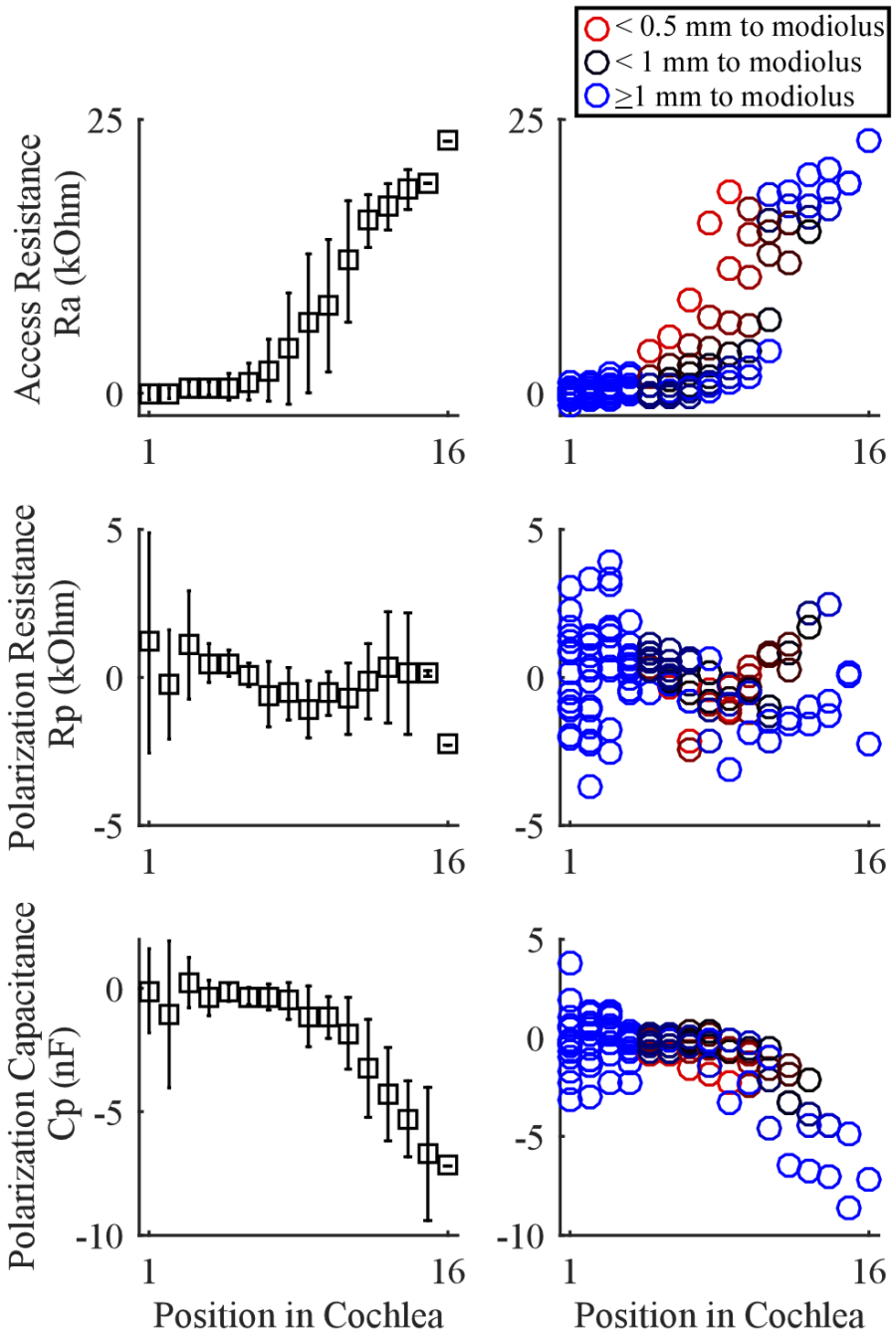


**Figure 5.9 - Changes in Impedance as a function of Cochlear Position**
Changes in access resistance, polarization resistance, and polarization capacitance as a function of cochlear position (left column). Incorporating microscopy data (right column), demonstrates proximity highly affects $R_a$ at a given insertion depth. $R_a$, $R_p$, and $C_p$ are normalized (values from saline subtracted out)

# REFERENCES


Adunka, O. F., C. K. Giardina, E. J. Formeister, B. Choudhury, C. A. Buchman and D. C. Fitzpatrick (2015). "Round window electrocochleography before and after cochlear implant electrode insertion." Laryngoscope.

Busby, P., K. Plant and L. Whitford (2013). "Electrode impedance in adults and children using the Nucleus 24 cochlear implant system." Cochlear implants international.

Clark, J. R., F. M. Warren and J. J. Abbott (2011). "A scalable model for human scala-tympani phantoms." Journal of Medical Devices 5(1): 014501.

Cohen, L. T., J. Xu, S. A. Xu and G. M. Clark (1996). Improved and simplified methods for specifying positions of the electrode bands of a cochlear implant array, LWW.

Davis, T. J., D. Zhang, R. H. Gifford, B. M. Dawant, R. F. Labadie and J. H. Noble (2016). "Relationship between electrode-to-modiolus distance and current levels for adults with cochlear implants." Otology & neurotology: official publication of the American Otological Society, American Neurotology Society [and] European Academy of Otology and Neurotology 37(1): 31-37.

DeVries, L., R. Scheperle and J. A. Bierer (2016). "Assessing the electrode-neuron interface with the electrically evoked compound action potential, electrode position, and behavioral thresholds." Journal of the Association for Research in Otolaryngology 17(3): 237-252.

Finley, C. C., T. A. Holden, L. K. Holden, B. R. Whiting, R. A. Chole, G. J. Neely, T. E. Hullar and M. W. Skinner (2008). "Role of electrode placement as a contributor to variability in cochlear implant outcomes." Otol Neurotol 29(7): 920-928.

Fitzpatrick, D. C., A. T. Campbell, B. Choudhury, M. P. Dillon, M. Forgues, C. A. Buchman and O. F. Adunka (2014). "Round window electrocochleography just before cochlear implantation: relationship to word recognition outcomes in adults." Otol Neurotol 35(1): 64-71.

Holden, L. K., C. C. Finley, J. B. Firszt, T. A. Holden, C. Brenner, L. G. Potts, B. D. Gotter, S. S. Vanderhoof, K. Mispagel, G. Heydebrand and M. W. Skinner (2013). "Factors Affecting Open-Set Word Recognition in Adults With Cochlear Implants." Ear Hear.

Hughes, M. (2012). Objective measures in cochlear implants, Plural Publishing.

Jones, G. L., J. Ho Won, W. R. Drennan and J. T. Rubinstein (2013). "Relationship between channel interaction and spectral-ripple discrimination in cochlear implant users a." The Journal of the Acoustical Society of America 133(1): 425-433.

Kratchman, L., D. Schuster, M. Dietrich and R. Labadie (2016). "Force Perception Thresholds in Cochlear Implantation Surgery." Audiology and Neurotology 21(4): 244-249.

Lazard, D. S., C. Vincent, F. Venail, P. Van de Heyning, E. Truy, O. Sterkers, P. H. Skarzynski, H. Skarzynski, K. Schauwers, S. O'Leary, D. Mawman, B. Maat, A. Kleine-Punte, A.

M. Huber, K. Green, P. J. Govaerts, B. Fraysse, R. Dowell, N. Dillier, E. Burke, A. Beynon, F. Bergeron, D. Baskent, F. Artieres and P. J. Blamey (2012). "Pre-, per- and postoperative factors affecting performance of postlinguistically deaf adults using cochlear implants: a new conceptual model over time." PLoS One 7(11): e48739.

Limnuson, K., H. Lu, H. J. Chiel and P. Mohseni (2014). "Real-time stimulus artifact rejection via template subtraction." IEEE transactions on biomedical circuits and systems 8(3): 391-400.

Mandala, M., L. Colletti, G. Tonoli and V. Colletti (2012). "Electrocochleography during cochlear implantation for hearing preservation." Otolaryngol Head Neck Surg 146(5): 774-781.

Maneva, S. M. (1970). The radiology report for cochlear implant: what the surgeon wants to know, European Congress of Radiology 2014.

McClellan, J. H., E. J. Formeister, W. H. Merwin, 3rd, M. T. Dillon, N. Calloway, C. Iseli, C. A. Buchman, D. C. Fitzpatrick and O. F. Adunka (2014). "Round window electrocochleography and speech perception outcomes in adult cochlear implant subjects: comparison with audiometric and biographical information." Otol Neurotol 35(9): e245-252.

Mens, L. H. (2007). "Advances in cochlear implant telemetry: evoked neural responses, electrical field imaging, and technical integrity." Trends in amplification 11(3): 143-159.

Miller, C. A., C. J. Brown, P. J. Abbas and S. L. Chi (2008). "The clinical application of potentials evoked from the peripheral auditory system." Hear Res 242(1-2): 184-197.

Mittmann, P., A. Ernst and I. Todt (2015). "Intraoperative electrophysiologic variations caused by the scalar position of cochlear implant electrodes." Otology & Neurotology 36(6): 1010-1014.

Nag, S., S. K. Sikdar, N. V. Thakor, V. R. Rao and D. Sharma (2015). "Sensing of stimulus artifact suppressed signals from electrode interfaces." IEEE Sensors Journal 15(7): 3734-3742.

Noble, J. H., R. H. Gifford, A. J. Hedley-Williams, B. M. Dawant and R. F. Labadie (2014). "Clinical evaluation of an image-guided cochlear implant programming strategy." Audiology and Neurotology 19(6): 400-411.

O'Connell, B. P., J. B. Hunter and G. B. Wanna (2016). "The importance of electrode location in cochlear implantation." Laryngoscope Investigative Otolaryngology 1(6): 169-174.

O'Connell, B. P., A. Cakir, J. B. Hunter, D. O. Francis, J. H. Noble, R. F. Labadie, G. Zuniga, B. M. Dawant, A. Rivas and G. B. Wanna (2016). "Electrode location and angular insertion depth Are predictors of audiologic outcomes in cochlear implantation." Otology & Neurotology 37(8): 1016-1023.

Pile, J., A. D. Sweeney, S. Kumar, N. Simaan and G. B. Wanna (2016). "Detection of modiolar proximity through bipolar impedance measurements." The Laryngoscope.

Radeloff, A., W. Shehata-Dieler, A. Scherzed, K. Rak, W. Harnisch, R. Hagen and R. Mlynski (2012). "Intraoperative monitoring using cochlear microphonics in cochlear implant patients with residual hearing." Otol Neurotol 33(3): 348-354.

Saunders, E., L. Cohen, A. Aschendorff, W. Shapiro, M. Knight, M. Stecker, B. Richter, S. Waltzman, M. Tykocinski and T. Roland (2002). "Threshold, comfortable level and impedance changes as a function of electrode-modiolar distance." Ear and hearing 23(1): 28S-40S.

Shepherd, R. K., S. Hatsushika and G. M. Clark (1993). "Electrical stimulation of the auditory nerve: the effect of electrode position on neural excitation." Hear Res 66(1): 108-120.

Tan, C. T., M. Svirsky, A. Anwar, S. Kumar, B. Caessens, P. Carter, C. Treaba and J. T. Roland (2013). "Real-time measurement of electrode impedance during intracochlear electrode insertion." The Laryngoscope 123(4): 1028-1032.

Tan, L., S. K. Holland, A. K. Deshpande, Y. Chen, D. I. Choo and L. J. Lu (2015). "A semi-supervised Support Vector Machine model for predicting the language outcomes following cochlear implantation based on pre-implant brain fMRI imaging." Brain and Behavior 5(12).

Tang, C., F. You, G. Cheng, D. Gao, F. Fu, G. Yang and X. Dong (2008). "Correlation between structure and resistivity variations of the live human skull." IEEE Transactions on Biomedical Engineering 55(9): 2286-2292. Tykocinski, M., L. T. Cohen and R. S. Cowan (2005). "Measurement and analysis of access resistance and polarization impedance in cochlear implant recipients." Otology & Neurotology 26(5): 948-956.

Vanpoucke, F., A. Zarowski, J. Casselman, J. Frijns and S. Peeters (2004). "The facial nerve canal: an important cochlear conduction path revealed by Clarion electrical field imaging." Otology & Neurotology 25(3): 282-289.

Vanpoucke, F. J., P.-P. B. Boermans and J. H. Frijns (2012). "Assessing the placement of a cochlear electrode array by multidimensional scaling." Biomedical Engineering, IEEE Transactions on 59(2): 307-310.

Vanpoucke, F. J., A. J. Zarowski and S. A. Peeters (2004). "Identification of the impedance model of an implanted cochlear prosthesis from intracochlear potential measurements." Biomedical Engineering, IEEE Transactions on 51(12): 2174-2183.

Wysocki, J. (1999). "Dimensions of the human vestibular and tympanic scalae." Hearing research 135(1): 39-46.

# THESIS CONCLUSIONS

The work presented includes detailed studies of attempts to monitor trauma during insertion - in light of the complex ECochG signal as a mixture of different sources that can be affected unequally by interaction of the array with cochlear tissue. This provides new and important baseline features that need to be understood for this technology to be adopted clinically.

# CHAPTER 6: ONGOING WORK

## Returning to Extracochlear ECochG: Hearing Preservation

Patterns of response were obtained at an extracochlear site (Chapter 2), but these results weren't correlated with hearing outcomes. For the subset of extracochlear recordings obtained from subjects with significant pre-operative hearing (HL at 250 Hz $\leq$ 80 dB HL), Fig. 6.1 demonstrates these response tracks for three different lateral wall arrays. The left column contains tracks whose responses, start to finish, were within 5 dB, whereas the right column demonstrates a permanent response drop greater than 5 dB. Similar to the color scheme introduced in Chapter 4, blue indicates subjects with preserved hearing and red indicates subjects whose hearing was lost as result of implantation. Additionally, the rows are separated by device type. The top row contains the shortest array in this dataset, the MEDEL Flex 24 array which typically has an insertion depth of 408° (IQ range 373°–449°) (O'Connell, Hunter et al. 2017). In this case, all 8 subjects had preserved hearing, regardless of whether the ECochG placed them in the 'atraumatic' or 'drop' category. The second row has the MEDEL Flex 28 array, which is slightly longer and typically reaches an insertion depth of 575° (IQ Range 465°–584°) (O'Connell, Hunter et al. 2017). This array had 6 subjects in the 'atraumatic' category, 3 of which had hearing preserved and 3 lost hearing. In the 'drop' category (n=4), the subject with the largest (20 dB) drop lost hearing, but significant (10 dB) drops were seen in subjects whose hearing was preserved. In the third row are the longest, 31.5 mm length MEDEL Standard arrays, whose insertion depth typically reaches 584° (IQ range 368°–643°) (O'Connell, Hunter et al. 2017). In the 'atraumatic' category (n=9), 7 lost hearing and 2 had preserved hearing. In the 'drop' category, 3 of the 4 subjects lost hearing. The bottom row illustrates all subjects, regardless of array length.

It is worthwhile to note the separation of hearing preservation rates by array length – that shorter arrays tended to have better postoperative hearing compared to longer arrays. This finding is generally consistent with most other studies, who attribute post-implant inflammation with longer arrays as a source of hearing loss that may be independent of intra-insertion trauma (Adunka, Pillsbury et al. 2009, O'Connell, Hunter et al. 2016, O'Connell, Hunter et al. 2017). The mechanism for this foreign body reaction occurs hours to weeks after implantation and is typically a function of implant size (Anderson, Rodriguez et al. 2008), thus it would be expected that longer (larger) arrays elicit greater intracochlear inflammation and would cause larger losses in hearing. Consistent with this reasoning, even for completely-within-ST insertions, longer arrays had significantly higher rates of hearing loss than shorter arrays (O'Connell, Hunter et al. 2017). This may explain why 7 of the 9 subjects with Standard arrays that exhibited 'atraumatic' ECochGs eventually lost hearing; that hearing loss occurred because of a more robust inflammatory reaction associated with the longer array rather than overt intra-insertion trauma. However, that large (10 dB) drops could be seen in the Flex 24 subjects despite preserved hearing still prompts investigation. A more thorough analysis of the nature of the drops, with the model of the ongoing response introduced in Chapter 3, is warranted.

## Simultanoues Intra- and Extra-cochlear ECochG

Investigators typically investigate extracochlear or intracochlear ECochG when studying the ECochG throughout CI insertion. However, as discussed in this dissertation and proposed by others (Dalbert, Pfiffner et al. 2015, Dalbert, Pfiffner et al. 2018), these signals are not inherently synonymous with one another. To characterize the differences, it is necessary to record simultaneous intra- and extra-cochlear ECochG to the same stimuli, and compare the signals directly. To this end, in 6 subjects we recorded RW responses and then concurrent extracochlear and intracochlear ECochG throughout CI insertion. A surgical image of the setup through the operating microscope (Fig. 6.2) shows the complexity of monitoring from such a cochlea, which likely explains why this approach has never been utilized elsewhere. Because the BioLogic setup allowed for 2-channel recording (Ch1 in-

tracochlear, Ch2 extracochlear) for the same stimulus (500 Hz, 90 dB nHL), it is possible to acquire signals simultaneously and ensure they are responding to the same exact stimuli at the same time.

In the 6 subjects, 2 received the CI512 modiolar array, and 4 received the CI522 lateral wall array for intended hearing preservation (Table 6.1). Post-operative audiometry determined all 4 subjects who were hearing preservation candidates had preserved thresholds after implantation. As a principal analysis, Round Window measurements were compared to the first simultaneous extracochlear and intracochlear measurement made in all 6 subjects (Fig. 6.3). Consistent with previous findings, the intracochlear response was typically 5.2 dB larger than that at the RW, and the extracochlear response was lower than the RW. Because the surgical field was somewhat cluttered with recording electrodes, it became necessary to shift the extracochlear electrode more anteriorly on the promontory. This likely explains why the responses were typically smaller than those acquired at the two sites evaluated in Chapter 2 of this dissertation. Still, responses at all recording sites were successfully obtained in all 6 subjects.

Example waveforms of simultaneous intra- and extra-cochlear ECochG throughout CI insertion in one subject (subject 5) are displayed in Fig. 6.4. Despite the large difference in scale bars (black vs. blue), clear responses can be seen at both sites. Magnitude and Phase Tracks for all six subjects are displayed in Fig. 6.5 (magnitude in top row, phase in bottom row). The left two columns are the CI512 cases, whereas the right four columns are the CI522 cases. The CI512 cases both show strong early intracochlear magnitude growth (Fig. 6.5A, blue), but in subject 1 there is a reversible drop after stylet removal while in subject 2 there is a permanent drop. In the extracochlear recordings (Fig. 6.5A, black), subject 1 showed an early and late permanent drop, while subject 2 had a large, reversible drop during stylet removal. The associated phases of these responses (Fig. 6.5B) demonstrated near-complete intracochlear phase inversion (blue) but only slight extracochlear phase changes (black) during the later stages of insertion when stylet removal occurs. In the CI522 cases, for intracochlear responses (Fig. 6.5C, blue), subject 3 demonstrates and early drop with subsequent growth, subject 4 demonstrates a steady response, subject 5 demonstrates a steady response and then growth, and subject 6 demonstrates growth and

then a slight drop at the end. Extracochlear recordings (Fig. 6.5C, black) demonstrate early, reversible drops in subjects 4 and 6, a late drop in subject 3, and a small response growth in subject 5. Intracochlear phases (Fig. 6.5D, blue) typically grew with insertion depth, but in subject 4 there was no phase change whatsoever, even at the extracochlear site (black). Extracochlear phases were typically steady in all CI522 subjects.

It is evident when taking these pilot results as a whole that 1) intracochlear magnitude and phase changes can occur independently from extracochlear magnitude and phase changes, and 2) intracochlear recordings tend to have growing amplitudes and latencies throughout insertion which are not seen on the extracochlear recordings. To investigate the relationship between intracochlear magnitudes and phases, and their relation to insertion depth, scatter plots were generated (Fig. 6.6). In panel A, intracochlear magnitude was found to significantly correlate with extracochlear magnitude for all recording pairs (Fig. 6.6A, $r=0.75$, $p<0.001$). Additionally, the difference in magnitude between these two sites significantly correlated with insertion depth (Fig. 6.6B, $r=0.49$, $p<0.01$). Phase relations between recording pairs were not found to be significant (Fig. 6.6C, $r=0.13$, $p=0.46$), and the phase difference between recording sites was not correlated with insertion depth (Fig. 6.6D, $r=-0.28$, $p=0.11$). Ongoing work will include further analysis of these waveforms with the model to determine if these recording sites are ultimately recording from distinct populations of generators.

## Estimation of Insertion Angle from an X-ray

CI insertion angle is an important factor in addressing CI outcomes (O'Connell, Hunter et al. 2016). The most robust approach to determine positioning requires post-operative CT imaging, however this remains mostly a research tool and is associated with some radiation risk. For this reason, post-operative CT imaging is only used in adults and will likely never be used in children. However, in nearly all CI cases, an intraoperative radiograph is obtained to ensure correct device placement. This clinical assessment is based on whether the array is grossly within the cochlea (rather than a vestibular canal) and that the array is not folded over.

When an X-ray is shot perfectly down the cochlear axis (horizontally level and 50 degrees from midline), it is possible to accurately obtain the CI insertion angle of each electrode contact. This radiographic view, called the Cochlear View (Xu, Xu et al. 2000), is necessary to both visualize the RW (angle reference point), the center of the cochlea, and ultimately ensure that the array is properly projected from the three-dimensional skull onto the 2D radiograph without skewing. When oriented properly, this view is sufficient to resolve insertion angle but this view cannot always be obtained at the time of surgery. Because the angle of the head can vary substantially (Svrakic, Friedmann et al. 2015), it would thus be useful to have a flexible tool to assess CI insertion angle from a 2D radiograph without knowing the angle the XRay was shot from.

The approach was to build a software tool which projected a standard cochlear spiral over a patient's 2D X-ray, and allow the user to manipulate the spiral's projection 3D until the array roughly matched the 2D spiral's path. A standard cochlear spiral has been often modelled as (1) and Fig. 6.7 (Clark, Warren et al. 2011):

$$R(\theta) = \left\{ \begin{array}{cc} C\big(1 - D\ln(\theta - \theta_0)\big) & \theta_1 \leq \theta < 100^\circ \\ Ae^{-B\theta} & 100^\circ \leq \theta < \theta_f \end{array} \right\} \tag{1a}$$

$$Z(\theta) = E\big(\theta - \theta_1\big) \tag{1b}$$

where $A = 3.762$

$B = 0.001317$

$C = 7.967$

$D = 0.1287$

$E = 0.003056$

$\theta_0 = 5.0^\circ$

$\theta_1 = 10.3^\circ$

$\theta_f = 910.3^\circ$

Because of variance in cochlear size, the software tool allows for scaling and stretching of the x, y, and z dimensions independently or as a whole. Additionally, using standard

isometric 3D projection techniques in MATLAB, it was straightforward to implement additional user options to rotate the cochlear spiral about 3 spatial planes independently, and also rotate the cochlea along its own central axis.

To test the tool, a real CI array was implanted into a cadaveric human temporal bone and imaged with a CT scanner. Using ImageJ, it was possible to deconstruct this 3D scan and create projected radiographs, wherein simulated X-rays at discrete viewing angles could be generated. The tool was then used to estimate the CI insertion angle for each projected X-ray. Although each radiograph had its own associated (known) X-ray angle, this information was blinded when attempting to fit the spiral to the image. Examples of fitted spirals at two X-ray projection angles are demonstrated in Fig 6.8, with the cochlear view in Fig. 6.8A and a standard Anterior-Posterior (AP) view in Fig. 6.8B. At an X-ray angle of 50° off from the cochlear axis (Fig. 6.8B), the predicted CI angular insertion depth was 298 degrees, just 11 degrees off from the angle of insertion calculated down the cochlear view (Fig. 6.8A). This result is consistent with others who evaluated the extent of error when the film angle was slightly off from the cochlear view (Svrakic, Friedmann et al. 2015). Ongoing work is being performed to validate this tool with intraoperative X-rays from 10 subjects, wherein the insertion angle is estimated immediately after insertion, and compared to the actual insertion angle as determined from a post-operative CT performed at a later date. Both intra-rater variance and inter-rater variance will be assessed.

# TABLES

Table 6.1: Subject Demographics

| | | | | | | HL at 500 Hz (dB HL) | | LF PTA (dB HL) | | |
|---|---|---|---|---|---|---|---|---|---|---|
| Subject | ID | Age/Sex | Etiology | Side | Device | Pre-operative | Post-operative | Pre-operative | Post-operative | HP Category |
| 1 | 472 | 5yo / M | Unknown | R | CI512 Contour Advance | 120.0 | N/A | 120.0 | N/A | N/A |
| 2 | 436 | 4yo / M | Unknown | R | CI512 Contour Advance | 85.0 | N/A | 78.7 | N/A | N/A |
| 3 | 466 | 3yo / M | ANSD | R | CI522 Slim Straight | 50.0 | 55.0 | 67.5 | 66.5 | Preserved |
| 4 | 447 | 5yo / F | *CLDN14* | L | CI522 Slim Straight | 45.0 | 50.0 | 42.5 | 46.3 | Preserved |
| 5 | 476 | 11yo / F | Unknown | L | CI522 Slim Straight | 75.0 | 80.0 | 67.5 | 78.7 | Preserved |
| 6 | 471 | 14yo / F | ANSD | L | CI522 Slim Straight | 50.0 | 60.0 | 31.2 | 38.8 | Preserved |

**Table 6.1 - Subject Demographics for Intra- and Extra-cochlear ECochG**
6 subjects were included, two receiving Cochlear Corporation's CI512 arrays and four receiving Cochlear Corporation's CI522 arrays. All 4 subjects with the CI522 had successful hearing preservation.

# FIGURES

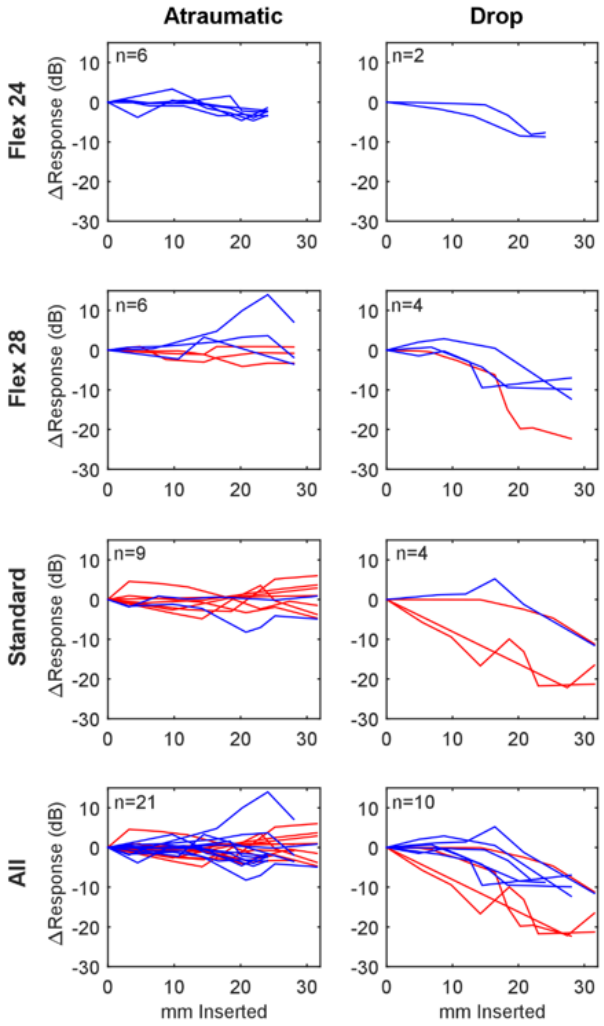


**Figure 6.1 - Extracochlear ECochG Tracks and Hearing Preservation**
Rates of hearing preservation (blue) vs. hearing loss (red) for Flex 24 (top row), Flex 28 (second row), Standard (third row), and all (fourth row) MEDEL arrays. The left column demonstrates ECochG tracks which never dropped more than 5 dB, whereas the right column includes tracks where the response dropped more than 5 dB. Hearing preservation rates (blue vs. red) were heavily influenced by array length - Flex 24 arrays had better hearing preservation than the Standard arrays.

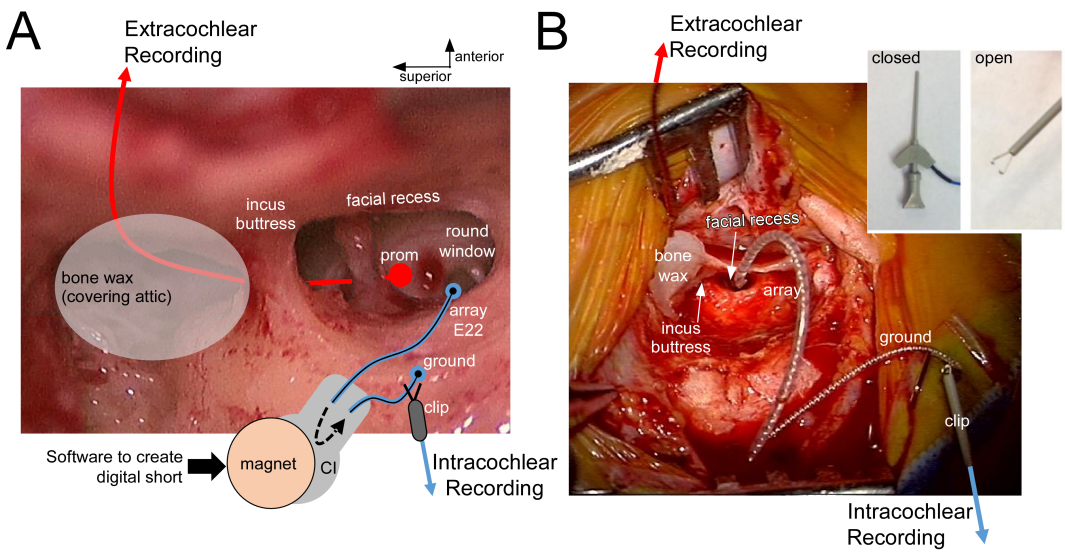


**Figure 6.2 - Surgical Field for Simultaneous Intra- and Extra-cochlear ECochG**
(A) A microscopic surgical view of a mastoidectomy with superimposed markers and (B) an actual setup. For extracochlear recording, the flexible electrode was advanced through the attic, onto the promontory, and fixed into place with bone wax. For the intracochlear setup, the device was seated, the magnet was connected, and a clip in the surgical field was attached to the ground of the implant. Insert: clip opened and closed.

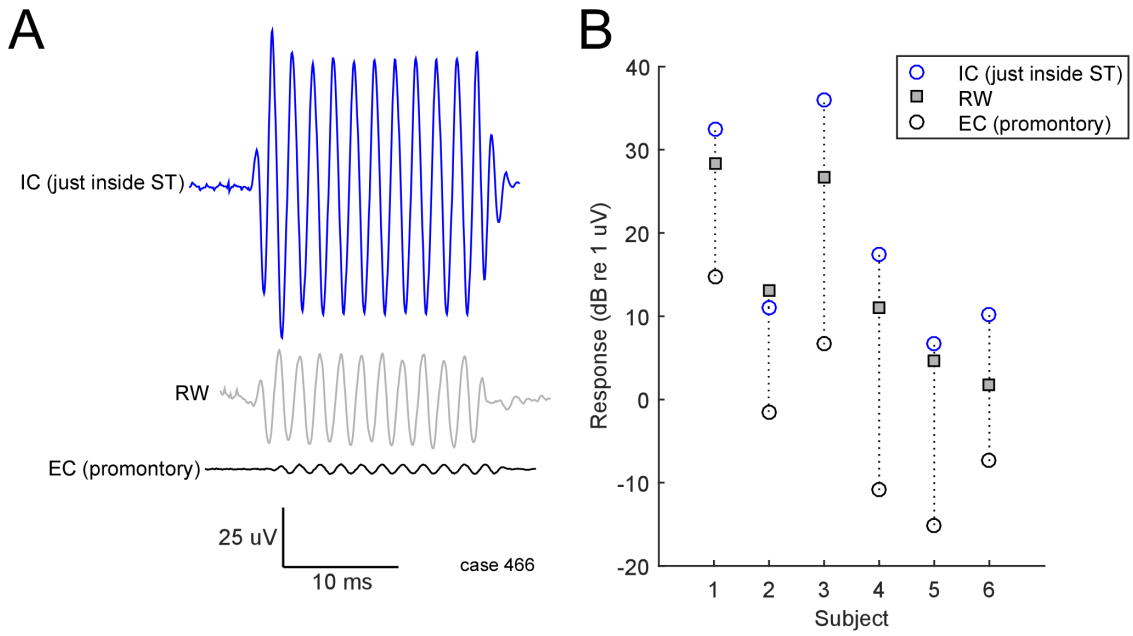


**Figure 6.3 - Magnitude differences between extra- and intra-cochlear recordings**
(A) Response waveforms for one subject shows an intracochlear response which is larger than that at the RW, and an extracochlear response which is smaller than that at the RW. (B) Across all 6 subjects, the median intracochlear response was 5.2 dB larger than that at the RW, but the promontory response was significantly lower. *note:* uV $= \mu V$

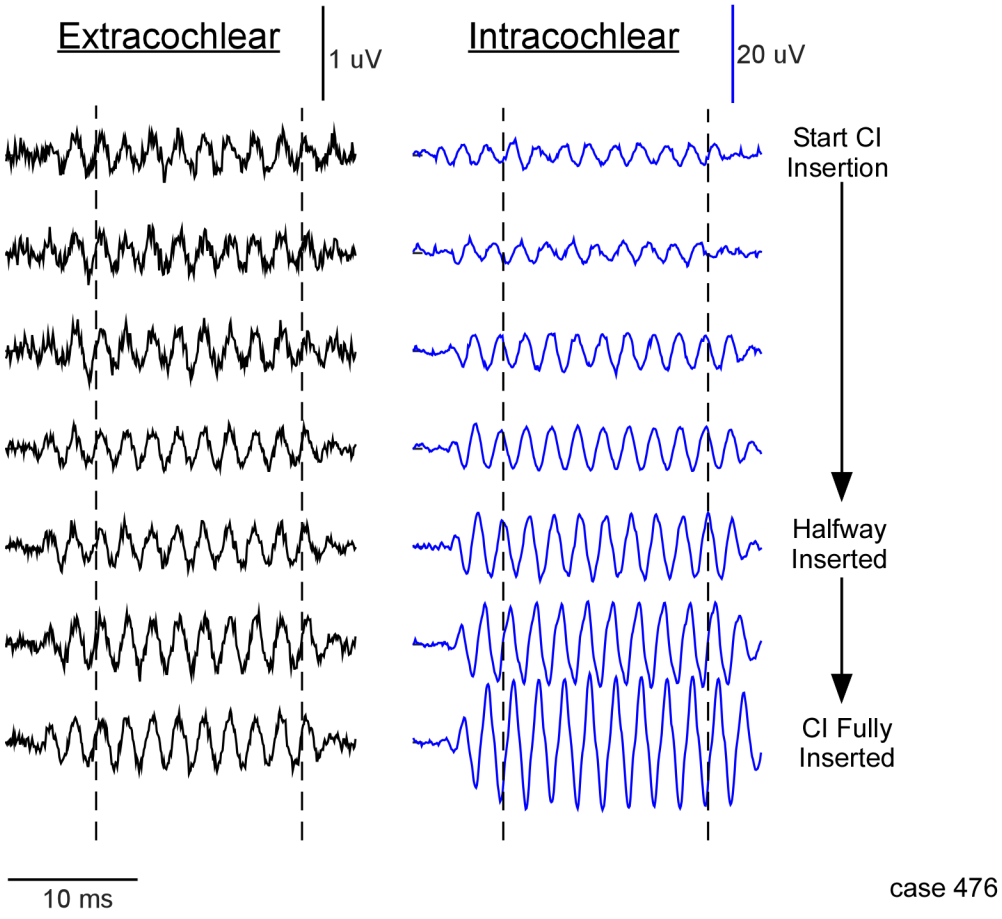


**Figure 6.4 - Waveforms of extra- and intra-cochlear recordings throughout CI insertion**

Extracochlear responses were much smaller than intracochlear responses at the start of CI insertion (top row, black vs. blue). Throughout CI insertion, the extracochlear response remained steady whereas the intracochlear response grew in magnitude (bottom row, black vs. blue). *note:* uV $= \mu V$

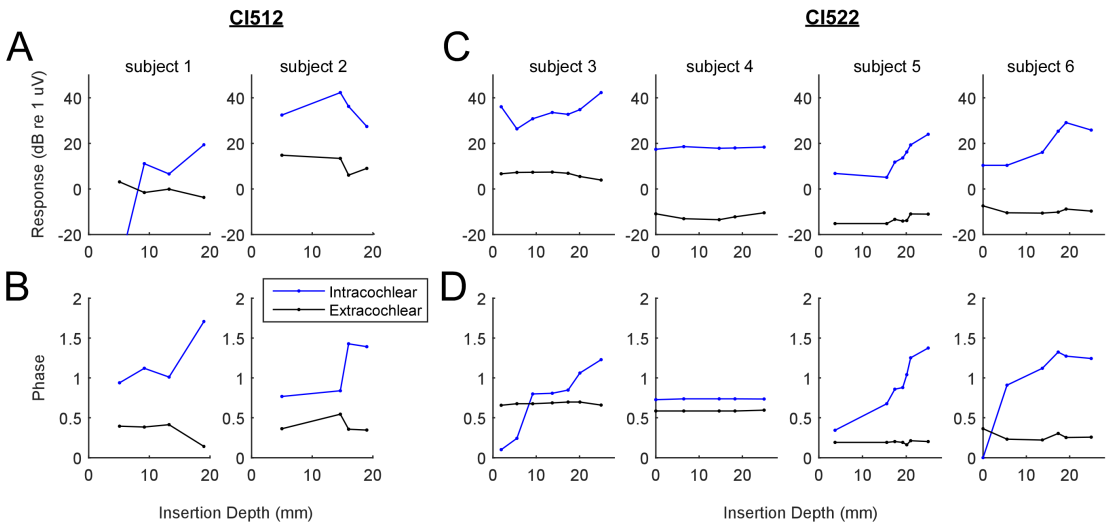


**Figure 6.5 - Magnitude and Phase Tracks for Intra- and Extra-cochlear ECochG**
Magnitude tracks (top row) and phase tracks (bottom row) are displayed for all 6 subjects, with intracochlear responses (blue) and extracochlear responses (black). In the CI512 subjects, fluctuations in intracochlear magnitudes are often observed with changes in intracochlear phase. In the CI522 subjects, intracochlear magnitudes could drop in the beginning and grow, remain steady, grow, or grow and then drop. These were typically associated with slowly lengthening latencies (elongating phases). Extracochlear responses showed early, reversible drops in subjects 4 and 6, but were largely stable. *note:* uV $= \mu V$

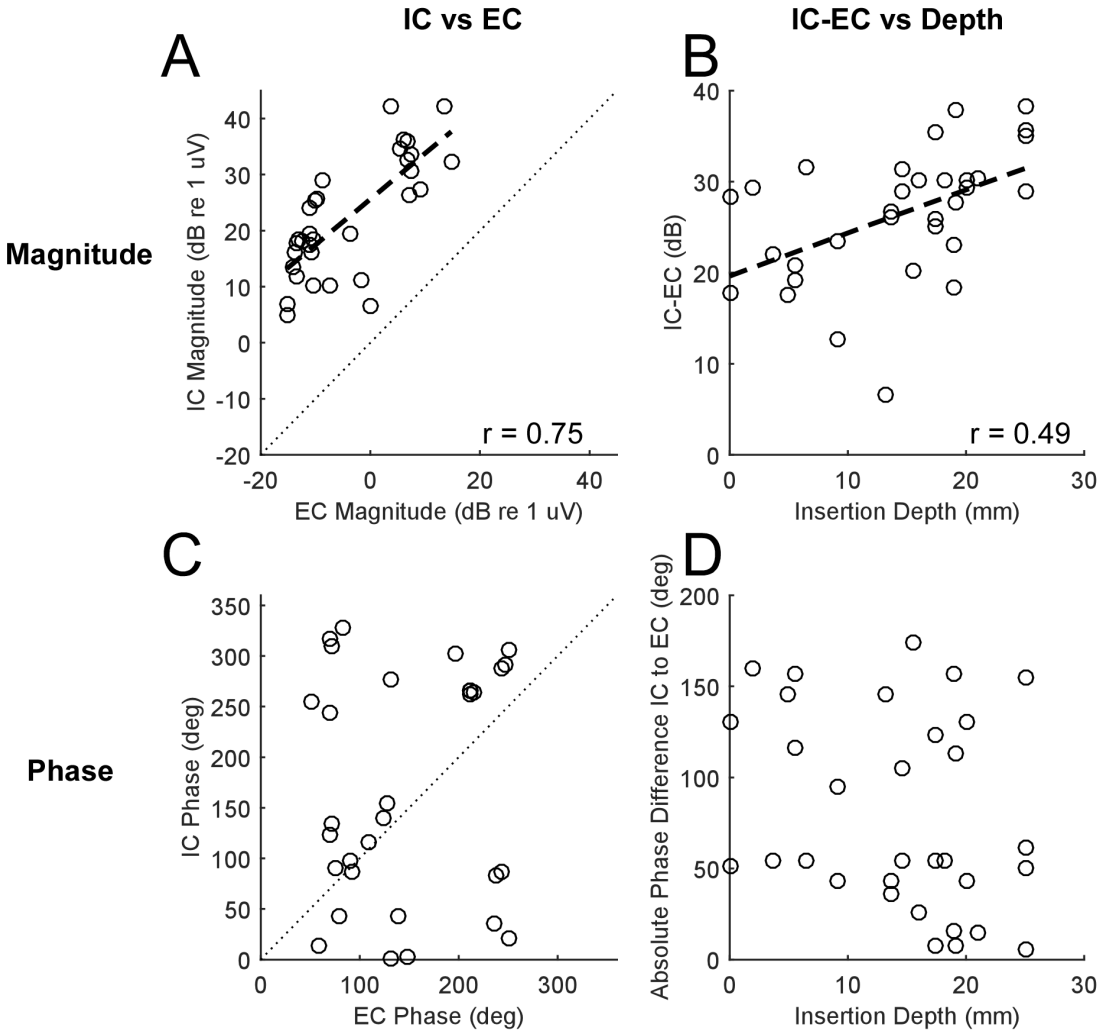


**Figure 6.6 - Relationship between Extracochlear and Intracochlear Recording Pairs**

Pooling all recording pairs from all subjects, it was found that (A) the intracochlear response magnitude was larger and correlated positively with the extracochlear response acquired at the same time (r=0.75). (B) Additionally, the difference in magnitude between intracochlear and extracochlear recording pairs was influenced by insertion depth (r=0.49). (C) Phase at the two sites were not correlated, and the difference in phase (D) was not influenced by insertion depth. *note:* uV $= \mu V$

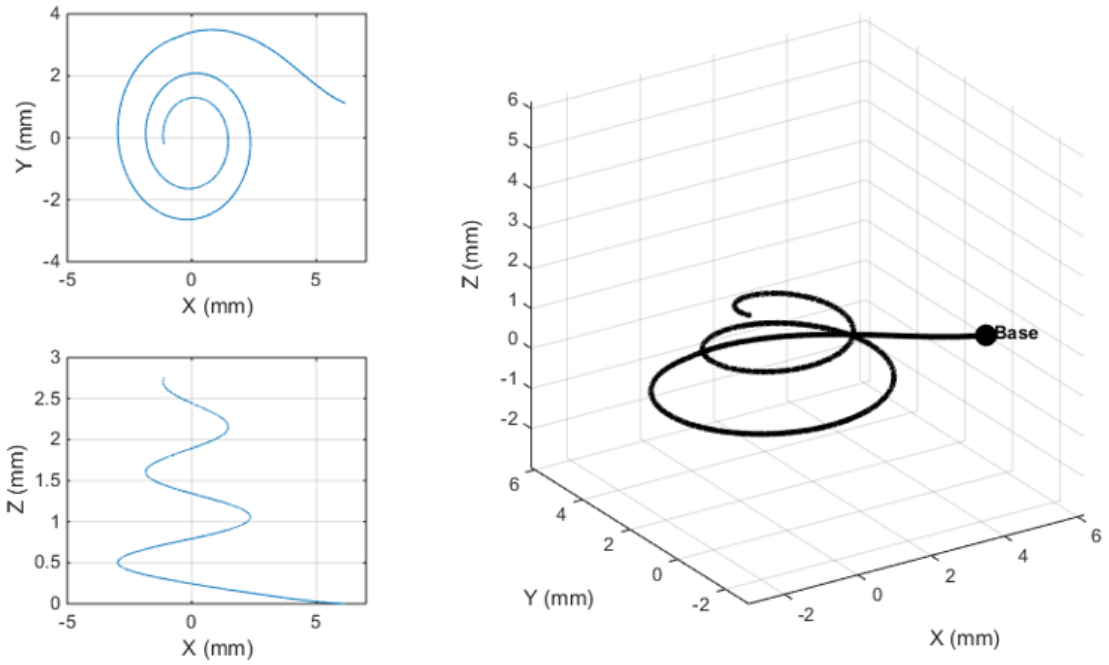


**Figure 6.7 - Helical Model of a Cochlear Scala Tympani**
The starting point for the model involves a 3D-modeled cochlea. The path here is that of the scala tympani (from Clark, Warren et al. 2011)

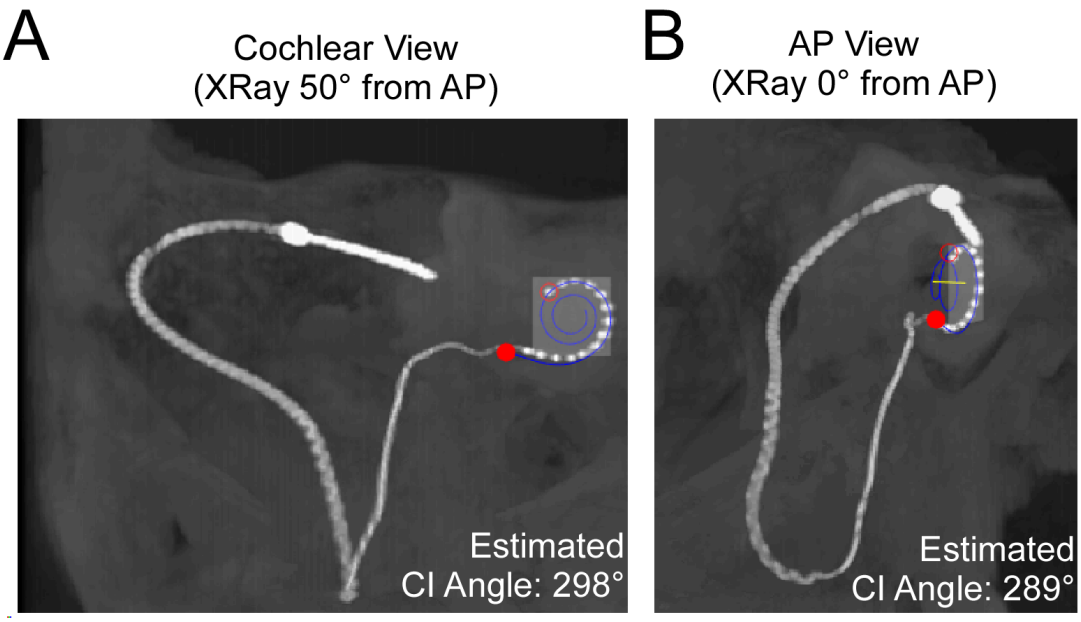


**Figure 6.8 - Implementation of 3D model on projected X-ray**
X-rays generated from a CT image from a single insertion at (A) "Cochlear View" and (B) down an Anteroposterior (AP) view. The cochlear spiral (blue) is overlayed over the scan, and user manipulation allows the Round Window (solid red dot), deepest contact (hollow red dot), and cochlear axis (yellow line) to be approximated. In this case, the known insertion angle (A) was 298° and when the X-ray was shot at an AP angle, the estimated insertion angle was 289°.

# REFERENCES


Adunka, O. F., H. Pillsbury and C. Buchman (2009). "Minimizing intracochlear trauma during cochlear implantation."

Anderson, J. M., A. Rodriguez and D. T. Chang (2008). Foreign body reaction to biomaterials. Seminars in immunology, Elsevier.

Clark, J. R., F. M. Warren and J. J. Abbott (2011). "A scalable model for human scala tympani phantoms." Journal of Medical Devices 5(1): 014501.

Dalbert, A., F. Pfiffner, M. Hoesli, K. Koka, D. Veraguth, C. Roosli and A. Huber (2018). "Assessment of Cochlear Function during Cochlear Implantation by Extra-and Intracochlear Electrocochleography." Frontiers in neuroscience 12: 18.

Dalbert, A., F. Pfiffner, C. Roeoesli, K. Thoele, J. H. Sim, R. Gerig and A. M. Huber (2015). "Extra-and Intracochlear Electrocochleography in Cochlear Implant Recipients." Audiology and Neurotology 20(5): 339-348.

O'Connell, B. P., J. B. Hunter, D. S. Haynes, J. T. Holder, M. M. Dedmon, J. H. Noble, B. M. Dawant and G. B. Wanna (2017). "Insertion depth impacts speech perception and hearing preservation for lateral wall electrodes." The Laryngoscope 127(10): 2352-2357.

O'Connell, B. P., J. B. Hunter and G. B. Wanna (2016). "The importance of electrode location in cochlear implantation." Laryngoscope Investigative Otolaryngology 1(6): 169-174.

Svrakic, M., D. R. Friedmann, P. M. Berman, A. J. Davis, J. T. Roland Jr and M. A. Svirsky (2015). "Measurement of cochlear implant electrode position from intraoperative post-insertion skull radiographs: a validation study." Otology & neurotology: official publication of the American Otological Society, American Neurotology Society [and] European Academy of Otology and Neurotology 36(9): 1486.

Xu, J., S.-A. Xu, L. T. Cohen and G. M. Clark (2000). "Cochlear view: postoperative radiography for cochlear implantation." Otology & Neurotology 21(1): 49-56.